EUMETSAT Satellite Application Facility on Climate Monitoring

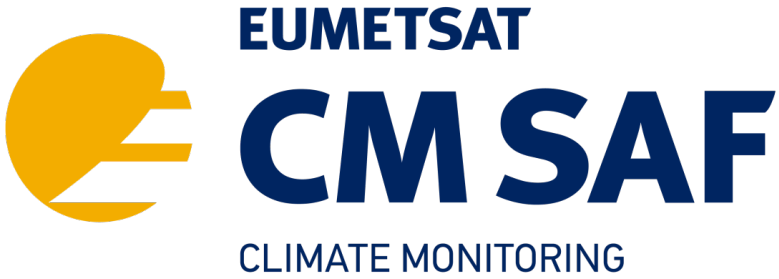

Algorithm Theoretical Basis Document

CM SAF Cloud, Albedo, Radiation data record, AVHRR-based, Edition 3 (CLARA-A3)

Top-of-Atmosphere Radiation

DOI: 10.5676/EUM_SAF_CM/CLARA_AVHRR/V003

TOA Reflected Solar Flux (RSF) **CM-11312**
TOA Outgoing Longwave Radiation (OLR) **CM-11342**

Reference Number: SAF/CM/RMIB/ATBD/GAC/TOA
Issue/Revision Index: 1.0
Date: 07.06.2021

Document Signature Table

	Name	Function	Signature	Date
Author	Tom Akkermans Nicolas Clerbaux	CM SAF scientist CM SAF scientist		27/04/2021 27/04/2021
Editor	Rainer Hollmann	Science Coordinator CM SAF		27/04/2021
Approval	CM SAF Steering Group			
Release	Rainer Hollmann	Project Manager		

Distribution List

Internal Distribution	
Name	**No. Copies**
DWD / Archive	1
CM SAF Team	1

External Distribution		
Company	**Name**	**No. Copies**
Public		1

Document Change Record

Issue/ Revision	Date	DCN No.	Changed Pages/Paragraphs
1.0	27.04.2021		Submitted for PCR

Applicable Documents

The following documents, of the exact issue shown, form part of this document to the extent specified herein. Applicable documents are those referenced in the Contract or approved by the Approval Authority. They are referenced in this document in the form [AD X].

Reference	Title	Code, Version, Date
AD 1	CM SAF CDOP3 Project Plan	SAF/CM/DWD/CDOP3_PP_1_6, Version 1.6, 03/07/2020
AD 2	CM SAF CDOP3 Product Requirement Document	SAF/CM/DWD/PRD, Version 3.7, 19/10/2020

Reference Documents

The reference documents contain useful information related to the subject of the project. These reference documents complement the applicable ones, and can be looked up to enhance the information included in this document if it is desired. They are referenced in this document in the form [RD X].

Reference	Title	Code, Version, Date
RD 1	CM SAF Requirements Review: AVHRR GAC Edition 3 data records (CLARA Ed.3)	SAF/CM/CDOP3/SMHI/RR32, Version 1.2, 08/05/2020
RD 2	ATBD CM SAF Cloud, Albedo, Radiation data record, AVHRR-based, Edition 3 (CLARA-A3): Cloud Products processing chain (level-1 – level-2/2b –level-3).	SAF/CM/DWD/ATBD/GAC v3.0
RD 3	Algorithm Theoretical Basis Document for Cloud Micro Physics of the NWC/PPS	NWC/CDOP3/PPS/SMHI/SCI/ATBD/CMIC, Issue 3.0, 26/04/2021
RD 4	Algorithm Theoretical Basis Document for the Cloud Probability of the NWC/PPS	NWC/CDOP3/PPS/SMHI/SCI/ATBD/ CloudProbability, Issue 2.0, 26/04/2021
RD 5	ATBD CM SAF Cloud, Albedo, Radiation data record, AVHRR-based, Edition 3 (CLARA-A3): Surface Radiation	SAF/CM/DWD/ATBD/CLARA/RAD, Issue 3.0
RD 6	The Data Set Generation Capability Description Document, AVHRR GAC Edition 3 (CLARA-A3)	SAF/CM/DWD/DGCDD/GAC/3, version 1.0
Documents from CDOP-2 and/or CLARA-A2:		
RD 7	Algorithm Theoretical Basis Document SAFNWC/PPS “Cloud mask”, PPS version 2014 patch 20150327 (OBS: in the text referred to as patch 1).	SAF/NWC/CDOP2/PPS/SCI/ATBD/1, Issue1.1, 13 March 2015
RD 8	ATBD: “Cloud Mask”, PPS version 2014	SAF/CM/SMHI/ATBD/CMA_AVHRR, Issue2.0, 19/08/2016

Reference	Title	Code, Version, Date
RD 9	ATBD Top of Atmosphere Radiation: SEVIRI/ GERB Data Record	SAF/CM/RMIB/ATBD/GERB, Issue2.4, 13/12/2016
RD 10	ATBD Top of Atmosphere Radiation: MVIRI/ SEVIRI Data Record	SAF/CM/RMIB/ATBD/MET_TOA, Issue1.3, 05/10/2016
RD 11	Scientific Validation Report: Top of Atmosphere Radiation: SEVIRI/GERB Data Records	SAF/CM/RMIB/VAL/GERB, Issue 1.1, 13/12/2016
RD 12	Scientific Validation Report: Top of Atmosphere Radiation: MVIRI/SEVIRI Data Record	SAF/CM/RMIB/VAL/MET_TOA, Issue1.1, 05/10/2016

Table of Contents

1. Introduction....10
1.1. Scope of the document....10
1.2. Short summary of the intended products' added value....10
1.3. Content of the document....10
2. Input data: description....11
2.1. FDR....11
2.1.1. Details on the visible and infrared calibration of AVHRR radiances....11
2.2. Input data from cloud processing package PPS (on GAC orbit grid)....13
2.2.1. Cloud mask....13
2.2.1.a. Probabilistic Cloud Mask (CMAPROB)....13
2.2.1.b. Classic cloud mask with snow detection flag (CMA-extended)....14
2.2.2. Cloud Physical Parameters (CPP)....14
2.2.2.a. Cloud phase and Cloud Optical Thickness....14
2.2.2.b. Common quality indicators flag (cpp_quality)....16
2.2.2.c. Common geophysical and processing conditions flag (cpp_conditions)....16
2.3. PPS auxiliary input data, mapped on GAC orbit grid....17
2.3.1. ERA5 snow depth....17
2.3.2. OSI SAF sea ice concentration....18
2.3.3. ERA5 10m wind speed....19
2.3.4. ERA5 surface temperature and integrated water vapor....19
2.3.5. USGS-based Land fraction....20
2.4. External input data....21
2.4.1. C3S daily Total Solar Irradiance (TSI) time series....21
2.4.2. Land cover data (IGBP)....22
2.4.3. CERES low-resolution land cover map....24
2.4.4. Hourly ERA5 Outgoing Longwave Radiation and Cloud cover....25
2.4.5. Climatology of CERES cloud optical thickness....26
2.4.6. CERES Shortwave Angular Distribution Models (ADMs) and albedo models....28
2.4.7. Twilight coefficients....29
2.4.8. Narrowband-to-broadband coefficients (shortwave)....30
2.4.9. Narrowband-to-OLR coefficients (longwave)....32
3. Retrieval of Reflected Solar Flux [CM-11312, RSF]....34
3.1. Part 1: Retrieval algorithm for instantaneous TOA albedo (level-2)....34
3.1.1. Overview (Fig.28)....34
3.1.2. Preparation of input data....35
3.1.2.a. Initialization of pixel value with input data: common part....35
3.1.2.b. Initialization of pixel value with input data: shortwave-only part....36
3.1.2.c. Preparation of cloud cover and surface types (Fig.*32*)....37
3.1.3. Sunglint treatment....43
3.1.3.a. Sunglint detection....43
3.1.3.b. Sunglint albedo calculation....45
3.1.4. Narrowband-to-broadband (NTB) conversion....46
3.1.5. Directional-to-hemispherical conversion (angular correction)....46
3.1.5.a. Scene type determination....46
3.1.5.b. Actual albedo calculation....47
3.1.5.c. Correcting interpolation-induced bias....47
3.1.6. Final error corrections....47
3.1.6.a. The resulting TOA albedo exceeds 100%....47
3.1.6.b. The resulting TOA albedo is lower than 6%....48
3.1.6.c. Order of corrections....49
3.1.7. Output....49
3.2. Part 2: Spatial aggregation from GAC orbit grid to regular CMSAF grid (level-2b)....51
3.2.1. Twilight coefficients....51
3.2.2. Aggregation procedure....51
3.2.2.a. Treatment of overlapping orbits....53
3.2.3. Nested 0.25° Processing Grid....54
3.2.4. Output....58
3.3. Part 3: Processing of instantaneous albedo to daily mean RSF (level-3)....58

3.3.1. Overview....58
3.3.2. Daylight conditions (SZA<84°): modeling albedo diurnal cycle....59
3.3.3. Twilight conditions (84°>SZA>100°)....66
3.3.4. Nighttime conditions (SZA>100°)....67
3.3.5. Daily integral....67
3.3.6. Output....68
3.4. Part 4: Temporal aggregation to monthly mean RSF (level-3b)....68
4. Retrieval of Outgoing Longwave Radiation [CM-11342, OLR]....70
4.1. Part 1: Retrieval algorithm of instantaneous OLR (level-2)....70
4.1.1. Overview....70
4.1.2. Preparation input data....71
4.1.2.a. Initialization of pixel value with input data: common part....71
4.1.2.b. Initialization of pixel value with input data: longwave-only part....71
4.1.3. Narrowband-to-OLR conversion (spectral+angular corrections)....73
4.2. Part 2: Spatial aggregation from GAC orbit grid to regular grid (level-2b)....75
4.3. Part 3: Processing of instantaneous to daily mean OLR (level-3)....75
4.3.1. Method....75
4.3.2. Output....77
4.4. Part 4: Temporal aggregation to monthly mean OLR (level-3b)....77
5. Error budget estimation....79
5.1. Theoretical sources of uncertainty....79
5.2. Evaluation based on preliminary products....80
6. Assumptions, limitations, future outlook....81
6.1. Input data: Snow cover....81
6.1.1. Problem statement....81
6.1.2. Future outlook....82
6.2. Input data: Land cover....82
6.3. Input data: ADMs (and aerosols)....82
7. Abbreviations and acronyms....83
8. Scientific references....84
9. Annex....87
9.1. Scene types for ADMs and albedo models: overview....87
9.1.1. CERES/TRMM Ed.2B ADMs, scene types and albedo models....87
9.1.2. CERES/Terra SSF Ed.2B ADMs, scene types and albedo models....100
9.1.3. CERES Terra/Aqua Edition4 ADMs....101
9.2. CERES TRMM SW ADM interpolation bias correction....101
9.3. Updated Narrowband-to-Broadband regressions....102
9.4. Application of NTB regressions on GAC/AVHRR pixel scale (new)....105
9.5. Land cover classes for NTB analyses....108
9.6. Bit Flags, and Bit Flag variable IDs....109
9.6.1. Bit flag variable ID's....109
9.6.2. Bit flags for Program Part 1....109
9.6.3. Bit flags for Program Part 3....110
9.7. Post-processing from ERA5 OLR and cloud cover....111

Table of Figures

Figure 1: Example of Level-1c brightness temperature (K) at 12µm, mapped on GAC orbit grid....11
Figure 2: Time-dependent curves for the slope parameter for converting AVHRR counts to reflectances for satellites in afternoon orbits. Upper panel: Results for the 0.6 µm channel (Ch1, left) and the 0.9 µm channel (Ch2, right). Lower panel: Differences relative to the calibration curves used for CLARA-A2. The new method used for CLARA-A3 is denoted SBAF-bases while the other method EXT is a modification applied to the CLARA-A2 extension in the years 2016-2019....12
Figure 3: Example of PPS Cloud Probability (%) on GAC orbit grid....14
Figure 4: Example of PPS CPP cloud phase (dimensionless) on GAC orbit grid. Ice in green, water in purple....15
Figure 5: Example of PPS CPP cloud optical thickness (dimensionless) on GAC orbit grid....15
Figure 6: Example of PPS CPP common quality indicators flag on GAC orbit grid. Yellow is 'good', blue is clearsky..16
Figure 7: Example of PPS CPP common geophysical/processing conditions flag (‘sunglint’) on GAC orbit grid....17
Figure 8: Example of ERA5 snow depth (cm) on GAC orbit grid....18
Figure 9: Example of OSI SAF sea ice concentration (%) on GAC orbit grid (dark brown=land)....19
Figure 10: Example of Surface Temperature (K) on GAC orbit grid....20
Figure 11: Example of Column Integrated Water Vapour (kg/m²) on GAC orbit grid....20
Figure 12: Example of USGS-based Land Fraction (%) on GAC orbit grid....21
Figure 13: C3S daily Total Solar Irradiance (TSI) timeseries v2.3....22
Figure 14: IGBP land cover map (high-res.)....22
Figure 15: IGBP land cover map (high-res.), zooming in on the Hawaiian Islands....23
Figure 16: IGBP land cover map (low-res.) with land extrapolated to sea and ice areas....23
Figure 17: IGBP land cover map (low-res.), extrapolated, zooming in on Hawaiian Islands....24
Figure 18: Low-resolution CERES land cover map....25
Figure 19: Example of ERA5 OLR daily input data for a single grid point....26
Figure 20: Example of ERA5 Cloud Cover daily input data for single grid point....26
Figure 21: Global multi-year monthly mean Cloud Optical Thickness for January (2000-2020)....27
Figure 22: Global multi-year monthly mean Cloud Optical Thickness for July (2000-2020)....27
Figure 23: Multi-year annual cycle of Cloud Optical Thickness (2000-20*20*) for single grid point....28
Figure 24: CERES TRMM SW albedo models for liquid-phase overcast ocean scene types....29
Figure 25: Twilight model with SZA-dependent solar flux for clearsky (left) and overcast (right) conditions; The red dotted lines are taken from Kato and Loeb, 2003....30
Figure 26: AVHRR- and CERES-carrying satellites’ orbital plane matching....30
Figure 27: Overview of the OLR (left) and RSF (right) processing chain....34
Figure 28: Flow chart for Program Part 1 and Part 2 (level-2 processing for RSF and OLR)....35
Figure 29: Flow chart: use of cloud masks: rules....36
Figure 30: Example of modified Cloud Optical Thickness (dimensionless) on GAC orbit grid....37
Figure 31: Example of ‘flag_coastal’ on GAC orbit grid....38
Figure 32: Flow chart: preparation of cloud cover and surface types....39
Figure 33: Flow chart: decision tree for determin*ing* surface type....40
Figure 34: Example of variable ‘CERESsurftype’ on GAC orbit grid....42
Figure 35: Relation between snow depth and snow cover in IFS (Dutra et al., 2010). In red: adaptation for our purposes, by putting a range limitation to 50%-100%....43
Figure 36: Example of variable ‘sun_glint_angle’ (units: degrees) on GAC orbit grid....44
Figure 37: Flow chart: processing of shortwave reflectance to broadband albedo....45
Figure 38: Schematic example of radiation incident on (top) horizontal area, (bottom) cloud edge....48
Figure 39: Photographic example of low-elevation sun rays incident on cloud edges (photo: ISS)....48
Figure 40: Example of variable ‘SW_alb_bb’ (broadband SW albedo) on GAC orbit grid....49
Figure 41: Example of final output "TOA SW albedo" ('SW_alb_bb') on GAC orbit grid....50
Figure 42: Example of final output “Cloud cover” on GAC orbit grid....50
Figure 43: Example of output “TOA albedo” (SW_alb_bb) aggregated on CMSAF 0.25° grid....51
Figure 44: Example: Number of GAC pixels contributing to each CMSAF 0.25°x0.25° grid box....52
Figure 45: Example of output “Cloud cover” aggregated on CMSAF 0.25° grid....52
Figure 46: Example of variable ‘UNIX Time’ with overlapping start and end of GAC orbit grid....53
Figure 47: Example of variable ‘VZA’ with overlapping start and end of GAC orbit grid....54
Figure 48: Example of variable ‘UNIX Time’ after aggregation (no overlap anymore)....54
Figure 49: non-nested regular CMSAF grid 0.25°x0.25° (orthographic projection)....55
Figure 50: Nested grid box size (km²) as function of latitude (°)....56
Figure 51: nested regular CMSAF grid 0.25°x0.25° (unprojected, a.k.a. plate carrée)....57
Figure 52: nested regular CMSAF grid 0.25°x0.25° (orthographic projection)....57

Figure 53: SZA for all temporal “5min bins” during a single UTC day on a single 0.25°x0.25° grid box. In this example, there is only one relevant Day Light Block....59
Figure 54: Conceptual example of modeling the albedo diurnal cycle (step 1)....60
Figure 55: Conceptual example of modeling the albedo diurnal cycle (step 2)....60
Figure 56: Conceptual example of modeling the albedo diurnal cycle (step 3)....61
Figure 57: Conceptual example of modeling the albedo diurnal cycle (step 4)....61
Figure 58: Conceptual example of modeling the albedo diurnal cycle (step 5)....62
Figure 59: Conceptual example of modeling the albedo diurnal cycle (step 6)....62
Figure 60: Number of DLB’s contributing to daily mean of UTC day 23/7/2010; Blue (0), yellow (1), red (2)....63
Figure 61: Conceptual example of DLB overlapping with start of the UTC day (00:00h UTC)....63
Figure 62: SZA during a single UTC day on a single grid box, during high-latitude wintertime....64
Figure 63: Number of SW instantaneous observations contributing to daily mean of UTC day 23/7/1983....65
Figure 64: Conceptual example of interpolating Twilight Coefficients A and B....66
Figure 65: TOA Daily mean Reflected Solar Flux for 2/1/1998....67
Figure 66: Number of SW daily means contributing to monthly mean RSF (January 1998)....69
Figure 67: Overview of the OLR (left) and RSF (right) processing chain....70
Figure 68: Flow chart: main structure of Program Part 1 (level-2 processing for RSF and OLR)....71
Figure 69: Spectral response curves of channels 4 and 5 of the different AVHRR-1/-2/-3 instruments (Frey et al., 2017) 72
Figure 70: example of SBAF calculator output: AVHRR channel 4 of TIROS-N to NOAA-19....73
Figure 71: Flow chart: processing of longwave narrowband T_b to OLR (AVHRR-2/-3)....74
Figure 72: Flow chart: processing of longwave narrowband Tb to OLR (AVHRR-1)....75
Figure 73: Example of OLR diurnal cycle for clear-sky desert pixel on 1/6/2012, modelled using a single satellite NOAA-19 (a) and using all available satellites (b). From Clerbaux et al. (2020)....76
Figure 74: TOA Daily mean Outgoing Longwave Radiation for 2/1/1998....77
Figure 75: Global monthly statistics CLARA-A3 w.r.t. ERA5, CERES, and HIRS (OLR)....80
Figure 76: Global monthly statistics CLARA-A3 w.r.t. CERES (RSF)....80
Figure 77: illustration of how land surface influences snow cover....81
Figure 78: Flux-equivalent Mean Bias (MB_{flux}) between observed and estimated broadband reflectance, for overcast conditions (update of Figure 4c in Akkermans and Clerbaux, 2020)....103
Figure 79: Flux-equivalent Mean Bias (MB_{flux}) between observed and estimated broadband reflectance, for (a) clear-sky and (b) all-sky conditions (update of Figure 5 in Akkermans and Clerbaux, 2020)....104
Figure 80: NTB regression validation in Akkermans and Clerbaux (2020)....106
Figure 81: NTB regression validation for individual GAC/AVHRR pixels....106
Figure 82: Mean bias of reflectance (in percentage points p.p.) between observed and estimated broadband reflectance, for all-sky conditions....107
Figure 83: Mean bias of flux-equivalent reflectance (in W/m^2) between observed and estimated broadband reflectance, for all-sky conditions....107
Figure 84: Clear-sky scaled radiance for AVHRR channels 1 and 2, stratified per IGBP class....108

Index of Tables

Table 1: PPS CPP common quality indicators bit flags....16
Table 2: C3S daily TSI time series v2.3: instrument adjustment factors....21
Table 3: Twilight model: scene type dependent sample size (n) and regression coefficients (A_c and B_c)....29
Table 4: NTB (Narrowband-to-Broadband) regression coefficients, here using 100% of the matched NTB pairs with strict matching criteria (update of Table 3 in Akkermans and Clerbaux, 2020)....31
Table 5: Example of Narrowband-to-OLR coefficients table (for AVHRR-2/-3)....32
Table 6: Example of Narrowband-to-OLR coefficients table (for AVHRR-1)....33
Table 7: Mapping of fresh snow and sea-ice to NTB, CERES, TWL surface types....41
Table 8: Mapping of IGBP class (water+land types) to NTB, CERES, TWL surface types....41
Table 9: CERES TRMM SW ADM scene types for clear-sky ocean....46
Table 10: Latitude segments of nested grid....56
Table 11: Satellite bit flags....66
Table 12: Linear regression coefficients (slope and offset) applied as spectral-band adjustment to measured brightness temperature (BT) of AVHRR channels 4 and 5 to mimic NOAA-19 AVHRR (Stengel et al., 2020)....72
Table 13: Slope and offset from linear relations between TIROS-N and NOAA-19....73
Table 14: ADM scene types (non-snow, non-ice)....87
Table 15: ADM scene types (permanent snow/ice, fresh snow, sea-ice)....100
Table 16: NTB: Number of matched NTB pairs with strict matching criteria (update of Table 2 in Akkermans and Clerbaux, 2020)....102
Table 17: NTB validation: Regression metrics based on calibration subset, here using 100% of the NTB pairs with strict matching criteria (update of Table 4 in Akkermans and Clerbaux, 2020)....102
Table 18: NTB validation: regression performance on expanded database with relaxed matching criteria (update of Table 6 in Akkermans and Clerbaux, 2020)....103
Table 19: NTB: Global stability statistics from bias map, based on expanded database, with relaxed matching criteria (update of Table 7 in Akkermans and Clerbaux, 2020)....105
Table 20: NTB: Global accuracy statistics from bias map, based on surface-type-dependent regressions from expanded database, with relaxed matching criteria (update of Table 8 in Akkermans and Clerbaux, 2020)....105
Table 21: Bit flag Variable ID's....109
Table 22: Bit flags for Program Part 1....109
Table 23: Bit flags for Program Part 3....110

1. Introduction

~~Basic accuracy requirements are defined in the Product Requirements Document [AD 2] and further specified and clarified in the Requirements Review document [RD 1].~~

The reader is referred to document [RD 2] which describes more details on the CLARA-A3 products and the overall processing chain from which the TOA Radiation products (RSF and OLR) are part of.

1.1. Scope of the document

The purpose of this document is to describe the algorithm implemented within the CM SAF to generate daily mean and monthly mean of Top-Of-Atmosphere (TOA) radiative fluxes data records from the AVHRR instrument on board the NOAA and MetOp satellites. The observations from the CERES radiometer are used to derive empirical narrowband-to-broadband relations for AVHRR.

This document focuses on the algorithm while details about the processing system are provided in the Dataset Generation Capability Description Document (DGCDD) [RD 6].

Two data records are generated with the following CM SAF identifiers:

CM SAF identifier	Content
CM-11312	TOA Reflected Solar Flux (RSF)
CM-11342	TOA Outgoing Longwave Radiation (OLR)

1.2. Short summary of the intended products' added value

Basic accuracy requirements are defined in the Product Requirements Document [AD 2] and further specified and clarified in the Requirements Review document [RD 1]. To remind the reader about the intended benefits of above mentioned (new) products, a short summary is provided here. Although the Clouds and the Earth's Radiant Energy System (CERES)[1] products are acknowledged to be the golden standard w.r.t. radiative flux data records, two major limitations can be identified: (1) the products are relatively recent, e.g. starting in year 2000 for the EBAF product, and (2) the products have a relatively coarse spatial resolution of 1°x1° (lat-lon equal angle grid). The products developed within CM SAF aim to bridge these gaps, respectively by (1) a prolongation back in time to the late 1970s and (2) by increasing the spatial resolution to 0.25°x0.25°. A third advantage of the new CDRs lies in their synergy and compatibility with the other CDRs from the CM SAF CLARA product family (cloud mask and other cloud parameters, surface radiation, surface albedo, etc.) sharing common algorithms and processing chains.

1.3. Content of the document

This Algorithm Theoretical Basis Document (ATBD) is structured as follows.

- **Section 2** provides basic information about the data used as input of the processing.
- **Sections 3 and 4** make up the core of the document, providing a complete description and justification of the main algorithms used to generate the data sets, respectively RSF (section 3) and OLR (section 4), each formatted according to the same subsection structure:
  - estimation of instantaneous TOA radiative fluxes
  - spatial aggregation to regular lat-lon grid of 0.25°x0.25°
  - estimation of daily mean flux
  - estimation of monthly mean flux
- **Section 5** presents a brief error budget estimation; this should not be considered as a validation (in which typically the generated data record is compared with an external 'ground truth' data record), which follows in the future Validation Report.
- **Section 6** concludes this document by discussing some important limitations, assumptions and proposed future product enhancements which are currently out of scope.

1 *URL: https://ceres.larc.nasa.gov/*

2. Input data: description

2.1. FDR

From AVHRR Global Area Coverage (GAC) Level-1c data, a Fundamental Data Record (FDR) is created using the PyGAC processor tool (Devasthale et al., 2016), performing the calibration and homogenization of the record. It is a Python package to read, calibrate and navigate NOAA and MetOp AVHRR GAC and LAC data[2].

Reflectance[3] (from shortwave channels 1+2, on 0.6µm and 0.8µm) and Brightness Temperature (from longwave channels 4+5, on 11µm and 12µm) are provided on their original irregular *GAC orbit grid* (with spatial coordinates for each pixel) together with the necessary metadata such as intercept and slope coefficients. Also included are the viewing and illumination geometry (SZA, VZA, RAA) and time stamp.

Figure 1 shows an example of channel 5 brightness temperature (K) taken from a single "GAC orbit file" for MetOp-A on 1/7/2011 roughly between 10h-11h UTC. An extracted area zooms in on Western Europe for better detail.

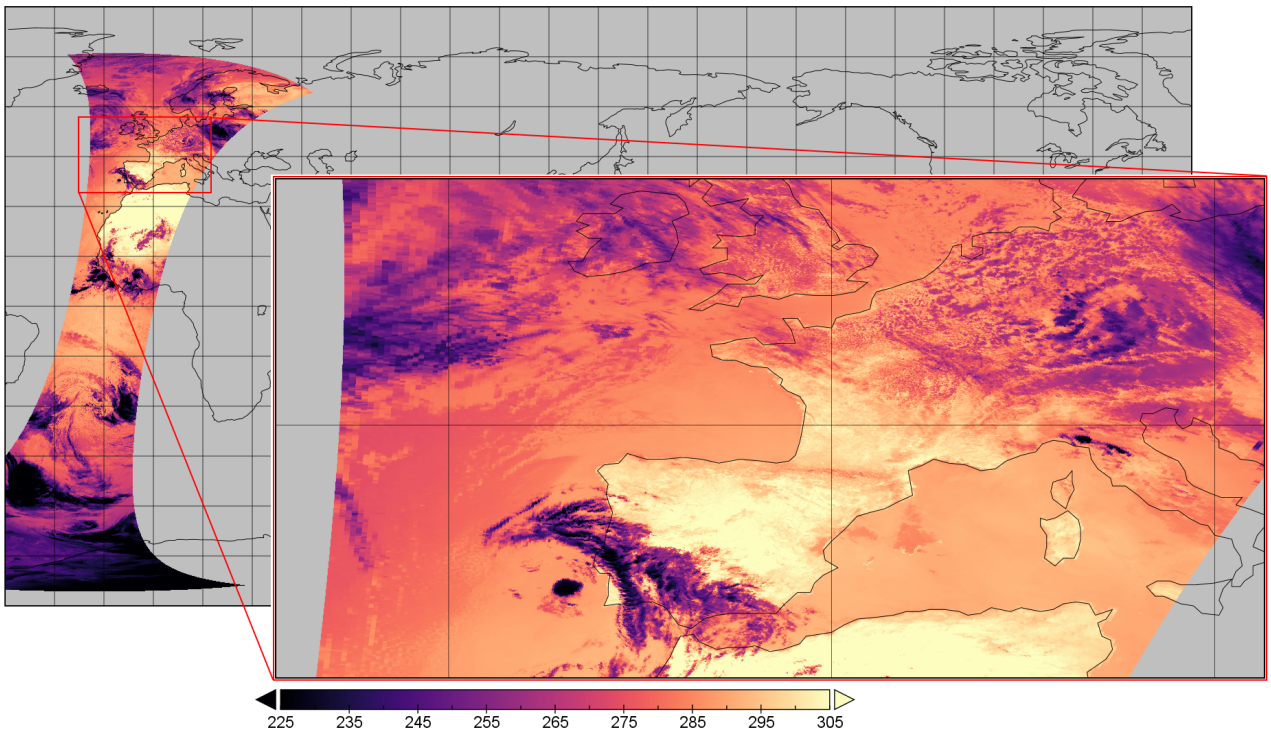

Figure 1: Example of Level-1c brightness temperature (K) at 12µm, mapped on GAC orbit grid

2.1.1. Details on the visible and infrared calibration of AVHRR radiances

Because of its fundamental importance for the quality of the derived products, we give in this sub-section more details on the used AVHRR calibration methods implemented in the PyGAC tool.

The calibration of the visible AVHRR channels at 0.6 µm, 0.9 µm and 1.6 µm is based on an original method introduced by Heidinger et al. (2010). Original AVHRR sensor counts are linked to calibrated radiances from corresponding spectral channels of the MODIS instrument on the Aqua and Terra satellites. MODIS uses an onboard solar diffuser as a calibration reference and is judged to deliver a stable and accurate calibration.

AVHRR and MODIS matchups are collected based on Simultaneous Nadir Observations (SNOs) and adjustments are made for spectral response differences. A quadratic relation is fitted to measurements for estimating the AVHRR sensor degradation with time in each spectral channel and for adjusting for inter-satellite sensor variations. For AVHRR sensors operating before the MODIS era, reference measurements over a number of invariant Earth targets are utilized. Reflectance characteristics are first estimated over these targets from MODIS and this information is then used as reference for the older AVHRR sensors. In addition, inter-satellite adjustments are estimated by also utilizing SNOs

2 *Github URL: https://github.com/pytroll/pygac*
3 *In fact it is the non-SZA-normalized reflectance a.k.a. 'scaled radiance'*

between co-existing pairs of NOAA satellites. The accuracy of the original method was estimated to 2-3 % in reflectance units. For CLARA-A3 we use a slightly updated version of the method making use of the latest MODIS collection (Collection 6.1) and introducing the use of Spectral Band Adjustment Factors (SBAFs) for the characterization of invariant Earth targets. This has led to more stable and balanced calibration of especially the 0.6 µm and 0.9 µm channels. Figure 2 below presents resulting calibration curves (i.e., time-varying slope/gains) for satellites in afternoon orbit compared to previous calibration curves used in CLARA-A2. Notable differences compared to CLARA-A2 are seen for some satellites (e.g., NOAA-14 and NOAA-19).

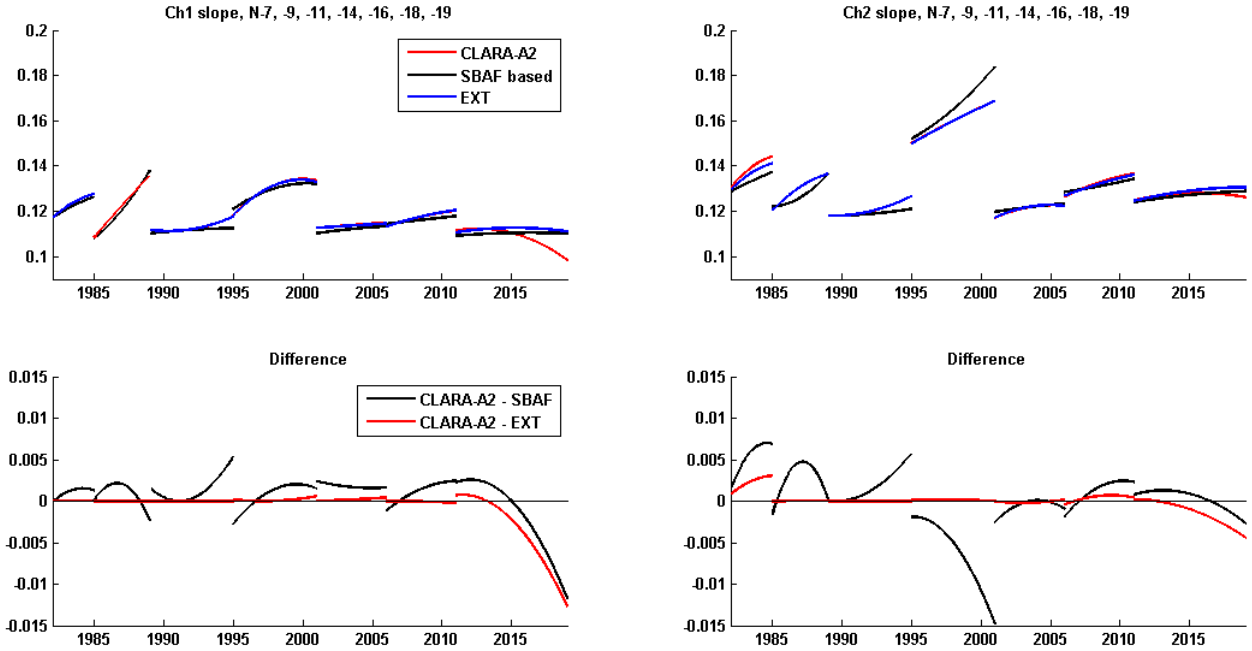

Figure 2: Time-dependent curves for the slope parameter for converting AVHRR counts to reflectances for satellites in afternoon orbits. Upper panel: Results for the 0.6 µm channel (Ch1, left) and the 0.9 µm channel (Ch2, right). Lower panel: Differences relative to the calibration curves used for CLARA-A2. The new method used for CLARA-A3 is denoted SBAF-bases while the other method EXT is a modification applied to the CLARA-A2 extension in the years 2016-2019.

The calibration of the three infrared channels at 3.7 µm, 11 µm and 12 µm is based on reference measurements to space and to an internal calibration target onboard each satellite. The method used is referred to as the Walton calibration method (Walton, 1998) and is the method used by default for the original L1b GAC dataset archived in the NOAA CLASS archive. The method is implemented in the PyGAC tool where some minor adjustments and refinements have also been introduced for CLARA-A3. Calibration coefficients have been estimated for subsets of 50 scanlines to reduce the effects of internal noise. A brightness temperature accuracy of 0.1-0.2 K is expected, although larger errors will be at hand for very cold Earth target temperatures due to a limited radiometric resolution of the AVHRR instrument.

Issues have been raised for potential flaws of the infrared calibration (e.g., Trishchenko, 2002 and Mittaz et al., 2007). In addition, comparisons with high-quality reference sensors have also revealed notable deviations (Mittaz et al., 2008 and Wang and Cao, 2008). Problems have been identified as linked to inconsistencies in the pre-launch calibration procedure and to various external factors (e.g., solar contamination of calibration payload and Earth shine noise effects). The EU-project FIDUCEO aimed at providing an improved AVHRR calibration of infrared channels where these problems would be taken care of and the original plan for CLARA-A3 was to make use of this new methodology. However, a final methodology could not be achieved within the available FIDUCEO project framework and further improvements here depend on whether this work can be continued in new projects in the future. However, the impact of inherent flaws of the infrared calibration is expected to be small for CLARA-A3. It is evident that the problems are more serious for applications requiring a very accurate calibration of brightness temperatures, such as the compilation of CDRs on Sea Surface Temperatures (SSTs). Past experience has also shown that it is possible to generate useful CDRs for other parameters despite these problems (e.g., as exemplified by CLARA-A2, PATMOS-X and ESA-CLOUD-CCI CDRs based on AVHRR GACdata).

In awaiting the realization of an improved AVHRR GAC FCDR, a specific EUMETSAT initiative has been made to collect and prepare (by using the latest version of the PyGAC tool) an AVHRR FDR that can be used as input to the CLARA-A3 TCDR but that also can be used by potential external users. This FDR will be officially released by EUMETSAT in parallel with the release of the CLARA-A3 data record in 2022. This FDR carries information (quality

flagging) on how to prevent the use of corrupt or inconsistent data (which is used to blacklist data for CLARA-A3 processing). It also enables data rescue for some data that was not available previously for CLARA-A2 because of lack of navigation information.

2.2. Input data from cloud processing package PPS (on GAC orbit grid)

The NWC SAF Polar Platform System (PPS) consists of a cloud processing software package for polar orbiting satellite data provided by the EUMETSAT NWC SAF project. The CLARA-A2 products were based on an upgraded version (patch 1, see [RD 7]) of the PPS Version 2014 cloud processing package (Dybbroe et al., 2005a and Dybbroe et al., 2005b), used to determine cloud fraction and cloud top properties. Since 2012, the NWC SAF PPS includes the Cloud Physical Properties (CPP) algorithm (Roebeling et al. 2006), which retrieves cloud thermodynamic phase, cloud optical thickness, cloud particle effective radius, and liquid/ice water path. For CLARA-A3, an upgraded version (PPSv2018-patch5) is used [RD 2].

Through the overall CLARA-A3 processing chain, all SAF NWC PPS output data are already regridded on the *GAC orbit grid* (matching the FDR's grid), which makes it easily available for TOA flux retrievals. Also a selection of its auxiliary input data (e.g. NWP variables), necessary to generate CLARA-A3 output (such as some PPS products), is available on the same GAC orbit grid: these input data can therefore also be easily re-used for other parts of the CLARA-A3 processing chain, such as the TOA radiative flux retrieval described in this document.

Hence, because most of this input data is already described and documented elsewhere, it will not be discussed in detail here, but rather briefly described and provided with references to the main relevant documents (see sections below).

2.2.1. Cloud mask

2.2.1.a. Probabilistic Cloud Mask (CMAPROB)

A detailed description of the probabilistic cloud mask is given in [RD 4], and the product's scientific development is additionally documented by Karlsson et al. (2020). Its main use in the TOA flux retrieval is to determine the scene type and corresponding shortwave ADM and albedo model (Tables 14 and 15), shortwave narrowband-to-broadband regression coefficients (Table 4) and twilight model coefficients (Table 3). The scene types simply distinguish "overcast" and "clear-sky" scenes: this fits within the scope of the TOA flux retrieval, which doesn't fully exploit the probabilistic cloud mask but converts it to a binary cloud mask by applying a 50 % threshold: lower is considered clear-sky (<50%), higher is considered overcast (≥50%). An illustrative example of the probabilistic cloud mask is given in Figure 3.

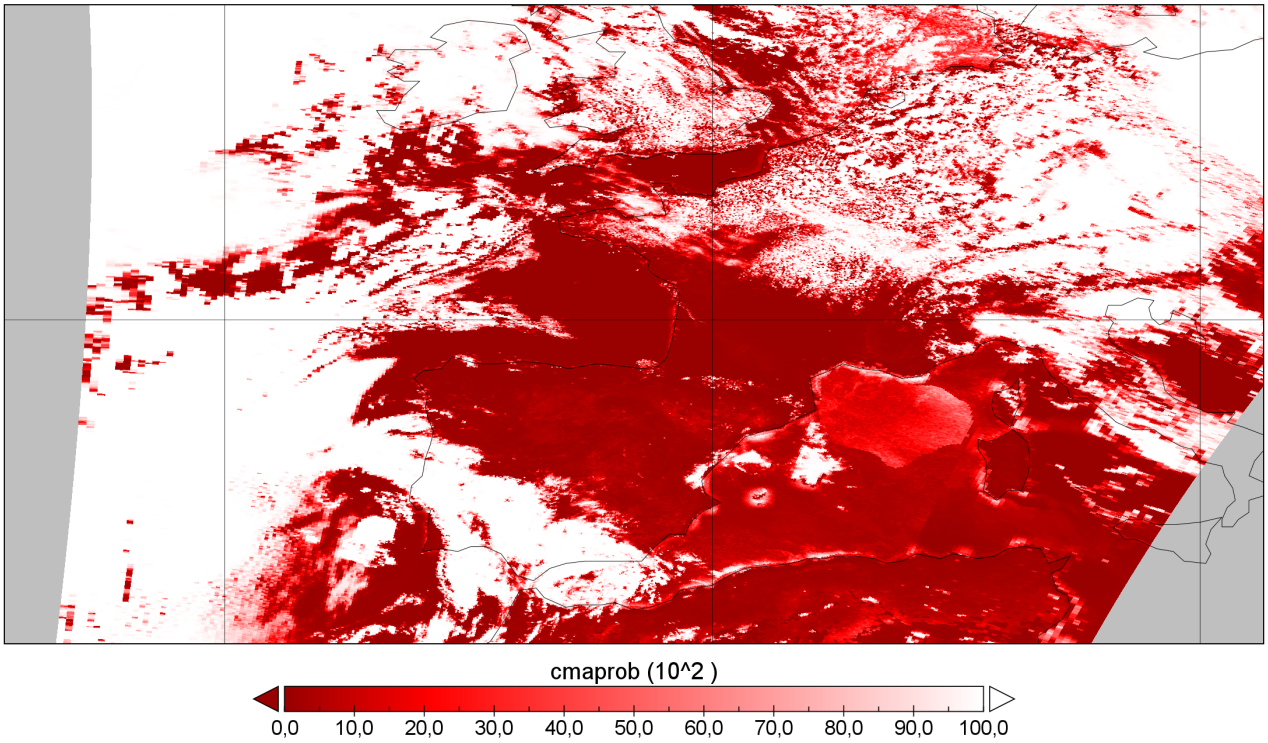

Figure 3: Example of PPS Cloud Probability (%) on GAC orbit grid

Note: should this threshold (i.e. 50%) need any adjustment, it could only be adjusted in the "clearsky-favorable direction" (e.g. ≥60% is overcast, <60% is clear-sky) because pixels <50% cloud probability are not assigned valid Cloud Physical Parameters (CPP) phase and optical thickness (see Section 2.2.2), which are required to further determine the exact ADM scene type.

2.2.1.b. Classic cloud mask with snow detection flag (CMA-extended)

A detailed description of the classic cloud mask is given in [RD 8]. In fact, it concerns a heritage product from CLARA-A2 (Karlsson et al., 2017) which is not actively maintained or developed anymore (*pers.comm. K.-G. Karlsson, 2020*). Besides the binary mask "CMA", an extended version ("CMA-extended") provides an additional flag indicating snow/ice contamination at the surface in clear-sky conditions. This flag is important for the TOA flux retrieval, as it is used in the decision tree to determine the correct scene type (distinction between clearsky land or clearsky snow/ice), which in turn is used to select the proper ADM and narrowband-to-broadband regression coefficients.

Note that the probabilistic cloud mask (Section 2.2.1.a) is considered superior to the classic mask as source of cloud detection, and is therefore used as primary data source for this purpose. Only in cases where the cloud probability falls below 50%, the surface snow/ice presence flag from the classic cloud mask is consulted.

The following values are used:

- CMAext = 0 : clear-sky
- CMAext = 1 : overcast
- CMAext = 2 : cloud-contaminated
- CMAext = 3 : clear-sky and snow/ice-contaminated

2.2.2. Cloud Physical Parameters (CPP)

2.2.2.a. Cloud phase and Cloud Optical Thickness

A detailed description of the Cloud Physical Parameters 'cloud phase' and 'cloud optical thickness' is given in [RD 3]. Their main use in the TOA flux retrieval is to determine the scene type and corresponding shortwave ADM and albedo model (Tables 14 and 15). The cloud phase is a binary variable with values 0 (liquid) or 1 (ice), an example of which is

shown in Figure 4. Cloud optical thickness is a continuous variable ranging between 0-100 (unitless), an example is shown in Figure 5. Both parameters are only defined for pixels that have a cloud probability ≥50% in the probabilistic cloud mask (Section 2.2.1.a).

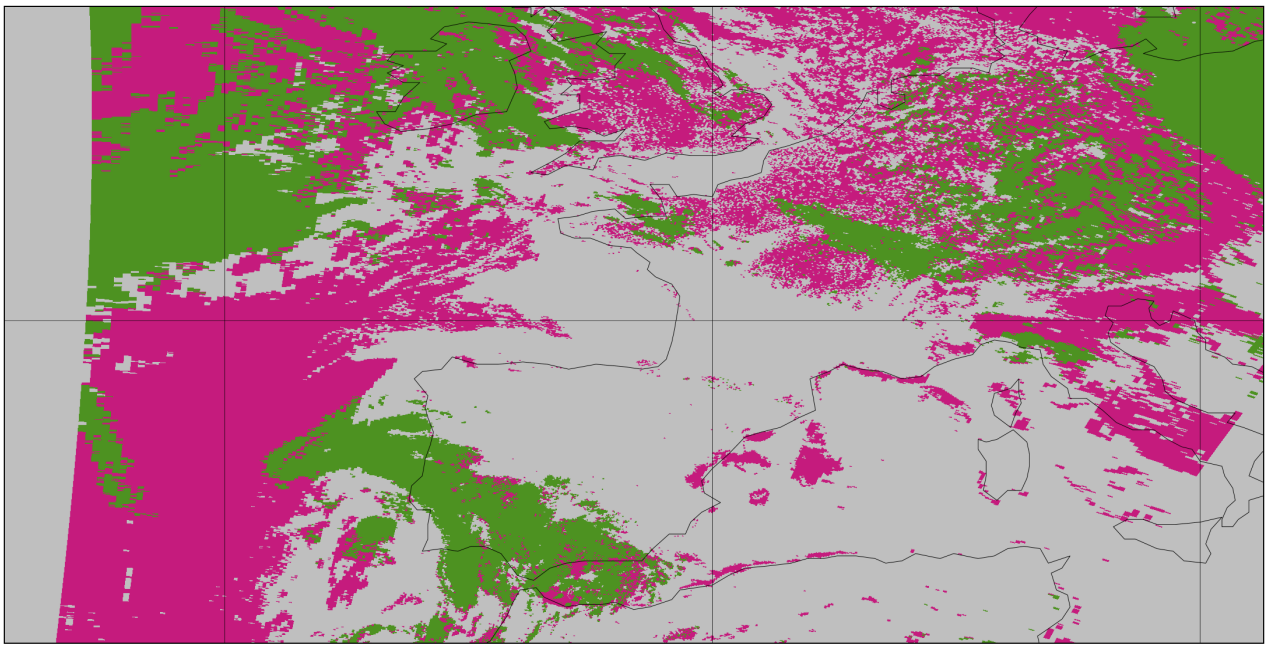

Figure 4: Example of PPS CPP cloud phase (dimensionless) on GAC orbit grid. Ice in green, water in purple.

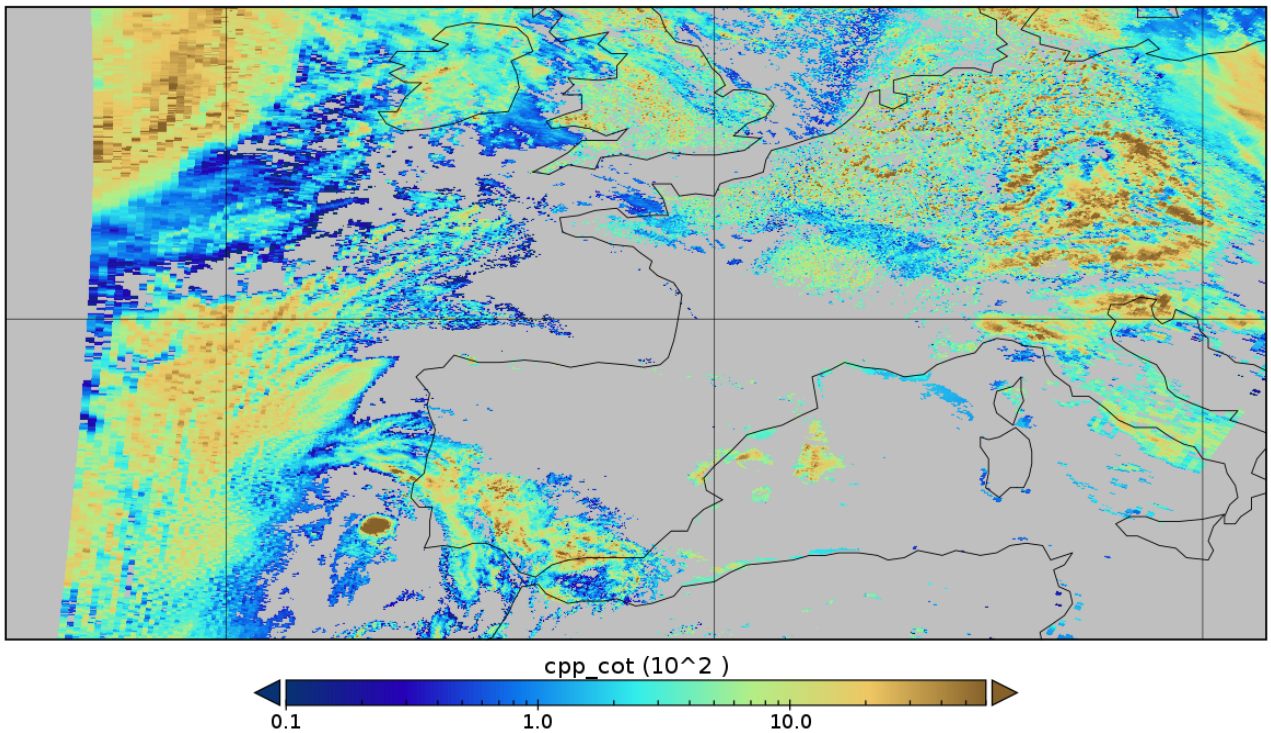

Figure 5: Example of PPS CPP cloud optical thickness (dimensionless) on GAC orbit grid

2.2.2.b. Common quality indicators flag (cpp_quality)

The **CPP quality flag** indicates the reliability of the cloud physical parameters. An overview of the possible bit flag combinations is given in Table 1. The fourth bit (value 8) indicates “good quality”.

Table 1: PPS CPP common quality indicators bit flags

Bit nr.	Binary representation	Value	Bitflag name	Interpretation and applicability
1	0000001	1	no_data	Clear-sky, so quality is not applicable.
2	0000010	2	*spare_bit*	
3	0000100	4	*spare_bit*	
4	**0001000**	**8**	**good**	**Only CPP information with this flag is allowed**
5	0010000	16	questionable	snow/ice situations
4+5	0011000	24	bad	
6	0100000	32	interpolated_reclassified	Set when the pixel has been reset to clear by the optical properties retrieval. When this corresponds to clearsky pixels in cloudmask, the COT will not be used anyway.

A spatially-explicit example of the quality flag is shown in Figure 6, where the yellow color indicates “good quality” CPP parameters.

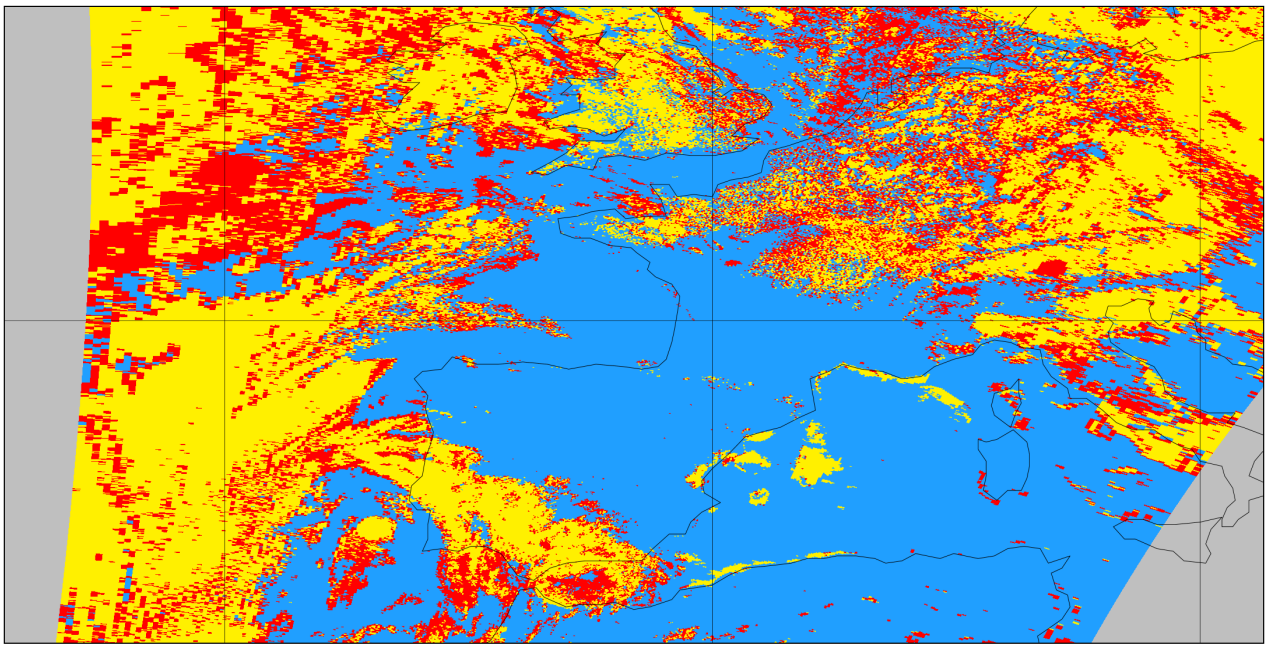

Figure 6: Example of PPS CPP common quality indicators flag on GAC orbit grid. Yellow is 'good', blue is clearsky.

2.2.2.c. Common geophysical and processing conditions flag (cpp_conditions)

Just like the quality flag (Section 2.2.2.b), the **conditions flag** is a ‘bit flag’, meaning that the data may contain a combination of multiple binary flags. However, the program only needs one of them: the PPS sunglint flag, shown in Figure 7.

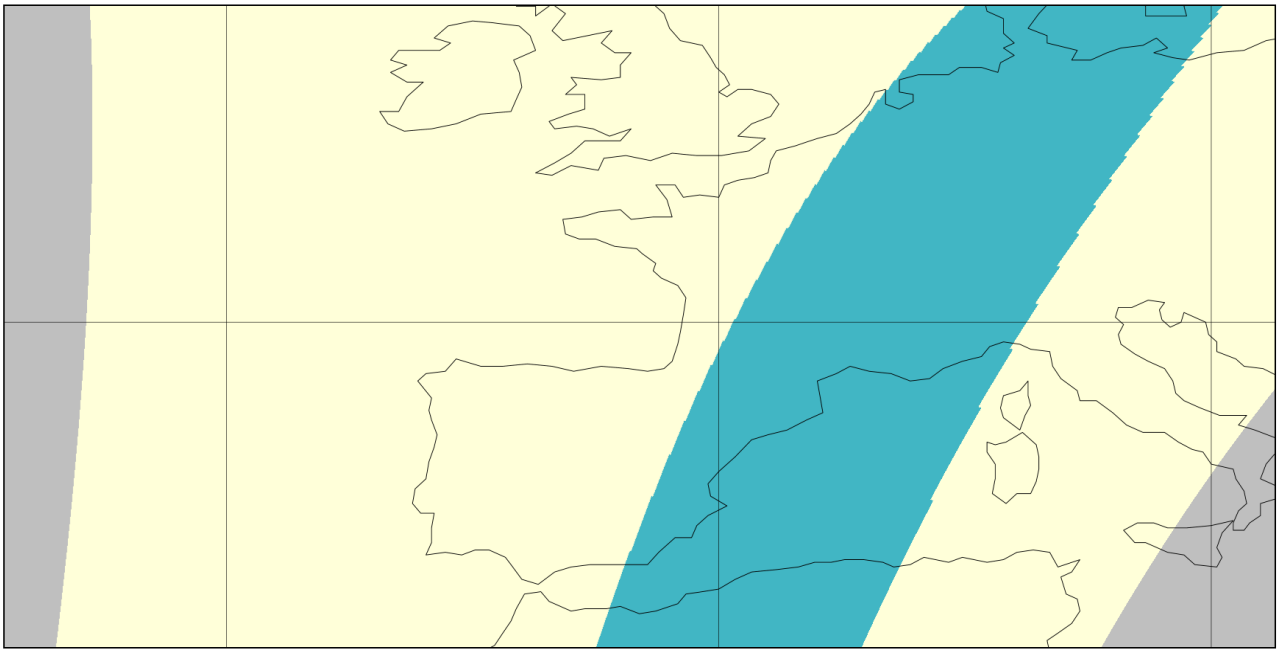

Figure 7: Example of PPS CPP common geophysical/processing conditions flag ('sunglint') on GAC orbit grid

The blue area in Figure 7 indicates pixels for which the PPS sunglint flag is active. The calculation is done purely on a basis of illumination and viewing geometry, so it provides the information for "**potential** sunglint conditions" (not taking into account other requirements such as the presence of clear-sky atmosphere and water surface).

2.3. PPS auxiliary input data, mapped on GAC orbit grid

The PPS data (serving as input for the TOA flux retrieval) contain many variables taken from external datasets which were then regridded onto the GAC orbit grid:

2.3.1. ERA5 snow depth

The main use of ERA5 snow depth in the TOA flux retrieval is to derive (areal) snow cover, and determine the scene type and corresponding shortwave narrowband-to-broadband regression coefficients (Table 4), shortwave ADM and albedo model (Table 15), and twilight model coefficients (Table 3), which all have dedicated fresh snow scene types.

In contrast to directly observed snow cover, the reanalysis data record from ERA5 (Hersbach et al., 2020) provides snow depth with a complete spatial and temporal coverage over the entire CDRs temporal range. ~~Snow depth is converted to snow cover using the depth-cover relation used by the ECMWF Integrated Forecasting System (Dutra et al., 2010).~~

Figure 8 shows an example of ERA5 snow depth (*cm*) taken from a single "*GAC orbit file*" for NOAA-15 on 1/7/2011 roughly between 20h-22h UTC. An extracted area zooms in on the Antarctic Peninsula for better detail.

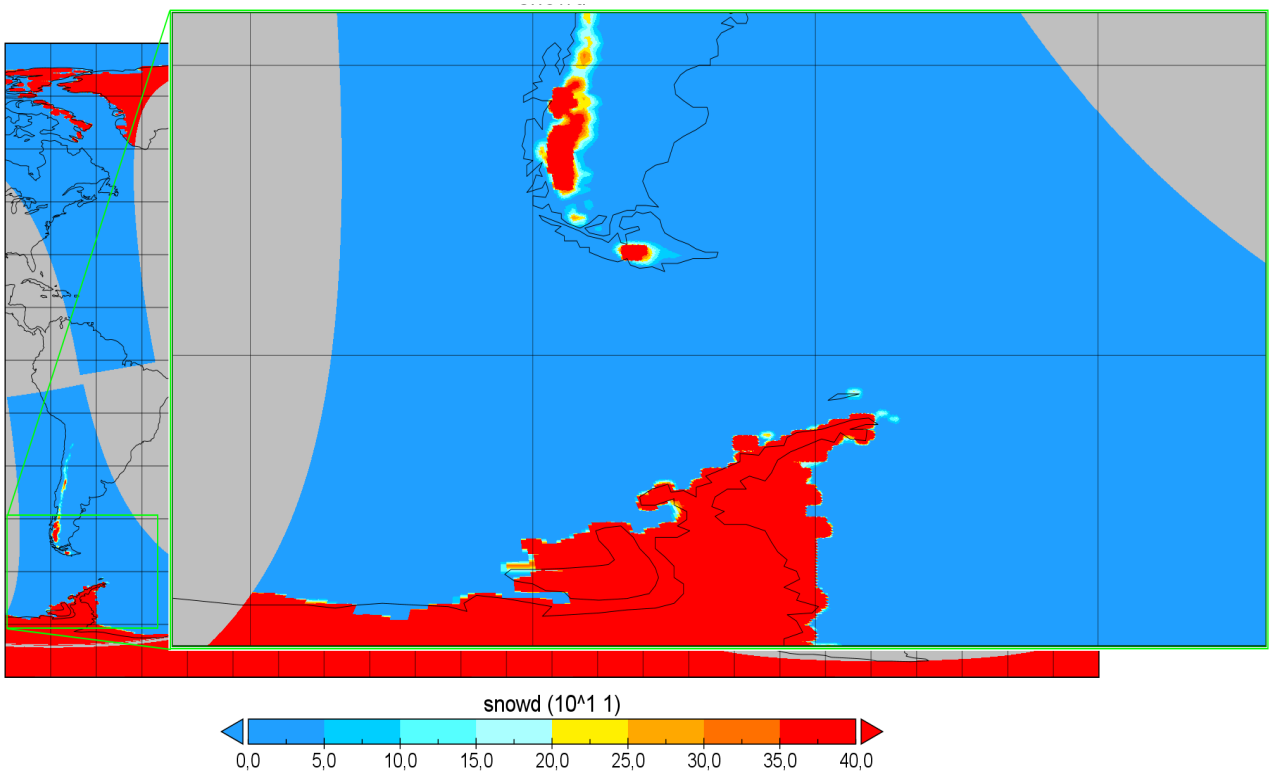

Figure 8: Example of ERA5 snow depth (cm) on GAC orbit grid

2.3.2. OSI SAF sea ice concentration

Sea ice concentration (%) is the areal coverage of sea ice in a certain area of open water, so in this case the areal proportion of a GAC pixel covered by sea ice, ranging between 0-100%. It is provided by the Ocean and Sea Ice Satellite Application Facility (OSI SAF) dataset (Tonboe et al., 2016), and an example is shown in Figure 9. As for the snow depth (Section 2.3.1), sea ice concentration is used to derive the scene type and corresponding NTB, SW ADM and Twilight model.

The OSI SAF products used here are OSI-450 & OSI-430-b. The retrieval is based on microwave sensors, allowing cloud-penetrating detection of sea ice. The spatial resolution is 25x25km.

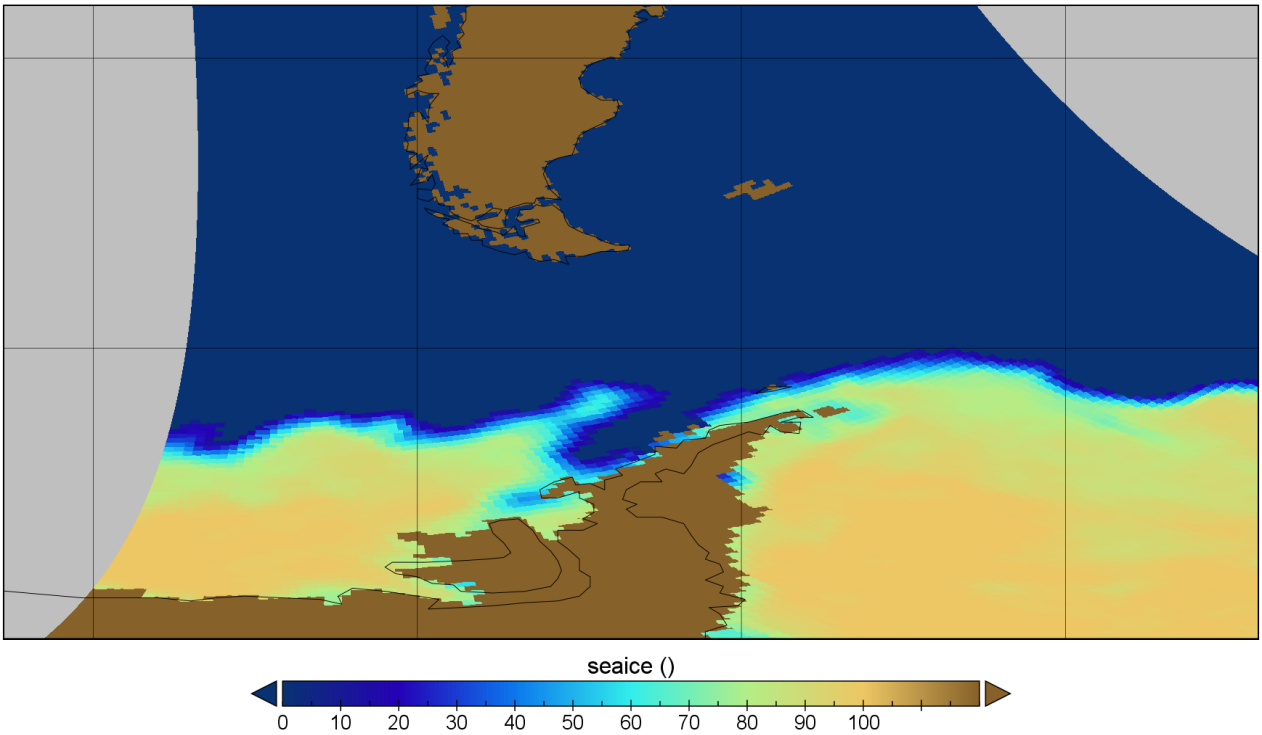

Figure 9: Example of OSI SAF sea ice concentration (%) on GAC orbit grid (dark brown=land).

2.3.3. ERA5 10m wind speed

The main use of ERA5 wind speed (*m/s*) in the TOA flux retrieval is to determine the scene type and corresponding shortwave ADM and albedo model for clear-sky ocean scenes (Table 14). It is a correction for the effects of ocean waves on the specular properties of the water surface.

Once the longitudinal and latitudinal wind speed components (10u, 10v) are converted to an absolute wind speed, it is discretized in some wind speed categories (Table 9). Each category refers to a different scene type and hence ADM and albedo model.

2.3.4. ERA5 surface temperature and integrated water vapor

ERA5 surface temperature (*K*) and column integrated water vapor (kg/m^2) are required in the longwave TOA flux retrieval: they constitute the meteorological predictors in the multivariate regressions that are used for the narrowband-to-OLR conversion (Clerbaux et al., 2020). Examples are shown in Figures 10 and 11, respectively.

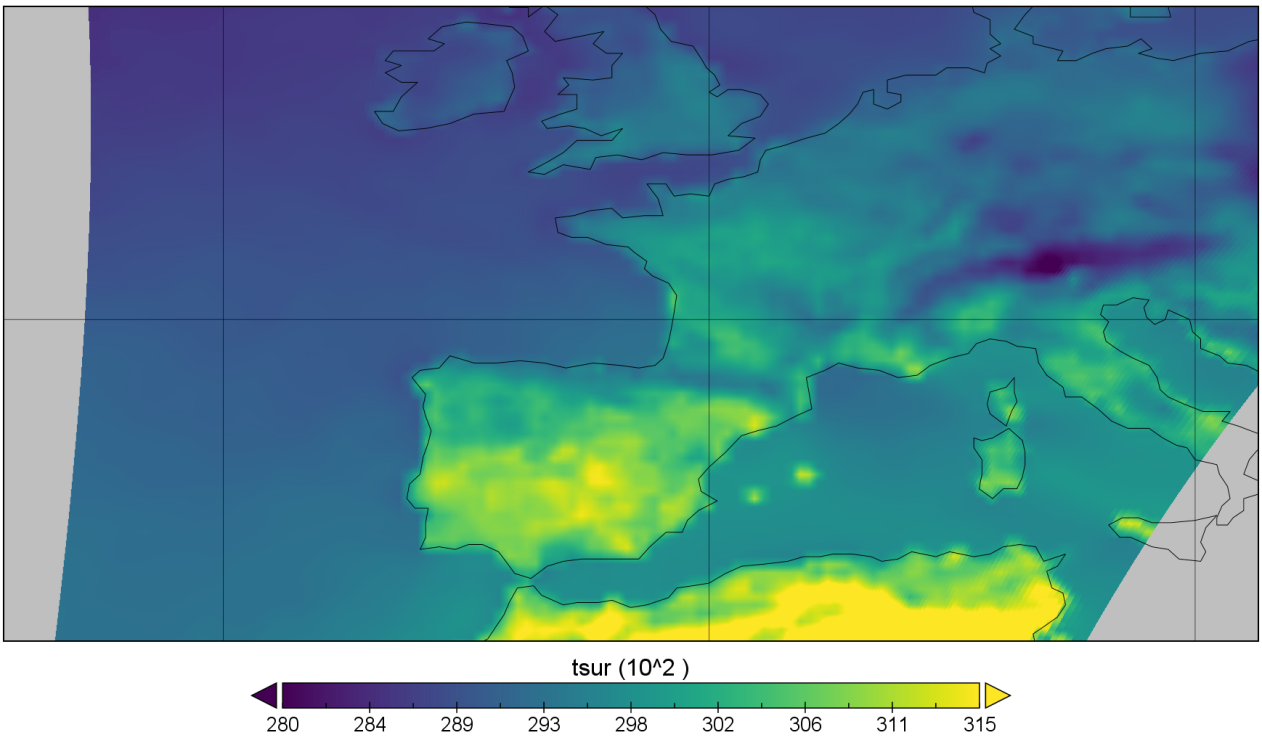

Figure 10: Example of Surface Temperature (K) on GAC orbit grid

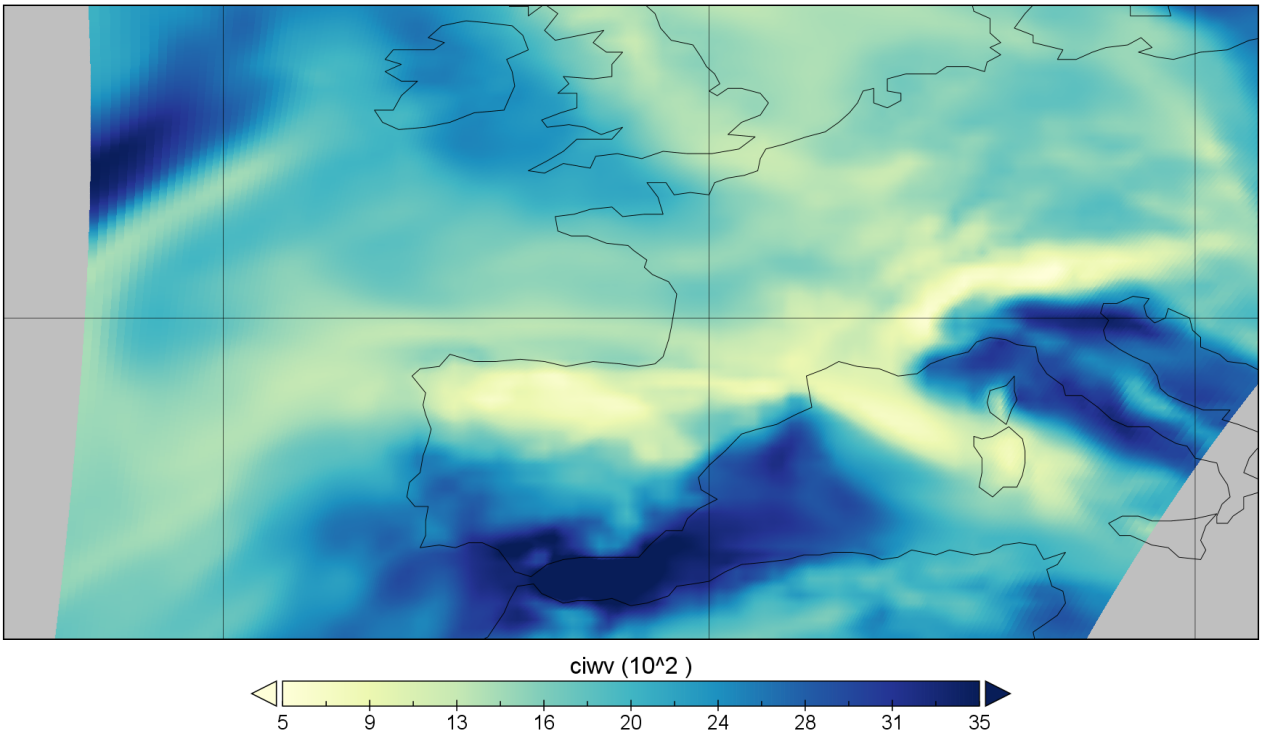

Figure 11: Example of Column Integrated Water Vapour (kg/m²) on GAC orbit grid

2.3.5. USGS-based Land fraction

The variable "land fraction" that is co-delivered with the PPS input data (on the same GAC orbit grid), is a continuous, fractional value derived as a moving average (44x44km moving window) of a binary land-sea mask, which in turn was created by reclassifying the USGS land cover map. In the TOA flux retrieval, it is used to determine whether a water pixel is situated in a "coastal region ~~(land fraction >0.0%), and more specifically whether this coastal water pixel contains mostly "inland water" (ponds, rivers, lakes,..) or mostly "open water" (large lakes, sea, ocean,..)"~~. It is, however, not to be interpreted as the physical sub-pixel areal fraction of non-water to total pixel area. An example is shown in Figure 12: note that the map's color legend is discretized purely for visualization purposes.

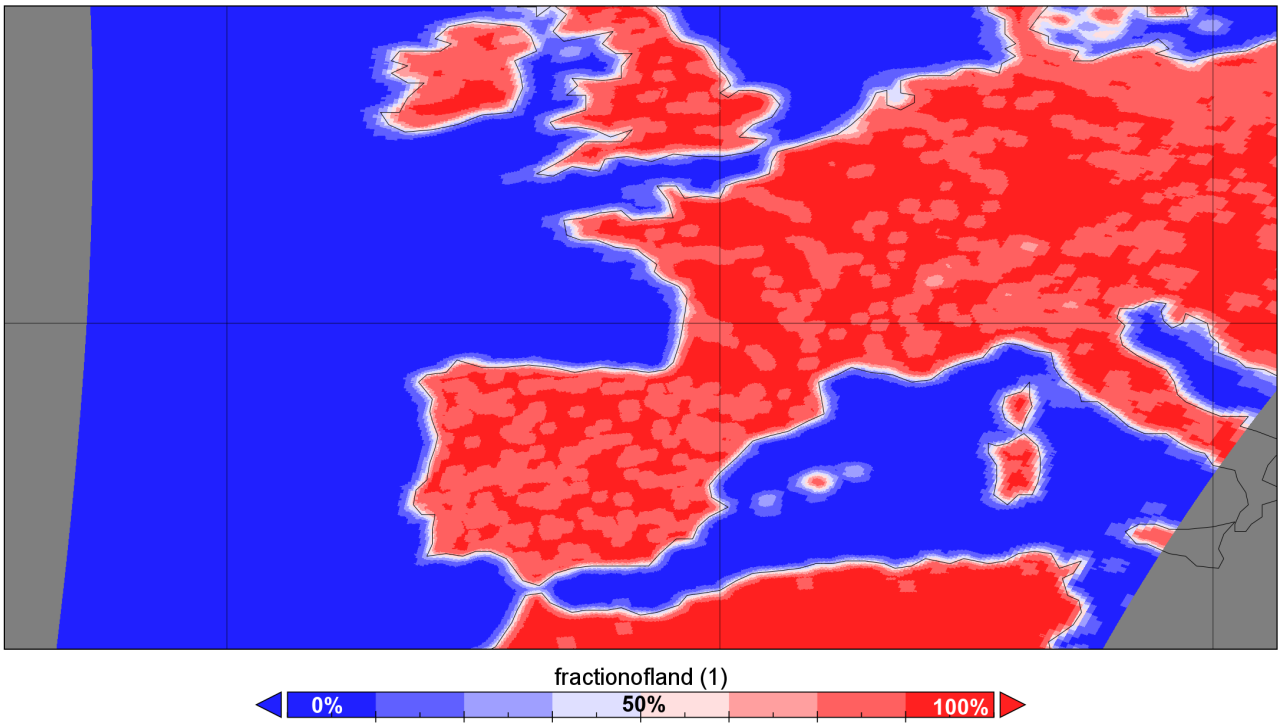

Figure 12: Example of USGS-based Land Fraction (%) on GAC orbit grid

2.4. External input data

These input data are taken from external sources, i.e. other than the FDR and PPS. For the spatially explicit data, this means that they are not provided on the *GAC orbit grid*.

2.4.1. C3S daily Total Solar Irradiance (TSI) time series

The TSI is the total amount of incoming solar radiation, i.e. integrated over all wavelengths, at mean Earth-Sun distance (1 *AU*). A time series of daily TSI (*W/m²*) is provided by the C3S TSI ICDR (v2.3)[4] which is recently developed at RMIB with methods based on Dewitte and Nevens (2016, 2017). It provides an estimate of the daily TSI between 1979-2020, computed as a composite of different space instruments, each with a certain adjustment factor (Table 2). The entire record is visualized in Figure 13. It is used primarily in the shortwave Level-3 processing, where the albedo diurnal cycle is converted to flux.

Table 2: C3S daily TSI time series v2.3: instrument adjustment factors

	Instrument	Adjustment factor
0	ERB (not used)	0.993204
1	ACRIM1	0.996232
2	ERBS (with temporal interpolation)	0.997864
3	ACRIM2	0.998587
4	DIARAD/VIRGO on SOHO	0.997241
5	PMO06/VIRGO on SOHO	0.997609
6	ACRIM3	1.000938
7	TIM on SORCE (aging corrected, ATBD)	1.001216
8	PREMOS	1.001085
9	Sovap	1.000518
10	TIM on TCTE	1.000633
11	TIM on TSIS1	1.000450
12	SATIRE (semi-empirical model)	1.000736

4 *URL: https://gerb.oma.be/tsi/C3S_RMIB_daily_TSI_composite_ICDR_v2.3.txt*

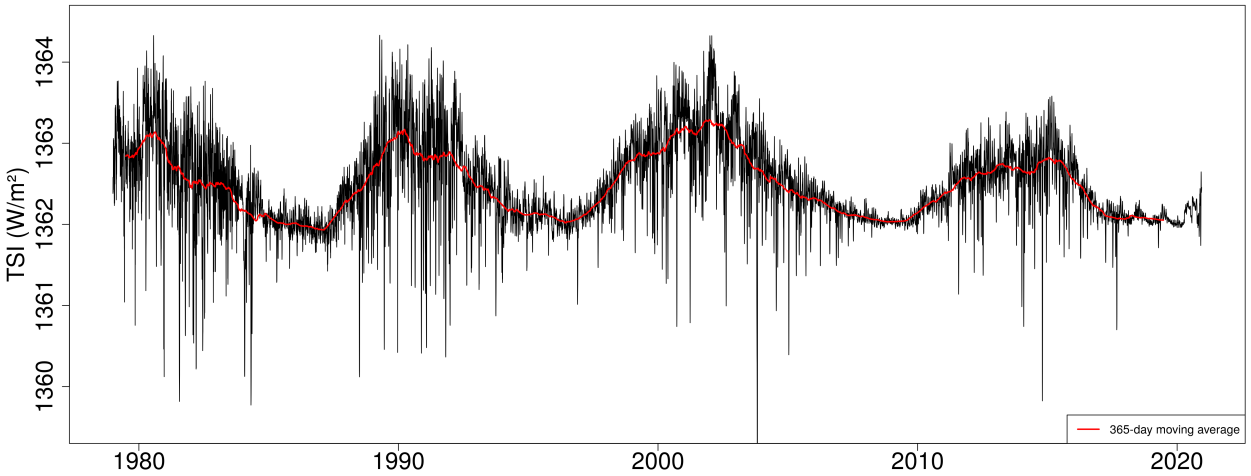

Figure 13: C3S daily Total Solar Irradiance (TSI) timeseries v2.3

2.4.2. Land cover data (IGBP)

Global Land Cover Characterization (GLCC)[5] is a series of global land cover classification datasets that are based primarily on the unsupervised classification of 1-km AVHRR 10-day NDVI (Normalized Difference Vegetation Index) composites. The AVHRR source imagery dates from April 1992 through March 1993. There are many possible land cover classifications that can be applied on the GLCC base dataset, the International Geosphere Biosphere Program (IGBP) Land Cover Classification being one of these (Loveland et al., 2000; Townshend, 1994). The GLCC with IGBP classification is used as static land cover dataset for this CDR, featuring 18 distinct classes (Figure 14). The raw data image has 43200 columns and 21600 lines, which corresponds to a spatial resolution of 30 arc-second per pixel in latitude and longitude.

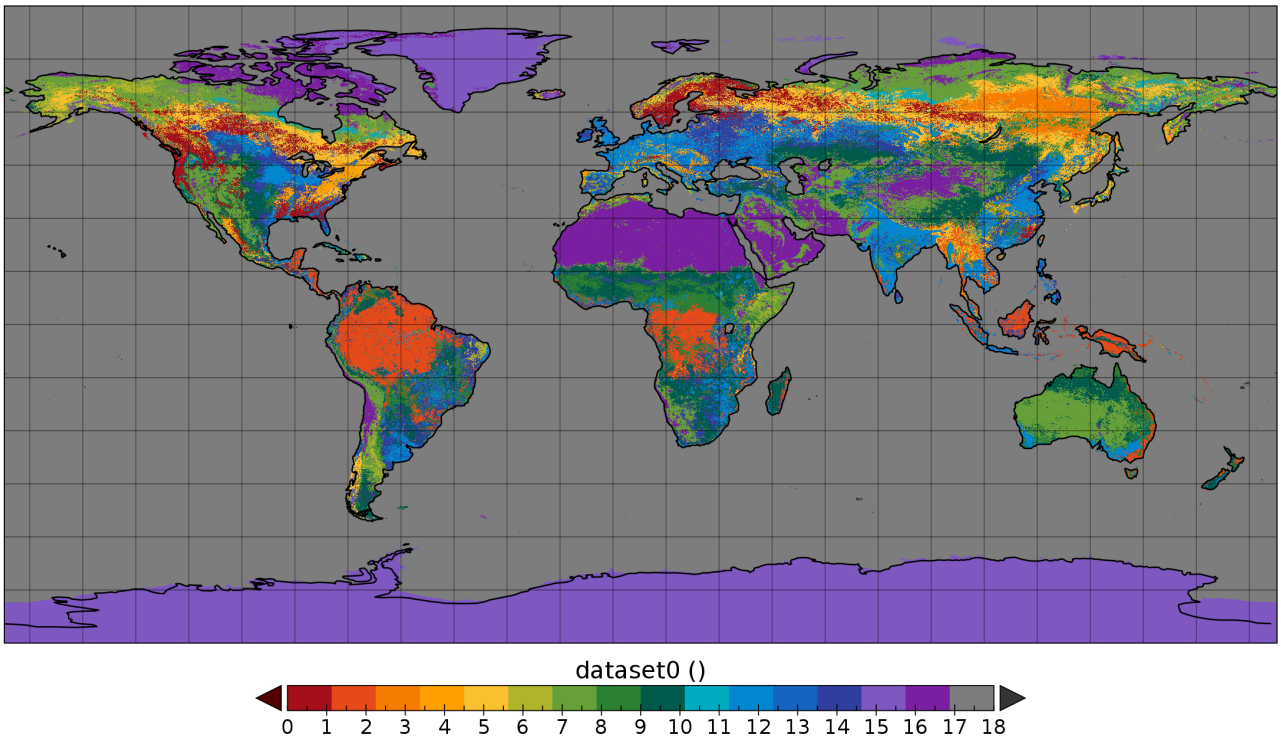

Figure 14: IGBP land cover map (high-res.)

Some significant land masses, however, are not included in this dataset (most notably islands, e.g. Hawaii, Fiji,..) and are designated with IGBP class "100" (=invalid, dark grey). An example is shown in Figure 15.

5 *URL: https://www.usgs.gov/centers/eros/science/usgs-eros-archive-land-cover-products-global-land-cover-characterization-glcc?qt-science_center_objects=0#qt-science_center_objects*

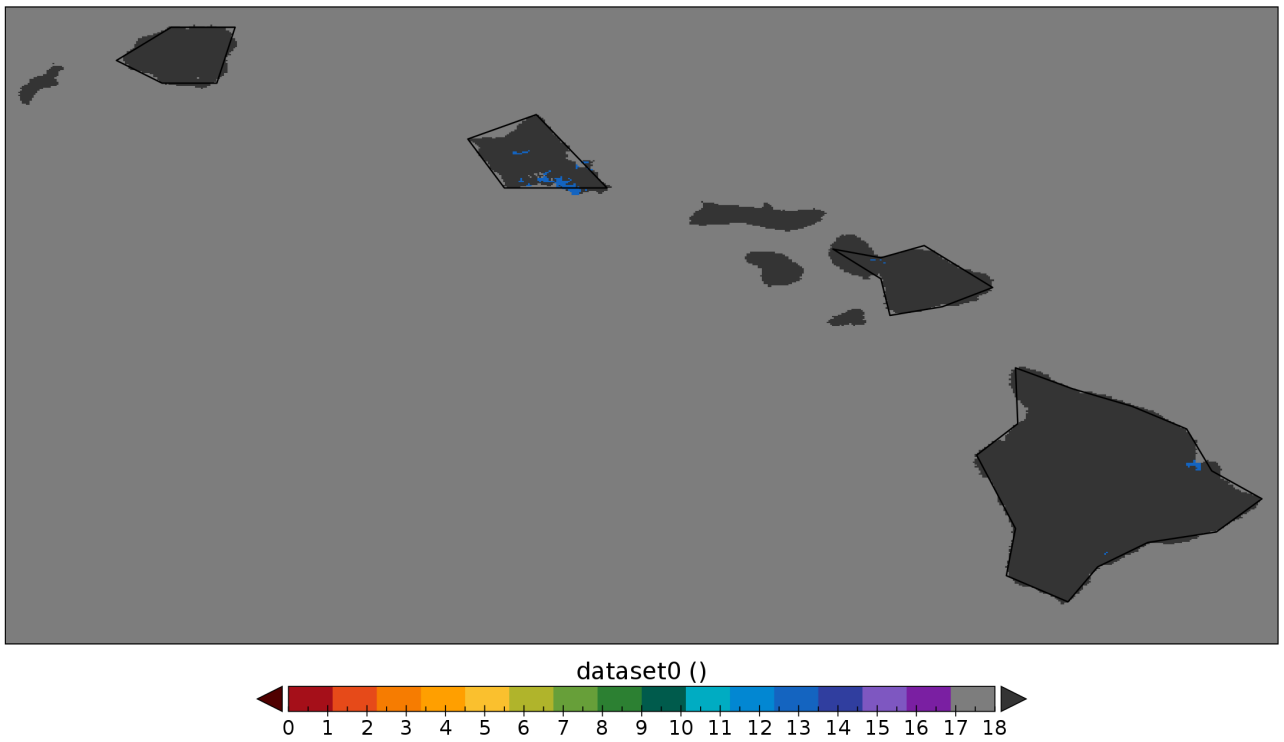

Figure 15: IGBP land cover map (high-res.), zooming in on the Hawaiian Islands

A work-around solution is to use a lower-resolution version (10-minute instead of 30 arc-second) land-only IGBP map, in which all water, snow and ice pixels are replaced by the nearest land-only land cover type. The resulting global map is shown in Figure 16, and a zoom-in on the Hawaiian islands is shown in Figure 17: now, none of the land pixels have an invalid land use anymore.

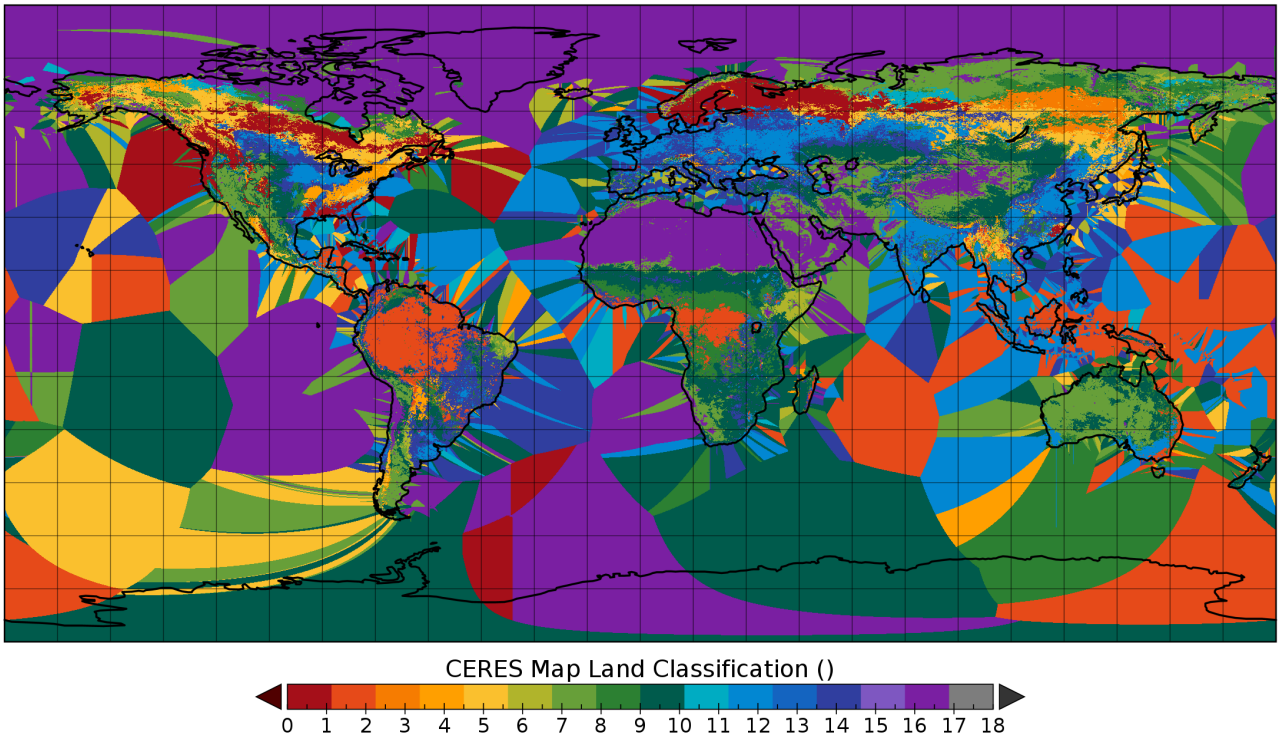

Figure 16: IGBP land cover map (low-res.) with land extrapolated to sea and ice areas

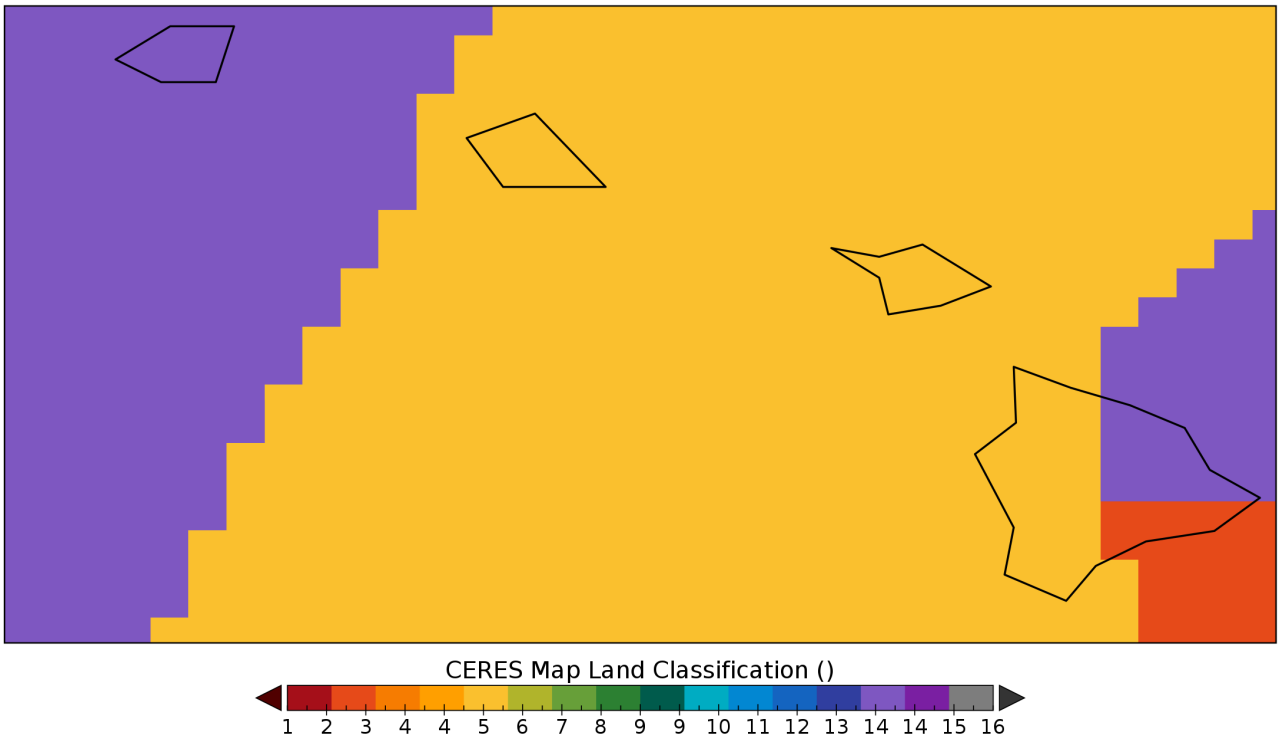

Figure 17: IGBP land cover map (low-res.), extrapolated, zooming in on Hawaiian Islands

In the first place, the IGBP land cover map serves as a land-water mask. Furthermore, it is used to remap the land cover according to three kinds of surface types (Tables 8 and 7):

- 8 CERES surface types: used to select ADM and albedo model
- 15 NTB surface types: used to select Narrowband-to-Broadband regression (parameters)
- 4 TWL surface types: used to select the Twilight model regression (parameters)

2.4.3. CERES low-resolution land cover map

The IGBP map does not provide a good discrimination between dark and bright deserts. For that purpose, an additional classification is required and used, which is based on a low-resolution land cover map from CERES (N.Loeb, *pers. comm.*). The map's spatial dimensions are 2160x1080 pixels, corresponding to a spatial resolution of 10 arc minutes. The map is shown in Figure 18, demonstrating the different sub-classification of desert areas: for instance the Sahara, Saudi, and Iranian deserts clearly have a different sub-classification compared to the IGBP map (Figure 14). Note that only classes "4" (dark desert) and "5" (bright desert) from this map are used, and only as a correction in case the (much more detailed) IGBP map prescribes one of the desert classes.

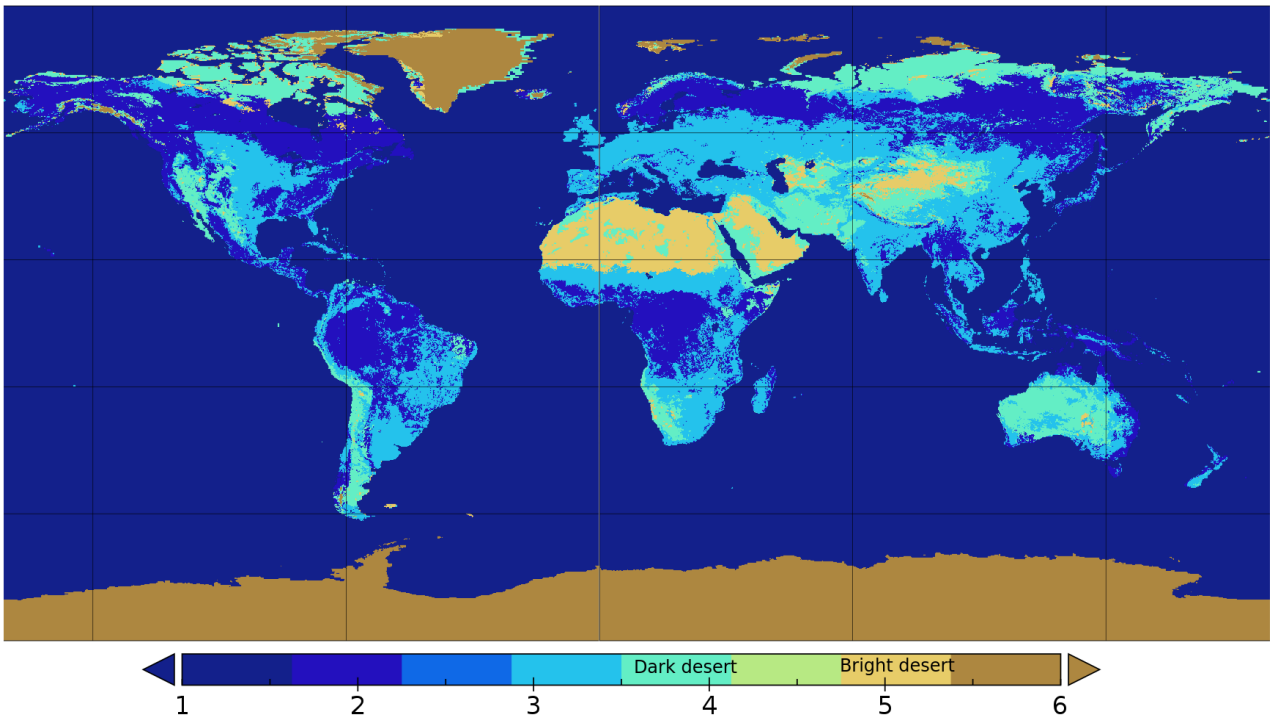

Figure 18: Low-resolution CERES land cover map

2.4.4. Hourly ERA5 Outgoing Longwave Radiation and Cloud cover

Hourly ERA5 outgoing longwave radiation and cloud cover are requested through the ECMWF Meteorological Archival and Retrieval System (MARS)[6], which also remaps the data on a regular lat-lon grid of 0.25°x0.25° resolution. The downloaded files are post-processed (more details in Annex 9.7), so that each UTC day is represented by a separate Netcdf file (global grid with 1440x720 grid boxes) containing a temporal range between previous day 11h UTC (instant.) until next day 13h UTC (instant.). Since the temporal dimension contains **hourly cumulated** values, it corresponds to 50 time slices.

These ERA5 data are used to model the longwave TOA flux diurnal cycle during clear-sky conditions over land. As an example, the extracted OLR for a certain grid point (21.5°N, 16.5°E) for UTC day "1 July 1979" is given in Figure 19. It concerns a clear-sky pixel over desert characterized by a pronounced diurnal cycle of OLR. Note that the x-axis indications are denoted as instantaneous times, but in fact refer to the hourly cumulation prior to the indicated time.

6 *URL: https://www.ecmwf.int/en/forecasts/datasets/archive-datasets*

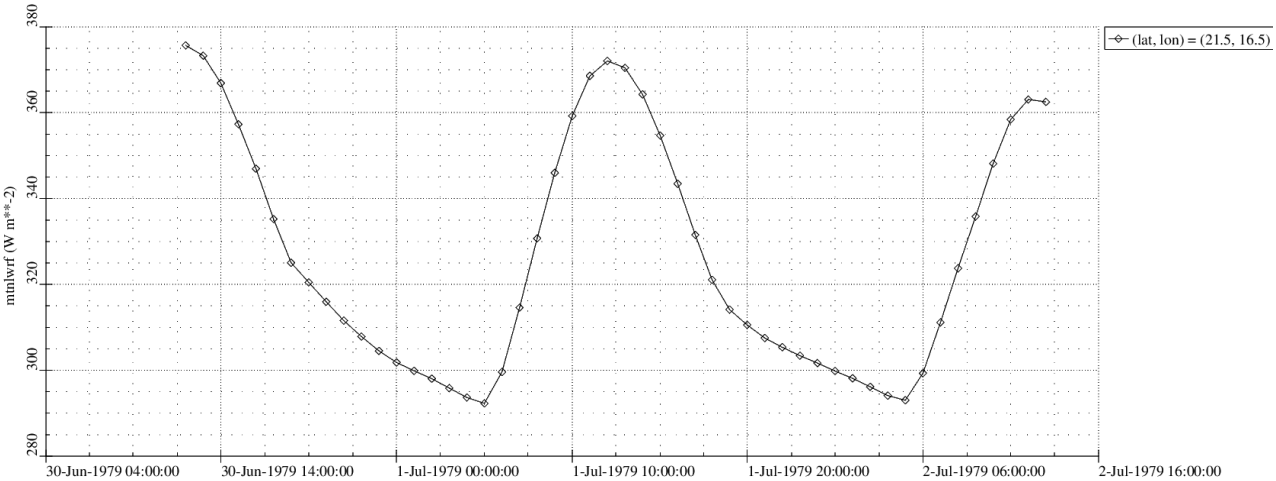

Figure 19: Example of ERA5 OLR daily input data for a single grid point.

Besides OLR, the same Netcdf file also contains ERA5 cloud cover, because the ERA5 OLR diurnal cycle is only used on **land** pixels during **clear-sky** conditions, which is determined by looking at the AVHRR input data (PPS cloudmask) as well as the ERA5 cloud cover: if both are below a certain threshold (10%), the ERA5 data is effectively used in the interpolation process. As an example, Figure 20 shows the corresponding cloud cover (as a fraction 0-1) for the same day and grid box, demonstrating clear-sky conditions during the full day.

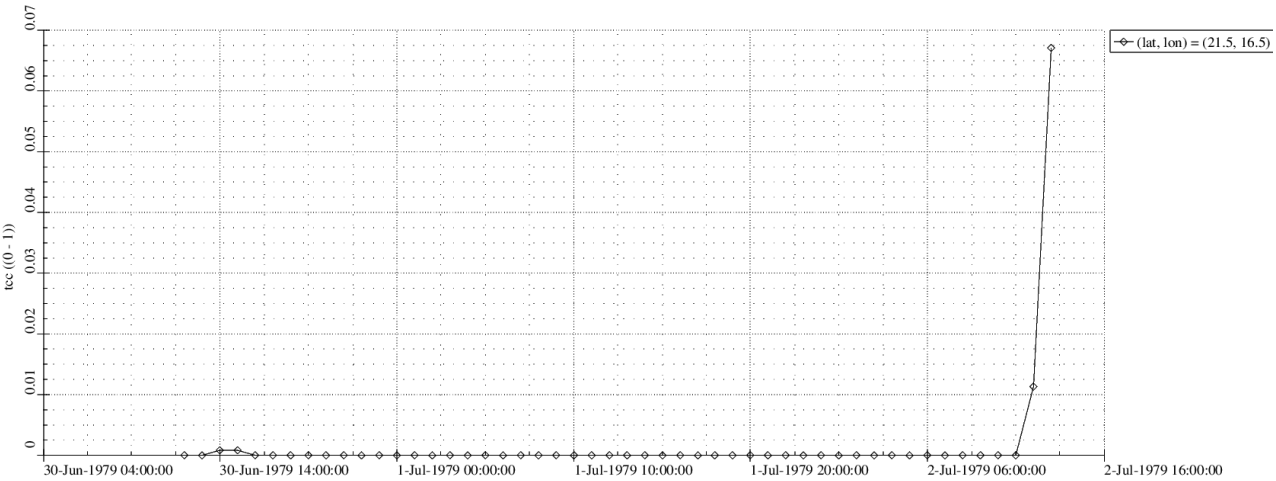

Figure 20: Example of ERA5 Cloud Cover daily input data for single grid point.

2.4.5. Climatology of CERES cloud optical thickness

Cloud optical thickness is required in the TOA flux retrieval to determine the scene type and corresponding shortwave ADM and albedo model; however, the observed PPS-CPP cloud optical thickness is only used when the quality flag indicates “good quality” (Section 2.2.2.a). Otherwise, the observed COT is replaced by a longterm-average annual cycle of COT from CERES: the data consists of 12 multi-year monthly means, each in a separate Netcdf file, that are calculated from all currently available years (2000-2020) on a global 1°x1° grid. The source of the data are the CERES EBAF-TOA Ed4.1 files[7] that contain, among other variables, also the cloud optical thickness. As an example, two of these multi-year monthly means are shown in Figures 21 (January) and 22 (July). The temporal dimension is demonstrated in Figure 23, where 12 multi-year monthly means are plotted for a single grid box (12.5°N, 21.5°E). It should be noted that this method is strictly meant to provide a realistic order of magnitude for COT on a given time and place; its bias is assumed to be smaller compared to the hypothetical bias due to a ‘bad quality’ COT observation.

7 *URL: https://ceres.larc.nasa.gov/data/*

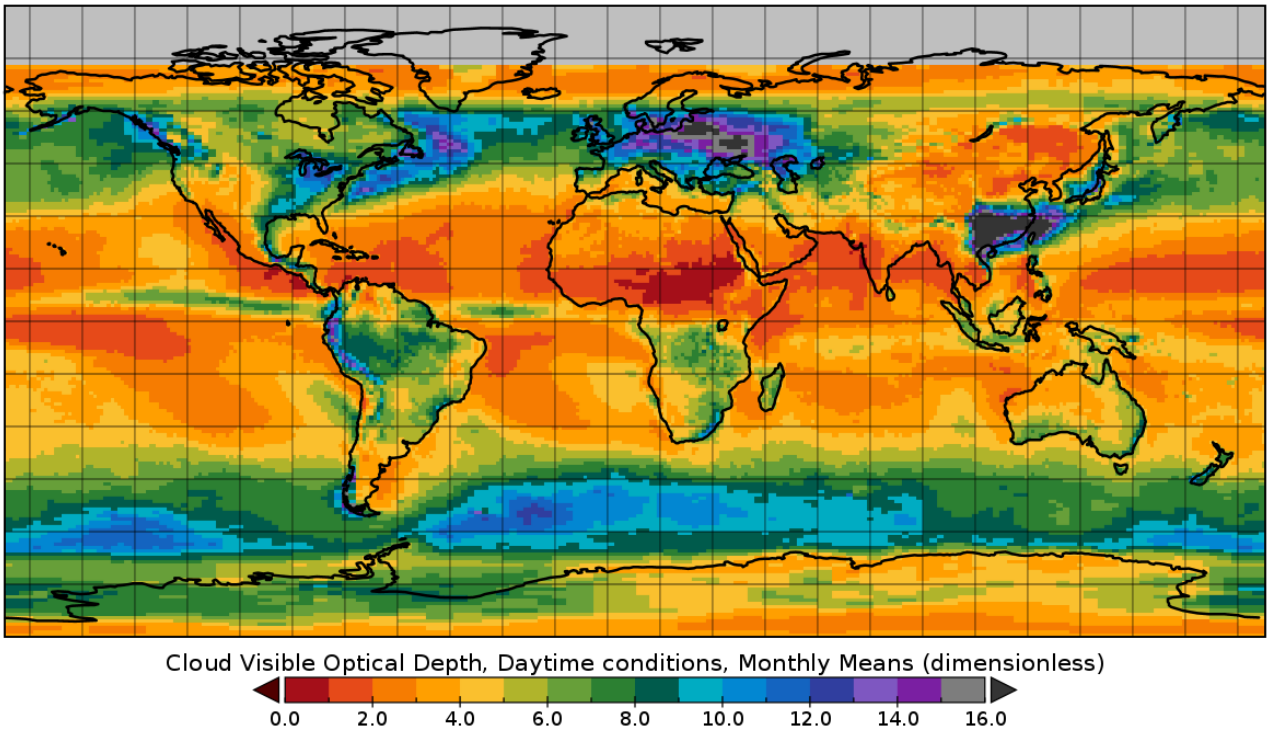

Figure 21: Global multi-year monthly mean Cloud Optical Thickness for January (2000-2020).

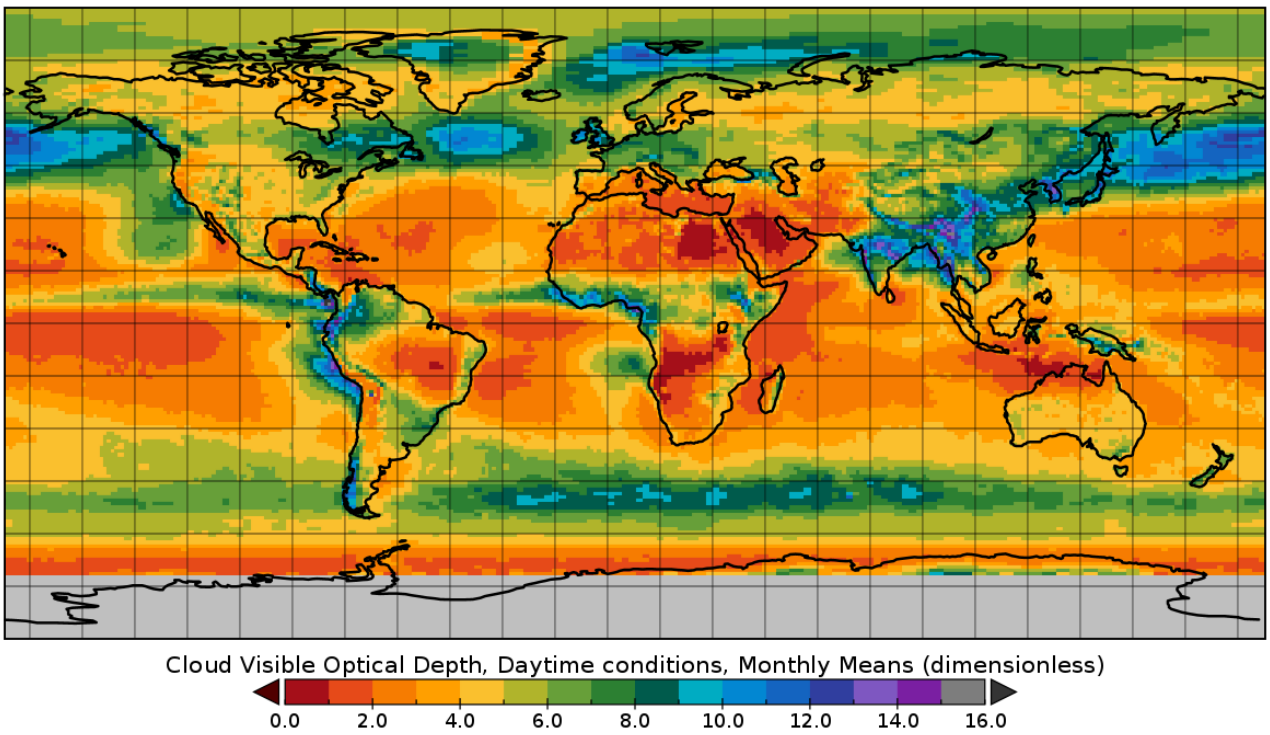

Figure 22: Global multi-year monthly mean Cloud Optical Thickness for July (2000-2020).

One pixel (12.5°N, 21.5°E) is shown in Figure 23 as example.

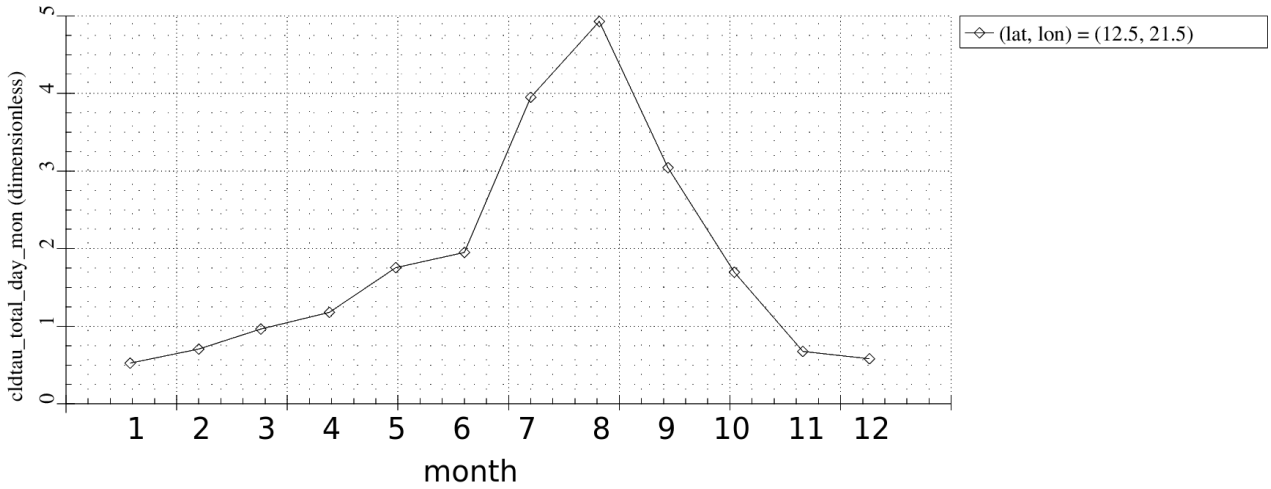

Figure 23: Multi-year annual cycle of Cloud Optical Thickness (2000-2020) for single grid point.

2.4.6. CERES Shortwave Angular Distribution Models (ADMs) and albedo models

The CERES TRMM Shortwave Ed.2B ADMs[8] (Loeb et al., 2003) are derived from 8 months of observations of the Clouds and Earth's Radiant Energy System (CERES) (Wielicki et al., 1996) instrument in Rotating Azimuth Plane Scan (RAPS) mode on board the Tropical Rainfall Measurement Mission (TRMM) satellite. The scene type information is inferred from the Visible and InfraRed Scanner (VIRS) imager on the same platform. Since the TRMM satellite was flying on a sun precessing orbit, these models span the entire SZA range, from the terminator (SZA≈90°) to the nadir illumination. This makes the TRMM orbit well suited to generate ADMs. On the other hand, as the inclination of the TRMM orbit was only 35° above the Equatorial plane, the mid- and high-latitude regions have not been sampled, which means that snow and ice scene types are not taken into account. The scene type classification is based on surface type, cloud cover, cloud phase, and cloud optical thickness. In theory, 590 CERES TRMM SW scene types and corresponding ADMs are available (Annex 9.1, Table 14). In practice, however, only the 'pure' clear-sky and overcast (i.e. cloud cover of 100%) scene types are used in both sets of ADMs.

The CERES Terra Shortwave Ed.2B ADMs[9] (Loeb et al., 2005) are used to complement the CERES TRMM SW ADMs. Indeed, the polar orbiting Terra satellite allowed the creation of dedicated models for permanent snow/ice, fresh snow, and sea ice. The scene type classification is based on surface type, cloud cover, visible sea ice concentration (i.e. 0% when cloud cover is 100%), visible snow cover, visible fresh snow cover, and cloud optical thickness. In theory, 59 CERES Terra SW scene types and corresponding ADMs are available (Annex 9.1, Table 15). In practice, however, only the 'pure' clear-sky and overcast scene types are used in both sets of ADMs.

Each of the 649 above mentioned CERES scene types (and corresponding ADMs) has a corresponding text file containing a pseudo[10] 3D matrix with as dimensions Solar Zenith Angle (SZA), Viewing Zenith Angle (VZA) and Relative Azimuth Angle (RAA) 'angular bins'. Every combination of those 3 angles can be identified in this 3D matrix, leading to the identification of the correct '3D bin' containing the corresponding anisotropic factor (or radiance, depending on which version of the ADMs we are working with). In short, depending on scene type and viewing/illumination geometry (3 angles), the correct anisotropy is determined, which is then used to convert a directional quantity (reflectance) into a hemispherical quantity (flux). This is an essential part of the Level-2 processing.

The above mentioned CERES ADMs also contain for each scene type a so-called "albedo model", describing the variation of average albedo with solar zenith angle, which is produced by hemispherically integrating the radiance field from all viewing zenith and relative azimuth angles. These albedo models are available for the same 649 scene types (from which in practice only the pure clear-sky and pure overcast are used). As an example, the albedo models for scene types "ocean with 100% cloud cover, liquid cloud phase" are shown in Figure 24, in which the different curves represent the variation in cloud optical thickness (COT), each corresponding to a different scene type, cfr. the scene type numbers ranging from low COT (nr.169) to high COT (nr.182). These albedo models are used in two different ways :

8 *URL: https://ceres.larc.nasa.gov/data/angular-distribution-models/#cerestrmm-ssf-edition2b-adms*
9 *URL: https://ceres.larc.nasa.gov/data/angular-distribution-models/#ceresterra-ssf-edition2b-adms*
10 *In reality it's a structured ASCII file with consecutive 2D tables that are read in an automated way.*

- In the Level-2 processing: to model the theoretical TOA albedo in sunglint conditions, i.e. when the observed reflectance is not useful. In that case, a 'surrogate albedo' is estimated from these albedo models by simply looking at the SZA.
- In the Level-3 processing: to model the theoretical TOA albedo variation between the different observations, i.e. as a 'smart' temporal interpolation method.

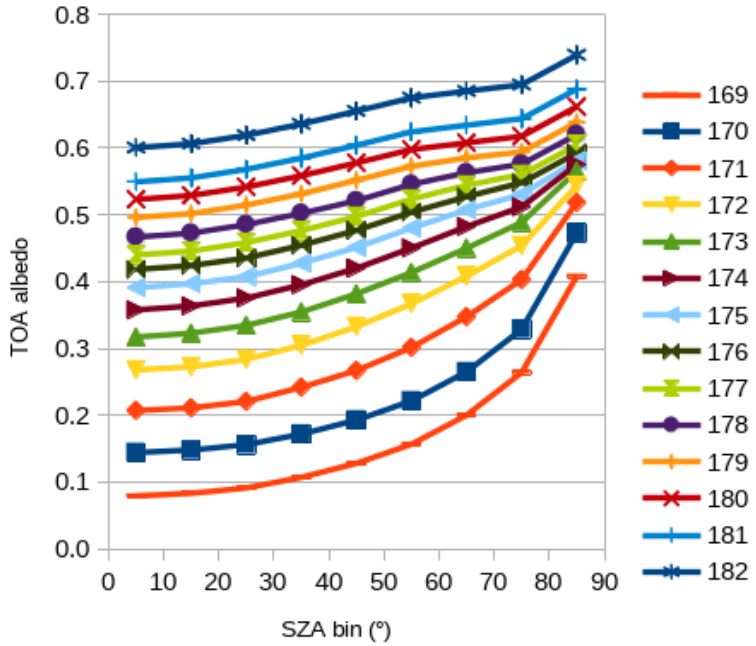

Figure 24: CERES TRMM SW albedo models for liquid-phase overcast ocean scene types.

Finally, the CERES Terra/Aqua Shortwave Ed.4 ADMs[11] (Su et al., 2015) are used in an experimental way for the scene type "overcast sea-ice". This particular scene type experiences problematic underestimations in daily and monthly RSF, which could be solved partially by upgrading the ADM to Ed.4. However, for the current version of the CLARA TOA flux product, it is not yet possible to implement the Edition 4 ADMs for all other scene types, because this newer generation ADMs requires much more input parameters given the more sophisticated scene types subdivisions. For instance, it requires a climate data record with Aerosol Optical Depth (AOD), and spatially and temporally explicit maps of Sea Ice Brightness Index (SIBI).

2.4.7. Twilight coefficients

For twilight conditions, the RSF is not taken from the AVHRR measurements but derived with a simple twilight model, in which the flux linearly depends on solar zenith angle. A regression model mimics the average flux-SZA relation in the CERES-SSF ~~observations~~TOA shortwave fluxes (in W/m²) with SZA ranging between 84°-86.5° for (parts of) years 2004, 2005, 2007, 2008, 2011, 2012. This is done for five different Twilight (TWL) surface types for both clear-sky and overcast conditions (so in total for 10 TWL scene types). The sample size (n) for each scene type is given in Table 3.

The linear regressions are shown in Figures 25 for clear-sky conditions (left) and overcast conditions (right): the solid lines represent the observations as SZA bin averages, demonstrating the linear nature of the flux-SZA relation, and its scene type dependency. From these observations, linear regressions were derived to allow a prediction of the flux for SZA higher than 86.5° (dotted lines). The intercept (A) and slope (B) of these regressions are called "twilight coefficients" and are listed for each of the 10 scene types in Table 3.

Table 3: Twilight model: scene type dependent sample size (n) and regression coefficients (A_c and B_c)

Cloud class	clearsky			overcast		
TWL Surface type	n	A_c	B_c	n	A_c	B_c
0 – water	34283	471.3169	-5.1139	4969304	1161.9394	-12.8346
1 – sea ice 100%	141835	1157.7694	-12.7842	375797	1237.6866	-13.6276

11 *URL: https://ceres.larc.nasa.gov/data/angular-distribution-models/#ceres-terraaqua-edition4-adms*

2 – perm.snow/ice	1626464	1330.8585	-14.6993	1879264	1418.4353	-15.7043
3 – fresh snow	86142	772.4400	-8.4760	652909	1238.9038	-13.6707
4 – land	7902	501.5476	-5.5098	102852	1155.6513	-12.7385
all surface types	*2160154*	***1239.9711***	***-13.6827***	*10981948*	***1213.5238***	***-13.3916***

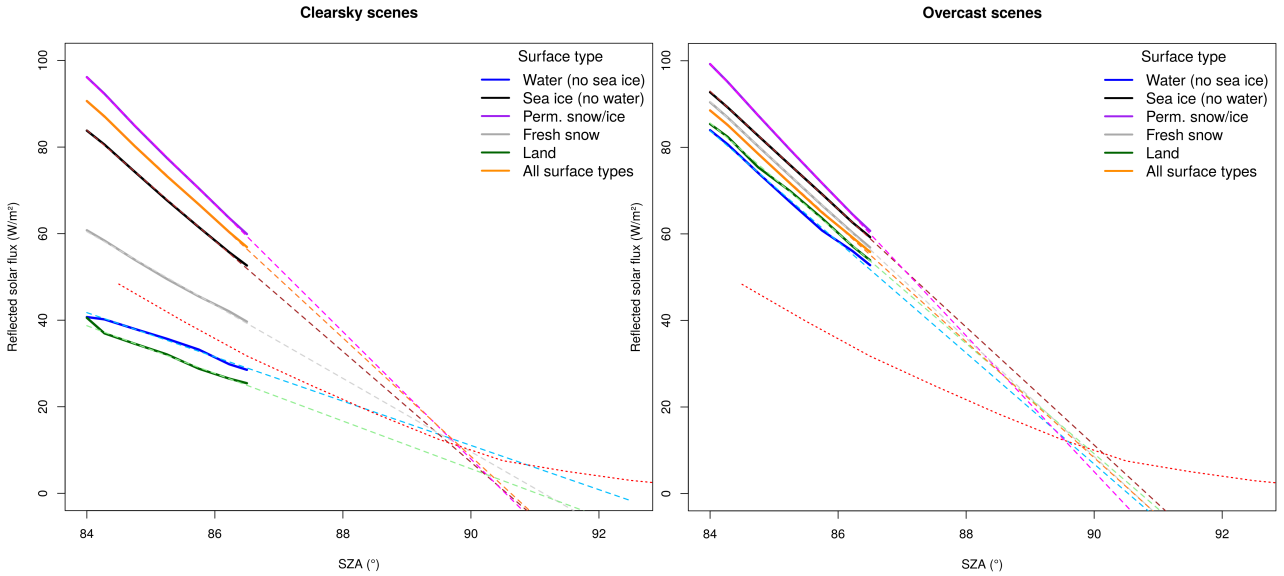

Figure 25: Twilight model with SZA-dependent solar flux for clearsky (left) and overcast (right) conditions; The red dotted lines are taken from Kato and Loeb, 2003.

2.4.8. Narrowband-to-broadband coefficients (shortwave)

Conversion of narrowband to broadband (NTB) reflectance was done empirically by creating multivariate linear regressions on *matched* (i.e. collocated, coangular, and simultaneous) AVHRR-CERES observations. The method is explained in detail by Akkermans and Clerbaux, 2020. The spatial resolution of AVHRR and CERES is respectively about 4km and 32 km at nadir, which requires a considerable spatial aggregation of AVHRR footprints to match a single CERES footprint. Achieving a sufficient matching sample size is only possible when the orbital planes of both CERES- and AVHRR-carrying satellites coincide, which limits the amount of useful data to these favorable periods (Figure 26).

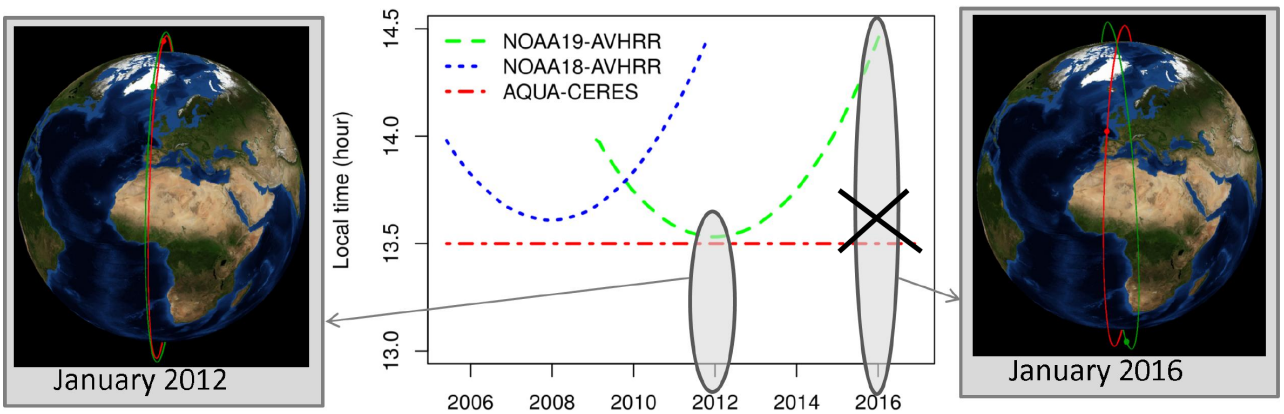

Figure 26: AVHRR- and CERES-carrying satellites' orbital plane matching

The main objective of Akkermans and Clerbaux (2020) was to derive regressions with high scene-specific accuracy, which is possible by narrowing down each scene type to a very homogeneous sample. However, there is a trade-off between the regression-specific theoretical accuracy (=internal), and the practical accuracy of the regressions when applied on the entire range of possible scene types (global result), including non-homogeneous and imperfect scenes.

Therefore, it was decided to slightly modify the regressions from Akkermans and Clerbaux (2020) by loosening the cloud cover range, thereby redefining the "clearsky" and "overcast" regressions:

- "clearsky": now defined as cloud cover from 0-10% (instead of strictly 0%)
- "overcast": now defined as cloud cover 90-100% (instead of strictly 100%)

Note that the cloud cover thresholds are imposed on both AVHRR and CERES cloud masks, e.g. for clear-sky *pixel matches* that means that both cloud masks should have cloud cover below 10%.

Furthermore, some small bug fixes in the code were found and solved. Together, the above mentioned adaptations result in updated coefficients, listed in Table 4, which is an update w.r.t. Table 3 in Akkermans and Clerbaux, 2020. ~~These coefficients should be used in the linear regression's equation (Eq. Error: Reference source not found).~~

	Clear-Sky (0-10%)					Overcast (90-100%)					All-Sky				
Surface Type	b_0	b_1	b_2	b_3	b_4	b_0	b_1	b_2	b_3	b_4	b_0	b_1	b_2	b_3	b_4
Ocean	1.811	1.148	-0.523	-0.043	0.390	4.013	0.313	0.447	0.709	1.286	2.938	0.334	0.447	0.719	1.115
Forests	1.471	0.480	0.377	1.358	1.211	3.622	0.366	0.395	0.905	1.542	2.571	0.410	0.371	0.921	1.643
Savannas	1.421	0.463	0.382	2.696	0.769	3.328	0.403	0.355	4.127	1.059	2.405	0.418	0.369	2.281	0.692
Grass/crop	2.575	0.443	0.339	1.101	1.430	3.704	0.393	0.368	1.093	1.893	2.836	0.431	0.348	0.860	1.792
Dark deserts	2.384	0.367	0.376	1.279	0.724	3.031	0.291	0.473	1.377	1.597	1.687	0.432	0.356	1.556	1.141
Bright deserts	3.225	0.365	0.335	1.467	1.291	1.305	0.462	0.317	2.648	1.419	1.594	0.553	0.207	2.490	1.523
Perm. snow/ice	7.511	0.202	0.479	-0.507	1.612	15.075	0.164	0.463	-1.231	6.254	20.261	0.078	0.467	-1.710	4.591
Fresh snow	1.598	0.310	0.412	1.627	3.213	2.487	0.334	0.430	1.223	3.272	1.637	0.306	0.450	1.148	3.399
Sea ice 100%	7.214	0.212	0.460	-0.163	4.139	8.590	0.270	0.423	0.029	4.896	21.573	0.180	0.324	-2.213	6.545
Sea ice 95-99%	8.486	0.220	0.437	-0.424	3.847	9.553	0.238	0.449	-0.266	4.424	12.541	0.281	0.343	-0.837	5.594
Sea ice 90-95%	6.376	0.253	0.430	-0.209	3.320	10.353	0.214	0.466	-0.466	4.176	10.396	0.174	0.503	-1.121	4.649
Sea ice 80-90%	3.619	0.345	0.367	0.191	2.635	9.456	0.207	0.484	-0.218	3.879	9.563	0.074	0.627	-0.793	4.032
Sea ice 60-80%	2.922	0.410	0.296	0.562	2.734	6.188	0.275	0.455	0.455	3.148	4.928	0.214	0.541	0.329	3.011
Sea ice 10-60%	2.540	0.458	0.227	0.492	4.172	4.259	0.290	0.472	0.444	2.518	3.264	0.265	0.516	0.417	2.551
Sea ice 0-10%	1.868	0.806	-0.121	0.382	2.267	4.195	0.326	0.436	0.392	2.839	3.167	0.348	0.432	0.499	2.839
(generic*)	2.485	0.336	0.384	1.232	1.929	3.846	0.362	0.394	0.932	2.449	2.963	0.390	0.363	0.887	2.810

b_0, b_1, b_2, b_3, b_4 : coefficients in Equation (2)
(*) surface-type-independent regression, that combines all matched NTB pairs (regardless the surface type)

Table 4: NTB (Narrowband-to-Broadband) regression coefficients, here using 100% of the matched NTB pairs with strict matching criteria (update of Table 3 in Akkermans and Clerbaux, 2020)

These coefficients should be used in the linear regression's equation (Eq. 1):

$$\rho_{SW} = b_0 + b_1 \cdot \rho_{0.6} + b_2 \cdot \rho_{0.8} + b_3 \cdot \ln\left(\frac{1}{\cos(\theta_0)}\right) + b_4 \cdot \ln\left(\frac{1}{\cos(\theta)}\right) \quad (1)$$

Overall, the updates are relatively small and did not affect the main analyses, results and conclusions of Akkermans and Clerbaux (2020). A complete overview of all updates of tables and figures w.r.t. Akkermans and Clerbaux (2020) is given in Annex 9.3.

Akkermans and Clerbaux (2020) constructed NTB regressions for three cloud classes: clear-sky, overcast and all-sky. Both calibration and validation were done at the relatively large CERES pixel scale (assumed footprint diameter of 32km at nadir):

- the "clear-sky" regression was calibrated by only considering CERES-AVHRR *pixel matches* in which both CERES cloud cover and aggregated AVHRR cloud cover were cloud-free. The same was done for the "overcast" category, but then with overcast footprint.
- For validation, the regressions were applied on the aggregated narrowband reflectances from AVHRR, i.e. **after** pixel aggregation. This validation method is sufficient for areas with relatively homogeneous cloud cover.

However, situations with mixed fields of "broken clouds" (patchwork of alternating clearsky and overcast AVHRR pixels) require a different validation approach, in which the regressions are applied on each individual AVHRR pixel, **before** pixel aggregation. This alternative validation is discussed and the results are shown in Annex 9.4, concluding that the NTB regressions are also performing well in these situations.

2.4.9. Narrowband-to-OLR coefficients (longwave)

Conversion of narrowband directional *brightness temperature* to broadband hemispherical *Outgoing Longwave Radiation (OLR)* is done empirically by creating multivariate linear regressions on *matched* (i.e. collocated, coangular, and simultaneous) AVHRR-CERES observations; the same matching database, as used for the shortwave NTB regressions (Figure 26; Akkermans and Clerbaux, 2020), is used for the longwave regressions. The regression's calibration and validation is documented in detail by Clerbaux et al. (2020). The absence of differentiation to cloud cover (and scene types in general) is a major difference with the SW processing. The main motivation for not using the cloud products for OLR estimation is the need to also process twilight and night time conditions. Although cloud detection is working during night time, this is not the main element affecting the OLR, which is mainly dependent on cloud top temperature and cloud transparency (high semi-transparent cirrus clouds have quite strong anisotropy in the longwave). This information is implicitly available through channel 4 (cloud top temperature) and the difference of T_B between channel 4 and 5 (indicator of cirrus clouds).

The quantities ***F*** (Flux in *W/m²*), $\boldsymbol{T_{ch4}}$ (BT in *K*) and ***IWV*** (Integrated Water Vapor in *kg/m²*) in equations 1 and 2 from Clerbaux et al. (2020) were in fact normalized for their absolute magnitude: indeed, the regression calibrations were designed to not depend on these quantities' absolute magnitude, so their normalization consists of subtracting the variable from its ~~bin-averaged mean value~~regression-specific mean value, i.e. the mean value of T, IWV and F that was recorded in the specific conditions leading to that specific regression model. This was only done for the terms in which the absolute magnitude of the value is of importance, and not for the terms in which it was already normalized, i.e. subtracted from a similar quantity, such as (T_{ch5}-T_{ch4}). Therefore, equation 1 from Clerbaux et al. (2020) should be interpreted as follows:

$$F=(\bar{F}+c_0)+c_1\cdot\Delta T_{ch4}+c_2\cdot(T_{ch5}-T_{ch4})+c_3\cdot(T_{ch4}-T_{surf})+c_4\cdot\Delta T_{ch4}^2+c_5\cdot\Delta T_{ch4}\cdot(T_{ch5}-T_{ch4})+c_6\cdot\Delta IWV \quad (2)$$

With the following substitutions, in which $\overline{X}$ stands for the bin-averaged mean value of X:

- $\Delta T_{ch4} = T_{ch4} - \overline{T}_{ch4}$
- $\Delta IWV = IWV - \overline{IWV}$

In total, there are coefficient values for 101088 combinations of month (12), longitude grid box (36), latitude grid box (18) and VZA bin (13), together constituting a table which is too long to include in this document. As an illustrative example, an extract of the table is shown in Table 5 for month November (longitude 350°-360°, latitude 170°-180°, all VZA bins) and month December (longitude 0°-10°, latitude 0°-10°, all VZA bins).

Table 5: Example of Narrowband-to-OLR coefficients table (for AVHRR-2/-3)

month	Lon box	Lat box	VZA bin	Sample size	$\overline{Tch4}$	$\overline{IWV}$	$\overline{F}$	c_0	c_1	c_2	c_3	c_4	c_5	c_6	Error
1-12	*0°-360°*	*0°-180°*	*0°-65°*	*#*	*[K]*	*[kg/m²]*	*[W/m²]*	-	-	-	-	-	-	-	*[W/m²]*
….	….	….	….	….	….	….	….	….	….	….	….	….	….	….	….
11	350-360	170-180	0-5	1704	247.6	2.95	178.8	8.32	1.62	-11.85	-0.22	-0.01	-0.22	-0.06	4.24
11	350-360	170-180	5-10	1438	247.5	2.91	179.4	7.72	1.53	-13.33	-0.09	0.00	0.23	-0.15	4.09
11	350-360	170-180	10-15	1337	247.7	2.90	179.5	7.13	1.85	-14.69	0.13	0.01	0.17	-1.23	4.04
11	350-360	170-180	15-20	1348	248.0	2.81	179.6	5.92	1.91	-10.85	0.03	0.00	-0.12	-0.97	4.46
11	350-360	170-180	20-25	1386	247.5	2.74	179.2	6.08	1.83	-11.45	-0.03	0.00	-0.14	-0.82	4.09
11	350-360	170-180	25-30	1395	247.2	2.71	179.0	5.45	1.64	-11.51	0.03	0.00	0.25	-0.63	3.53
11	350-360	170-180	30-35	1369	246.9	2.68	178.3	3.84	1.67	-8.31	0.11	0.00	0.14	-0.98	3.27
11	350-360	170-180	35-40	1397	247.2	2.62	179.0	1.57	1.70	-6.25	0.27	0.01	0.29	-1.57	3.02
11	350-360	170-180	40-45	1668	247.1	2.59	178.4	2.01	1.66	-6.15	0.20	0.00	0.31	-1.21	3.27
11	350-360	170-180	45-50	1664	245.8	2.65	175.7	3.09	1.49	-4.87	-0.02	0.00	0.23	-0.26	3.21
11	350-360	170-180	50-55	1284	246.0	2.64	176.4	1.69	1.41	-4.60	0.08	0.01	0.39	-0.29	2.86
11	350-360	170-180	55-60	1156	246.8	2.60	178.4	0.10	1.77	-2.17	0.12	0.02	0.23	-2.04	3.07
11	350-360	170-180	60-65	1016	246.0	2.61	176.6	0.82	1.46	-1.32	-0.06	0.03	0.43	-1.59	3.25
12	0-10	0-10	0-5	1186	260.4	4.08	219.6	2.79	1.67	-1.60	-0.23	-0.01	0.03	0.21	2.26
12	0-10	0-10	5-10	943	260.0	4.06	218.7	1.67	1.88	-1.39	0.00	-0.01	0.03	-0.47	2.30
12	0-10	0-10	10-15	1022	259.8	4.04	217.8	0.68	2.10	-1.37	0.16	0.00	0.00	-0.88	2.39
12	0-10	0-10	15-20	1020	259.7	4.01	217.1	2.26	2.11	-1.77	-0.11	0.01	-0.09	-0.92	2.43
12	0-10	0-10	20-25	1114	258.7	4.00	215.1	2.78	1.91	-1.19	-0.26	0.00	-0.02	-0.51	2.50
12	0-10	0-10	25-30	1236	257.2	3.76	212.6	1.91	1.95	-1.14	-0.11	0.00	0.01	-0.09	3.09
12	0-10	0-10	30-35	1284	255.5	3.40	209.9	0.79	2.32	-2.13	0.20	0.00	-0.12	-0.54	2.99
12	0-10	0-10	35-40	1299	254.3	2.96	207.5	1.82	2.27	-2.34	0.13	0.00	-0.11	-0.44	2.83
12	0-10	0-10	40-45	1477	251.7	2.68	203.0	1.33	2.23	-1.74	0.10	0.00	-0.11	-0.54	2.74
12	0-10	0-10	45-50	1296	250.9	2.50	201.5	1.26	2.20	-1.98	0.13	0.00	-0.08	-0.93	2.57
12	0-10	0-10	50-55	1372	251.5	2.83	203.2	1.23	2.23	-1.72	0.07	0.00	-0.11	-0.74	2.61
12	0-10	0-10	55-60	952	250.4	2.79	201.3	-1.21	2.35	-1.68	0.36	0.00	-0.10	-1.30	2.70
12	0-10	0-10	60-65	730	249.7	2.19	200.3	0.18	2.15	-0.62	0.04	0.00	-0.07	-0.67	2.40
….	….	….	….	….	….	….	….	….	….	….	….	….	….	….	….

For the AVHRR/1 instrument, a different set of regressions has been compiled since there is no channel 5. Analogous to the dual-channel situation, equation 2 from Clerbaux et al. (2020) should be interpreted as follows:

$$F = (\overline{F} + c_0) + c_1 \cdot \Delta T_{ch4} + c_2 \cdot (T_{ch4} - T_{surf}) + c_3 \cdot \Delta T_{ch4}^2 + c_4 \cdot \Delta IWV \quad (3)$$

With the following substitutions, in which $\overline{X}$ stands for the bin-averaged mean value of X:

- $\Delta T_{ch4} = T_{ch4} - \overline{T}_{ch4}$
- $\Delta IWV = IWV - \overline{IWV}$

The single-channel equivalent of the coefficients table is shown in Table 6.

Table 6: Example of Narrowband-to-OLR coefficients table (for AVHRR-1)

month	Lon box	Lat box	VZA bin	Sample size	$\overline{Tch4}$	$\overline{IWV}$	$\overline{F}$	c_0	c_1	c_2	c_3	c_4	Error
1-12	*0°-360°*	*0°-180°*	*0°-65°*	*#*	*[K]*	*[kg/m²]*	*[W/m²]*	-	-	-	-	-	*[W/m²]*
….	….	….	….	….	….	….	….	….	….	….	….	….	….
11	350-360	170-180	0-5	1704	247.6	2.95	178.8	5.39	1.17	-0.75	-0.01	-0.03	4.24
11	350-360	170-180	5-10	1438	247.5	2.91	179.4	3.43	1.39	-0.44	-0.01	-0.23	4.09
11	350-360	170-180	10-15	1337	247.7	2.90	179.5	1.60	1.65	-0.20	-0.01	-0.77	4.04
11	350-360	170-180	15-20	1348	248.0	2.81	179.6	1.89	1.67	-0.30	-0.01	-0.68	4.46
11	350-360	170-180	20-25	1386	247.5	2.74	179.2	2.31	1.56	-0.38	-0.01	-0.26	4.09
11	350-360	170-180	25-30	1395	247.2	2.71	179.0	1.97	1.51	-0.35	0.00	-0.41	3.53
11	350-360	170-180	30-35	1369	246.9	2.68	178.3	1.06	1.62	-0.11	-0.01	-1.00	3.27
11	350-360	170-180	35-40	1397	247.2	2.62	179.0	0.05	1.69	0.04	-0.01	-1.52	3.02
11	350-360	170-180	40-45	1668	247.1	2.59	178.4	0.87	1.53	-0.18	0.00	-1.00	3.27
11	350-360	170-180	45-50	1664	245.8	2.65	175.7	2.25	1.46	-0.30	-0.01	-0.33	3.21
11	350-360	170-180	50-55	1284	246.0	2.64	176.4	0.48	1.55	-0.09	0.00	-0.47	2.86
11	350-360	170-180	55-60	1156	246.8	2.60	178.4	-0.70	1.83	0.02	0.02	-2.03	3.07
11	350-360	170-180	60-65	1016	246.0	2.61	176.6	0.69	1.69	-0.16	0.01	-1.67	3.25
12	0-10	0-10	0-5	1186	260.4	4.08	219.6	1.62	1.79	-0.31	-0.01	0.09	2.26
12	0-10	0-10	5-10	943	260.0	4.06	218.7	0.39	1.99	-0.03	-0.01	-0.54	2.30
12	0-10	0-10	10-15	1022	259.8	4.04	217.8	-0.28	2.14	0.08	0.00	-0.55	2.39
12	0-10	0-10	15-20	1020	259.7	4.01	217.1	1.50	1.96	-0.35	0.01	-0.52	2.43
12	0-10	0-10	20-25	1114	258.7	4.00	215.1	2.31	1.82	-0.43	0.01	-0.17	2.50
12	0-10	0-10	25-30	1236	257.2	3.76	212.6	1.42	1.90	-0.24	0.00	0.21	3.09
12	0-10	0-10	30-35	1284	255.5	3.40	209.9	-1.37	2.22	0.19	0.00	-0.41	2.99
12	0-10	0-10	35-40	1299	254.3	2.96	207.5	-0.46	2.14	0.09	0.00	-0.24	2.83
12	0-10	0-10	40-45	1477	251.7	2.68	203.0	0.69	1.98	-0.07	0.00	0.17	2.74
12	0-10	0-10	45-50	1296	250.9	2.50	201.5	-0.33	2.07	0.06	0.00	-0.59	2.57
12	0-10	0-10	50-55	1372	251.5	2.83	203.2	-0.21	2.07	0.02	0.00	-0.45	2.61
12	0-10	0-10	55-60	952	250.4	2.79	201.3	-3.18	2.26	0.38	0.00	-1.29	2.70
12	0-10	0-10	60-65	730	249.7	2.19	200.3	-0.32	2.04	0.02	0.00	-0.45	2.40
….	….	….	….	….	….	….	….	….	….	….	….	….	….

3. Retrieval of Reflected Solar Flux [CM-11312, RSF]

The current chapter focuses on the retrieval of shortwave "Reflected Solar Flux" (RSF), schematized in the rightmost bluish sections of Figure 27. The processing chain is subdivided in four separate modules, denominated "Parts 1 – 4" in the leftmost column of Figure 27.

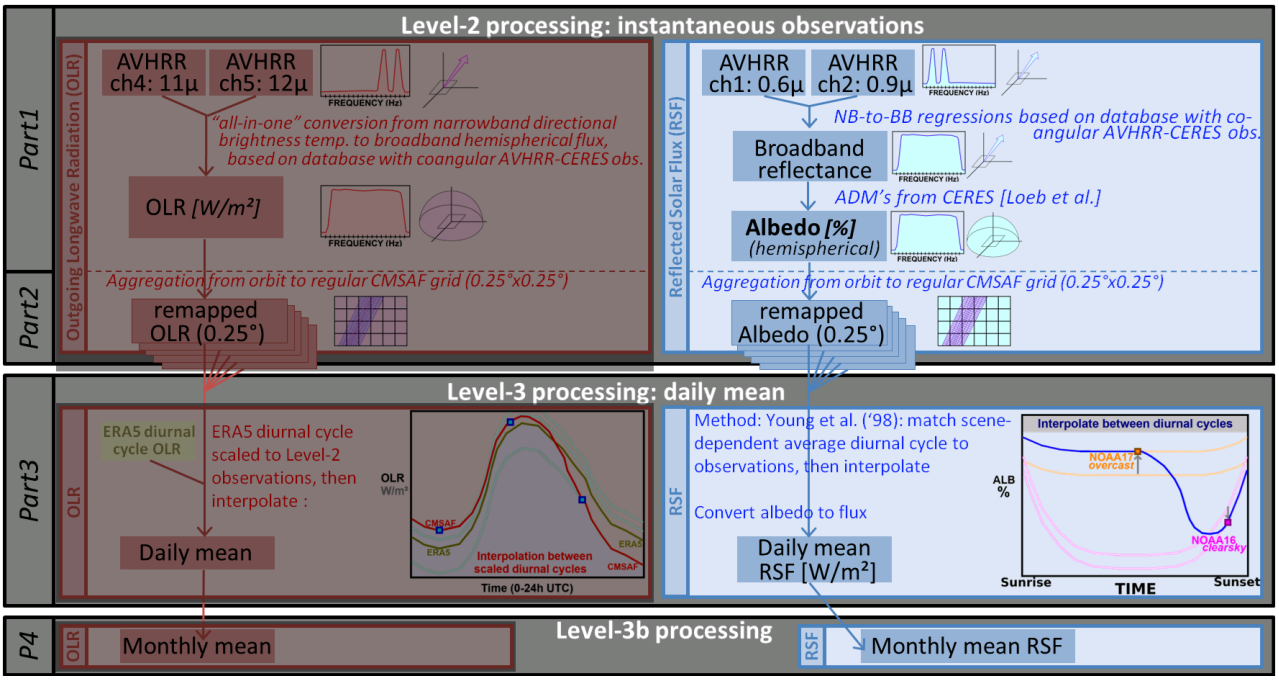

Figure 27: Overview of the OLR (left) and RSF (right) processing chain

The four following sections in this chapter refer to these four specific modules that may be executed and managed separately. "Part 1" refers to the module "Program Part 1", etcetera.

3.1. Part 1: Retrieval algorithm for instantaneous TOA albedo (level-2)

3.1.1. Overview (Fig.28)

Program Part 1 retrieves the **instantaneous TOA shortwave albedo** (broadband hemispherical) from the narrowband directional reflectance (1 or 2 channels) and all the various input data sources, and creates the Level-2 output which consists of a single NetCDF file corresponding to each *GAC orbit inputfile*. Creating separate shortwave and longwave output files would not be efficient, as there are many common auxiliary variables which need to be propagated to the next program parts, and which hence should be stored to disk twice.

Program Part 1 takes as input a single AVHRR GAC file (i.e. the "*reference input file*" containing reflectances). Corresponding auxiliary files (containing auxiliary input data such as PPS, meteorological reanalysis, sea ice cover, etc.) are located automatically based on the filename of the reference input file.

A loop then iterates over all AVHRR GAC pixels, and all subsequent processing is done on each single pixel separately (Flowchart Fig. 28). A distinction is made between shortwave and longwave processing, either manually for all pixels (enabling/disabling the LW- and/or SW-processing for all pixels by modifying the relevant flag in configuration file) or automatically per pixel (e.g. SW is automatically disabled if invalid SW-specific inputdata is detected, or when SZA>84°).

When terminating the processing for a given pixel, incl. abrupt/premature terminations due to invalid input data, certain data is always written to the output before proceeding to the next pixel in the iteration. It concerns the following variables:

- bit flags
- bit flag variable ID
- time stamp (UNIX time)

When the loop is finished, all pixels are written to a Netcdf file. This Level-2 data serves as input for the Surface Radiation processing [RD 5] as well as for the subsequent part of the TOA flux retrieval (Program Part 2, Section 3.2).

The **bit flags** are for each pixel by default set to zero, and may be modified during the processing; their main purpose is to deliver pixel-specific information about the processing, including potential reasons for increased uncertainty, or even for missing output. The total bit flag value is composed of multiple bits each representing a separate binary flag. A complete overview of all the flag meanings can be found in Appendix 9.6.2 (Table 22). The accompanying "**bit flag variable ID"** indicates *which variable* is affected when a bit flag is activated; a list with their associated default ID numbers is also available in Annex 9.6.1 (Table 21).

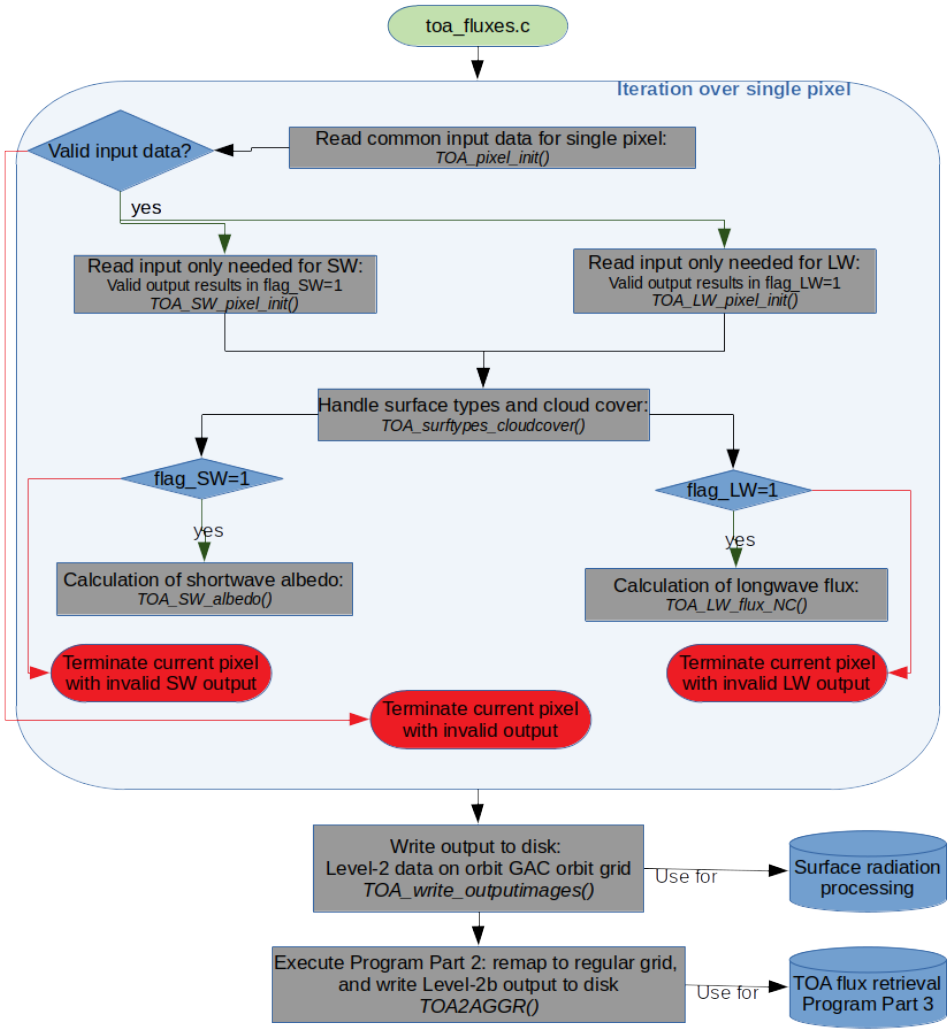

Figure 28: Flow chart for Program Part 1 and Part 2 (level-2 processing for RSF and OLR)

3.1.2. Preparation of input data

3.1.2.a. Initialization of pixel value with input data: common part

First, the input data required for **both** shortwave and longwave processing are read (Flowchart Fig. 28). It concerns the following variables:

- Longitude and latitude coordinates (*Section 2.1*),
- Viewing zenith angle and solar zenith angle (*Section 2.1*),
- Land fraction (*Section 2.3.5*),
- Classic cloud mask 'CMAext' (*Section 2.2.1.b*),

- Probabilistic cloud mask 'CMAPROB' (*Section 2.2.1.a*),
- Sea ice concentration (*Section 2.3.2*),
- Snow depth (*Section 2.3.1*).

Any invalid value would terminate the routine, thus resulting in invalid outputs for that pixel. Note that the SZA is not needed for the longwave part, but is used to distinguish the limit for "daytime" and thus shortwave processing (SZA<84°). VZA>70° is also considered 'invalid' thereby terminating the routine and resulting in invalid output.

The probabilistic cloud mask (*CMAPROB*) is used as only source to determine whether the pixel is either clear or overcast. The classic cloudmask (*'CMAext(ended)'*), only used for surface snow cover detection, is corrected to be consistent with CMAPROB following Flowchart Fig. 29.

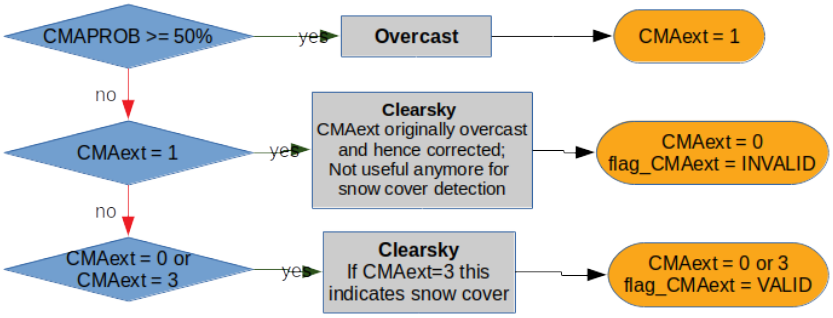

Figure 29: Flow chart: use of cloud masks: rules

When probabilities<50% despite an overcast classic cloud mask, the latter is not useful anymore for snow cover detection, and a corresponding flag is set (flag_CMAext=INVALID).

3.1.2.b. Initialization of pixel value with input data: shortwave-only part

The shortwave-specific input data (Flowchart Fig. 28) consist of the following variables:

- Cloud Physical Parameters (CPP): phase, optical thickness, quality flag (*Section 2.2.2.a*).
- Bitwise flags 'cpp_quality' (*Section 2.2.2.b*) and 'cpp_conditions' (*Section 2.2.2.c*)
- Relative azimuth angle (*Section 2.1*),
- Wind speed: u and v components (*Section 2.3.3*),
- Channel 1 (0.6µm) and channel 2 (0.9µm) non-SZA-normalized reflectance a.k.a. 'scaled radiance' (*Section 2.1*).

Any invalid value would terminate the SW processing, thus resulting in an invalid output for that pixel.

The channel 1 (λ=0.6µm) and channel 2 (λ=0.9µm) *scaled radiance* (SR_λ)[12] which are available in the *GAC orbit files*, are already normalized to account for the changing Earth-Sun distance (as a function of day of year). Equation 4 clarifies what exactly is already included in the SR_λ input data.

$$SR_\lambda = \frac{d^2 \cdot L_\lambda \cdot \pi}{SSI_\lambda} \quad (4)$$

where d is the Earth–Sun distance factor in astronomical units, L_λ is the spectral radiance ~~($W \cdot sr^{-1} \cdot m^{-2} \cdot nm^{-1}$)~~, and SSI_λ is the spectral solar irradiance ~~($W \cdot m^{-2} \cdot nm^{-1}$)~~. The "true isotropic reflectance" (Heidinger et al., 2010), here simply referred to as 'narrowband reflectance' (ρ_λ), is calculated by applying a further normalization using the cosine of solar zenith angle, $cos(\theta_0)$, which compensates the increasing surface-projected area of incident solar radiation[13]:

$$\rho_\lambda = \frac{SR_\lambda}{\cos(\theta_0)} \quad (5)$$

12 *According to Heidinger et al. (2010), the quantity called 'scaled radiance' is not yet normalized for earth-sun distance, so the quantity in the GAC file is something between the 'scaled radiance' and 'true isotropic reflectance'.*

13 *In fact, θ_0 is an approximation of the angle between the incident radiation and the normal vector, assuming that the projected area (surface) is horizontal, i.e. parallel with the earth's ellipsoid.*

The resulting reflectance is considered invalid if it exceeds 200%, which would lead to the termination of the SW processing and an invalid TOA albedo for the current pixel.

To save computation time, other parameters are only read if they are required: the cloud physical parameters (CPP) cloud phase and optical thickness are only read for pixels with overcast cloud mask (CMAext=1). For Cloud Optical Thickness (COT) another requirement is that the CPP quality flag indicates 'good quality' for this pixel (cpp_quality=8). If not, the COT is instead taken from a multi-year climatology of monthly means (Section 2.4.5) calculated from the CERES, which serves as surrogate for the observed COT. Based on the latitude and longitude of the AVHRR pixel, it locates the corresponding 1°x1° COT grid box. It provides a COT value which is realistic for a given region, and representative on long time scale. For wintertime polar regions the surrogate value of the COT annual cycle is invalid. This is mostly not a problem as pixels in those regions are anyway mostly exceeding the "daytime threshold" (SZA>84°) and therefore not even processed in the shortwave part (RSF); but nevertheless, when it is required in those cases, an arbitrarily chosen value of COT=5.0 is assumed.

Hence, the resulting COT (Figure 30) is modified w.r.t. the original input COT (Figure 5). The modified COT values in Figure 30 can be noticed by larger homogeneous clusters of light-greenish color in some regions, most notably in the area indicated with red circle: these correspond with pixels that do not have "good quality" in the *cpp_quality* flag (Figure 6).

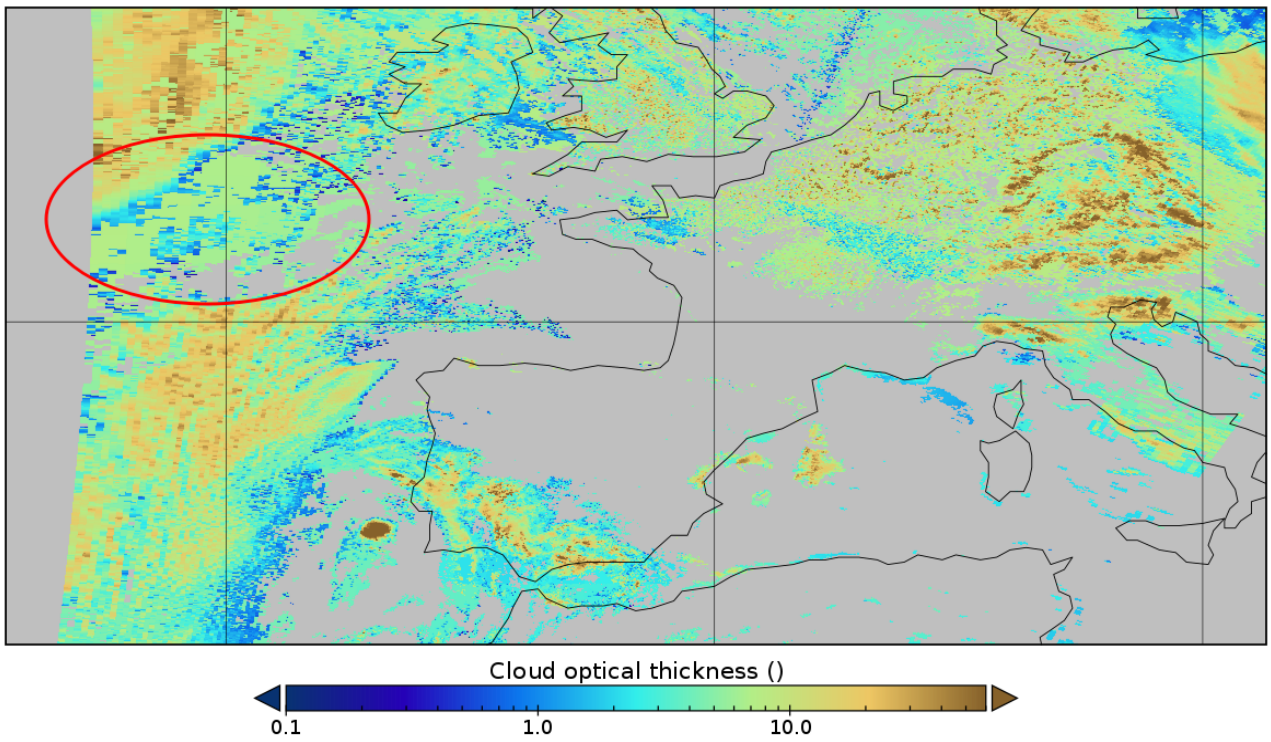

Figure 30: Example of modified Cloud Optical Thickness (dimensionless) on GAC orbit grid

ERA5 10m wind speed components are read when the scene type is "clearsky ocean". In that case, the Pythagorean wind speed magnitude is calculated from the U and V wind components. Because the scene type requires knowledge about the surface type, wind speed data is only effectively read after the routines discussed in next Section 3.1.2.c, Flowchart Fig.28.

3.1.2.c. Preparation of cloud cover and surface types (Fig.32)

After the shortwave-specific input data are read, the processing of cloud cover and surface types starts (cfr. overall Flowchart Fig.28). This is governed by a subroutine depicted in Flowchart Fig.32. First, the IGBP land cover class for the current pixel is determined from the IGBP map (Section 2.4.2) by means of the nearest neighbor method.

Then (Fig.32), the USGS-based land fraction (Section 2.3.5) is used to determine whether a pixel is situated in a "coastal region" (land fraction between 1% and 99%), and more specifically if this coastal pixel contains "mostly inland water" (ponds, rivers, lakes,..) or "mostly open water" (large lake, sea, ocean,..). ~~Note that "coastal" here means having a mixture of water and land in a 44x44km (moving) window.~~ **'flag_coastal'** is defined, resulting in three categories (Figure 31):

- Land fraction 0% or 100%: flag_coastal=0 (inland or open water), **blue** in Figure 31
- Land fraction 1-50% : flag_coastal=1 (coastal, mainly open water), white in Figure 31
- Land fraction 50-99%: flag_coastal=2 (coastal, mainly inland water), **red** in Figure 31

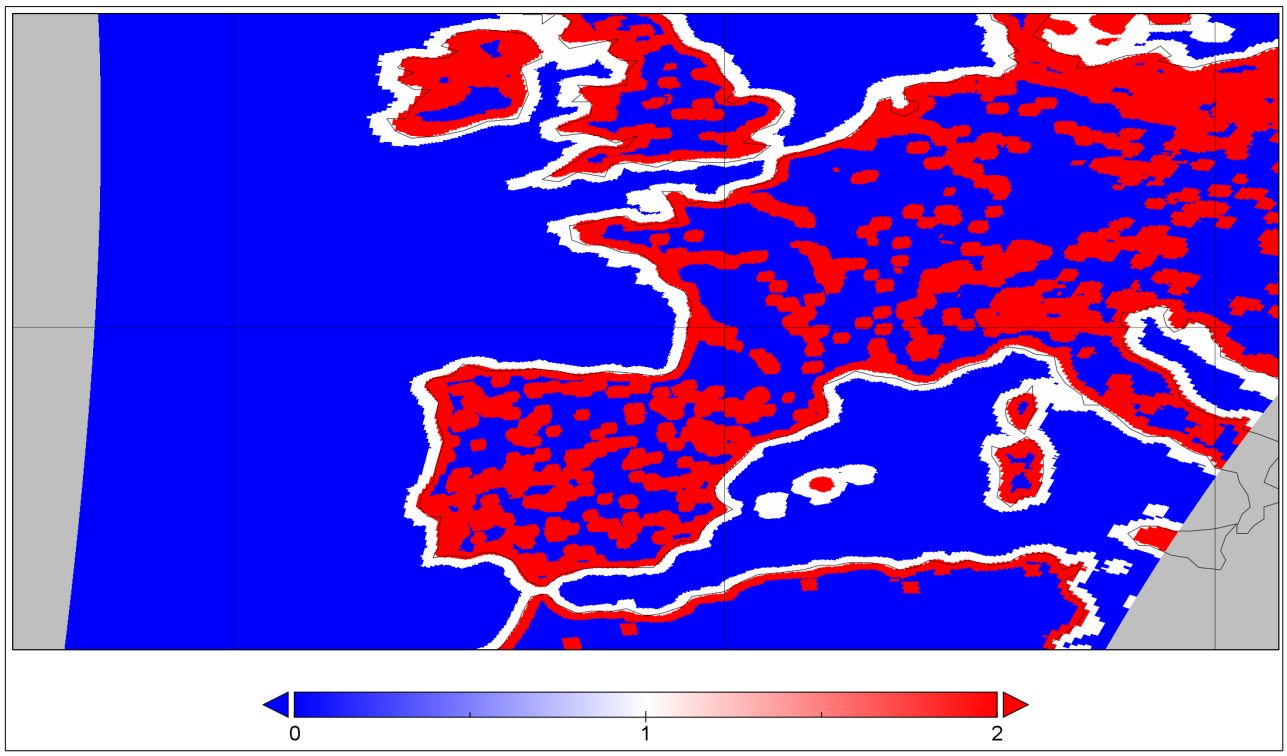

Figure 31: Example of 'flag_coastal' on GAC orbit grid

The only use of the land fraction information, as input data, is the determination of the coastal flag. This flag is used in the decision tree for determining the surface type (Flowchart Fig.33).[14]

14 *It is nót subsequently used to determine whether a pixel is considered land or water: instead, the original land fraction value is erased and re-assigned to either 0% (water) or 100% (land) depending on the previously determined IGBP-derived land cover class. This distinction is thus strictly binary, which leads to a division between 'water pixels' and 'land pixels', a.k.a. land-sea mask.*

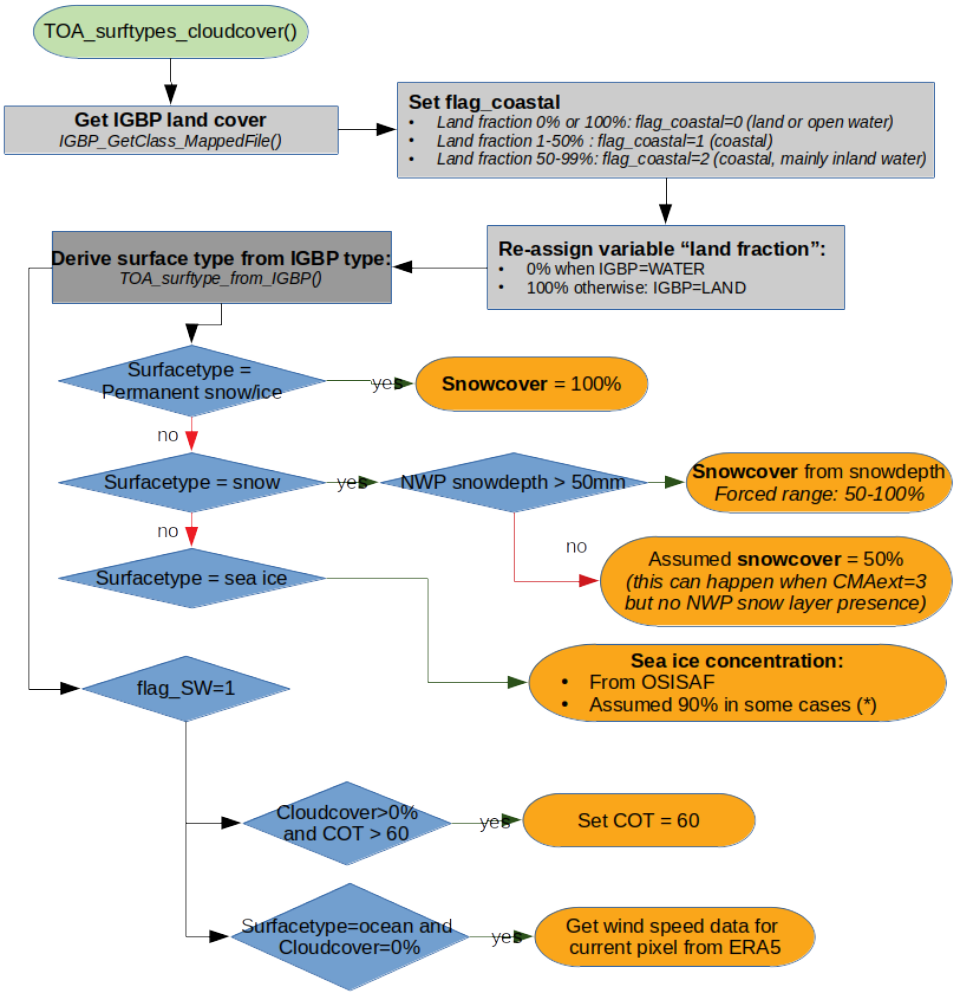

Figure 32: Flow chart: preparation of cloud cover and surface types

Subsequently the surface types are derived for narrowband-to-broadband conversion ("NTB surface types"), for the ADM and albedo model ("CERES surface types"), and for the Twilight model ("TWL surface types"), as shown in Flowchart Fig.33. The main difficulty here is that the different input data sources (IGBP map, ERA5 snow depth/cover, OSI SAF sea ice) have different coverage in terms of coast line and land/sea mask: for instance the border between sea ice and permanent snow/ice may be separated by "coverage gaps" or they may be overlapping. This complicates the combined use of these datasets, and explains the rather complex way of determining the final surface type for a pixel.

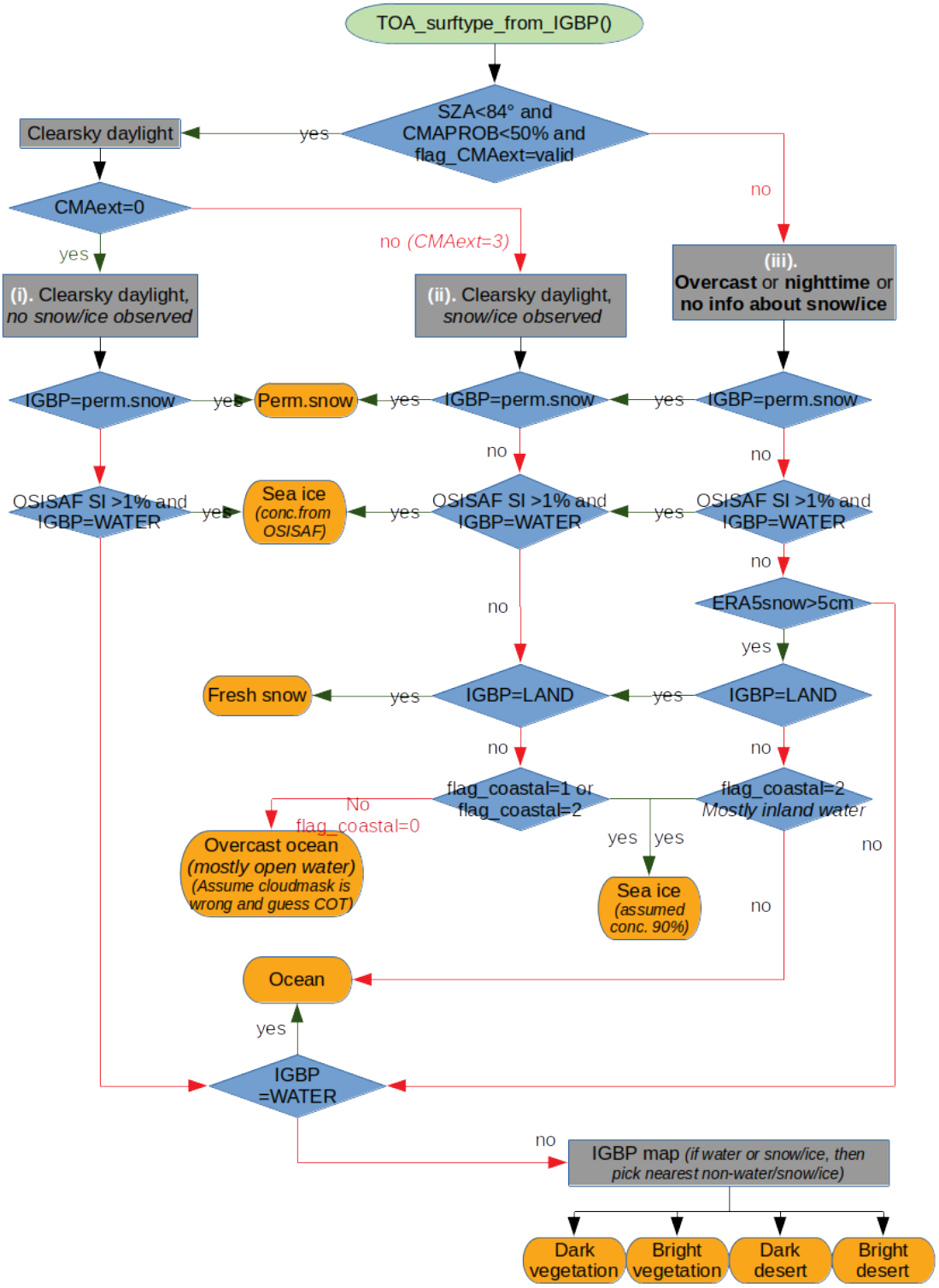

Figure 33: Flow chart: decision tree for determining surface type

An important first step in Flowchart Fig.33 is separating conditions of (i) clearsky daylight without observed snow/ice, (ii) clearsky daylight with observed snow/ice, and (iii) all other cases, i.e. overcast, or nighttime, or no information about snow/ice. This is done using variables SZA, CMAPROB, corrected CMAext and flag_CMAext (the latter two defined by Flowchart Fig.29). In all three conditions, the IGBP class 'permanent snow/ice' gets full priority in the decision tree, and the corresponding surface type ('permanent snow/ice') is selected without further criteria. Next in the decision tree is the OSI SAF sea ice, which leads to the "sea ice" surface type as soon as its concentration exceeds 1% in water pixels. Table 7 describes the mapping of sea ice and fresh snow to NTB and CERES surface type; the NTB surface type "NTB_SEAICE" is subdivided according to OSI SAF sea ice concentration. Subsequently, fresh snow is

only an option on land pixels in conditions (ii) and (iii), with respectively an observation based detection (ii) and a model-based assumption (iii) of fresh snow. Using the information from the coastal flag, the remaining combinations are resolved (Flowchart Fig.33) such as observed snow/ice in a coastal water pixel without a matching OSI SAF sea ice concentration.

Table 7: Mapping of fresh snow and sea-ice to NTB, CERES, TWL surface types

OSI SAF sea ice concentration	**NTB surface type**	**CERES surface type (ADM, albedo model)**	**TWL surface type**
100%	NTB_SEAICE_100 (NTB surface type 9)	(CERES surface type 8) SURF_SEAICE	(TWL surface type 1) SEAICE_100%
95-99%	NTB_SEAICE_95_99 (NTB surface type 10)		*n.a.*
90-94%	NTB_SEAICE_90_94 (NTB surface type 11)		
80-89%	NTB_SEAICE_80_89 (NTB surface type 12)		
60-80%	NTB_SEAICE_60_79 (NTB surface type 13)		
10-60%	NTB_SEAICE_10_59 (NTB surface type 14)		
1-10%	NTB_SEAICE_00_09 (NTB surface type 15)		
Snow cover	**NTB surface type**	**CERES surface type (ADM, albedo model)**	**TWL surface type**
100%	NTB_FRESH_SNOW (NTB surface type 8)	(CERES surface type 7) SURF_FRESHSNOW	(TWL surface type 3) FRESHSNOW_100%
1-99%			*n.a.*

Finally (Fig.33), when the pixel does not contain permanent snow/ice, fresh snow or sea ice, the IGBP class is mapped to ***NTB surface type*** and ***CERES surface type*** according to Table 8. The IGBP-to-NTB surface type mapping uses the same IGBP class clusters as Loeb et al. (2005) used for their longwave and window ADM's (but also supported by comparing AVHRR narrowband reflectance stratified by IGBP class, see Annex 9.5, Figure 84), while the IGBP-to-CERES mapping is based on the IGBP class clusters used in Loeb et al. (2003) i.e. the dedicated surface types for the shortwave CERES TRMM ADMs. Since the IGBP classes are not sufficient to have a good discrimination between dark and bright desert, the desert CERES surface types are split according to the CERES classification (and more specifically to the albedo) (Ipe, 2011; Loeb et al, 2003). This post-discrimination process is performed using a coarser CERES surface type map at 10' resolution (Section 2.4.3), and the method is identical as applied in [RD 10].

Table 8: Mapping of IGBP class (water+land types) to NTB, CERES, TWL surface types

IGBP class	**NTB surface type**	**CERES surface type (ADM, albedo model)**	**TWL surface type**
17) Water	(NTB surface type 1) NTB_WATER	(CERES surface type 1) SURF_OCEAN	(TWL surface type 0) WATER
1) Evergreen Needleleaf Forest	(NTB surface type 2) NTB_FOREST	(CERES surface type 2) SURF_VEGETATION_DARK	(TWL surface type 4) LAND
2) Evergreen Broadleaf Forest			
3) Deciduous Needleleaf Forest			
4) Deciduous Broadleaf Forest			
5) Mixed Forest			
6) Closed Shrublands	n.a.		
11) Wetlands			
8) Woody Savannas	(NTB surface type 3) NTB_SAVANNA		
9) Savannas		(CERES surface type 3) SURF_VEGETATION_BRIGHT	
10) Grasslands	(NTB surface type 4) NTB_GRASS_CROP		
12) Croplands			
14) Cropland/Natural Vegetation Mosaic			
6) Closed Shrublands		n.a.	
11) Wetlands			
13) Urban and Built-Up		(CERES surface type 4) SURF_DESERT_DARK or*	
7) Open Shrubland	(NTB surface type 5) NTB_DESERT_DARK		
18) Tundra			

16) Barren or Sparsely Vegetated	(NTB surface type 6) NTB_DESERT_BRIGHT	(CERES surface type 5) SURF_DESERT_BRIGHT	
15) Permanent Snow and Ice	(NTB surface type 7) NTB_PERM_SNOW_ICE	(CERES surface type 6) SURF_SNOW	(TWL surface type 2) PERM_SNOW_ICE
(*) for CERES surface types, the discrimination between dark and bright desert is done using the CERES 10' map			

In most cases, the surface type is homogeneous in the entire AVHRR pixel. There are two exceptions:

- Surface type "sea ice" (only allowed in pixels where IGBP=water) contains a certain areal proportion of pure sea ice, according to its sea ice concentration (%), and may also contain water, i.e. the remaining portion of the pixel.
- Surface type "Fresh snow" (only allowed in pixels where IGBP≠water) contains an areal proportion of pure snow, according to its snow cover (%), and may also contain 'undefined land', i.e. the remaining portion of the land. In line with the CERES ADM scene type definitions, ~~Please note that~~ this ~~undefined~~generic 'non-snow covered land' does not have a further specified land cover type (such as desert, forest, etc.); their differences are negligible compared to the sharp contrast between the reflectance from the snow and non-snow pixel fractions.

Note that the **surface type** mapping shown in Tables 7 and 8 is not sufficient to select the correct **scene-type**-dependent NTB, ADM, and TWL models, since a surface type is just one of the parameters that make up a scene type. Other criteria are e.g. snow cover, cloud cover, cloud properties,.. For example, the CERES surface type "SURF_SEAICE" is not sufficient to determine the correct ADM. In fact, it simply specifies the range of scene type numbers (600-620) from which the correct scene type (and corresponding model) is chosen by additionally considering sea ice concentration and cloud cover (see Annex 9.1).

Figure 34 shows an example of the resulting "CERES surface type" for an area in which all the pixels are observed during nighttime, i.e. condition III in Flowchart Fig.33, meaning that all the fresh snow pixels (*CERES_surface_type=7*) are determined using ERA5 snow depth; in this example these pixels are mainly situated in the southern Andes region.

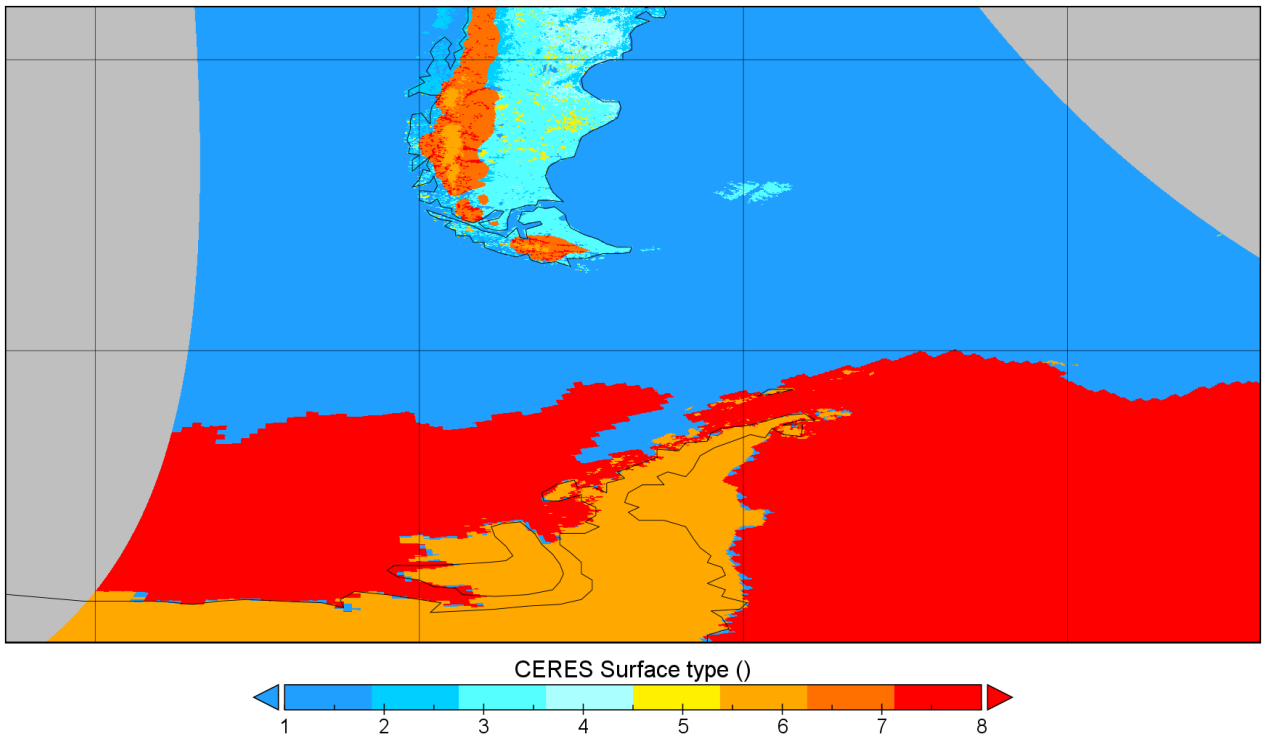

Figure 34: Example of variable 'CERESsurftype' on GAC orbit grid

Once the surface types have been determined (Tables 7 and 8), the routine *TOA_surftypes_cloudcover()* continues (Flowchart in Figure 32).

As already explained, the **clear-sky snow cover** (*i.e. conditions (I) in Flowchart Fig.33*) is detected by making use of the classic cloud mask ("CMA extended" or "CMAext") which has an additional category for clear-sky "surface snow/ice contamination" (CMAext=3; Fig.29). This snow detection flag only indicates the *presence* of snow, but does not provide quantitative information about the within-pixel areal coverage of the snow: instead, this information is derived from the ERA5 snow depth (Hersbach et al., 2020) which~~. Snow depth~~ is converted to *snow cover* using the depth-cover relation used by the ECMWF Integrated Forecasting System (Dutra et al., 2010), as shown in Figure 35. The snow detection flag (indicating the presence of snow) is based on observations, whereas the NWP snow depth only depends on models (i.e. less reliable): therefore, a minimum of 50% snow cover is imposed whenever the snow detection flag is active, even if the NWP snow depth is lower than 5cm. Using such a threshold is based on the assumption that the uncertainty of modelled snow cover decreases with layer depth (layer of 7 cm is more certain than layer of 1 cm).

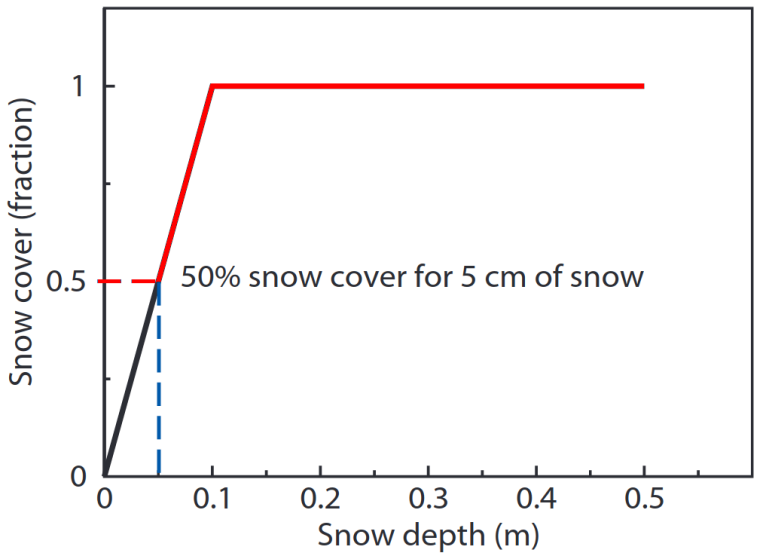

Figure 35: Relation between snow depth and snow cover in IFS (Dutra et al., 2010). In red: adaptation for our purposes, by putting a range limitation to 50%-100%

This observation-based detection of snow presence is not performed for **overcast conditions**, or when the probabilistic cloud mask indicates clear-sky conditions (CMAPROB<50%) while the deterministic cloud mask indicates overcast conditions (CMAext=1), thereby not providing sufficient information to determine the presence of snow at the surface (*in this case, flag_CMAext=INVALID*). In these cases (*i.e. conditions (III) in Flowchart Fig.33*) snow depth from ERA5 reanalysis is used as 'surrogate' dataset for **both** the areal coverage ánd the mere presence of snow. Also here, the minimum of 5cm snow depth (i.e. 50% snow) is used as threshold, so every overcast pixel with more than 5cm snow depth is considered "snow covered", and otherwise "snow free". The downside of ERA5-derived snow cover is that it is heavily based on models, which may lead to large biases w.r.t. observed snow cover. However, using the ERA5-derived snow cover on long time scales (climatology) will still be better than using no snow cover at all.

3.1.3. Sunglint treatment

3.1.3.a. Sunglint detection

The overall Flowchart Fig.28 shows that after reading the input data [*TOA_pixel_init() and TOA_SW_pixel_init()*] and processing the surface types and cloud cover [*TOA_surftypes_cloudcover()*], the main routine for the shortwave processing is initiated [*TOA_SW_albedo()*]. It starts (Flowchart Fig.37) with the detection of potential sunglint conditions [*TOA_detect_sunglint()*]. The resulting TOA albedo in sunglint conditions is not based on the actual AVHRR observations but on other assumptions.

The calculation of the sunglint angle (γ) is itself also computationally demanding, so the pre-calculated **PPS sunglint flag** (Figure 7 in Section 2.2.2.c) is used to narrow down the number of potential sunglint affected pixels.

- When the flag is **disabled**, the program's internal glint flag ('*flag_sunglint*') is automatically set to 0, meaning 'no sunglint conditions', which entirely skips the sunglint angle calculation and proceeds to the regular albedo calculation (starts with section 3.1.4).

- When the flag is **enabled**, the "*exposed water fraction*" is calculated: this is the areal fraction (%) of the AVHRR pixel that is covered by visible water on the surface, i.e. the part not covered by land, clouds or sea ice (*since landmask and cloudmask are both binary, only the sea ice concentration in water pixels could cause the exposed water fraction to vary between 0% and 100%*):
  - When the *exposed water fraction* is **lower** than a certain threshold (10% by default, but adjustable in configuration file with parameter GLINT_MIN_WATER_FRACTION), the sunglint flag is automatically set to 0, meaning 'no sunglint conditions', which entirely skips the sunglint angle calculation and proceeds to the regular albedo calculation (starts with Section 3.1.4).
  - However, when the *exposed water fraction* is **higher** than the threshold, the sunglint angle (γ) is effectively calculated, an example of which is shown in Figure 36. It is the angle (°) between the direction of the Sun specular reflection and the direction of observation, given by Equation (6), where θ_0 is the solar zenith angle (SZA), θ the viewing zenith angle (VZA), and φ_0 the relative azimuth angle (RAA), all in degrees:

$$\gamma = \arccos\left[\sin(\theta_0)\cdot\sin(\theta)\cdot\cos(\phi_0) + \cos(\theta_0)\cdot\cos(\theta) \right] \quad (6)$$

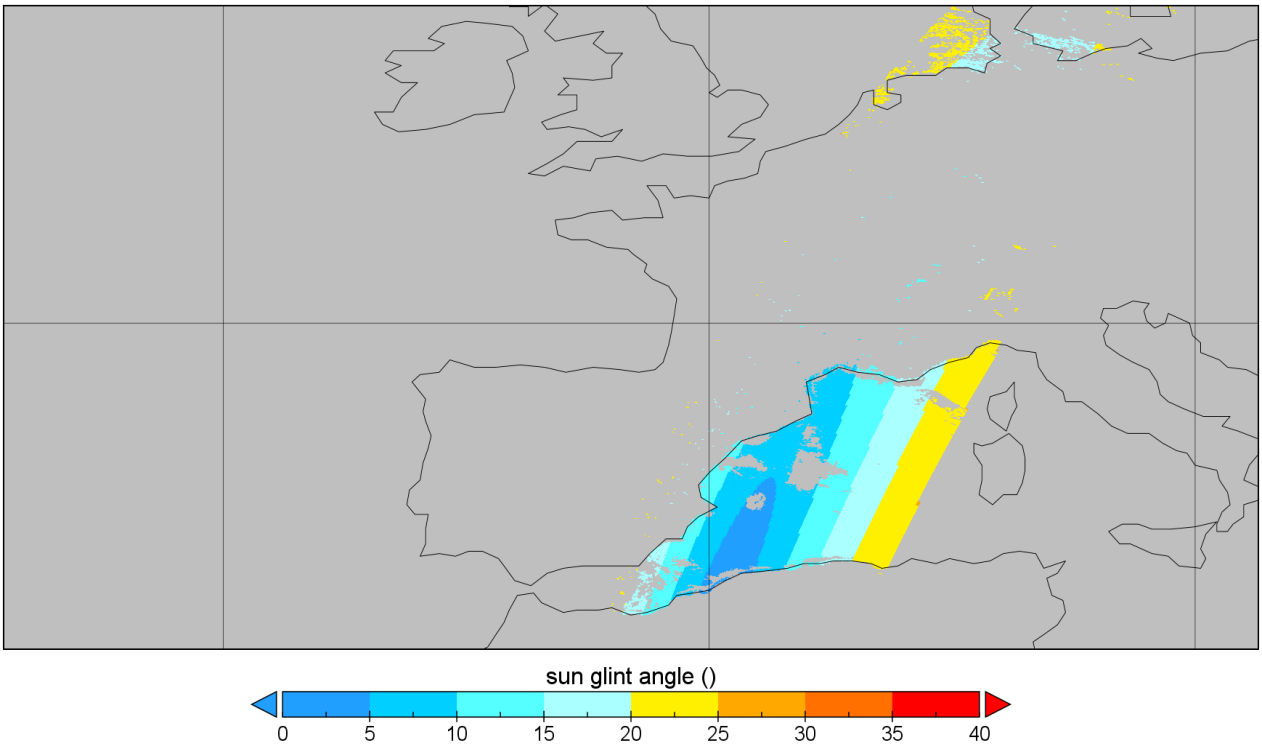

Figure 36: Example of variable 'sun_glint_angle' (units: degrees) on GAC orbit grid

This 'sunglint angle' is then compared to a threshold, which is by default 25° (but also adjustable in the configuration file with parameter GLINT_ANGLE_THRESHOLD_MILD):

- When higher than 25° (colors orange to red in color legend Fig.36), the sunglint flag is automatically set to 0, meaning 'no sunglint conditions', which entirely skips the sunglint angle calculation and proceeds to the regular albedo calculation (starts with Section 3.1.4). Figure 36 only shows the sunglint angle lower than the threshold, explaining why no orange or red colors are visible.
- When lower than 25° (colors blue to yellow in color legend of Fig.36), the sunglint flag is set to 1, meaning 'sunglint conditions': the regular albedo calculation is skipped (thereby avoiding redundant computations), and the sunglint albedo calculation is activated (Section 3.1.3.b).

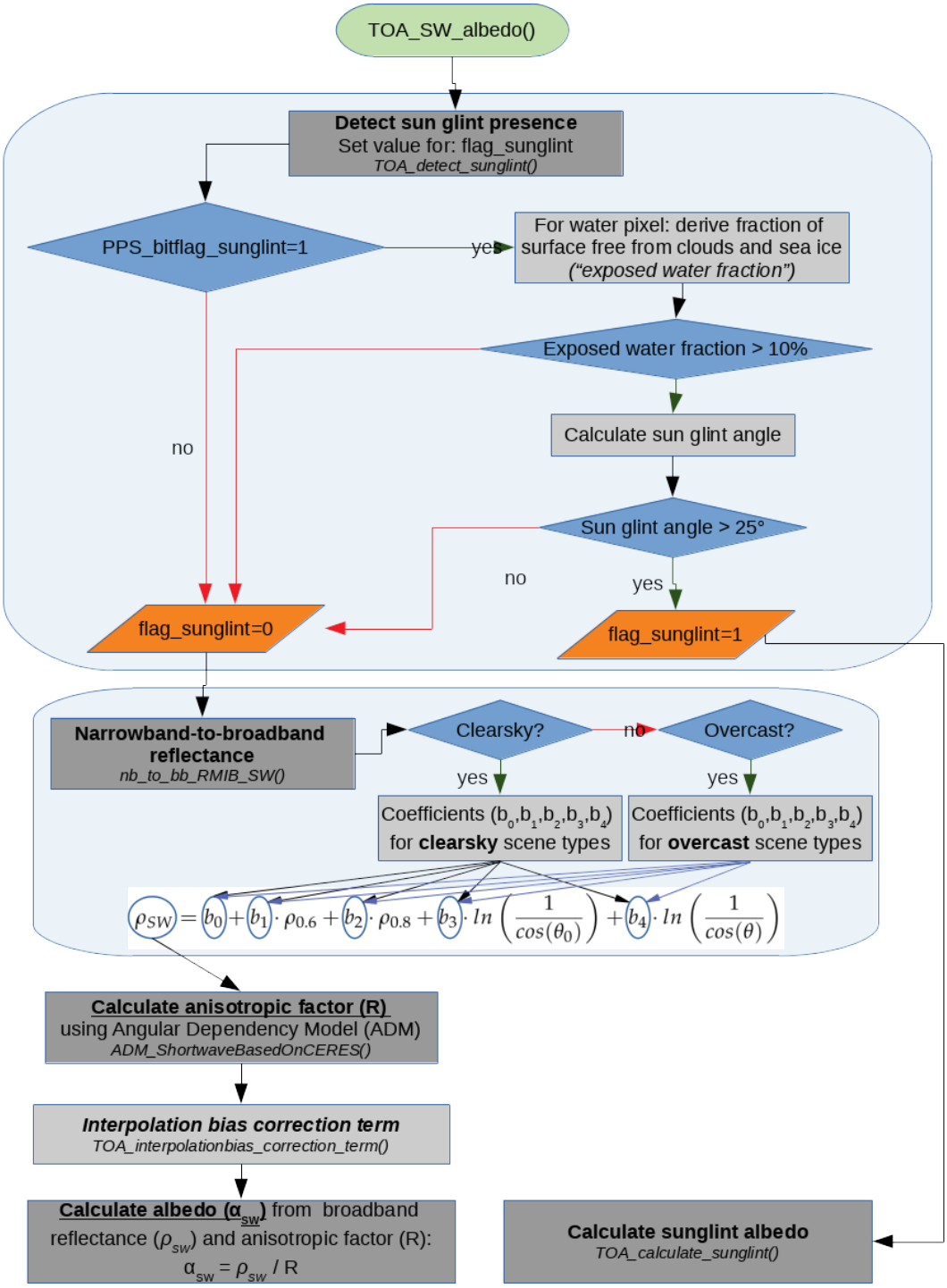

Figure 37: Flow chart: processing of shortwave reflectance to broadband albedo

3.1.3.b. Sunglint albedo calculation

In sunglint conditions, the SW albedo is derived from the CERES albedo models (Section 2.4.6 and Annex 9.1), which are available together with the CERES ADMs and which describe the variation of albedo with respect to the solar elevation. For each scene type, the albedo is given for a number of solar zenith angle bins (example shown in Figure 24), and the final albedo is calculated by linear interpolation in SZA.

More detailed information on the determination of scene type is given in Section 3.1.5.a where the same scene type identification is used (scene types for albedo models are identical to those for ADMs). Note that also for the albedo models, a weighted scene type approach is used.

3.1.4. Narrowband-to-broadband (NTB) conversion

When no sunglint is detected (flag_sunglint=0) the NTB routine is activated (Flowchart Fig.37). Depending on the scene type, which is a combination of cloud cover and 15 NTB surface types, the regression coefficients $\{b_i\}$ are selected (*Section 2.4.8, Table 4*); because of the binary cloud mask, only the clear-sky and overcast cloud categories are used. These coefficients are then applied with the **narrowband** isotropic reflectances (*from Eq.5 from Section 3.1.2.b*) in Equation ~~Error: Reference source not found~~1 to obtain the "**broadband** shortwave reflectance" ρ_{SW} (Akkermans and Clerbaux, 2020), a.k.a. "shortwave isotropic albedo".

~~(7)~~

The resulting broadband reflectance ρ_{SW} is considered invalid if it is lower than 0%, or if it exceeds 200%, which would both lead to the termination of the routine and an invalid TOA albedo for the current pixel. A negative broadband reflectance may occur in e.g. clear-sky water pixels when $\rho_{0.8}$ is much higher than $\rho_{0.6}$, given the negative value for the coefficient b_2 (*Section 2.4.8, Table 4*); a possible reason could be a coastal situation where the (real) sub-pixel land-sea mask is mixed, whereas the NTB regressions were calibrated on (and intended for) pure water or pure land pixels.

3.1.5. Directional-to-hemispherical conversion (angular correction)

Following the narrowband-to-broadband conversion, the shortwave Angular Distribution Model (ADM) routine is initiated (Flowchart Fig.37). The ADMs (Section 2.4.6) are used to determine the correct anisotropic factor (*R*) needed to convert **directional** to **hemispherical** albedo.

3.1.5.a. Scene type determination

The scene type is a combination of surface and cloud properties, and in case of clear-sky water also wind speed. The basic scene type selection is straightforward, by using the look-up tables (*Annex 9.1, Tables 14 and 15*) in which surface type and cloud physical parameters are classified in discretized bins, with each combination of parameter bins leading to a single scene type and corresponding ADM and albedo model (Section 2.4.6).

However, when selecting a **single scene type** (combination of surface type, cloud cover, cloud properties, wind speed) and deriving the single corresponding ADM (and anisotropic factor) for a given combination of viewing and illumination angles (SZA, VZA, RAA), there is an issue with the discretization of the scene type criteria. An example is given for the parameter wind speed (*ws*) over clear-sky ocean: for each discretized bin of wind speed, a separate scene type is available, and hence a separate ADM and anisotropic factor (Table 9).

Table 9: CERES TRMM SW ADM scene types for clear-sky ocean

Scene: Ocean, clear-sky (0% clouds)	
Wind speed (m/s)	**ADM/Scene type nr.**
$ws \leq 3.5$	1
$3.5 < ws \leq 5.5$	**2**
$5.5 < ws \leq 7.5$	3
$ws > 7.5$	4

With an observed wind speed (*ws*) of 5.4 m/s, scene type number #2 would normally be selected, since $3.5<ws\leq5.5$. However, this would introduce a discretization error because the observed wind speed is not representative for the bin center (which is 4.5 m/s). Therefore, it makes sense to derive a **weighted mean** anisotropic factor, thereby minimizing biases due to scene type discretization. In this case it would mean a weighted mean of scene types #2 ($3.5<ws\leq5.5$) and #3 ($5.5<ws\leq7.5$); the weighting consists of the relative distance between the observed value and the lower and upper bin centers. For cloud cover and cloud optical thickness this is done in a similar way, but here the lower/upper bin centers are situated on 2 axes (cloud cover and COT): that means 4 combinations of 'extremes' between which should be interpolated, i.e. for each of which a weighting is calculated and applied (furthermore, COT is interpolated logarithmically instead of linearly). An overview of all scene types and their discretized categorization criteria can be found in Annex 9.1, Table 14.

3.1.5.b. Actual albedo calculation

Once the number of relevant scene types (maximum 4) and their relative weights have been determined, the corresponding anisotropic factors are retrieved from the ADMs by linearly interpolating between the angular bins from a given scene type, and a scenetype-weighted mean anisotropic factor is calculated.

The instantaneous TOA albedo is then obtained by dividing the broadband reflectance (ρ_{SW}) by the scenetype-weighted mean anisotropic factor (R).

$$\alpha_{SW} = \frac{\rho_{SW}}{R} \tag{8}$$

3.1.5.c. Correcting interpolation-induced bias

Besides the scene type discretization, an additional potential source of bias is the linear interpolation between viewing and illumination angular bins (SZA, VZA, RAA)[15] in which the originally collected observations sometimes vary non-linearly (Loeb et al., 2003). This effect is minor for most of the angular bins. To remove it, a scene- and angular-dependent correction term ($\delta\alpha_{SW}$) is added to the instantaneous albedo:

$$\alpha_{SW} = \frac{\rho_{SW}}{R} + \delta\alpha_{SW} \tag{9}$$

Unlike Loeb et al. (2003) the correction term is here applied in terms of albedo, instead of flux. Annex 9.2 documents how exactly this affects the retrieval of this correction term.

3.1.6. Final error corrections

After the main processing, some threshold values are used for final corrections to the TOA albedo.

3.1.6.a. The resulting TOA albedo exceeds 100%

The resulting TOA albedo can exceed 100% for some reasons. For instance, errors in the scene type classification, which would lead to a wrong ADM or narrowband-to-broadband regression: these regressions are calibrated for a certain range (e.g. ocean→dark→low range) and extrapolating these in much higher range for which they were not intended (bright surfaces, e.g. sea ice), could therefore lead to an unrealistically high broadband reflectance.

Another reason is the normalization with SZA (Equation 5), which should correct for the increasing ‘spread’ of the radiation over a larger area with higher SZA, proportional to its cosine (Figure 38a). In fact, the SZA is used here as an approximation of the angle between illumination and the surface normal vector, which assumes a plane-parallel horizontal surface. However, this assumption is violated for significantly sloped surfaces such as mountain ranges or edges of tall clouds (large cloud top height variations). In these cases, the surface normal vector is tilted (Figure 38b) but the cos(SZA)-normalization is still applied in the same way, leading to an over-correction and hence albedo overestimation. Especially for bright surfaces (snow covered mountains, thick clouds,..) in combination with low sun elevation (i.e. high solar zenith angle) the sloped object may cause the apparent albedo to exceed 100%. A photographic example of this *cloud slope effect* is shown in Figure 39. When aggregating to larger pixels, this cloud effect is mostly compensated by an underestimated albedo at shadow side, and therefore the albedo of clouds is allowed to exceed unity (to a maximum of 120%) when solar zenith angle exceeds 60°.

15 *In order to retrieve the correct anisotropic factor*

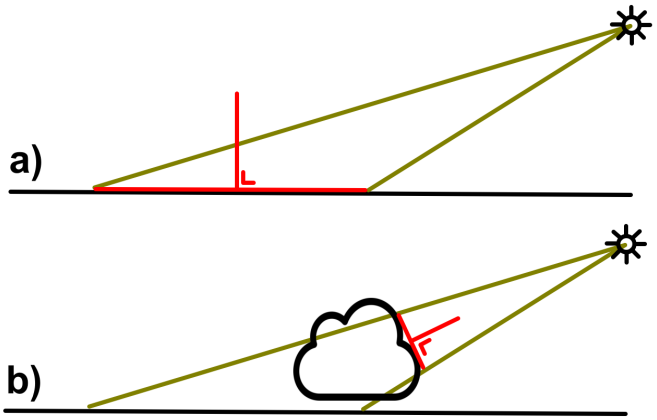

Figure 38: Schematic example of radiation incident on (top) horizontal area, (bottom) cloud edge

Figure 39: Photographic example of low-elevation sun rays incident on cloud edges (photo: ISS)

Corrections are not considered: this would require a fully three-dimensional spatially-explicit cloud model to detect the sun-facing and shadow cloud surfaces that would be subject to respectively over- and underestimation. Instead, we consider the spatial averaging to 0.25°x0.25° sufficient to smooth out these small-scale biases. Analogous to the overcast areas, there is also no correction for terrain topography in clear-sky conditions.

3.1.6.b. The resulting TOA albedo is lower than 6%

In some cases the resulting TOA albedo is much too low because the surface type is erroneously assumed "water" whereas in reality it's "mixed water/land" or "completely land". As a consequence, the wrong narrowband-to-broadband regression is used, leading to an underestimated broadband reflectance. This kind of surface type mismatch typically happens in coastal zones (Figure 31). Therefore, coastal water pixels with **any** albedo lower than 6% (even in the 0-4% range) are corrected to 6% and considered "valid". In all other situations, the same correction is applied but only in the 4-6% range, while an albedo below 4% is always set to "invalid".

3.1.6.c. Order of corrections

The corrections are done in the following order (with an if-else logic to increase computational efficiency):

- Albedo>120%: final albedo value is (always) set to missing value. Bitflag BITFLAG_ERROR is added.
- Albedo between 100%-120% :
  - SZA>60° **and** cloudcover>50%: albedo allowed to exceed 100% (max 120%). Bitflag BITFLAG_CORR added.
  - SZA<60° or cloudcover<50%: albedo set to missing value. Bitflag BITFLAG_ERROR added.
- Water pixel in 'coastal zone' (incl. rivers): Albedo between 0%-6%? → final albedo value set to 6% *[Note: for coastal water pixels, albedo cannot be lower than 6% (these are often actually mixed or land, misleading the NTB). This feature can be disabled using the configuration file flag FLAG_COASTAL_CORRECTION].* Bitflags BITFLAG_CORR and BITFLAG_COAST are added.
- Albedo <4%: albedo value set to missing value. Bitflag BITFLAG_ERROR is added.
- Albedo between 4%-6%: albedo set to 6%. Bitflag BITFLAG_ERROR is added.

An example of the resulting TOA shortwave (broadband) albedo is shown in Figure 40.

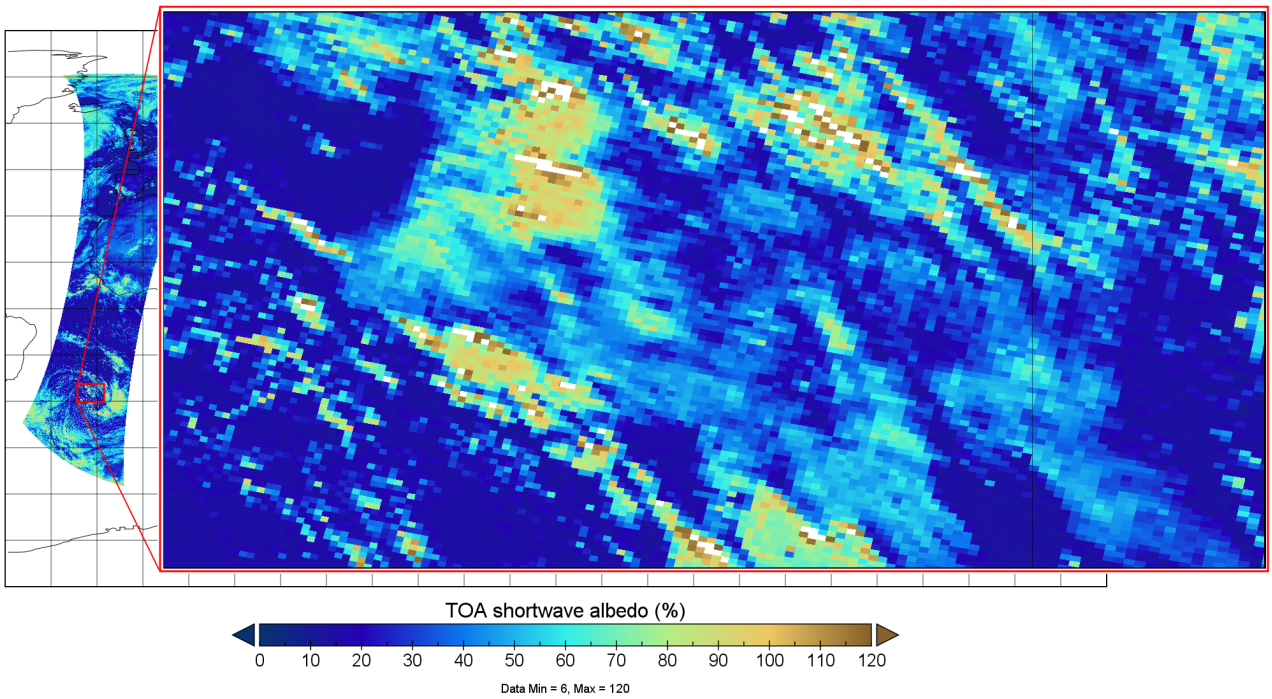

Figure 40: Example of variable 'SW_alb_bb' (broadband SW albedo) on GAC orbit grid

Clearly visible are some white pixels (missing value), which are invalid because their TOA albedo exceeds 120%. The dark brown colored pixels are situated in the 100-120% range and are only allowed because they represent clouds with SZA>60%.

3.1.7. Output

The output of Program Part 1 consists of a single Netcdf file with spatial dimensions and properties identical to the input file (i.e. the GAC orbit grid). The following variables are stored in this output file, and will subsequently be used in Program Part 2 (aggregation to regular grid, Section 3.2) and serve as input for the Surface Radiation processing [RD 5].

- Shortwave albedo, instantaneous (%), an example is provided in Figure 41.
- Shortwave broadband reflectance, a.k.a. isotropic albedo, instantaneous (%)
- Wind speed (m/s) → *only for clearsky ocean pixels*
- Cloud optical thickness, and Cloud phase → *only for overcast pixels*
- Fresh snow cover (%)
- Cloud cover (%) → *binary, so only 0% or 100%, an example is provided in Figure 42.*
- Time → *UNIX time, i.e. seconds since 1/1/1970*
- CERES Surface type (1-8)
- Sea ice concentration (%) → *only for (at least partly) sea ice covered pixels*

- Bit flags, and Bit flag variable ID
- Longitude (°E) and Latitude (°N)
- Viewing zenith angle (°)

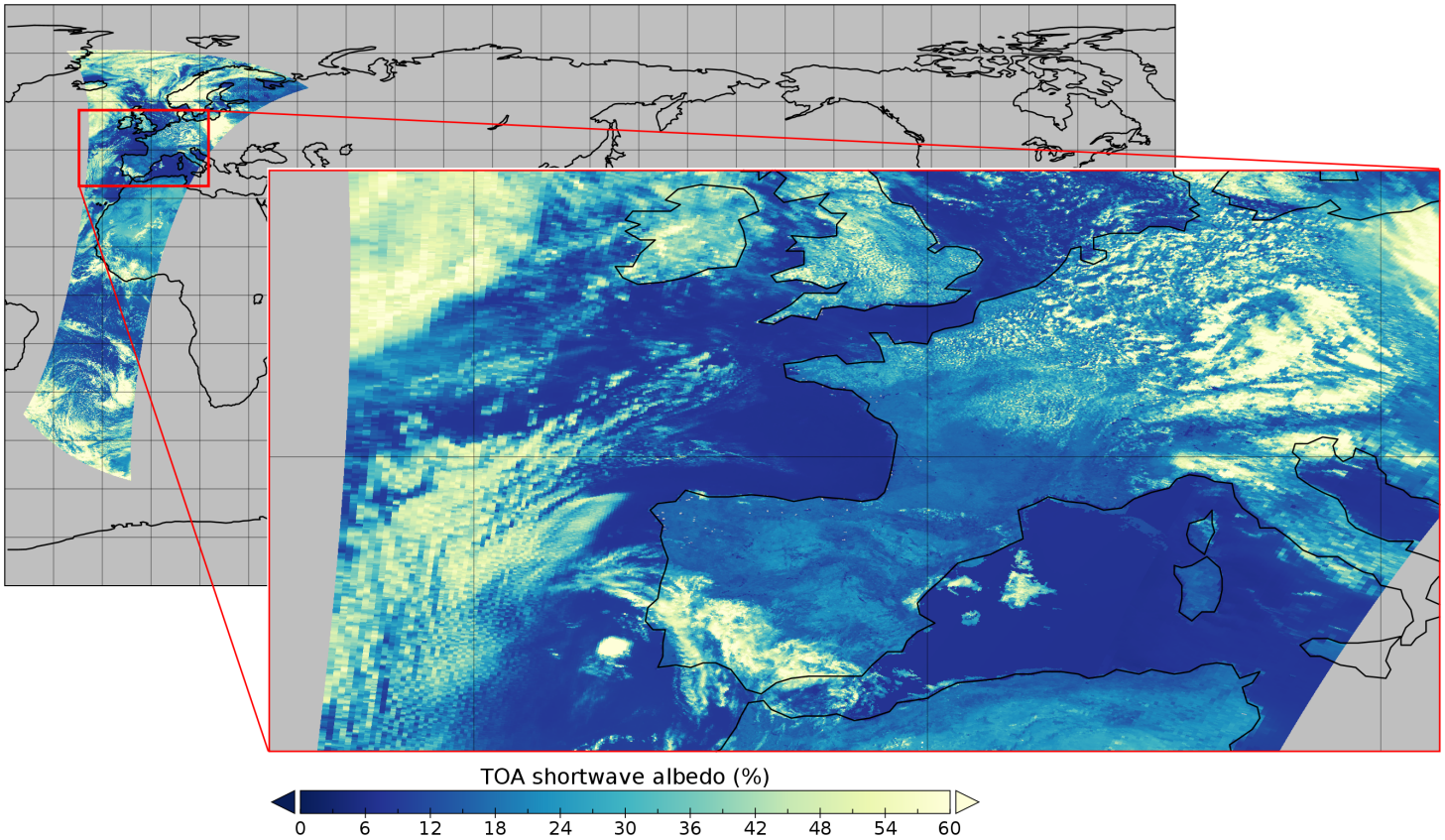

Figure 41: Example of final output "TOA SW albedo" ('SW_alb_bb') on GAC orbit grid

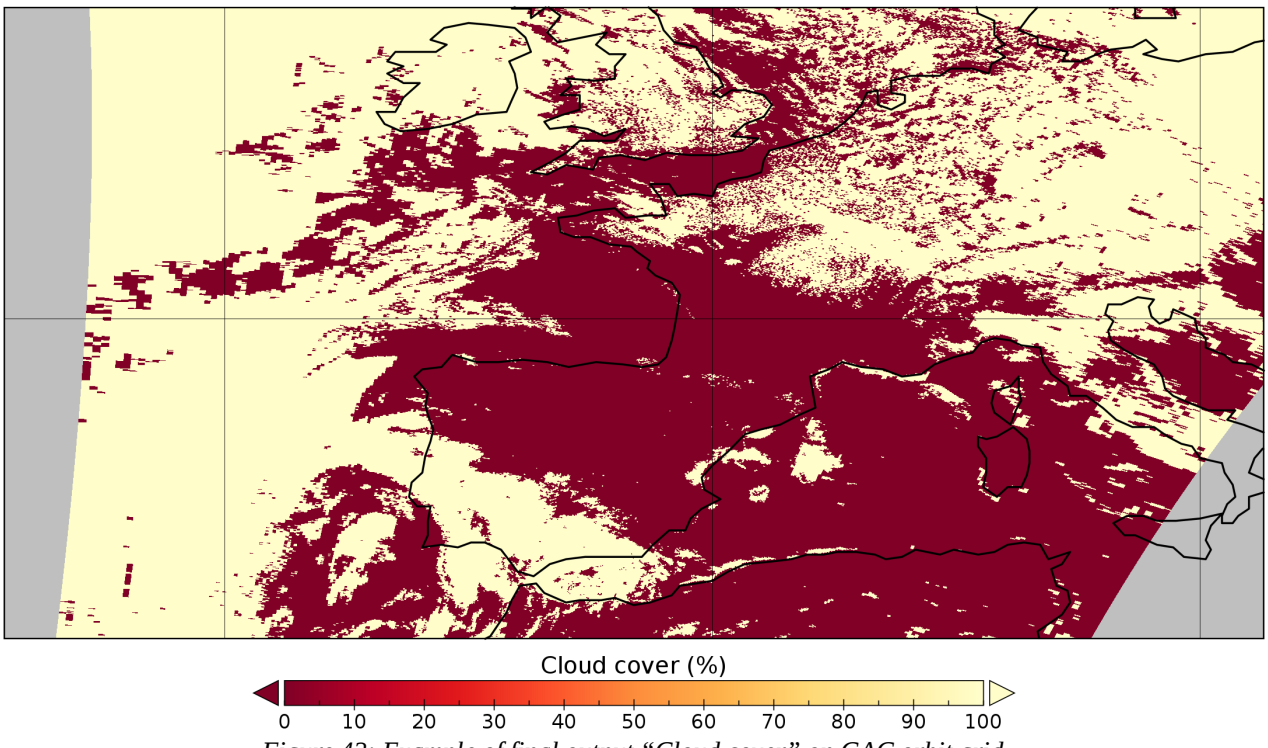

Figure 42: Example of final output "Cloud cover" on GAC orbit grid

3.2. Part 2: Spatial aggregation from GAC orbit grid to regular CMSAF grid (level-2b)

Program Part 2 mostly consists of remapping and aggregating all the output of Part 1 (Section 3.1.7) to a regular lat-lon grid (0.25°x0.25°). It is an optional program, and by default called as a routine [*TOA2AGGR()*] in Program Part 1, but it may also be used as standalone binary.

3.2.1. Twilight coefficients

The twilight linear regression coefficients A (intercept) and B (slope) are determined in Program Part 2 for each individual AVHRR pixel, just before they are aggregated to the 0.25°x0.25° grid. In fact, this determination could as well be done in Program Part 1, since it is applied per individual AVHRR pixel level (GAC orbit grid), but for practical reasons it's moved to the second program part[16].

The determination consists of selecting the proper A and B coefficients from the table supplied as input data (Table 3 in Section 2.4.7), which depends on the scene type, i.e. the combination of *TWL surface type* and cloud cover. A_c en B_c are the clear-sky coefficients, A_o en B_o are the overcast coefficients (Table 3). There is no need for cloud cover weighting, since the cloud mask is binary (either overcast or clear-sky). However, for surface type there is some need for weighting, more specifically for the sea ice: the TWL surface type "***(1) sea ice, 100%***" is for pure sea ice surfaces. Hence, a weighted average is made for sea ice and water depending on their relative areal share of sea ice in the pixel.

3.2.2. Aggregation procedure

All the variables included in the output of Program Part 1 (Section 3.1.7) are remapped from their irregular *GAC orbit grid* to a regular lat-lon grid with a spatial resolution of 0.25°x0.25°, using the nearest neighbor method. The aggregated value is calculated as the average of all contributing GAC/AVHRR pixels in each 0.25°x0.25° grid box. As an example, Figure 43 shows the remapped and aggregated result obtained from the original TOA albedo (Figure 41).

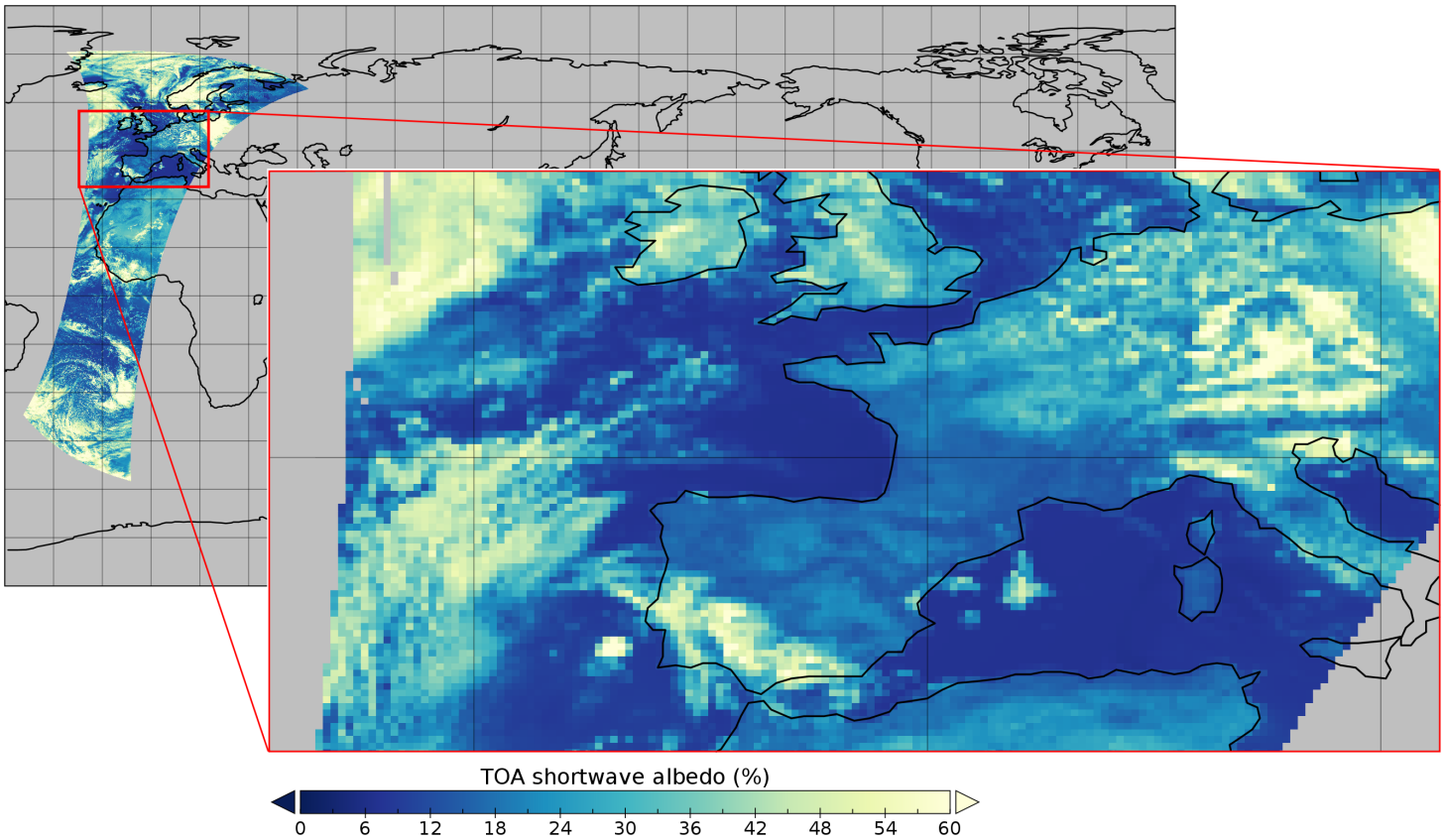

Figure 43: Example of output "TOA albedo" (SW_alb_bb) aggregated on CMSAF 0.25° grid

16 *Since the twilight coefficients could still be subject to updates, only Program Part 2 has to be re-run (and not also Program Part 1 which is much more computationally demanding).*

Due to the increasing AVHRR footprint size (caused by the VZA-dependent area projection, as well as by the earth's curvature), the number of AVHRR pixels ('observations') contributing to a single 0.25°x0.25° aggregated grid box typically decreases from nadir towards swath edges (Figure 44).

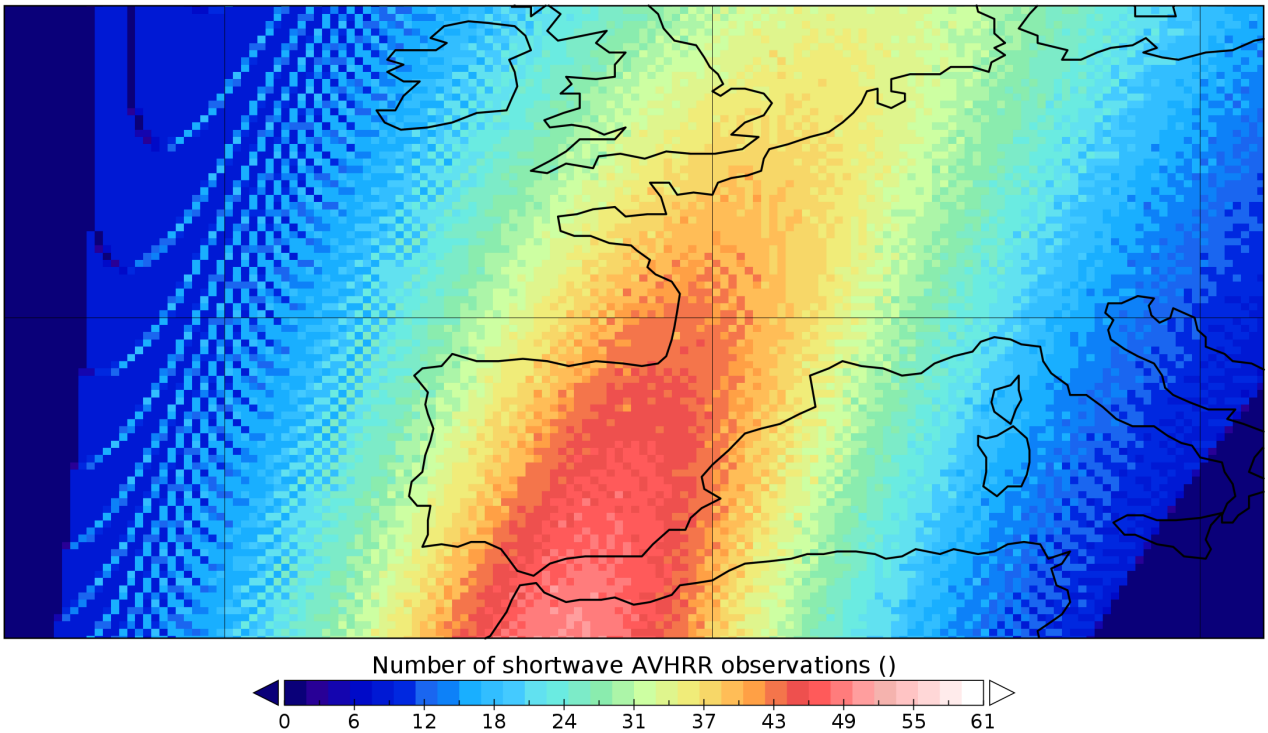

Figure 44: Example: Number of GAC pixels contributing to each CMSAF 0.25°x0.25° grid box

Near the swath edges, only about 8 AVHRR pixels per grid box are counted; decreasing the grid box size to e.g. 0.05°x0.05° (i.e. decreasing it's area by factor 25) would thus introduce large gaps in the orbit and prevent a spatially continuous analysis. There is also a latitudinal effect: towards the poles, a decrease of AVHRR pixels per grid box is observed, due to the decreasing area of a grid box as a consequence of the regular lat-lon projection.

Due to the aggregation, some (originally binary) variables, such as cloud cover and cloud phase, become fractional. As an example, Figure 45 shows the remapped and aggregated result obtained from the original cloud cover (Figure 42).

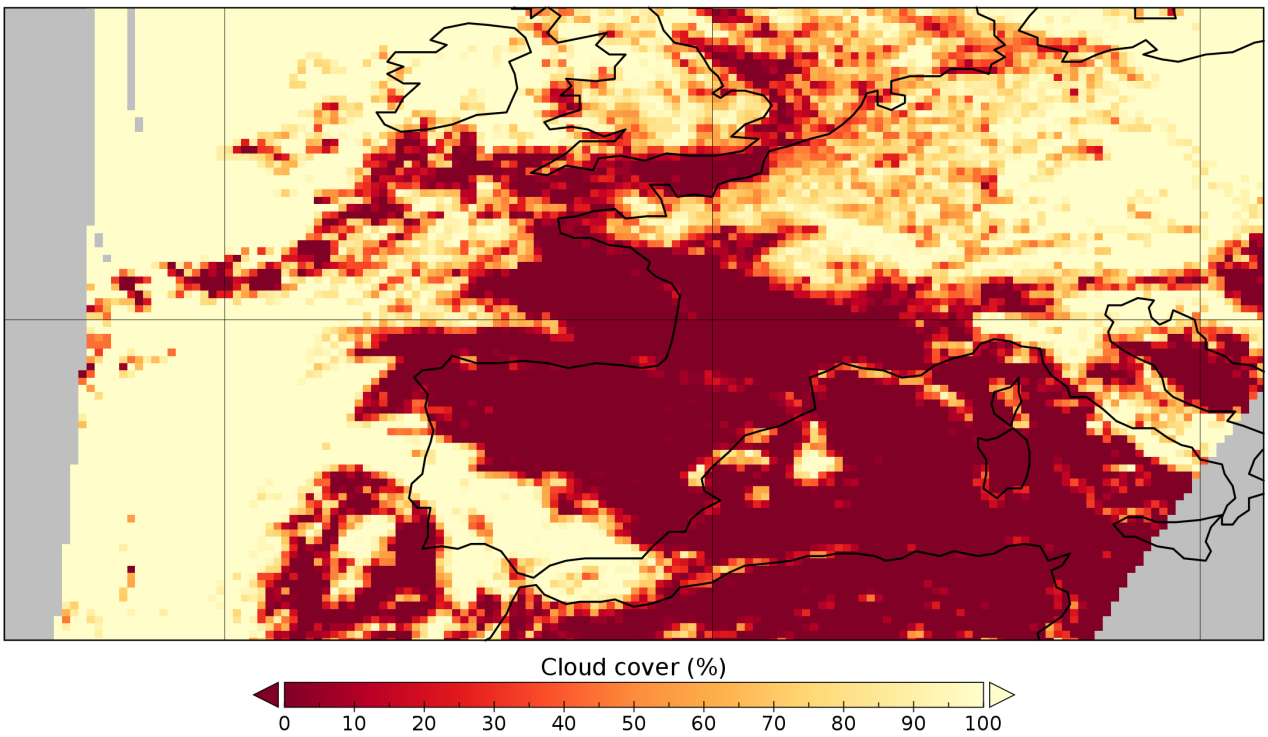

Figure 45: Example of output "Cloud cover" aggregated on CMSAF 0.25° grid

3.2.2.a. Treatment of overlapping orbits

The beginning and ending of a *GAC orbit grid* (i.e. input and output grid from Program Part 1) may sometimes have a considerable spatial overlap; an example can be seen in Figure 46, showing the variable "UNIX time" for each AVHRR pixel (the overlapping region effectively consists of two overlapping data layers, from which only the orbit ending is visible, and sits on top of the orbit start). In those cases, the aggregation of several GAC pixels into a single 0.25°x0.25° grid box is done by using pixels from either the beginning **or** from the ending, but never a mixture of both. The reason is that this time stamp should not be averaged because the temporal information is needed in Program Part 3 (diurnal cycle modeling; Section 3.3) and should be as close as possible to the real observation time.

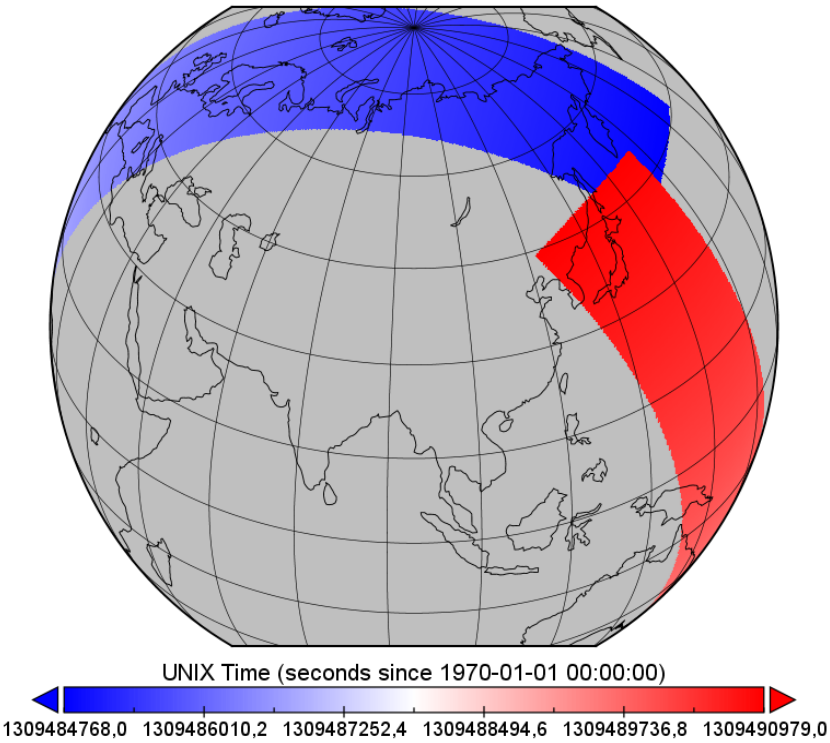

Figure 46: Example of variable 'UNIX Time' with overlapping start and end of GAC orbit grid

During the iteration over all AVHRR (GAC) pixels, every AVHRR pixel is assigned to a CMSAF grid box according to its longitude and latitude coordinates, but only if one of the following three criteria is fulfilled:

- it concerns the first AVHRR pixel assigned to the corresponding CMSAF grid box
- the time difference between current and previous AVHRR pixel is less than 60 seconds (strong indication that it doesn't belong to an overlapping part of the *GAC orbit grid*)
- (*in case the second criterion is not met, i.e. the time difference is >60 seconds*): VZA is more than 5 degrees closer to Nadir (where VZA=0°). This guarantees that in case of grid overlap, only the AVHRR pixels having a significantly better VZA are selected in favor of the overlapping orbit. In this case, the aggregated CMSAF grid box is reset (i.e. existing contributions of AVHRR pixels are removed) and aggregation starts again but now only for the favorable orbit with better VZA.

To illustrate this process, the previously shown example of overlapping orbit (Figure 46) is used again, but now showing the variable "Viewing Zenith Angle" (Figure 47).

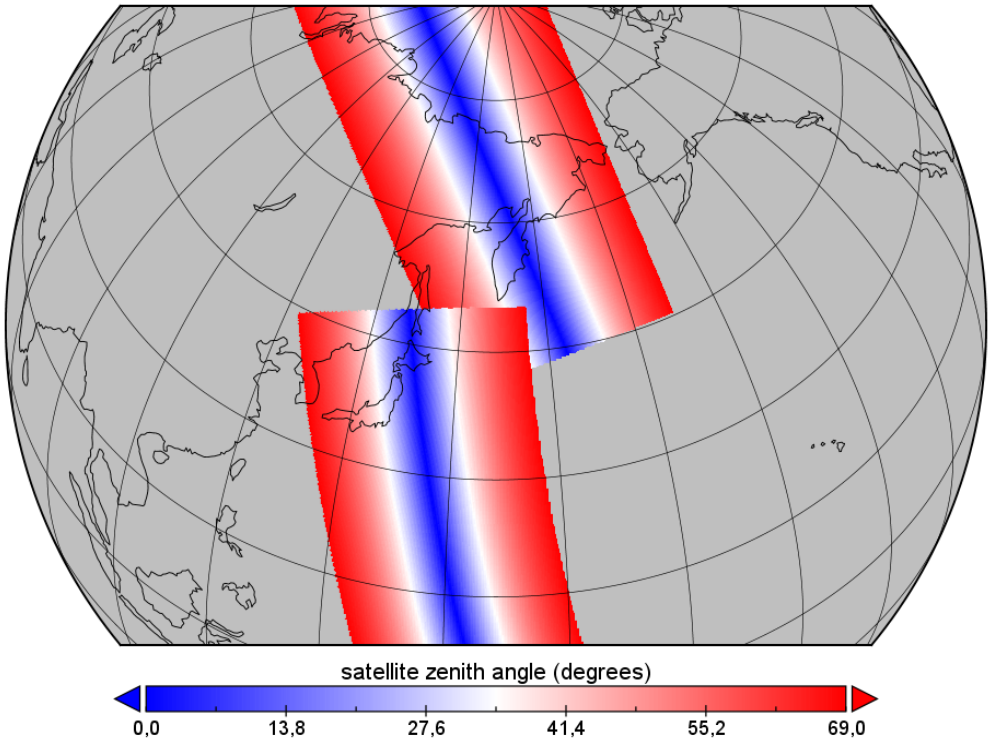

Figure 47: Example of variable 'VZA' with overlapping start and end of GAC orbit grid

Within the overlapping region, it can be seen that the VZA is different for the start and for the end of the orbit. It will determine which part of the orbit is preferred to perform the aggregation. Figure 48 then shows the final aggregated result, but here again in terms of (UNIX) time, similar to Figure 46. As can be seen from the aggregated result, the overlap is split roughly 50%-50% between orbit start and orbit end, with each part allocated to the lowest VZA.

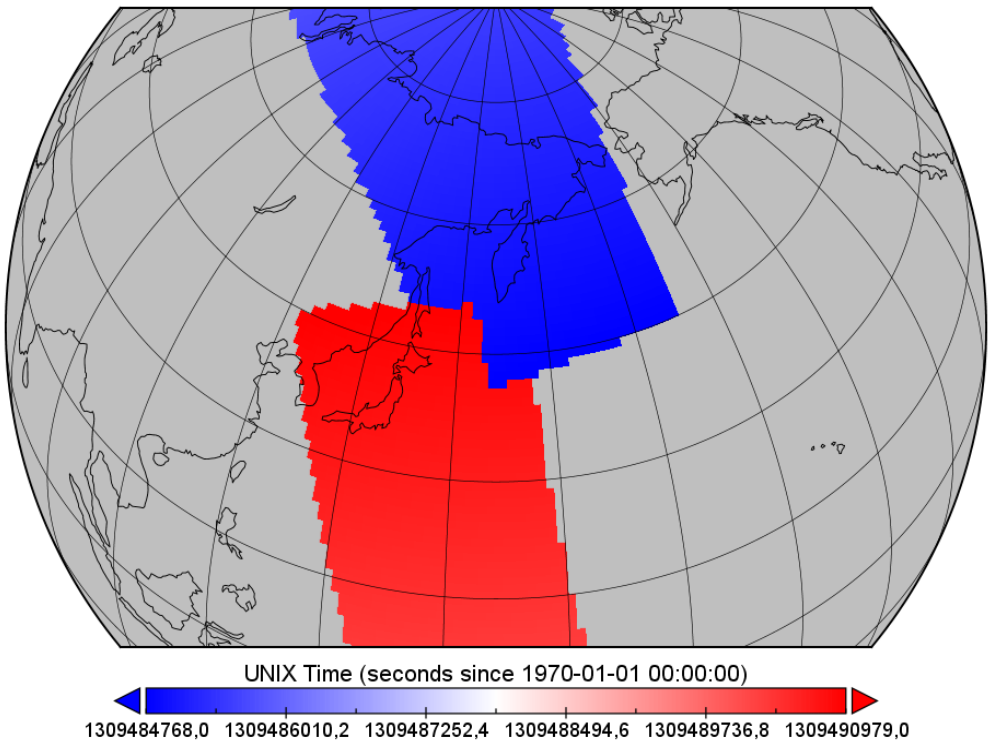

Figure 48: Example of variable 'UNIX Time' after aggregation (no overlap anymore).

3.2.3. Nested 0.25° Processing Grid

In Program Part 2, all output fields from Program Part 1 are remapped from their irregular '*GAC orbit grid*' to the regular (lat-lon) 0.25°x0.25° CMSAF grid. However, such a regular grid causes an enormous pixel size distortion towards the poles (per unit area: a lot more pixels which each are a lot smaller), an example of which is shown in

Figure 49 (depicting a 0.25°x0.25° grid, mapped with an orthographic projection). This is a major disadvantage of using regular lat-lon grids.

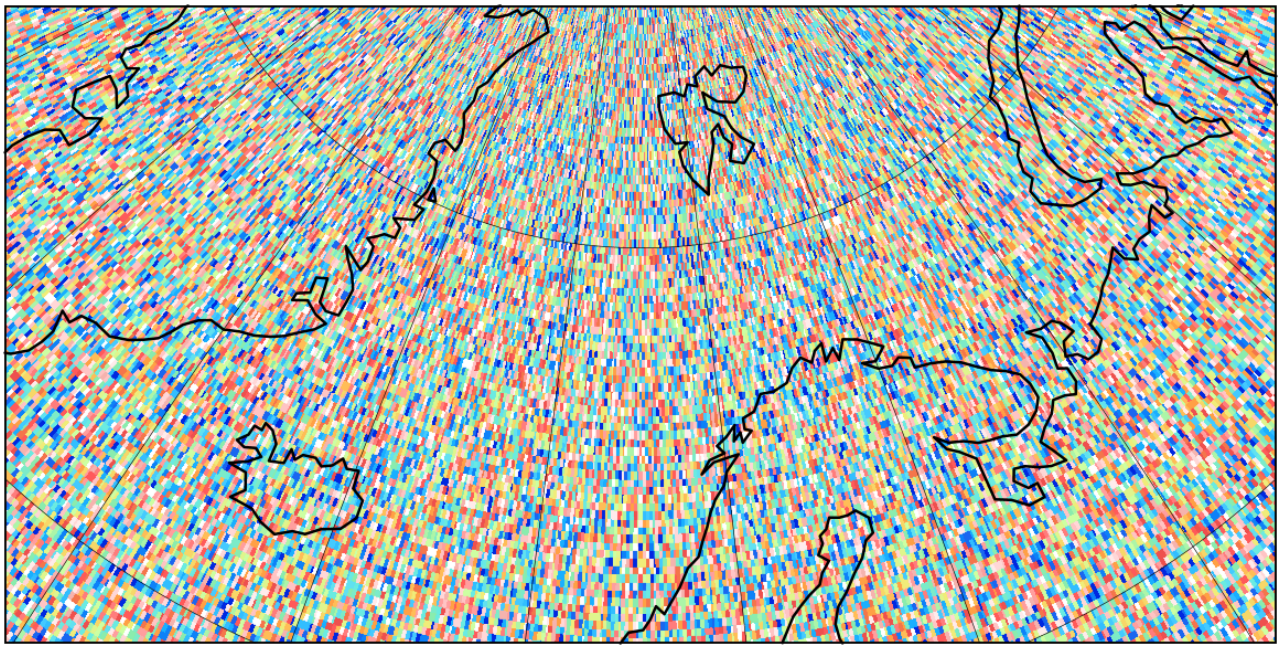

Figure 49: non-nested regular CMSAF grid 0.25°x0.25° (orthographic projection)

To solve this issue, during the remapping, the grid boxes are systematically merged –in longitudinal direction– towards both poles (N and S) according to their combined area; this does not mean that a true "equal area" grid is created, but rather that the enormous areal distortions towards both poles are minimized. The concept is similar to what is done operationally in the CERES processing[17].

This alternative 'nested' grid configuration is based on a set of objective criteria:

- For each latitude, all merged pixels should be completely merged (i.e. no half-merged pixels). With other words, the number of merged pixels per latitude should be an integer (i.e., the longitudinal merged pixel size should be a divisor of 1440, which is the total number of original 0.25°x0.25° pixels per latitude).
- The merged pixel area can never exceed the maximum original pixel area, corresponding to the area of a 0.25°x0.25° grid box at the equator (772,8 km²). For instance, when iterating latitudes from equator towards the North pole, merging two neighboring pixels can only occur if the combined pixel size decreases below 772,8km², which happens at 60°N (Figure 50).

17 *URL: https://ceres.larc.nasa.gov/data/general-product-info/#ceres-nested-10-processing-grid*

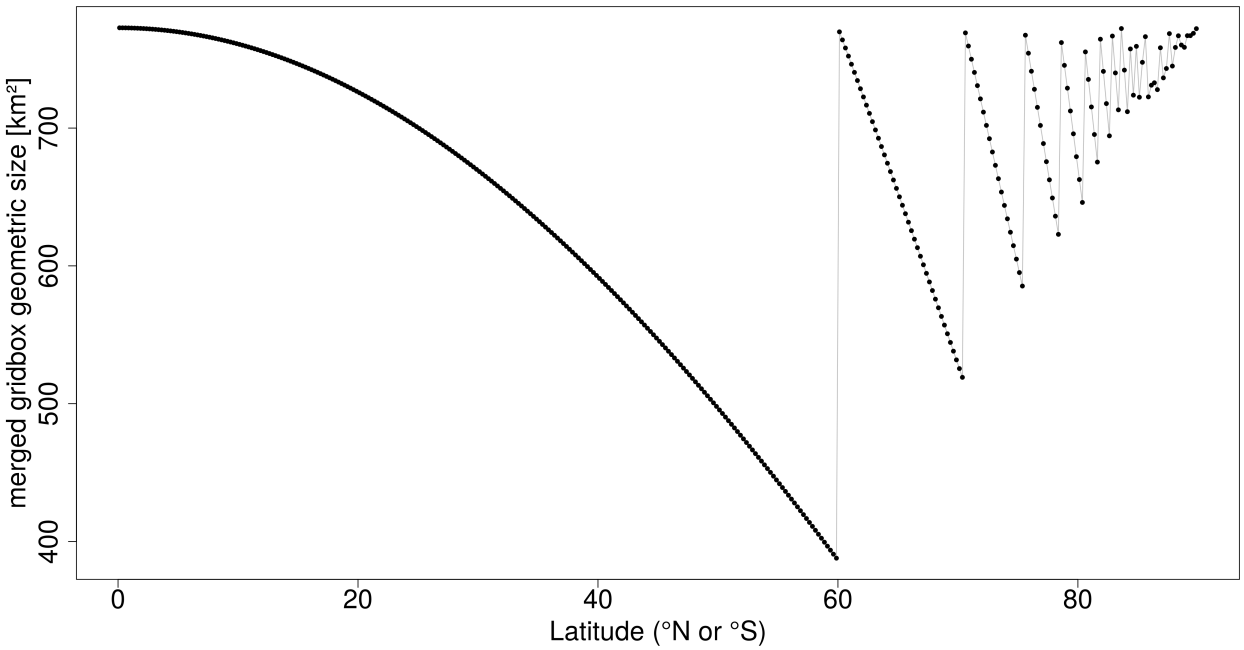

Figure 50: Nested grid box size (km²) as function of latitude (°).

The resulting nested grid is summarized in Table 10.

Table 10: Latitude segments of nested grid

Latitude Segment (°N or °S)	# of zones* in segment	Longitudinal pixel count	Longitudinal pixel extent (°)
Equator to 60.00°	**240**	**1440**	**0.25°**
60.00°-70.50°	42	720	0.50°
70.50°-75.50°	20	480	0.75°
75.50°-78.50°	12	360	1.00°
78.50°-80.50°	8	288	1.25°
80.50°-82.75°	9	240	1.50°
82.75°-83.50°	3	180	2.00°
83.50°-84.25°	3	160	2.25°
84.25°-85.25°	4	144	2.50°
85.25°-86.00°	3	120	3.00°
86.00°-86.50°	2	96	3.75°
86.50°-86.75°	1	90	4.00°
86.75°-87.25°	2	80	4.50°
87.25°-87.50°	1	72	5.00°
87.50°-88.00°	2	60	6.00°
88.00°-88.25°	1	48	7.50°
88.25°-88.50°	1	40	9.00°
88.50°-88.75°	1	36	10.00°
88.75°-89.00°	1	30	12.00°
89.00°-89.25°	1	24	15.00°
89.25°-89.50°	1	16	22.50°
89.50°-89.75°	1	10	36.00°
89.75°-90.00°	1	3	120.00°
Total (global)	***180***		
(*) a single 'zone' is a row of pixels, only varying in longitude, so 1x1440 pixels.			

An illustrative example of the varying pixel width in longitudinal direction is given for Northern Europe (Figure 51), showing the gradient between nested pixels sized 0.25°x0.25° (South) to nested pixels sized 0.25°x120° (North). Note that the map is not projected, so it's a regular 'flat' lat-lon representation.

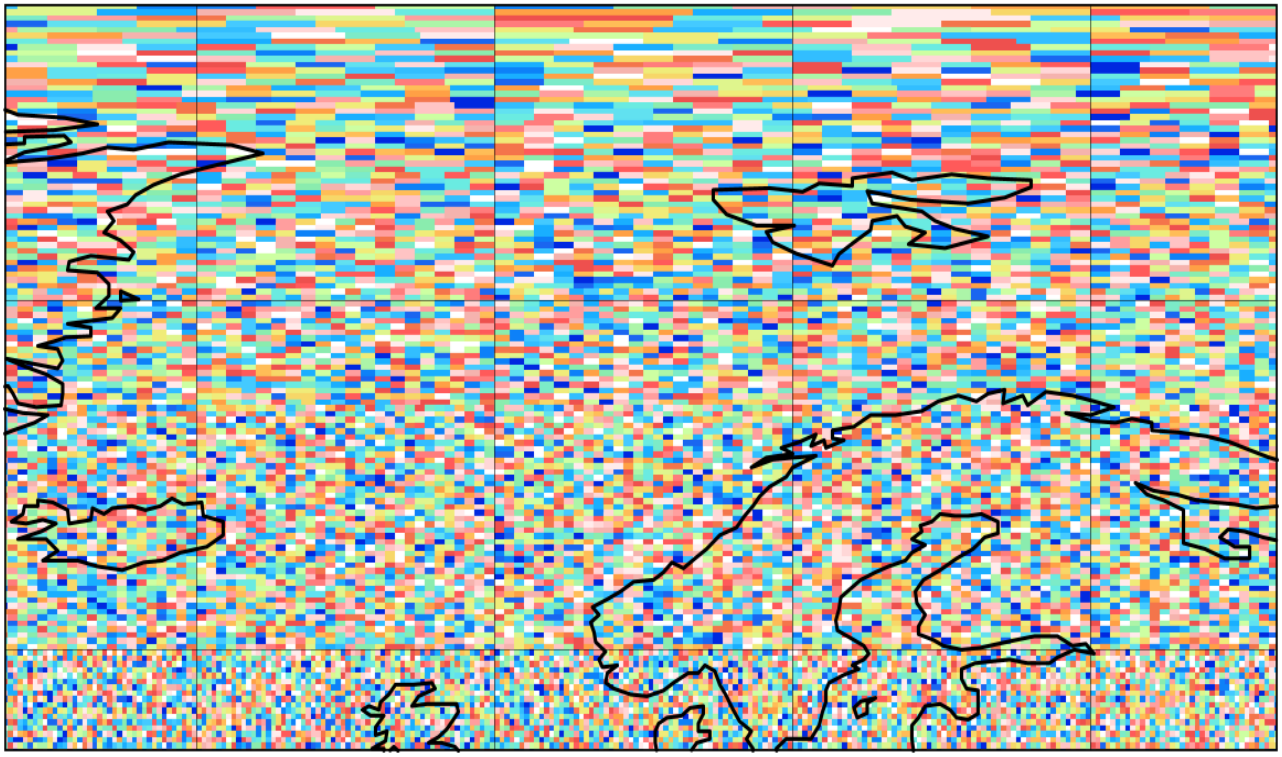

Figure 51: nested regular CMSAF grid 0.25°x0.25° (unprojected, a.k.a. plate carrée)

The advantage of using a nested grid becomes clear when it is shown on a projected map, in this case using an orthographic projection, showing pixels that are much more uniform in size (Figure 52; to be compared with original grid in Figure 49).

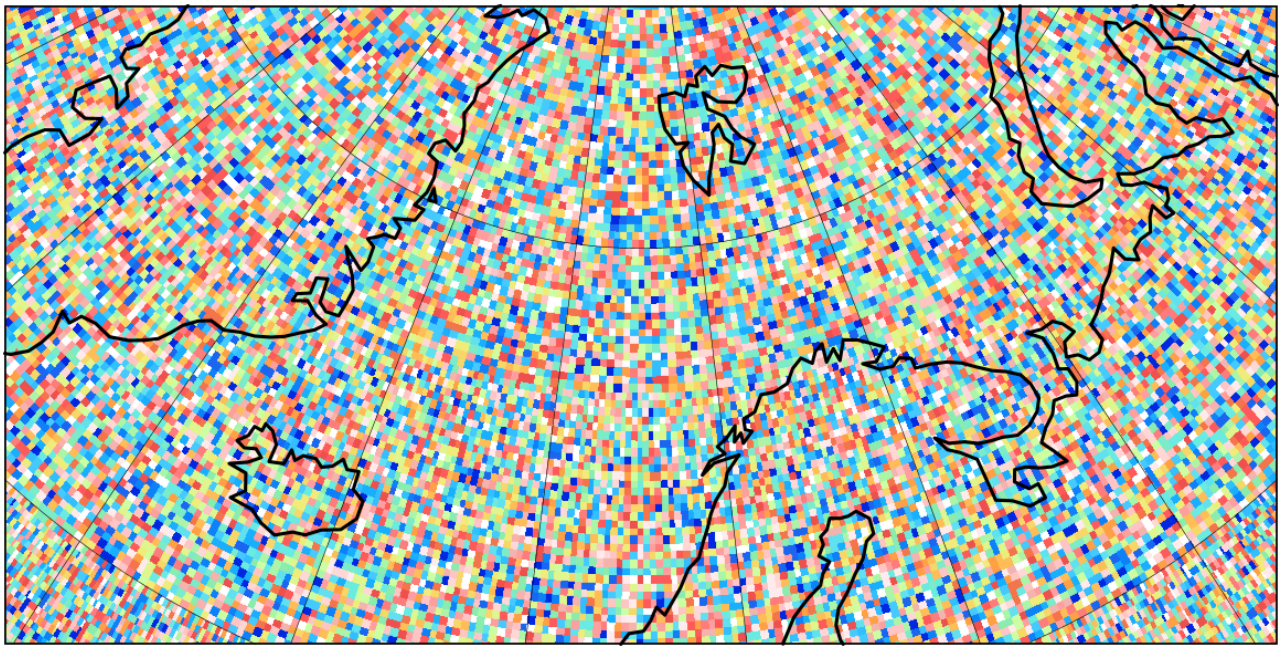

Figure 52: nested regular CMSAF grid 0.25°x0.25° (orthographic projection)

After the Level-3 processing (Sections 3.3 and 3.4), the CLARA-A3 TOA nested grid output is converted back into a regular lat-lon (equal angle) grid, as specified in the CMSAF CLARA-A3 products requirements. However, the user should be aware that a significant number of pixels are 'oversampled' due to nested grid structure. This also has implications for validation: when comparing 1:1 to a reference dataset with the same spatial resolution (1440x720

pixels, i.e. 25°x25° globally), the reference dataset should first be re-gridded to the same nested grid as CLARA-A3. As the spatial variability within CLARA-A3 "nested grid cells" is per definition zero, it will consequently introduce artificial bias w.r.t. the reference dataset if the latter does have spatial variability in those regions. In fact, this is similar to the principle of validating a high-resolution product with a low-resolution reference, for which the high-resolution product should always be aggregated to match the grid of the low-resolution reference data.

3.2.4. Output

The output of Program Part 2 consists of a single Netcdf file with spatial dimensions 1440x720, structured in a global regular lat-lon grid with 0.25°x0.25° resolution. The following variables are stored in this output file, and will subsequently be used in Program Part 3 (calculation of diurnal cycle and daily mean):

1. *Longwave flux aka OLR, instantaneous (W/m²) → see Section 4.*
2. *Longwave processing counts (number of AVHRR GAC pixels contributing to the aggregated longwave 0.25°x0.25° pixel) → see Section 4.*
3. Shortwave albedo, instantaneous (%)
4. Shortwave processing counts *(number of AVHRR GAC pixels contributing to the aggregated shortwave 0.25°x0.25° pixel)*
5. Shortwave sunglint counts (number of AVHRR GAC pixels contributing to the aggregated shortwave 0.25°x0.25° pixel, and which are characterized by sunglint)
6. Wind speed (m/s) → only for (at least partly) clearsky ocean pixels
7. Cloud optical thickness → only for (at least partly) cloudy pixels
8. Cloud phase → only for (at least partly) cloudy pixels
9. Twilight coefficient 'A'
10. Twilight coefficient 'B'
11. Fresh snow cover (%)
12. Cloud cover (%)
13. Time → *UNIX time, i.e. absolute seconds since 1/1/1970*
14. Fraction of surface type 1, water (%)
15. Fraction of surface type 2, dark vegetation (%)
16. Fraction of surface type 3, bright vegetation (%)
17. Fraction of surface type 4, dark desert (%)
18. Fraction of surface type 5, bright desert (%)
19. Fraction of surface type 6, permanent snow/ice (%)
20. Fraction of surface type 7, fresh snow (%)
21. Fraction of surface type 8, sea ice (%)
22. Sea ice concentration (%) → only for (at least partly) sea ice covered pixels

3.3. Part 3: Processing of instantaneous albedo to daily mean RSF (level-3)

3.3.1. Overview

Program Part 3 reads the instantaneous Level-2 albedo observations remapped on regular 0.25°x0.25° grid (i.e. output from Program Part 2) and integrates these to a daily mean SW flux on the same 0.25°x0.25° grid. This Level-3 output consists of two NetCDF files per day: one containing all shortwave quantities, the other containing all longwave quantities. A 'day' is understood in terms of UTC time, i.e. considered identical for all grid boxes 00:00:00UTC-23:59:59UTC; to stress this fact, it will be referred to as "*UTC day*".

By default, **bit flags** in Program Part 3 are set to zero (similar to Program Part 1), and may be modified during the processing; their main purpose is to deliver pixel-specific information about the processing, including potential reasons for increased uncertainty, or even for missing output. The total bit flag value is composed of multiple bits each representing a separate binary flag. A complete overview of all the flag meanings can be found in Appendix 9.6.3 (Table 23).

Program Part 3 reads as input (a list containing) all instantaneous 0.25°x0.25° ***Level-2 orbit files*** belonging to previous, current and next *UTC day*; the number of files mostly depends on the number of satellites during that period and may vary roughly between 30 and 240. An example of a single *Level-2 orbit file* is shown in Figure 43.

First, a (global) spatial iteration starts over all 0.25°x0.25° grid boxes, i.e. in total 1440x720 iterations. All the steps described below are performed for every single one of these grid boxes:

For each 0.25°x0.25° grid box, the UTC day (24 hours) is subdivided in 288 temporal bins of 5 minutes each (*referred to as "5min bins"*)[18]. For every of these temporal *5min bins*, the solar zenith angle is calculated based on location and time. This allows the day to be subdivided in 3 types of *5min bins* (Figure 53), corresponding to 3 components of the daily mean, which are processed separately:

- daylight bins, for which SZA<84° (Section 3.3.2)
- twilight bins, for which 84°≥SZA>100° (Section 3.3.3)
- nighttime bins, for which SZA≥100° (Section 3.3.4)

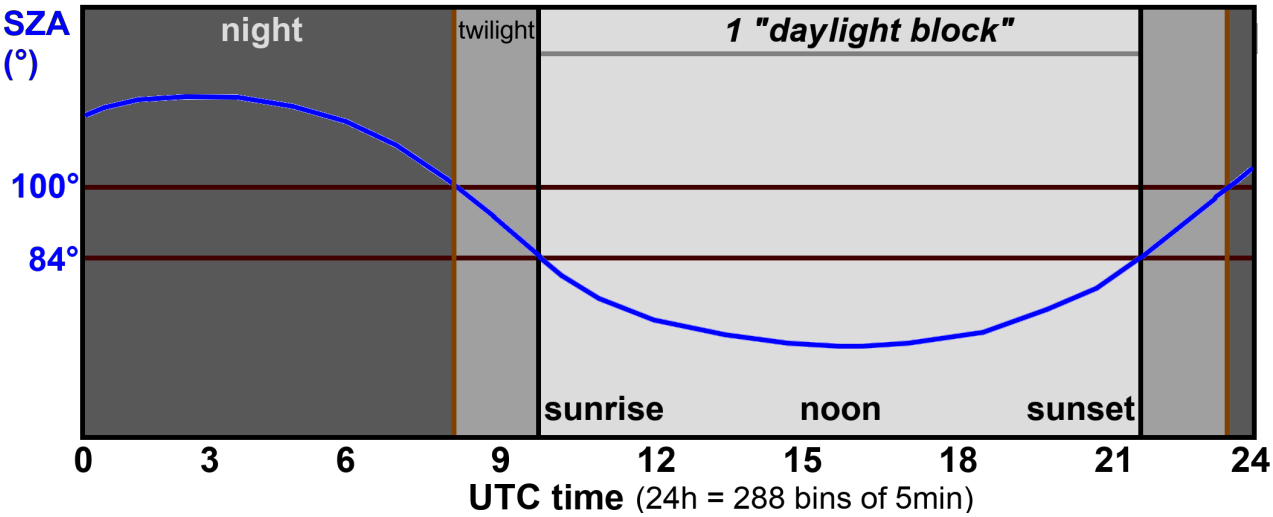

Figure 53: SZA for all temporal "5min bins" during a single UTC day on a single 0.25°x0.25° grid box. In this example, there is only one relevant Day Light Block.

3.3.2. Daylight conditions (SZA<84°): modeling albedo diurnal cycle

A consecutive time period of *5min bins* with daylight conditions (SZA<84°) is called a "*daylight block (DLB)*" (Figure 53). Depending on the grid boxes' location, a single UTC day may contain (or overlap with) more than one DLB.

A second (nested) iteration loops over the different Day Light Blocks (mostly only one or two), in which each DLB is processed separately:

The variables "UNIX time" (*Figure 46; variable #13 in Section 3.2.4*) and "number of contributing AVHRR pixels" (*Figure 44; variable #4 in Section 3.2.4*) are extracted from all the *Level-2 orbit files* (that were loaded at the start of Program Part 3) for the current 0.25°x0.25° grid box's coordinates, resulting in 2 corresponding vectors, each with as much elements as there are *Level-2 orbit files*. We refer to these 'elements' as '*Level-2 observations*': From these, only the observations are kept that follow both these requirements:

1. The observation's UNIX time falls within the temporal range of the day light block (about 10:00h to 21:30h UTC in the example of Figure 53).
2. The observation's number of contributing AVHRR pixels is higher than zero. Note that this is mostly not the case: indeed, one Level-2 orbit file spatially covers only a single orbit, so most of the global (1440x720) grid boxes have no (zero) AVHRR pixels.

The resulting selection of Level-2 observations (for current 0.25°x0.25° grid box) are referred to as "*valid observations*". Each *valid observation* is 'assigned' to the temporally nearest *5min bin* (more specifically to its bin center). In cases where more than one observation falls within the same 5min bin, priority is given to the observation with the lowest temporal difference with the 5min bin center.

Temporal interpolation

18 *Technically, also the previous and next day are included, resulting in 864 bins of 5 minutes each*

The temporal interpolation method used here, called "*constant meteorology method*", has been documented extensively by Young et al. (1998) and used subsequently in the CERES processing, where it is also called the "*CERES-only (CO) method*" (Doelling et al., 2013).

An illustrative example for a hypothetical DLB is shown in Figure 54, showing a DLB having 2 '*valid observations*', in this case from a NOAA-17 and a NOAA-16 orbit file. Each observation has an associated scene type, i.e. combination of surface type and cloud properties (cover, phase, optical thickness): this is simplified in the conceptual example, which just shows respectively 'overcast' and 'clearsky'.

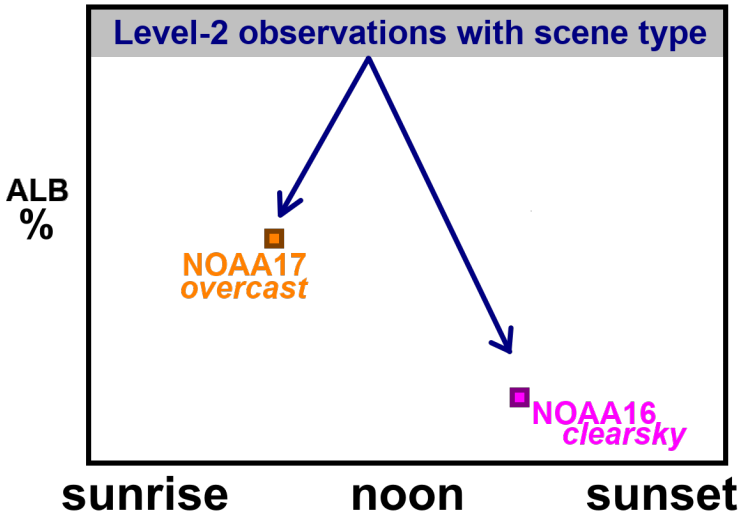

Figure 54: Conceptual example of modeling the albedo diurnal cycle (step 1)

Then, an iteration is started over all valid observations associated with the DLB (in this example that would be 2). The scene type of each observation is used to select its corresponding **albedo model**, which describes the **average diurnal cycle** of TOA albedo depending on the Solar Zenith Angle (Figure 24; Section 9.1). Each *5min bin* of the DLB has its own solar zenith angle (Figure 53), and hence can be assigned an albedo value based on the selected albedo model. This is shown for the first observation (NOAA-17; overcast) in Figure 55.

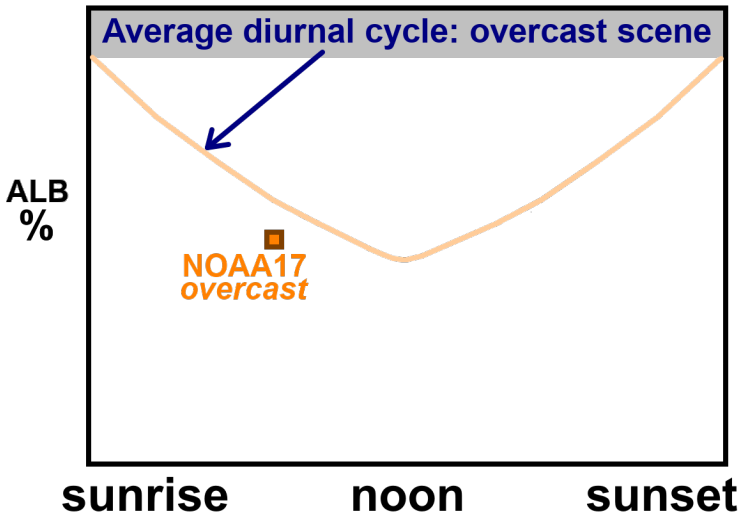

Figure 55: Conceptual example of modeling the albedo diurnal cycle (step 2)

Normally, the diurnal cycle's albedo shouldn't be too far off the observed albedo, but there will be a difference in most cases because the albedo model provides an average value and not an instantaneous observation. However, rather than the absolute magnitude, it's mostly the shape of this curve which is important. Therefore, the diurnal cycle curve (albedo model) is scaled so that it matches the observation, as shown in Figure 56. This is done by first calculating the ratio of observed to modeled albedo in the *5min bin* containing the observation: this ratio is subsequently multiplied with the modeled albedo in each of the 5min bins to obtain the **scaled diurnal cycle** (i.e. scaled albedo model) that matches the observation (Equation 4 in Young et al., 1998).

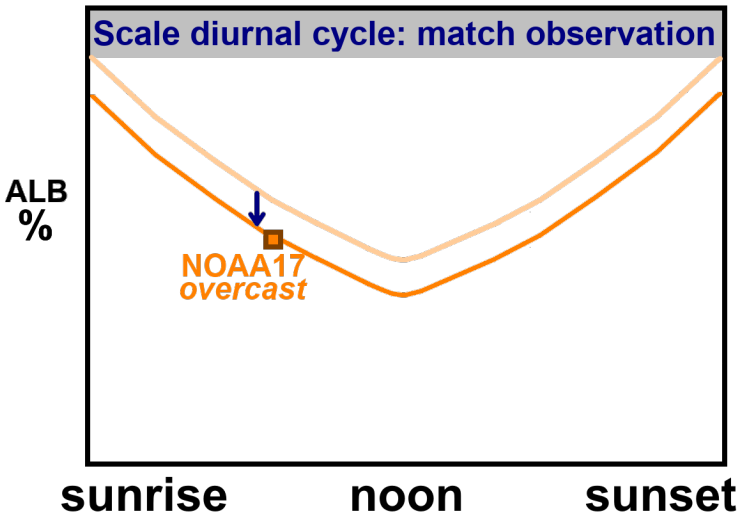

Figure 56: Conceptual example of modeling the albedo diurnal cycle (step 3)

Some situations require additional corrections. For instance when an observation around solar noon (lowest albedo during the day) has a relatively **high observed albedo with 'flat' diurnal cycle** (*e.g. 60%, typically overcast with high optical thickness*) but due to errors in the auxiliary input data (e.g. cloud mask), and hence scene type, the **diurnal cycle is much lower and more curved** (*e.g. 30%, typically lower cloud cover and/or lower optical thickness*): the scaling could then lead to albedo's exceeding 100% around sunrise and sunset. In these cases, iterative corrections are applied to correct the scene type: +25% cloud cover (until it reaches maximum) and +15 optical thickness (until it reaches maximum), which 'flattens' the albedo model and hence decreases the risk of excessive scaling (which would lift albedo's over 100%). As soon as the (iteratively modified) diurnal cycle does not exceed 100%, it is accepted.

The iteration will then proceed to the next observation, in this example NOAA-16 with clear-sky scene type. The same steps are applied to this observation, i.e. determination of the albedo model's diurnal cycle (Figure 57) and scaling of the albedo model's diurnal cycle (Figure 58).

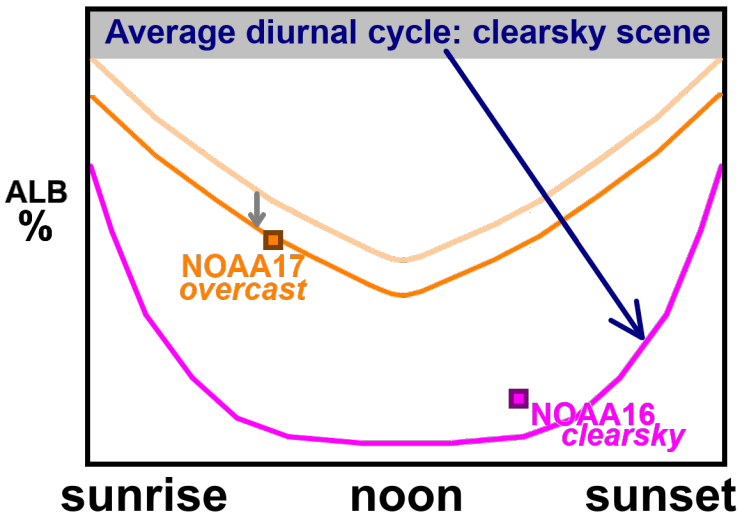

Figure 57: Conceptual example of modeling the albedo diurnal cycle (step 4)

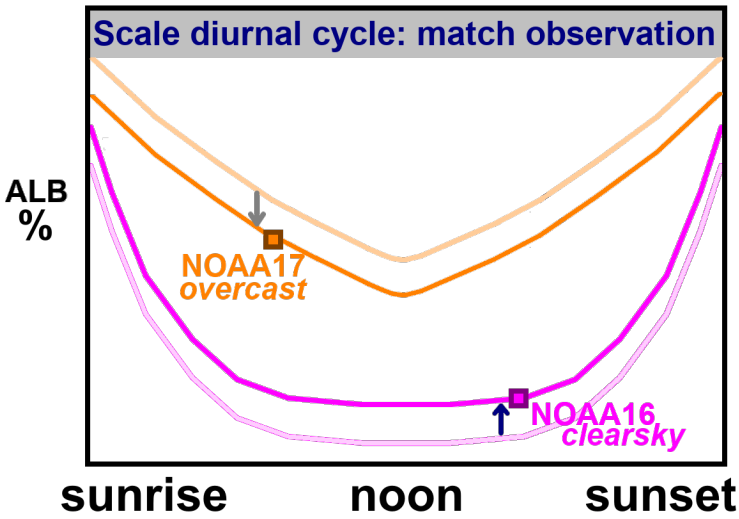

Figure 58: Conceptual example of modeling the albedo diurnal cycle (step 5)

After the iteration over all observations in the current DLB (in this case there are only 2 observations), there are as many 'scaled diurnal cycles' as there are observations (in this case 2). The final step consists of interpolating between these scaled diurnal cycles (Figure 59). This is done by calculating a weighted mean between the closest preceding and closest following observations for each 5min bin. The weight of each observation is simply the interpolated relative 'temporal distance' until the other observation. This method assumes that the scene types (cloud properties) evolve linearly between the observations.

Before the first observation in the current DLB (in this case NOAA-17; overcast), and after the last observation in current DLB (in this case NOAA-16; clear-sky), there is no interpolation, since there is only one applicable albedo model to be used. The final result is obtained by connecting the interpolated albedo models, cfr the blue curve in Figure 59: this is the final TOA albedo (α_{SW}) for each 5min bin.

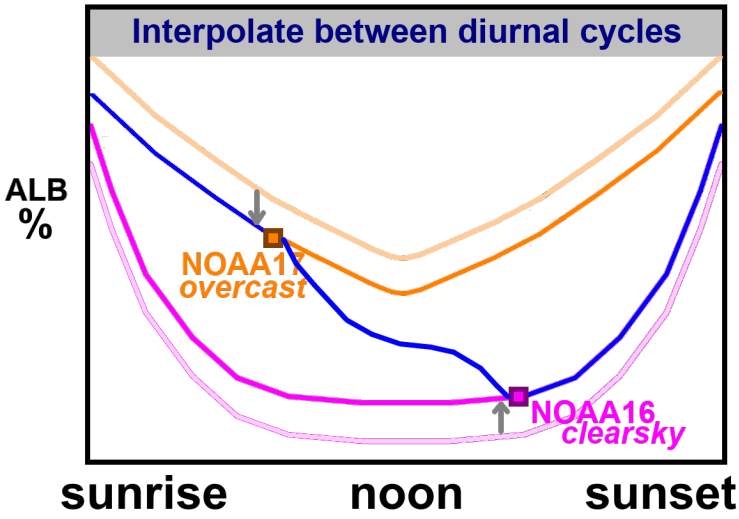

Figure 59: Conceptual example of modeling the albedo diurnal cycle (step 6)

In this conceptual example, the DLB was entirely situated within the 24h temporal range of the UTC day (hence, only a single DLB contributes to the daily mean calculation). In reality, however, for many regions the UTC day partially contains 2 DLB's, typically with the first DLB having an overlap at 0h UTC and the second DLB having an overlap at 24h UTC (cfr regions around the Pacific, exact delineation depends on season; see example in Figure 60).

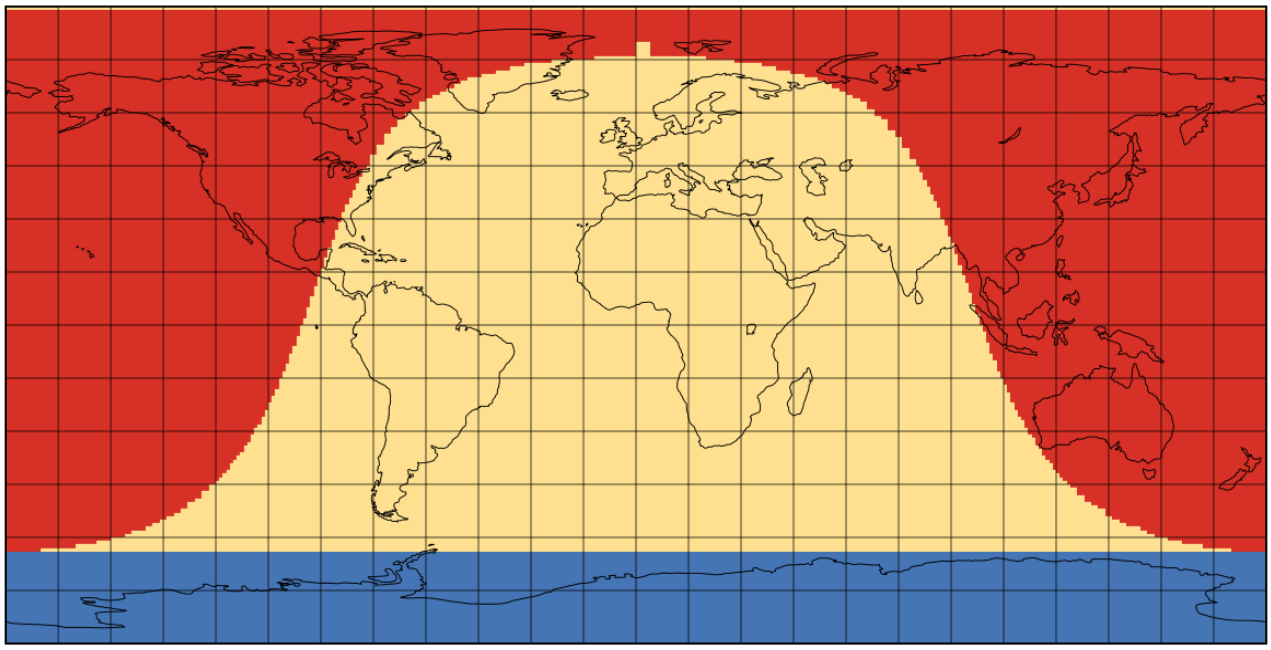

Figure 60: Number of DLB's contributing to daily mean of UTC day 23/7/2010; Blue (0), yellow (1), red (2)

In these cases, where DLB's overlap the UTC day range limits, the following situations will occur:

- **The first DLB** overlaps with the start of the UTC day (00:00h UTC): to save computation time, the DLB temporal range is limited by letting it start from the last valid Level-2 observation from the preceding UTC day onwards (example see Figure 61): this observation is still necessary for the interpolation across the UTC day boundary (00:00h UTC).
- **The second DLB** overlaps with the end of the UTC day (23:59h UTC): for this DLB, only the first valid Level-2 observation of the next UTC day is used. (analogous to the DLB overlapping start of UTC day).

Shrinking the DLB's temporal range is done for computational reasons; it means that no redundant interpolation work is performed (*especially when there are other valid observations in the first part of that DLB, i.e. before the NOAA-17 observation in the example of Figure 61*): only the shrunken DLB is kept in memory and used in the calculations.

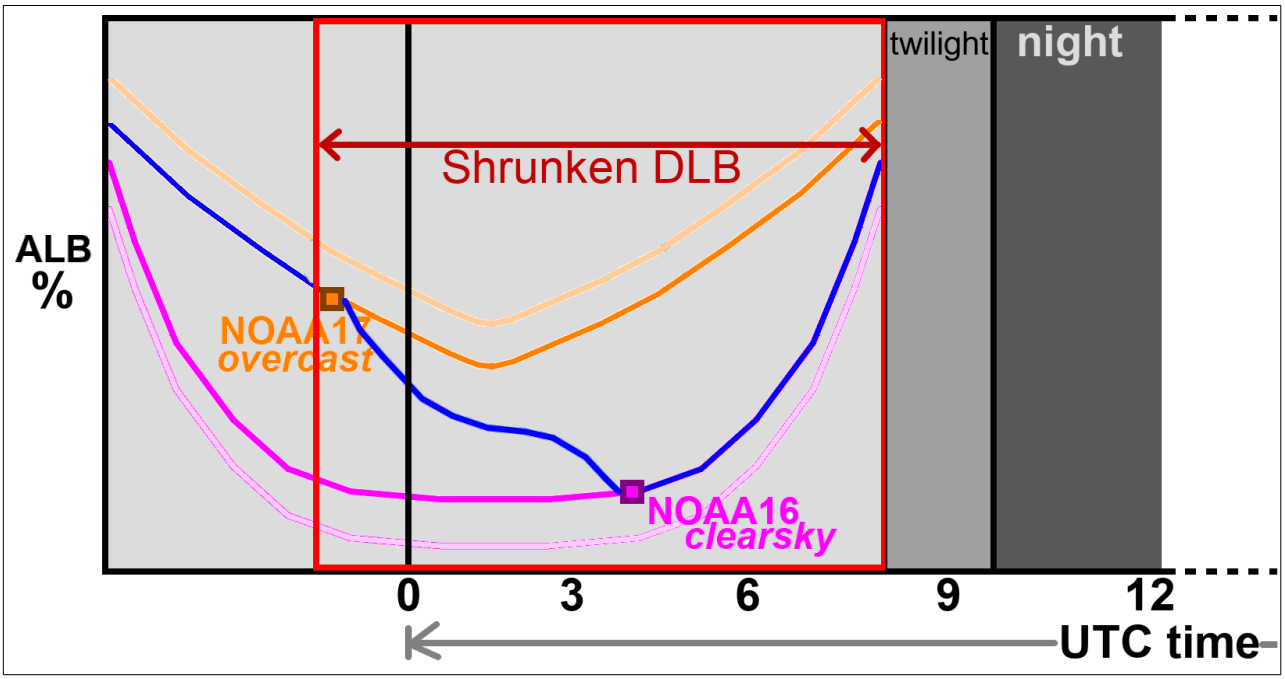

Figure 61: Conceptual example of DLB overlapping with start of the UTC day (00:00h UTC)

Hence, in cases where the DLB overlaps with the 00:00h or 23:59h UTC limits, the temporal range of the DLB is re-defined (DLB is limited to a 'shrunken DLB') and the steps explained in Figures 54 to 59 are performed only on the

shrunken DLB. In these cases, an additional last step is required (*after the TOA albedo has been interpolated, cfr blue line in Figure 61*), i.e. cutting off the redundant part(s) of the diurnal cycle that do not belong to the current UTC day. In the conceptual example shown in Figure 61, that would mean cutting of the first part of the DLB between the NOAA-17 observation and 00:00h UTC which marks the start of the UTC day.

Finally, for every 5min bin in the daylightblock, the albedo (α_{SW}) is converted to daylight flux $F_{daylight}$ (W/m²) as follows:

$$F_{daylight} = \left(\frac{\alpha_{SW} \cdot TSI \cdot \cos(\theta_0)}{d^2} \right) \cdot \left(\frac{r_e}{r_e + h_{20}} \right)^2 \quad (10)$$

The first term contains the daily Total Solar Irradiance (*TSI*, W/m²) supplied as input data cfr. Section 2.4.1. The Sun-Earth distance (*d*) is calculated using the Bretagnon method and coefficient look-up tables (Bretagnon and Simon, 1986). Its value is also supplied in the daily mean output file (as global ancillary metadata).

The second term in Equation 10 is a correction to scale the surface reference level to a reference level of 20km, according to Loeb et al., 2003 (Eq.18 in that reference), and is defined in Equation 11.

$$\left(\frac{r_e}{r_e + h_{20}} \right)^2 = \left(\frac{6371\,km}{6371\,km + 20\,km} \right)^2 = 0.993751 \quad (11)$$

If the DLB does not contain any '*valid observations' (cfr. first paragraphs of Section 3.3.2)*, the entire daily mean is flagged as invalid. This may happen because the Level-2 input data is corrupted or invalid. Another, more frequent reason is that the duration of the DLB is very short, typically occurring in wintertime at high latitudes, which decreases the chance of having an observation falling within its temporal range. This demonstrated in Figure 62, where the observations (red squares) fall outside the limited DLB temporal range.

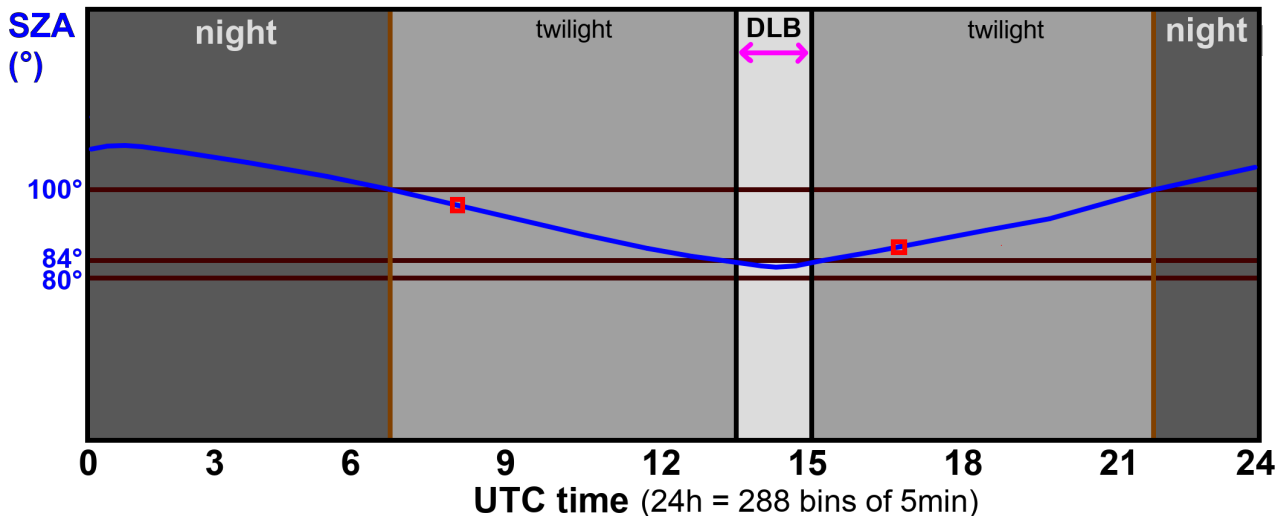

Figure 62: SZA during a single UTC day on a single grid box, during high-latitude wintertime

To avoid too many daily mean grid boxes being flagged as invalid, an exception is made for these situations: if the minimum solar zenith angle (SZA) in a DLB is not lower than 80°, then the entire DLB will be re-categorized to "twilight" and processed as such (Section 3.3.3), meaning that the twilight model is exceptionally extended to the range of 80°>SZA>84°. The example shown in Figure 62 illustrates how the minimum SZA still remains higher than 80°. This exception is a trade-off between data coverage (avoiding too much missing grid boxes) and accuracy (not relying too much on modeling by setting requirements to the minimum contribution of observations).

Number of shortwave instantaneous (Level-2) observations contributing to diurnal cycle

The number of shortwave instantaneous Level-2 observations that have been used to create the albedo's diurnal cycle is stored and written to the output file under the variable name "*Number of SW instantaneous observations contributing to daily mean*". In the conceptual example of Figures 54-59, this number would be 2 (one from NOAA-17 and one

from NOAA-16) from the one and only DLB. Note that in case of multiple DLB's, these are added and the total number is provided as output.

An example for the daily mean of 23/7/1983 is shown in Figure 63. Latitudinal variation is seen in ~~T~~the winter hemisphere (here ~~North~~South) which is characterized by shorter day light blocks, i.e. by more observations falling outside the DLB's limits. In the ~~southern~~summer hemisphere (here North), the dominant feature is an increase towards the pole due to overlapping orbits.

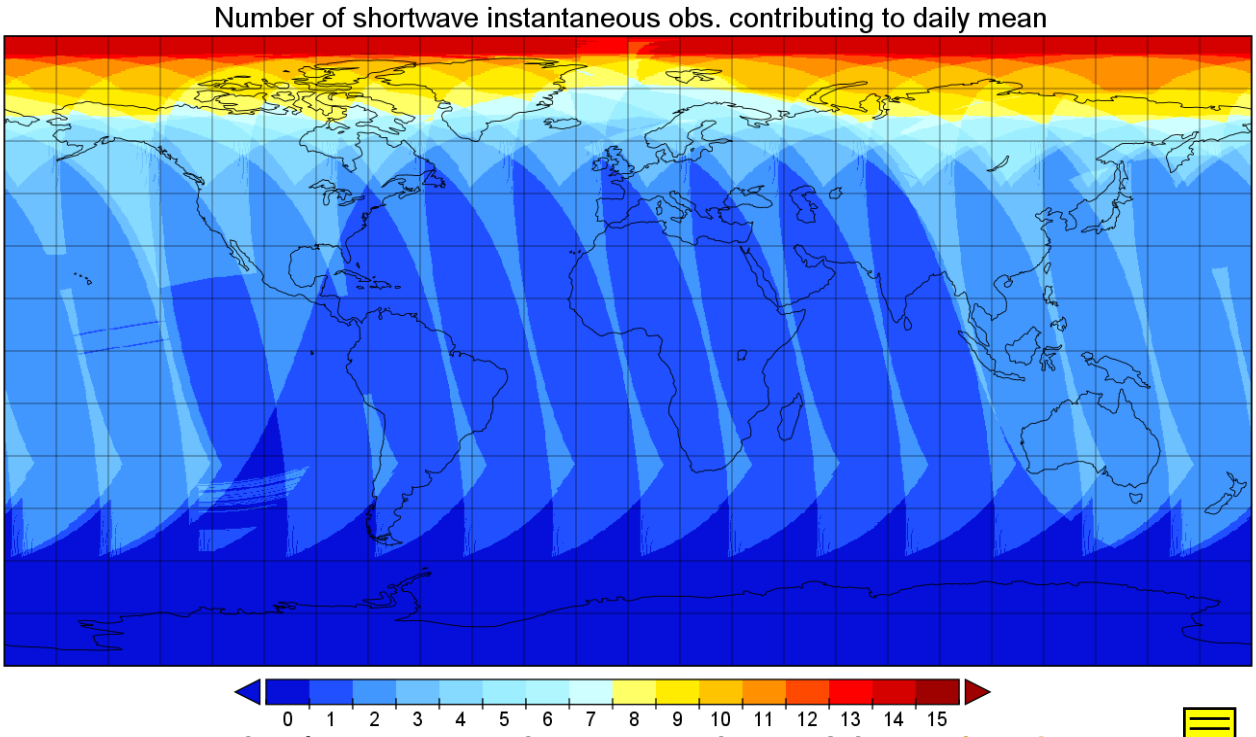

Figure 63: Number of SW instantaneous observations contributing to daily mean of UTC day 23/7/1983

Furthermore, there is longitudinal variation due to:

- number of DLB's per UTC day: because each DLB should have at least 1 observation, regions with 2 DLB's have at least 2 observations (leading to a pattern like in Figure 60).
- sideways overlap of consecutive orbits, i.e. where the swath edges of each orbit overlap with the edges of next orbit, resulting in a double temporal frequency compared to the center part of the swath. Similar to the latitudinal sampling variation due to overlapping orbits, this is considered as an inherent feature of polar orbiting satellite processing, and the increased temporal sampling is fully used (i.e. there is no selection) since it increases the observational impact of the diurnal cycle compared to the modeling/interpolation impact. This is illustrated for a single day with a single satellite in Figure 63.

From this total number of "*contributing SW instantaneous observations*", a certain fraction (0-100%) is contaminated by sunglint and hence created with different Level-1 routines. This fraction is also stored and written to the daily mean output file under the variable name called "*relative share of sunglint-affected to all instantaneous observations*".

Satellite bit flags

The daily mean output file gets an additional bit flag variable (called '*satellite bit flag*') identifying the satellite(s) from which observations are involved in the construction of each pixel's daily mean. The flags simply indicate the presence of each satellite according to Table 11. Besides the pixel-specific flags, also a single global satellite bit flag is calculated: it contains a bit flag for each satellite that is used for at least 1 grid box (from the 1440x720 grid) and is added in the ancillary metadata from the variable "Satellite_bitflags_sw" (as 'global_value').

Table 11: Satellite bit flags

Bit nr.	Binary representation	Value	Satellite Bitflag	Sensor
1	0000000000000000001	1	TIROS-N	AVHRR
2	0000000000000000010	2	NOAA-6	
3	0000000000000000100	4	NOAA-7	
4	0000000000000001000	8	NOAA-8	
5	0000000000000010000	16	NOAA-9	
6	0000000000000100000	32	NOAA-10	
7	0000000000001000000	64	NOAA-11	
8	0000000000010000000	128	NOAA-12	
9	0000000000100000000	256	NOAA-14	
10	0000000001000000000	512	NOAA-15	
11	0000000010000000000	1024	NOAA-16	
12	0000000100000000000	2048	NOAA-17	
13	0000001000000000000	4096	NOAA-18	
14	0000010000000000000	8192	NOAA-19	
15	0000100000000000000	16384	METOP-A	
16	0001000000000000000	32768	METOP-B	
17	0010000000000000000	65536	METOP-C	
18	0100000000000000000	131072	S-NPP	VIIRS
19	1000000000000000000	262144	NOAA-20	

3.3.3. Twilight conditions (84°>SZA>100°)

The interpolated twilight coefficients A (intercept) and B (slope) are used in combination with the time-varying Solar Zenith Angle to determine the twilight flux for every 5min bin.

Similar to the processing of daylight conditions (Section 3.3.2), each valid observation within the current 0.25°x0.25° grid box is assigned to the temporally closest 5min bin, together with all its attributes, among which the scenetype-dependent twilight coefficients A and B, cfr Section 3.2.1. However, for twilight conditions, this is done for **all** valid observations in the current 0.25°x0.25° grid box during the current UTC day, **regardless day- or nighttime**. Subsequently, both coefficient A and coefficient B are linearly interpolated, so each 5min bin is assigned an interpolated value for A and for B (*orange and lightblue lines in Figure 64*).

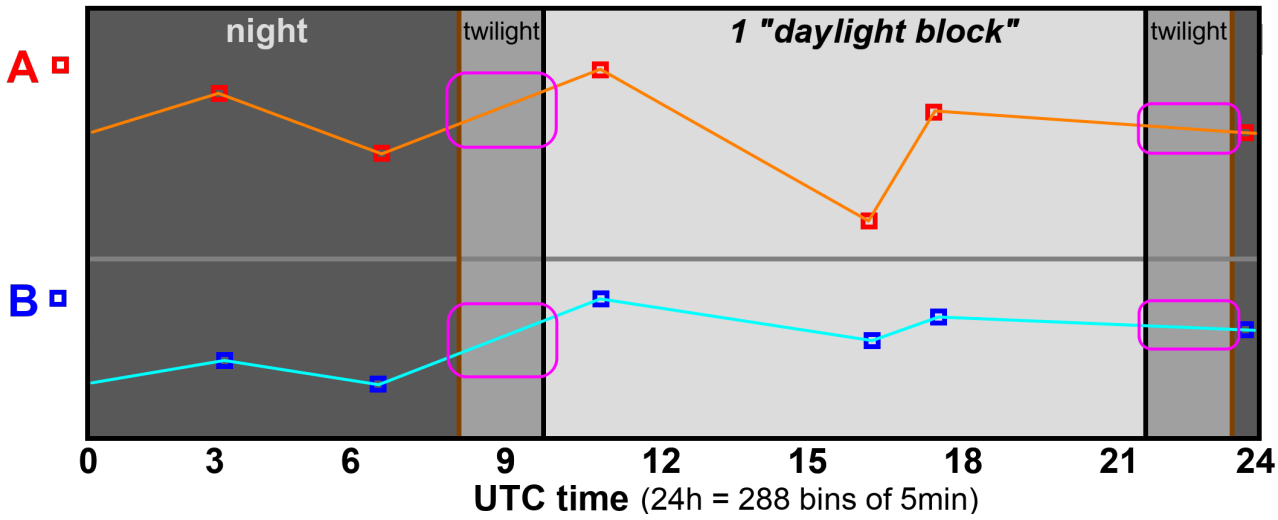

Figure 64: Conceptual example of interpolating Twilight Coefficients A and B

Finally, for each *5min bin* belonging to the "twilight regime" (*purple boxes in Figure 64*), a twilight flux ($F_{twilight}$; *W/m²*) is calculated by combining the bin-specific interpolated A and B coefficients with their corresponding bin-specific Solar Zenith Angle (θ_0, *degrees*):

$$F_{twilight} = A_{interpolated} + \left(B_{interpolated} \cdot \theta_0\right) \quad (12)$$

where $F_{twilight}$ stands for Flux during twilight conditions (W/m²), $A_{interpolated}$ en $B_{interpolated}$ are the linearly interpolated twilight coefficients, and θ_0 is the Solar Zenith Angle (SZA). When the result is lower than the generic all-sky twilight model by Kato and Loeb (2003), it is matched to the latter (see red dotted lines in Figure 25).

3.3.4. Nighttime conditions (SZA>100°)

For all the 5min bins with nighttime conditions (SZA>100°) the flux is set to **0.0 W/m²**.

$$F_{night} = 0.0\,Wm^{-2} \tag{13}$$

3.3.5. Daily integral

The daily mean Reflected Solar Flux ($RSF_{dailymean}$; Eq.14) is calculated by taking the average of all *5min bins* that have been processed either with conditions for **daylight** ($F_{daylight}$, Section 3.3.2), **twilight** ($F_{twilight}$, Section 3.3.3) or **nighttime** (F_{night}, Section 3.3.4), with the number of contributing *5min bins* for the three components being respectively I, J and K. As the *UTC day* has 288 temporal 5 min bins, it follows that I+J+K=288.

$$RSF_{daily\,mean} = \frac{1}{I+J+K}\cdot\left(\sum_{i=1}^{I} F_{daylight,i} + \sum_{j=1}^{J} F_{twilight,j} + \sum_{k=1}^{K} F_{night,k}\right) \tag{14}$$

An example of the $RSF_{dailymean}$ for UTC day 2/1/1998 is given in Figure 65.

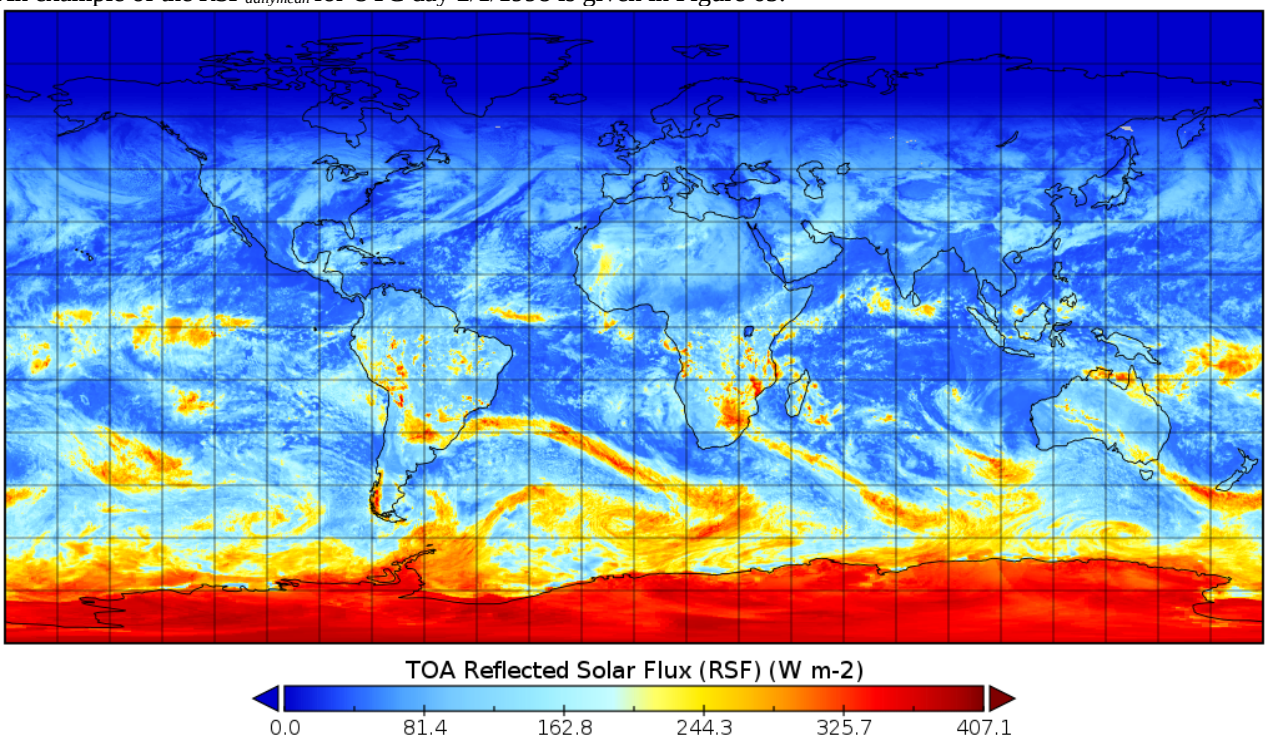

Figure 65: TOA Daily mean Reflected Solar Flux for 2/1/1998

The twilight-specific daily mean flux ($RSF_{twilight,mean}$) is calculated as the average flux during twilight conditions only, given by Equation 15:

$$RSF_{twilight\,mean} = \frac{1}{J}\cdot\left(\sum_{j=1}^{J} F_{twilight,j}\right) \tag{15}$$

The fractions of each components' number of *5min bins* (I, J, K) to the total number of *5min bins* (I+J+K) are called "*relative temporal share (RTS)*", and are provided as auxiliary output variables (units: %). They are indicative for the

relative importance of each component in the calculation of the daily mean, and their calculation is given by Equations 16 and 17. Note that RTS_{night} can be calculated as $100 - RTS_{daylight} - RTS_{twilight}$.

$$RTS_{daylight} = 100 \cdot \left(\frac{I}{I+J+K} \right) \quad (16)$$

$$RTS_{twilight} = 100 \cdot \left(\frac{J}{I+J+K} \right) \quad (17)$$

3.3.6. Output

The output of Program Part 3 consists of two NetCDF files per day: one containing all shortwave quantities, the other containing all longwave quantities. The files both have spatial dimensions of 1440x720, structured in a regular lat-lon global grid with 0.25°x0.25° resolution. The following variables are stored in the SW outputfile:

- **Reflected Shortwave Flux, daily mean; $RSF_{daily\ mean}$ (W/m^2)**
- Reflected Shortwave Flux, twilight mean; $RSF_{twilight\ mean}$ (W/m^2)
- Relative temporal share daylight to daily mean; $RTS_{daylight}$ (%)
- Relative temporal share twilight to daily mean; $RTS_{twilight}$ (%)
- Number of day light blocks
- Number of SW instantaneous observations
- Relative share of sunglint-affected to all instantaneous observations (%)
- Bit flags (bitwise quality flags)
- Satellite bit flags

3.4. Part 4: Temporal aggregation to monthly mean RSF (level-3b)

The monthly mean Reflected Solar Flux ($RSF_{monthlymean}$; Eq.18) is calculated by taking the average of all *RSF daily means* that have been processed in Section 3.3, with D being the number of contributing daily means (which should ideally equal the number of days during that month).

$$RSF_{monthly\ mean} = \frac{1}{D} \cdot \left(\sum_{d=1}^{D} RSF_{dailymean,d} \right) \quad (18)$$

Ideally, all grid boxes have a complete temporal coverage for all days of the month. This is logged by the variable "*Number of SW daily means contributing to monthly mean*" for which an example is shown in Figure 66, taken from the month January 1998: note that most of the grid boxes have a complete temporal coverage (31/31 days), while some smaller regions have one or two days missing (cfr bluish colors, with 30/31 or 29/31 days).

The user is strongly encouraged to verify this auxiliary variable before doing analyses on the main results (i.e. monthly mean RSF). Two bit flags are added to help diagnosing this issue:

- **MISSINGDAYS_WARNING**: this flag is set when the temporal coverage is not complete, and the number of missing days ranges between 1-4. The monthly mean RSF is not entirely representative since some days are missing, but can still be used (depending of course on the application or analysis).
- **MISSINGDAYS_INVALID**: this flag is set when the temporal coverage is not sufficient, with the number of missing days being 5 or more. The monthly mean RSF is considered invalid and the **user is advised not to use it**.

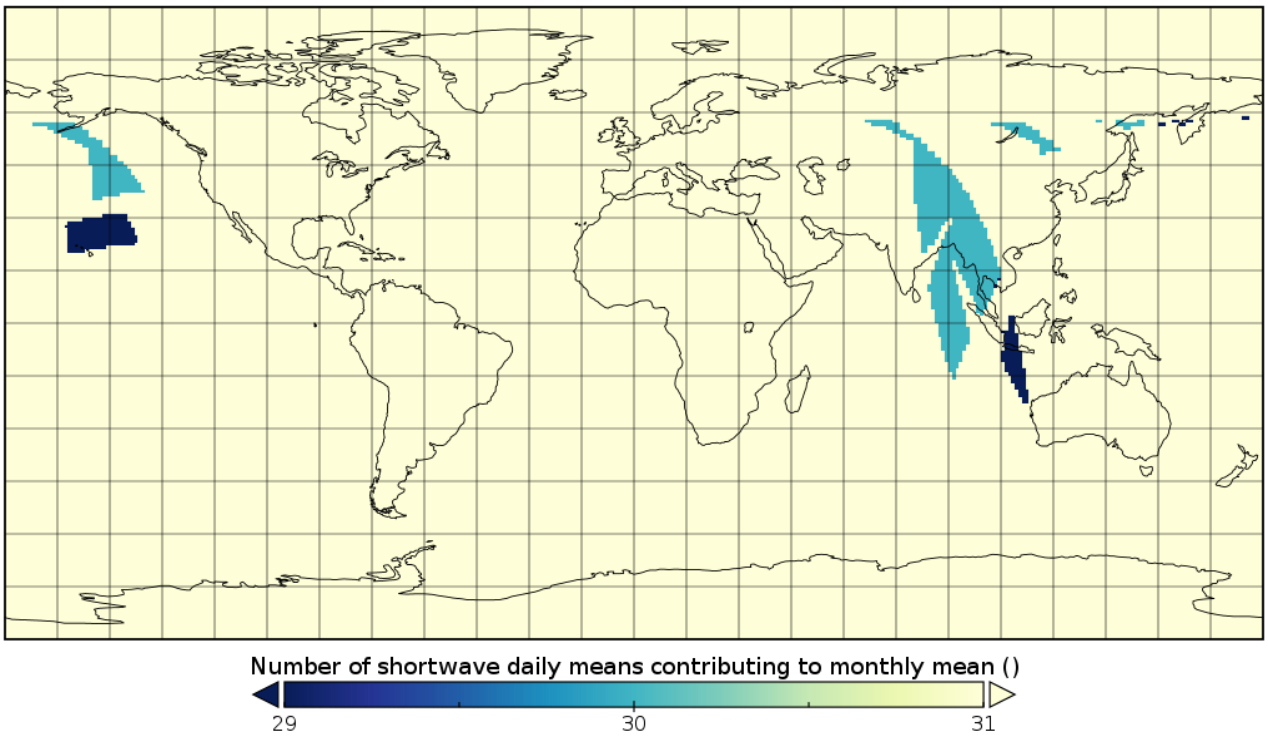

Figure 66: Number of SW daily means contributing to monthly mean RSF (January 1998)

Some of the auxiliary variables created by the daily mean program (Part 3) are propagated to the monthly mean Program Part 4, which creates a monthly mean from them.

The output from Program Part 4 is as follows:

- **Reflected Shortwave Flux, monthly mean; $RSF_{monthly\ mean}$ (W/m^2)**
- Reflected Shortwave Flux, twilight mean; $RSF_{twilight\ monthly\ mean}$ (W/m^2)
- Relative temporal share daylight to dailymean; $RTS_{daylight}$ (%)
- Relative temporal share twilight to dailymean; $RTS_{twilight}$ (%)
- Number of SW instantaneous observations
- Relative share of sunglint-affected to all instantaneous observations (%)
- Bit flags (bitwise quality flags)

4. Retrieval of Outgoing Longwave Radiation [CM-11342, OLR]

The current chapter focuses on the longwave "Outgoing Longwave Radiation" (OLR), cfr the leftmost reddish sections in overview figure below. The software designed to produce the CDR is subdivided in separate software modules (See figure below, Parts 1 – 4 in the leftmost column).

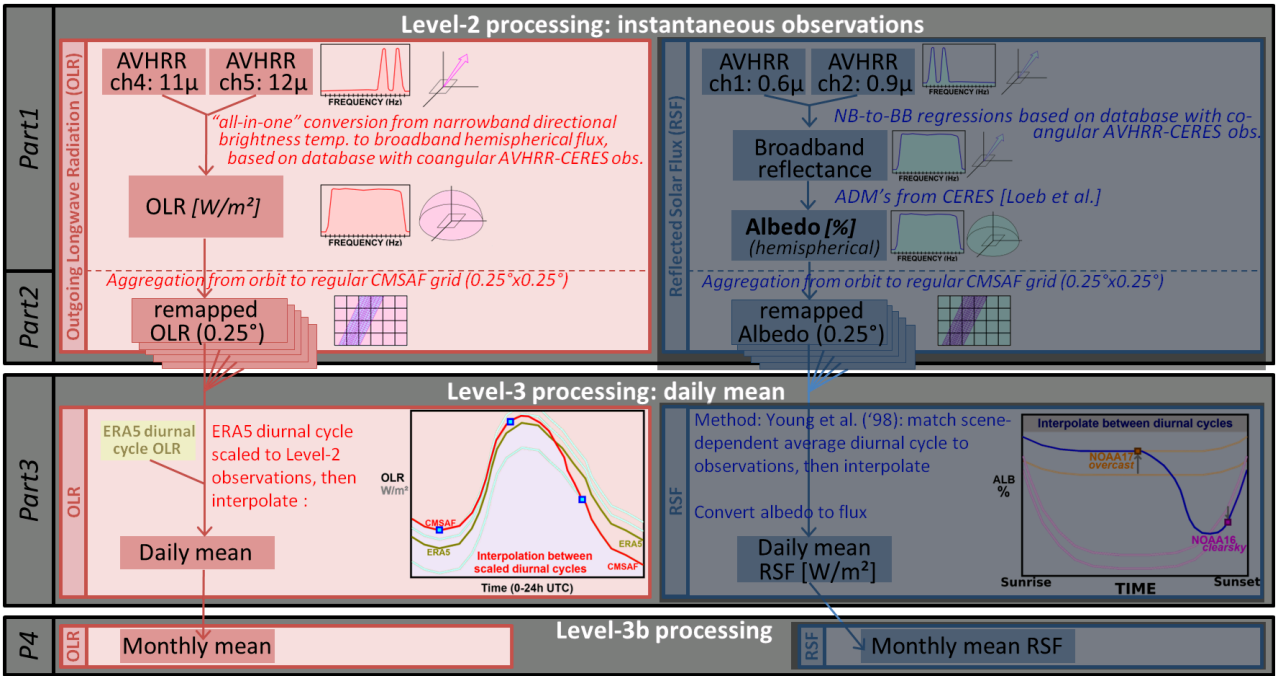

*Figure 67: Overview of the **OLR (left)** and RSF (right) processing chain*

The four sections in this chapter refer correspond to these specific software modules that may be executed and managed separately. "Part 1" refers to the software "Program Part 1", etcetera.

4.1. Part 1: Retrieval algorithm of instantaneous OLR (level-2)

4.1.1. Overview

Program Part 1 retrieves the instantaneous **Outgoing Longwave Radiation** (broadband and hemispherical) from the narrowband brightness temperature (channels 4+5) and all the various input data sources, and creates the Level-2 output which consists of a single NetCDF file corresponding to each *GAC orbit inputfile*. Creating separate shortwave and longwave output files would not be efficient, as there are many common auxiliary variables which need to be propagated to the next program parts, and which hence should be stored to disk twice.

Program Part 1 takes as input a single AVHRR GAC file (i.e. the "*reference input file*" containing reflectances). Corresponding auxiliary files (containing auxiliary input data such as meteorological reanalysis, sea ice cover, etc.) are located automatically based on the filename of the reference input file.

A loop then iterates over all AVHRR GAC pixels, and all subsequent processing is done on each single pixel separately (Flowchart Fig. 68). A distinction is made between shortwave and longwave processing, either manually for all pixels (enabling/disabling the LW- and/or SW-processing for all pixels by modifying the relevant flag in configuration file) or automatically per pixel (e.g. SW is automatically disabled if invalid SW-specific inputdata is detected, or when SZA>84°).

When terminating the processing for a given pixel, incl. abrupt/premature terminations due to invalid input data, certain data is always written to the output before proceeding to the next pixel in the iteration. It concerns the following variables:

- bit flags
- bit flag variable ID
- time stamp (UNIX time)

When the loop is finished, all pixels are written to a Netcdf file.

The **bit flags** are for each pixel by default set to zero, and may be modified during the processing; their main purpose is to deliver pixel-specific information about the processing, including potential reasons for increased uncertainty, or even for missing output. The total bit flag value is composed of multiple bits each representing a separate binary flag. A complete overview of all the flag meanings can be found in Appendix 9.6.2 (Table 22). The accompanying "**bit flag variable ID"** indicates *which variable* is affected when a bit flag is activated; a list with their associated default ID numbers is also available in Annex 9.6.1 (Table 21).

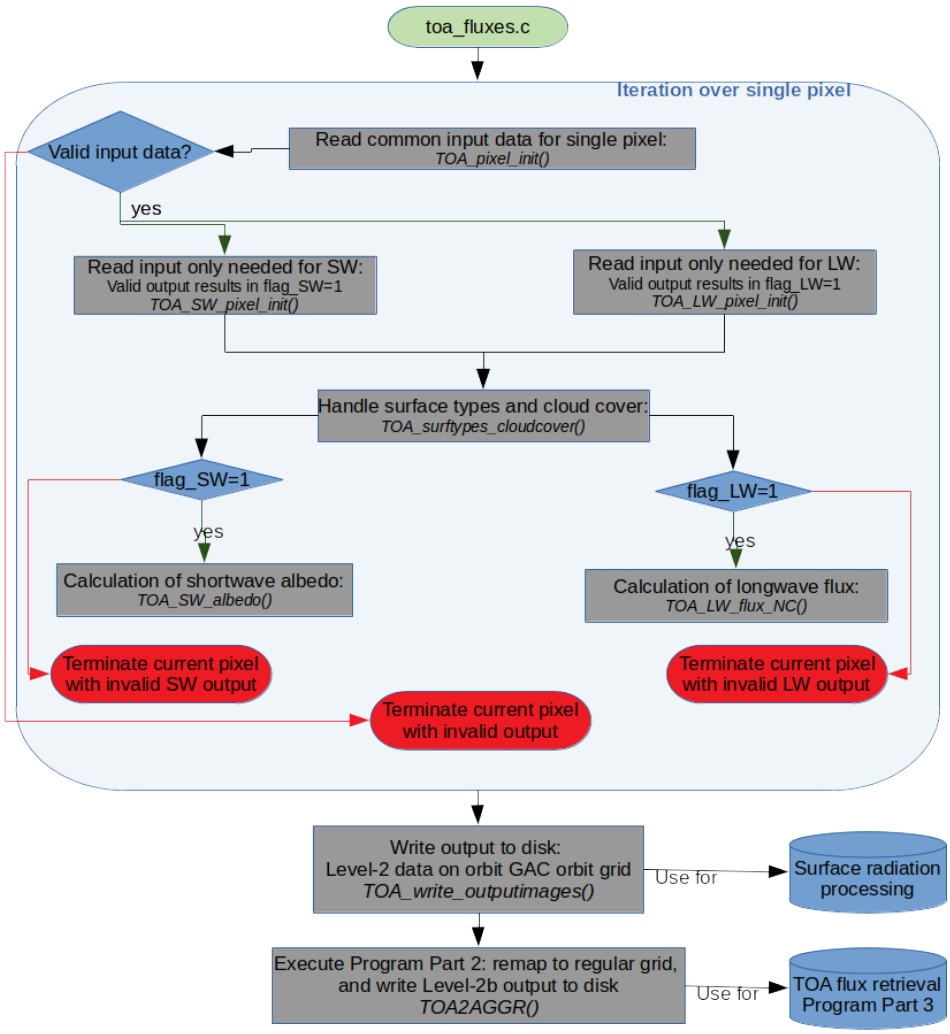

Figure 68: Flow chart: main structure of Program Part 1 (level-2 processing for RSF and OLR)

4.1.2. Preparation input data

4.1.2.a. Initialization of pixel value with input data: common part

First, the input data required for **both** shortwave and longwave processing are ingested (Flowchart Fig. 68). The reader is referred to Section 3.1.2.a, as its contents are identical.

4.1.2.b. Initialization of pixel value with input data: longwave-only part

If all common input data are successfully ingested, the longwave-specific input data are read (Flowchart Fig.68). It concerns the following variables:

- Integrated water vapor (*Section 2.3.4*),
- Surface temperature (*Section 2.3.4*),

- Channel 4 (λ=11µm) and channel 5 (λ=12µm) brightness temperature (T_b) (*Section 2.1*).

Any invalid value would terminate the routine, thus resulting in invalid outputs for that pixel (for longwave part).

Unlike the visible channels, instrument-specific differences in spectral response from the thermal channels are not accounted for by the FDR. Therefore, in a subsequent step a spectral response correction is applied to the brightness temperatures. The relative spectral response curves are shown in Figure 69 (Frey et al., 2017). Note that for instrument AVHRR/1 (orange/reddish tones) only channel 4 is applicable.

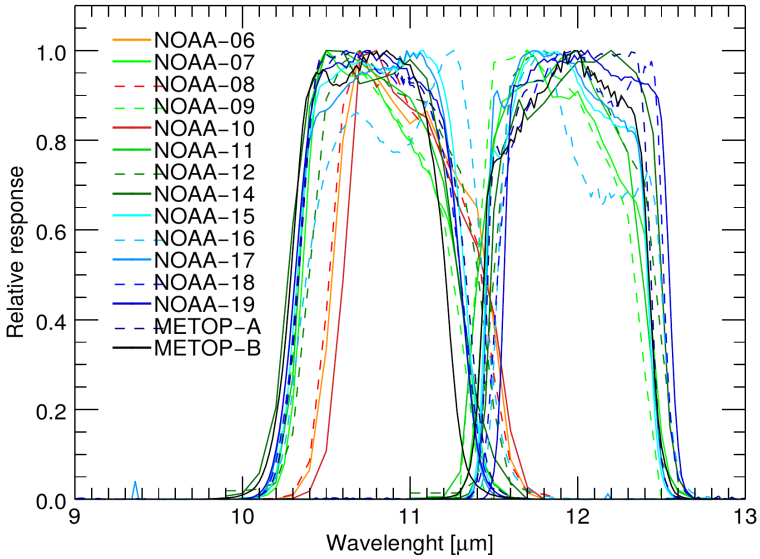

Figure 69: Spectral response curves of channels 4 and 5 of the different AVHRR-1/-2/-3 instruments (Frey et al., 2017)

That correction is implemented using a look-up table which contains for each AVHRR-carrying satellite the corresponding correction parameters (offset and slope) with NOAA-19 as reference spectral response (Table 12).

Table 12: Linear regression coefficients (slope and offset) applied as spectral-band adjustment to measured brightness temperature (BT) of AVHRR channels 4 and 5 to mimic NOAA-19 AVHRR (Stengel et al., 2020)

Satellite	Instrument	Channel 4 (11µm)		Channel 5 (12µm)	
		Slope	*Offset*	*Slope*	*offset*
NOAA-5	VHRR	0.999	0.236	n.a.	
TIROS-N*	AVHRR/1	1.0014*	-0.043*		
NOAA-6		0.999	0.300		
NOAA-8		0.999	0.201		
NOAA-10		0.999	0.469		
NOAA-7	AVHRR/2	1.000	-0.198	0.991	1.991
NOAA-9		1.000	-0.215	0.988	2.770
NOAA-11		1.000	-0.170	0.989	2.443
NOAA-12		1.001	-0.212	0.994	1.383
NOAA-13		1.000	0.000	1.000	0.000
NOAA-14		1.001	-0.446	0.995	1.081
NOAA-15	AVHRR/3	1.000	-0.136	0.990	2.145
NOAA-16		1.000	-0.095	0.997	0.561
NOAA-17		1.000	-0.185	0.990	2.112
NOAA-18		1.000	-0.214	0.997	0.626
NOAA-19		**1.000**	**0.000**	**1.000**	**0.000**
METOP-A		1.000	-0.196	0.991	1.981
METOP-B		1.000	-0.165	0.990	2.300
METOP-C		1.00052	-0.31908	1.00562	-1.43378
NOAA-20	VIIRS	1.000	0.000	1.000	0.000
(*) Coefficients not taken from Stengel et al. (2020) but from the web-based SBAF calculator					

These coefficients are taken from ESA Cloud_cci (Stengel et al., 2020) where NOAA-19 AVHRR is mimicked by all other AVHRRs. Slope and offset values were calculated by applying different AVHRR spectral response functions to the same collection of measurements. The coefficients are expressed in terms of brightness temperature (K) and taken

from the web-based *Spectral Band Adjustment Factor (SBAF) calculator*[19] based on IASI IR hyperspectral data. The IASI-based SBAFs are computed from algorithms and online tools developed at NASA-LaRC with IASI L1C data obtained from EUMETSAT (Scarino et al. 2016, Cayla 2001, Chalon et al. 2001). Figure 70 illustrates the result for channel 4 conversion of TIROS-N to NOAA-19 for the MSG region:

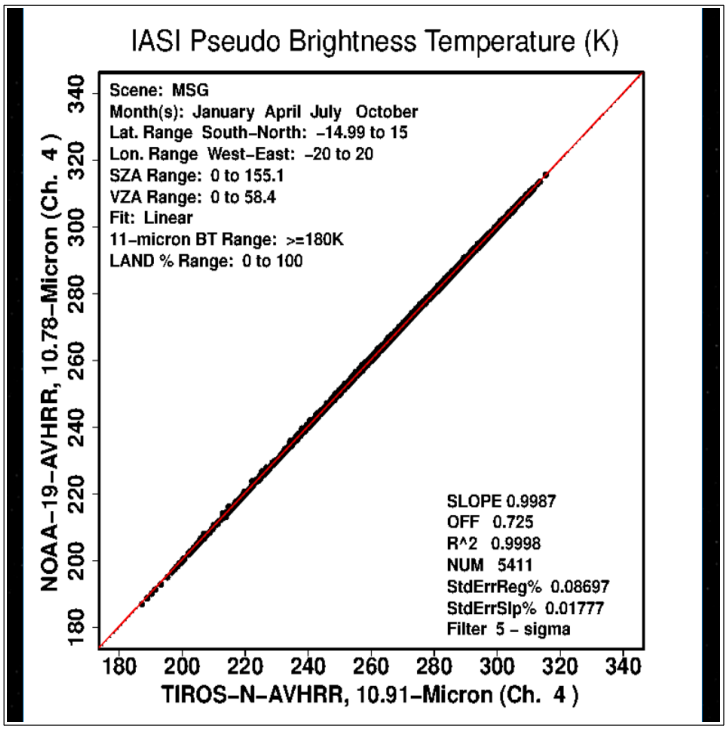

Figure 70: example of SBAF calculator output: AVHRR channel 4 of TIROS-N to NOAA-19

However, there are also coefficients for other regions, and a rounded mean is calculated from all regions (Table 13).

Table 13: Slope and offset from linear relations between TIROS-N and NOAA-19

Earth Spectra (IASI)	TIROS-N	
	AVHRR channel 4	
	slope	offset
GOES-E	1.001	0.047
GOES-W	1.000	0.247
Indian Ocean	1.001	0.169
MSG	0.999	0.725
North Pole	1.003	-0.685
South Pole	1.003	-0.558
TWP	1.003	-0.246
MEAN	1.001429	-0.043000
MEAN_round	**1.0014**	**-0.043**

The corresponding satellite- and channel-dependent slope and offset is then applied to obtain the channel-specific Brightness Temperature corrected for spectral response (Equation 19).

$$T_{b,\lambda} = offset_{sat,\lambda} + \left(slope_{sat,\lambda} \cdot T_{b,\lambda}\right) \quad (19)$$

4.1.3. Narrowband-to-OLR conversion (spectral+angular corrections)

Unlike the shortwave processing, where the spectral corrections (NTB; Section 3.1.4) and angular corrections (ADM; Section 3.1.5) are separated, the longwave processing combines these steps into a single narrowband-to-OLR conversion. The method is explained by Clerbaux et al., 2020, and summarized here in Flowchart Fig.71.

19 *URL: https://satcorps.larc.nasa.gov/cgi-bin/site/showdoc?mnemonic=SBAF&mode=IR*

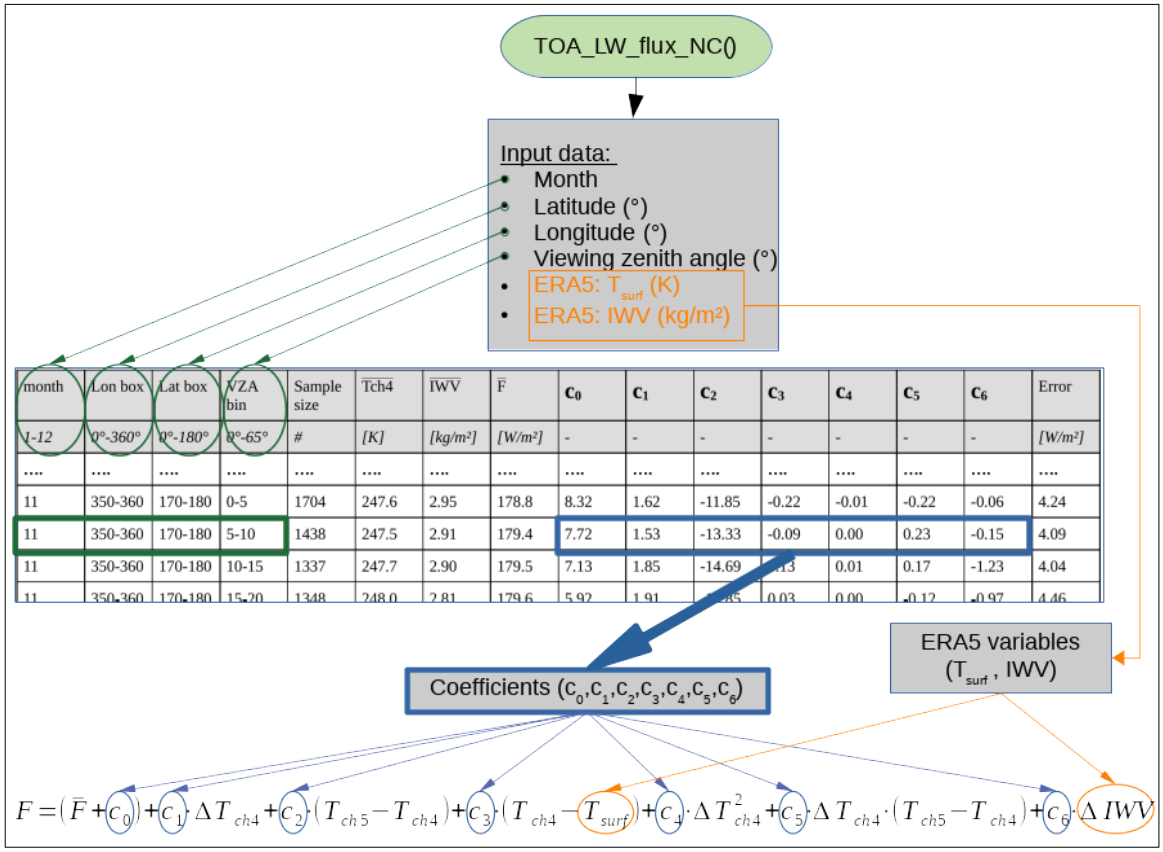

month	Lon box	Lat box	VZA bin	Sample size	Tch4	IWV	F̄	c0	c1	c2	c3	c4	c5	c6	Error
1-12	0°-360°	0°-180°	0°-65°	#	[K]	[kg/m²]	[W/m²]	-	-	-	-	-	-	-	[W/m²]
....	....	....	....	....	....	....	....	....	....	....	....	....	....	....	....
11	350-360	170-180	0-5	1704	247.6	2.95	178.8	8.32	1.62	-11.85	-0.22	-0.01	-0.22	-0.06	4.24
11	350-360	170-180	5-10	1438	247.5	2.91	179.4	7.72	1.53	-13.33	-0.09	0.00	0.23	-0.15	4.09
11	350-360	170-180	10-15	1337	247.7	2.90	179.5	7.13	1.85	-14.69	-0.13	0.01	0.17	-1.23	4.04
11	350-360	170-180	15-20	1348	248.0	2.81	179.6	5.92	1.91	-15.85	0.03	0.00	-0.12	-0.97	4.46

Figure 71: Flow chart: processing of longwave narrowband T_b to OLR (AVHRR-2/-3)

The narrowband-to-OLR conversion is based on a set of multivariate regressions from empirical relations between narrowband brightness temperature from AVHRR, and broadband fluxes from CERES (Section 2.4.9). The regressions are made for each of the following discretized parameter combinations:

- Month (12),
- Latitudinal 10°x10° grid box (18) ,
- Longitudinal 10°x10° grid box (36),
- VZA bin (13).

Hence, in total there are coefficient values for 101088 combinations, resulting in a large table with 101088 regression coefficients (*table in Flowchart Fig.71*). The continuous predictors in every regression are:

- Surface temperature (K)
- Integrated water vapor (kg/m²)

The method (*Flowchart Fig.71*) consists of using the month, spatial coordinates and viewing zenith angle to determine the regression and corresponding regression coefficients c_0 *to* c_6. Then, the channel brightness temperatures T_{ch4} and T_{ch5} together with the predictors *IWV* and T_{surf} are plugged into the obtained regression (Equation 20), which is solved for the resulting flux (*F; W/m²*). More details on the regression coefficients table, and the use of these coefficients, was given in Section 2.4.9.

$$F = (\bar{F} + c_0) + c_1 \cdot \Delta T_{ch4} + c_2 \cdot (T_{ch5} - T_{ch4}) + c_3 \cdot (T_{ch4} - T_{surf}) + c_4 \cdot \Delta T_{ch4}^2 + c_5 \cdot \Delta T_{ch4} \cdot (T_{ch5} - T_{ch4}) + c_6 \cdot \Delta IWV \quad (20)$$

The above mentioned method is valid for two channels (11µm and 12µm). For the AVHRR/1 instrument, the single-channel method (11µm only) is summarized in Flowchart Fig.72.

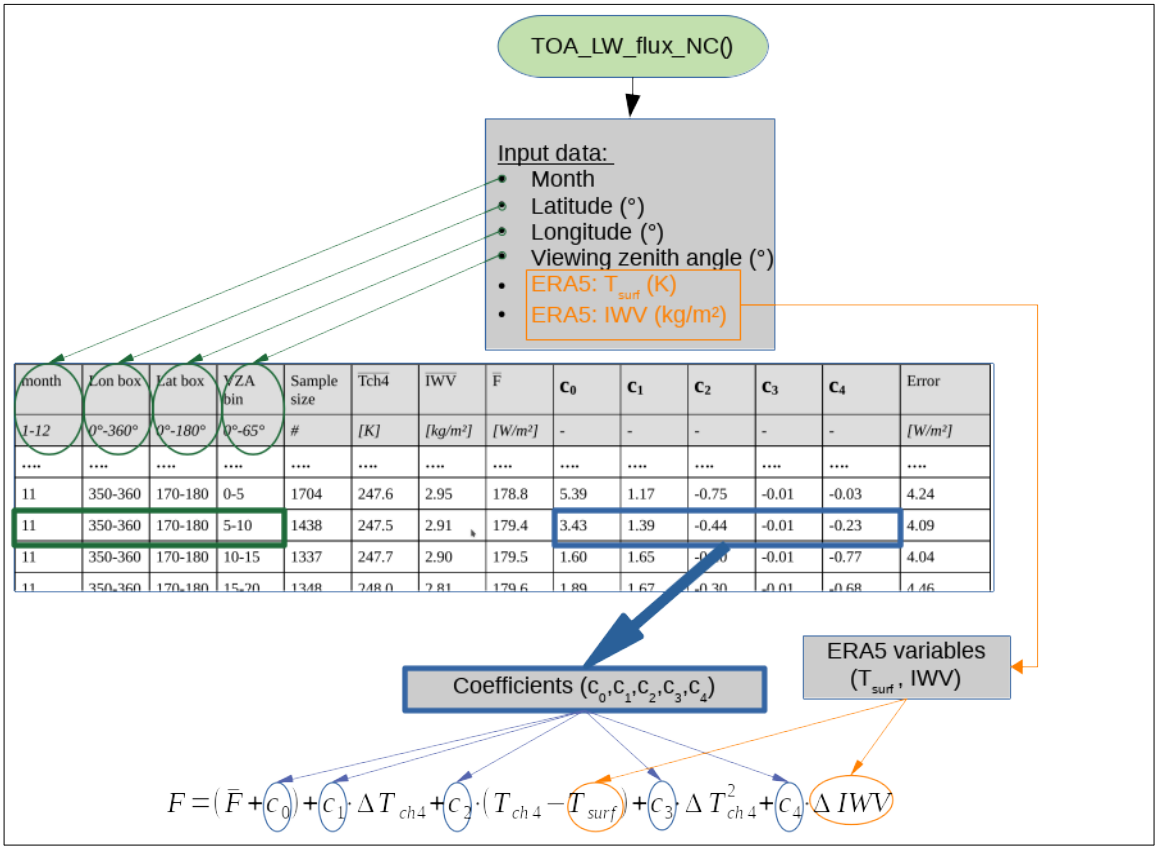

Figure 72: Flow chart: processing of longwave narrowband Tb to OLR (AVHRR-1)

The determination and application of the regression is done in a similar way as for the 2-channel approach. However, a different set of regressions is used in this case (with coefficients c_1 to c_4) which have the format as given in Equation 21.

$$F = (\bar{F} + c_0) + c_1 \cdot \Delta T_{ch4} + c_2 \cdot (T_{ch4} - T_{surf}) + c_3 \cdot \Delta T_{ch4}^2 + c_4 \cdot \Delta IWV \quad (21)$$

4.2. Part 2: Spatial aggregation from GAC orbit grid to regular grid (level-2b)

The reader is referred to Section 3.2, as its contents are identical (spatial aggregation is the same for longwave and shortwave variables).

4.3. Part 3: Processing of instantaneous to daily mean OLR (level-3)

4.3.1. Method

The method is explained in Clerbaux et al. (2020) and involves the use of hourly ERA5 OLR and cloud cover as input data (Section 2.4.4). Figure 73a shows an illustrative OLR diurnal cycle from ERA5 (black curve) together with the instantaneous AVHRR observations from NOAA-19 acquired during this time period (blue dots). For each AVHRR observation, a factor was determined between the ERA5 and the observed OLR, which was used to scale the entire ERA5 diurnal cycle (dotted grey curves). These scaled diurnal cycles were then temporally interpolated (inversely weighted to their temporal difference) so that the cycle passed exactly through all observations (red curve). This was only done for observations over land that were considered “clear-sky” by both AVHRR and ERA5 (as was the case for

all observations in Figure 73); for all other cases (i.e., ocean or cloudy), the observations were simply linearly interpolated (dashed red curve), similar to the interpolation of the twilight coefficients (Section 3.3.3, Figure 64).

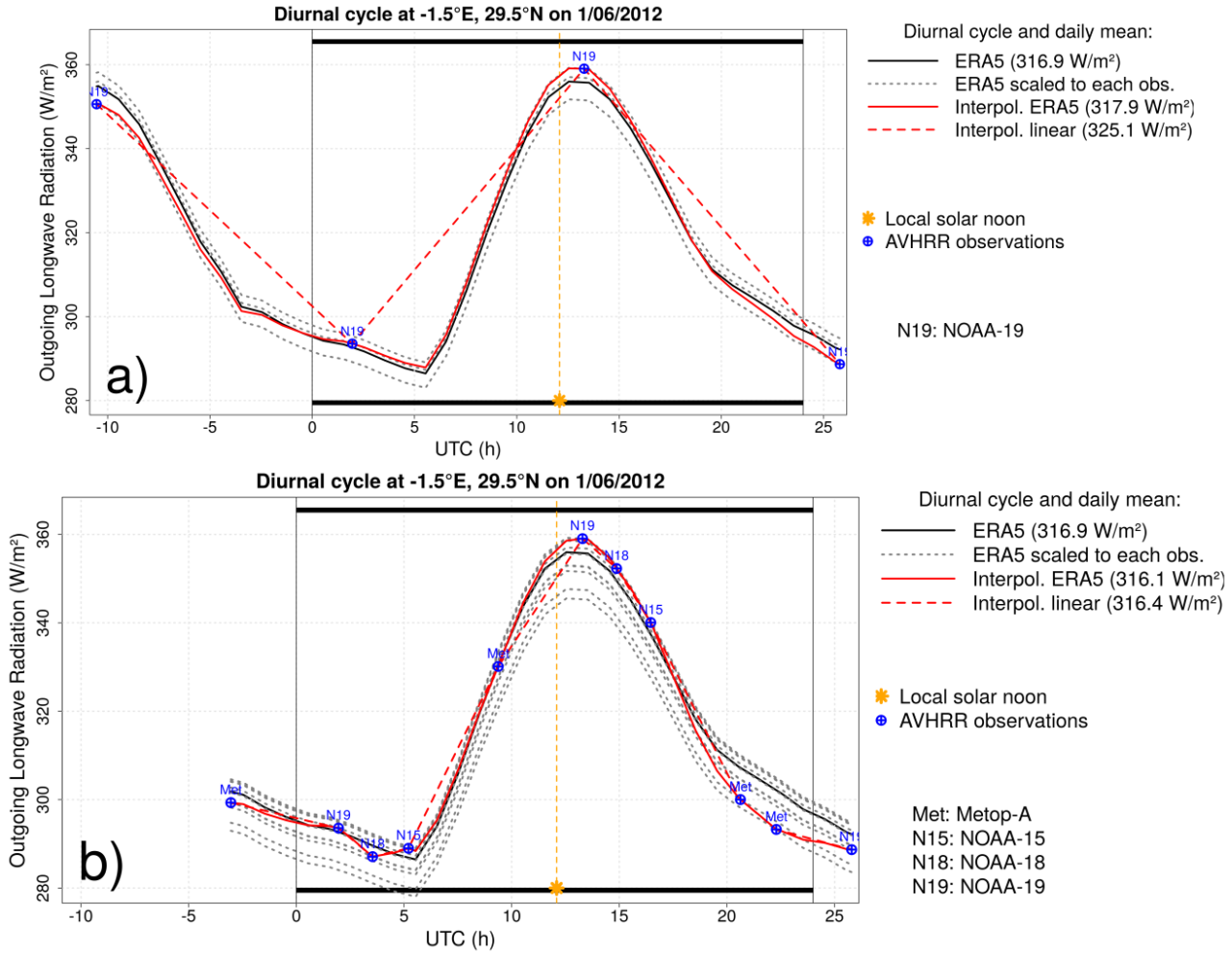

Figure 73: Example of OLR diurnal cycle for clear-sky desert pixel on 1/6/2012, modelled using a single satellite NOAA-19 (a) and using all available satellites (b). From Clerbaux et al. (2020).

The daily mean Outgoing Longwave Radiation ($OLR_{dailymean}$; Eq.22) is then calculated by averaging the interpolated diurnal cycle (dashed/solid red curves) over the entire UTC day, i.e., 0–24 h UTC, equivalent to 288 temporal bins of 5 minutes each (N=288).

$$OLR_{daily\ mean} = \frac{1}{N} \cdot \left(\sum_{n=1}^{N} OLR_n \right) \tag{22}$$

where OLR_n is the interpolated-diurnal-cycle OLR for the nth temporal *5min bin*. In this example, the linear interpolation of observations resulted in a daily mean of 325.1 W/m² (dashed red curve), while the ERA5-scaling interpolation significantly decreased the daily mean by 7.2 W/m² to 317.9 W/m² (solid red curve).

The method could be applied, and a daily mean value could be calculated, as long as there is at least one observation during that day. Obviously, more observations spread over the day made the resulting daily mean product less sensitive to the ERA5-scaling: this is shown in Figure 73b, for which eight daily observations, from four different satellites, were used.

An example of the $OLR_{dailymean}$ for UTC day 2/1/1998 is given in Figure 74.

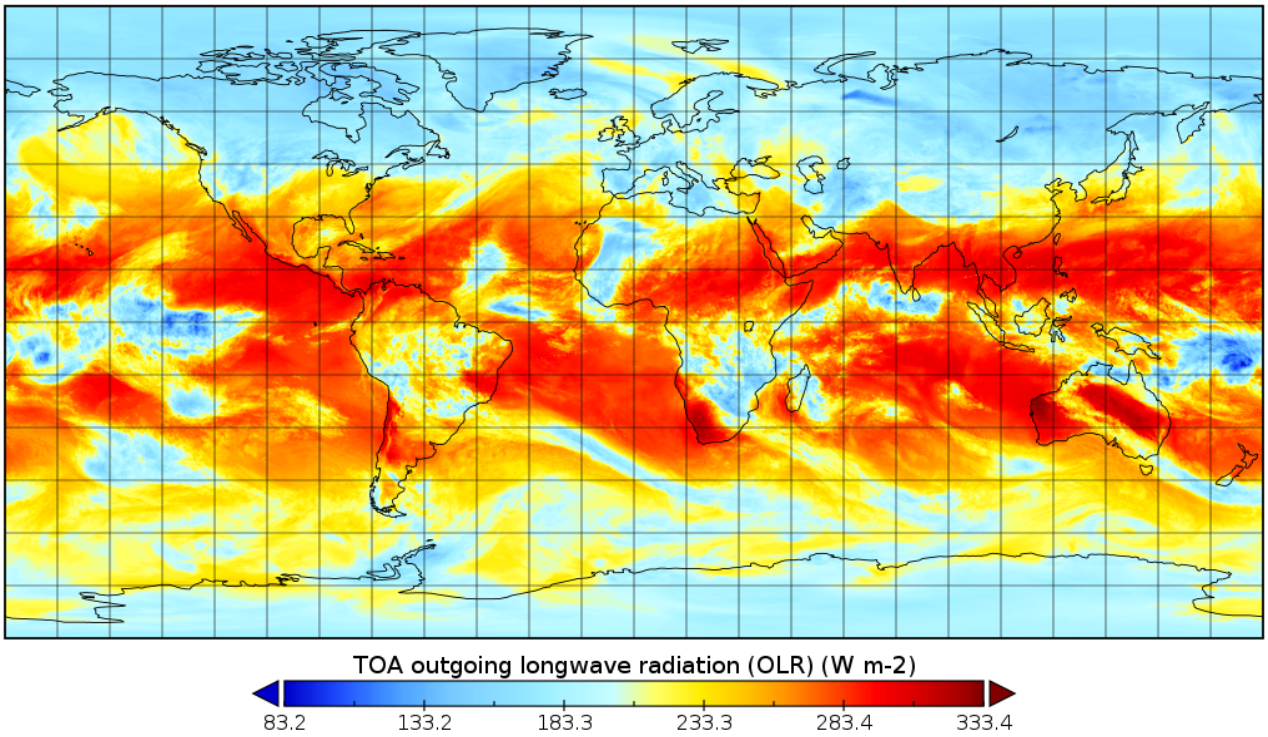

Figure 74: TOA Daily mean Outgoing Longwave Radiation for 2/1/1998

4.3.2. Output

The output of Program Part 3 consists of two NetCDF files per day: one containing all shortwave quantities, the other containing all longwave quantities. The files both have spatial dimensions of 1440x720, structured in a regular lat-lon global grid with 0.25°x0.25° resolution. The following variables are stored in the LW outputfile:

- **Outgoing Longwave Radiation, daily mean; $OLR_{daily\ mean}$ (W/m^2)**
- Number of LW instantaneous observations
- Bit flags (bitwise quality flags)
- Satellite bit flags

4.4. Part 4: Temporal aggregation to monthly mean OLR (level-3b)

The monthly mean Outgoing Longwave Radiation ($OLR_{monthlymean}$; Eq.23) is calculated by taking the average of all *OLR daily means* that have been processed in Section 4.3, with the number of contributing daily means being respectively D (which should ideally be the number of days during that month).

$$OLR_{monthly\ mean} = \frac{1}{D} \cdot \left(\sum_{d=1}^{D} OLR_{dailymean,d} \right) \quad (23)$$

Ideally, all grid boxes have a complete temporal coverage for all days of the month. This is logged by the variable "*Number of SW daily means contributing to monthly mean*" for which an example is shown in Figure 66, taken from the month January 1998: note that most of the grid boxes have a complete temporal coverage (31/31 days), while some smaller regions have one or two days missing (cfr bluish colors, with 30/31 or 29/31 days).

The user is strongly encouraged to verify this auxiliary variable before doing analyses on the main results (monthly mean OLR). Two bit flags are added to help diagnosing this issue:

- **MISSINGDAYS_WARNING**: this flag is set when the temporal coverage is not complete, and the number of missing days ranges between 1-4. The monthly mean OLR is not entirely representative since some days are missing, but can still be used (depending of course on the application or analysis).

- **MISSINGDAYS_INVALID**: this flag is set when the temporal coverage is not sufficient, with the number of missing days being 5 or more. The monthly mean OLR is considered invalid and the **user is advised not to use it**.

Some of the auxiliary variables created by the daily mean program (Part 3) are propagated to the monthly mean Program Part 4, which creates a monthly mean from them.

The output from Program Part 4 is as follows:

- **Outgoing Longwave Radiation, daily mean; $OLR_{daily\ mean}$ (W/m^2)**
- Number of LW instantaneous observations
- Bit flags (bitwise quality flags)

5. Error budget estimation

5.1. Theoretical sources of uncertainty

The following tables provide an error estimate of the different components in the TOA retrieval algorithm. Note that these should be added to the pre-existing error sources associated with e.g. FDR geolocation, FDR calibration, etc. Some components are not yet known at the time of writing, but will be clarified in the Validation Report.

On instantaneous scale:

Error source	***shortwave***	***longwave***
Spectral response correction	*(included in FDR)*	*(not yet known)*
SW narrowband-to-broadband LW narrowband-to-OLR	~11 to 16 W/m² (5% to 7% rel.RMSE) range*	4.86 W/m² (***)
CERES SW TRMM ADMs	10 W/m² (Loeb et al.,2005**; +own analysis) *(i.e.~5%)*	*n.a.*
TOTAL	$\sqrt{(11^2+10^2)}$ = 14.9 W/m²	$\sqrt{(4.86^2)}$ = 4.86 W/m²
(*) Relative RMSE between AVHRR-derived and CERES-observed broadband reflectance. 7% is likely an overestimation as it includes uncertainty due to scene type identification (surface/cloud properties) and to spatial-temporal matching of AVHRR-CERES observations. *(**) 1° regional instantaneous TOA flux uncertainty* *(***) Clerbaux et al., 2020*		

On daily scale: this depends on number of satellites and their equatorial crossing time, which varies across the record (e.g. mid-morning orbit only available from 2002 onwards).

Error source	***shortwave***	***longwave***
Spectral response correction	*(included in FDR)*	*(not yet known)*
SW narrowband-to-broadband LW narrowband-to-OLR	*~6%, i.e. 6W/m² (*)*	*(not yet known)*
CERES SW TRMM ADMs	~5%, i.e. 5 W/m² (*)	*n.a.*
Diurnal cycle model	~7 W/m² (own analysis**)	2.4 W/m² (Doelling,2013)
TOTAL	$\sqrt{(6^2+5^2+7^2)}$ = 10.5 W/m²	
*(*) Assuming the daily equals the instantaneous **relative** uncertainty, and a global daily mean RSF of 100 W/m² and OLR of 240 W/m²* *(**) by comparing daily mean RSF calculated from only 2 satellites (early morning and afternoon) and from all available satellites (incl.mid-morning) for July 2011.*		

On monthly scale:

Error source	***shortwave***	***longwave***
Spectral response correction	*(included in FDR)*	
SW narrowband-to-broadband LW narrowband-to-OLR	*~6%, i.e. 6W/m² (*)*	*(to be checked with NC)*
CERES SW TRMM ADMs	~5%, i.e. 5 W/m² (*)	*n.a.*
Diurnal cycle model	~2 W/m² (own analysis**)	
TOTAL	$\sqrt{(6^2+5^2+2^2)}$ = 8 W/m²	
(**) by comparing monthly mean RSF calculated from only 2 satellites (early morning and afternoon) and from all available satellites (incl.mid-morning) for July 2011. *(***) Assuming the monthly equals the instantaneous **relative** uncertainty, and a global monthly mean RSF of 100 W/m² and OLR of 240 W/m²*		

5.2. Evaluation based on preliminary products

Here follow some preliminary validation results, based on a test run of the software on a selection of months. Please note that this does not concern the final software, not the final results, and thus not the final validation results. Also, it is very limited in terms of performance indicators. The main objective is here to give the reader a very first impression of the retrieval algorithms' performance, which is done by comparing monthly means with several external reference data: ERA5 reanalysis, CERES SYN1deg monthly Ed4.1, CERES EBAF-TOA Ed4.1, and HIRS OLR. For each month, the global mean bias and (bias-corrected) RMSE w.r.t. each of the reference data is calculated and plotted in Figures 75 and 76.

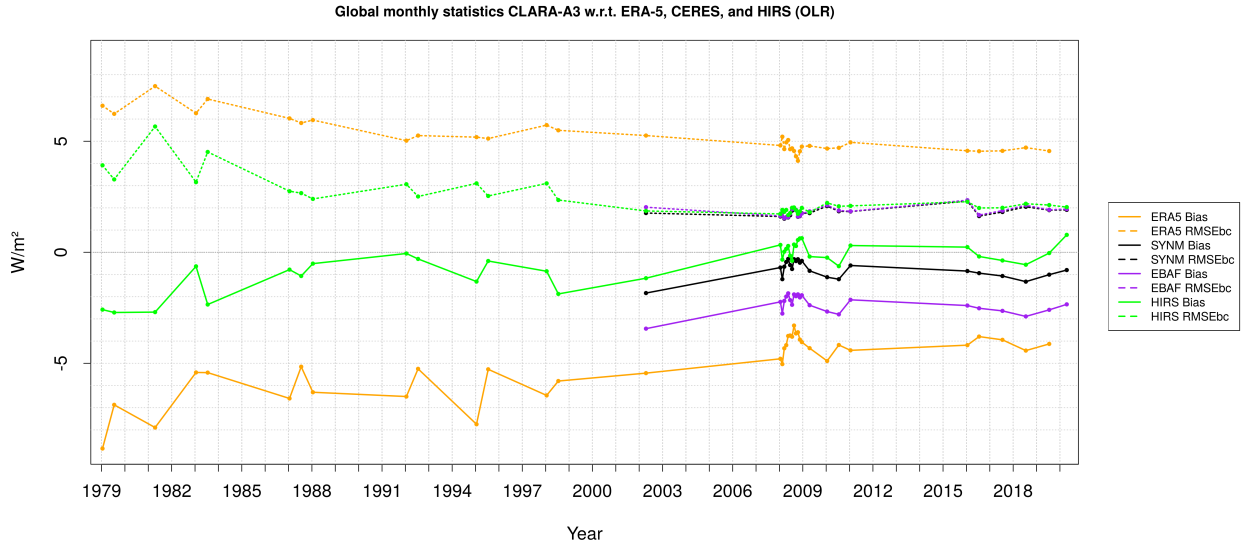

Figure 75: Global monthly statistics CLARA-A3 w.r.t. ERA5, CERES, and HIRS (OLR)

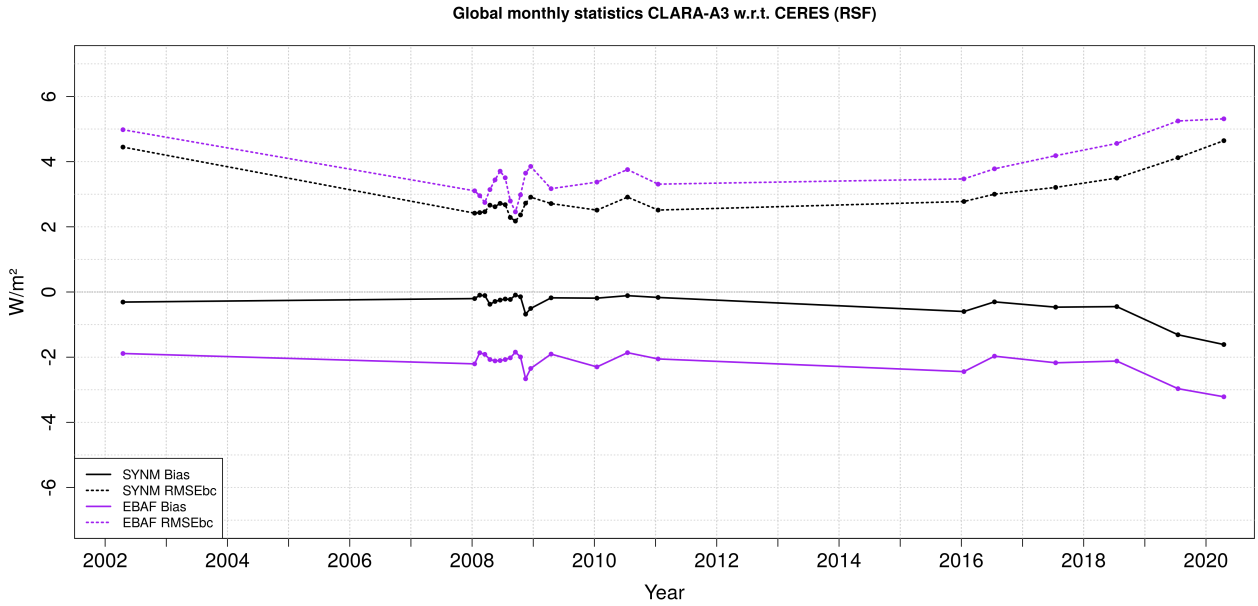

Figure 76: Global monthly statistics CLARA-A3 w.r.t. CERES (RSF)

These very preliminary validation results show a relatively stable product with an acceptable bias, and an RMSE which in most cases falls within the “target” accuracy requirement [RD 1].

6. Assumptions, limitations, future outlook

6.1. Input data: Snow cover

6.1.1. Problem statement

Spatially and temporally variable snow cover is taken into account, but only very roughly.

For clearsky conditions, the **presence of snow** is detected with a category from the cloudmask ("CMA extended") but this is known to be inaccurate when channel 5 is not available (12µm), which is the case for AVHRR/1 instrument (satellites TIROS-N, NOAA-6/-8/-10).

The observation-based snow presence detection is supplemented with snow depth from reanalysis (ERA5) and then converted to within-pixel fractional **snow cover** (with a minimum of 5cm snowdepth, i.e. 50% cover). This snow depth is heavily based on modeling, so its accuracy can be questioned.

We can identify some situations that may cause biases:

- CMAextended fails to detect snow presence: especially important for AVHRR/1 (TIROS-N, NOAA-6/-8/-10). The opposite is also a risk (false positives).
- CMAextended snow presence flag is optimized for "pure" snow surfaces, where snow-covered areas dominate the FOV. For forested regions this parameter may not be trustworthy (*K.-G. Karlsson, pers.comm., 2020*); see Figure 77.
- ERA5 snow depth dataset is inaccurate (spatial, temporal, and meteorological errors); since the minimal coverage is 50%, the potential errors could maximally be:
  - setting snow coverage to 50% whereas in reality it's 100%
  - setting snow coverage to 100% whereas in reality it's 0%
- ERA5 snow depth–cover relation does not take into account the surface variability and the relation with the underlying surface type: tundra and grassland typically leave vast white blankets, while forests and mountainous terrain are typically less prone to complete snow coverage (see Figure 77).

Figure 77: illustration of how land surface influences snow cover

For overcast or nighttime scenes, both snow presence ánd coverage are identified using the ERA5 reanalysis. However, in these cases its accuracy is less essential compared to clearsky scenes, since the potential biases are lower (difference between overcast snow-free and overcast snow-covered surface is minimal).
ERA5 assimilates snow cover from IMS 4km product. However, this is only the case after 2004.

6.1.2. Future outlook

The current way of snow cover determination is not accurate enough. Furthermore, CMAextended is part of the classic (deterministic) cloud mask, from which the development will not be continued because the new probabilistic cloud mask is now implemented (which does not contain a “snow/ice contamination flag”). Ideally next CLARA releases should also take satellite-based snow cover into account, e.g.:

- the ***Northern Hemisphere EASE-Grid 2.0 Weekly Snow Cover and Sea Ice Extent, Version 4***
  - https://nsidc.org/data/NSIDC-0046
  - covering years 1978-2019.
  - https://daacdata.apps.nsidc.org/pub/DATASETS/nsidc0046_weekly_snow_seaice/data/
- the ***NOAA Climate Data Record (CDR) of Northern Hemisphere (NH) Snow Cover Extent (SCE), v.1***
  - Snow cover extent for this data set is based on the NOAA/NCDC Climate Data Record (CDR) of Northern Hemisphere (NH) Snow Cover Extent (SCE) by D. Robinson (2012) and regridded to the EASE-Grid. The NOAA/NCDC CDR of Northern Hemisphere Snow Cover Extent data were derived from the manual interpretation of AVHRR, GOES, and other visible-band satellite data (Helfrich et al. 2007).
  - https://www.ncei.noaa.gov/access/metadata/landing-page/bin/iso?id=gov.noaa.ncdc:C00756

6.2. Input data: Land cover

Land use is not static, and for some regions very dynamic in time. This can be on inter-annual scale (e.g. seasonal vegetation in Sahel) or on long term (e.g. drying out of lakes).
Since the IGBP map is from the early 90s (1992-1993), it is situated in the middle of the timeseries (ranging between 1979-2019) and can therefore be considered as a “representative average situation”. However, for certain parts of the record there will certainly be mismatches leading to errors in scene type selection, and consequently the resulting RSF and/or OLR.

6.3. Input data: ADMs (and aerosols)

In future versions of the CLARA TOA flux product, we aim for a systematic implementation of the Ed.4 ADMs (Su et al., 2015) for all scene types. This means that the older Ed.2B ADMs will be completely replaced.
These new ADM's also contain aerosol-specific scene types. Since aerosols are currently not taken into account, this would likely improve the retrieval's performance. It should be investigated well in advance whether the auxiliary aerosol input data will be retrieved as part of the future CLARA TOA flux product, or if it would be a general CLARA add-on product, or if it would be a completely external aerosol optical depth data record.

7. Abbreviations and acronyms

Abbreviation or acronym	
ADM	Angular Distribution Model *(also: Angular Dependency Model)*
AVHRR	Advanced Very High Resolution Radiometer
CDR	Climate Data Record *(see also: FCDR)*
CERES	Clouds and the Earth's Radiant Energy System
CLASS	The Comprehensive Large Array-data Stewardship System (NOAA)
CDR	Climate Data Record *(see also: FCDR)*
CMAext(ended); CMAprob	Cloud Mask Extended (legacy); Cloud Mask Probabilistic (new)
CM SAF	Climate Monitoring Satellite Application Facility
COT	Cloud Optical Thickness *(also: Cloud Optical Depth)*
DLB	Day Light Block
ERA5	Fifth generation ECMWF reanalysis
F(C)DR	Fundamental (Climate) Data Record
FIDUCEO	Fidelity and uncertainty in climate data records from Earth Observations (EU FP7 project)
GAC	Global Area Coverage
GAC orbit grid	Irregular grid with each pixel representing an AVHRR/GAC observation on its original location
IGBP	International Geosphere Biosphere Program
IWV	Integrated Water Vapor
LW	Longwave
MODIS	Moderate Resolution Imaging Spectroradiometer (on Aqua and Terra satellites)
NOAA	National Oceanic and Atmospheric Administration
NOAA-X	NOAA satellite numbered X
NTB	Narrowband-to-broadband
NWC SAF	Nowcasting Satellite Application Facility
OLR	Outgoing Longwave Radiation (W/m²)
OSI SAF	Ocean and Sea Ice Satellite Application Facility
PPS	Polar Platform System
RAA (φ)	Relative Azimuth Angle (°)
RSF	Reflected Solar Flux (W/m²)
SBAF	Spectral Band Adjustment Factors
SNO	Simultaneous Nadir Observations
SST	Sea Surface Temperatures
SW	Shortwave
SZA (θ_0)	Solar Zenith Angle (°)
TCDR	Thematic Climate Data Record
TIROS-N	Television InfraRed Observation Satellite -N
TOA	Top of Atmosphere
TRMM	Tropical Rainfall Measuring Mission
TWL	Twilight
VIRS	Visible Infrared Scanner
VZA (θ)	Viewing Zenith Angle (°)

8. Scientific references

Akkermans, T., & Clerbaux, N. (2020). Narrowband-to-Broadband Conversions for Top-of-Atmosphere Reflectance from the Advanced Very High Resolution Radiometer (AVHRR). Remote Sensing, 12(2), 305.

Bretagnon, P., & Simon, J. L. (1986). Planetary Programs and Tables from-4000 to+ 2800. *pptt*.

Clerbaux, N., Akkermans, T., Baudrez, E., Velazquez Blazquez, A., Moutier, W., Moreels, J., & Aebi, C. (2020). The Climate Monitoring SAF Outgoing Longwave Radiation from AVHRR. *Remote Sensing*, *12*(6), 929.

Devasthale, A., Raspaud, M., Schlundt, C., Hanschmann, T., Finkensieper, S., Dybbroe, A., ... & Karlsson, K. G. (2016). PyGAC: an open-source, community-driven Python interface to preprocess more than 30-year AVHRR Global Area Coverage (GAC) data.

Dybbroe, A., Karlsson, K. G., & Thoss, A. (2005). NWCSAF AVHRR cloud detection and analysis using dynamic thresholds and radiative transfer modeling. Part I: Algorithm description. Journal of applied meteorology, 44(1), 39-54.

Dybbroe, A., Karlsson, K. G., & Thoss, A. (2005). NWCSAF AVHRR cloud detection and analysis using dynamic thresholds and radiative transfer modeling. Part II: Tuning and validation. Journal of Applied Meteorology, 44(1), 55-71.

Dewitte, S., & Nevens, S. (2016). The total solar irradiance climate data record. *The Astrophysical Journal*, *830*(1), 25.

Dewitte, S., & Clerbaux, N. (2017). Measurement of the earth radiation budget at the top of the atmosphere—a review. *Remote Sensing*, *9*(11), 1143.

Doelling, D. R., Loeb, N. G., Keyes, D. F., Nordeen, M. L., Morstad, D., Nguyen, C., ... & Sun, M. (2013). Geostationary enhanced temporal interpolation for CERES flux products. *Journal of Atmospheric and Oceanic Technology*, *30*(6), 1072-1090.

Frey, C. M., Kuenzer, C., & Dech, S. (2017). Assessment of Mono-and Split-Window Approaches for Time Series Processing of LST from AVHRR—A TIMELINE Round Robin. *Remote Sensing*, *9*(1), 72.

Heidinger, A.K., Straka, W.C., Molling, C.C., Sullivan, J.T. and Wu, X.Q. (2010): Deriving an inter-sensor consistent calibration for the AVHRR solar reflectance data record. Int. J. Rem. Sens., 31(24), 6493-6517.

Hersbach, H., Bell, B., Berrisford, P., Hirahara, S., Horányi, A., Muñoz-Sabater, J., ... & Thépaut, J. N. (2020). The ERA5 global reanalysis. *Quarterly Journal of the Royal Meteorological Society*, *146*(730), 1999-2049.

Ipe, A. (2011). *Cloud properties retrieval for climate studies from geostationary orbit* (Doctoral dissertation, Ph. D. Thesis, Vrije Universiteit Brusssel, Brusssel, Belgium, 30 June 2011. Available online: http://gerb. oma. be (accessed on 17 February 2017)).

Karlsson, K. G., Anttila, K., Trentmann, J., Stengel, M., Meirink, J. F., Devasthale, A., ... & Benas, N. (2017). CLARA-A2: the second edition of the CM SAF cloud and radiation data record from 34 years of global AVHRR data. *Atmospheric Chemistry and Physics*, *17*(9), 5809-5828.

Karlsson, K. G., Johansson, E., Håkansson, N., Sedlar, J., & Eliasson, S. (2020). Probabilistic Cloud Masking for the Generation of CM SAF Cloud Climate Data Records from AVHRR and SEVIRI Sensors. Remote Sensing, 12(4), 713.

Kato, S., & Loeb, N. G. (2003). Twilight irradiance reflected by the earth estimated from Clouds and the Earth's Radiant Energy System (CERES) measurements. Journal of climate, 16(15), 2646-2650.

Loeb, N. G., Manalo-Smith, N., Kato, S., Miller, W. F., Gupta, S. K., Minnis, P., & Wielicki, B. A. (2003). Angular distribution models for top-of-atmosphere radiative flux estimation from the Clouds and the Earth's Radiant Energy System instrument on the Tropical Rainfall Measuring Mission satellite. Part I: Methodology. *Journal of applied meteorology*, *42*(2), 240-265.

Loeb, N. G., & Coakley, J. A. S. Kato, K. Loukachine, and N. Manalo-Smith, 2005: Angular distribution models for top-of-atmosphere radiative flux estimation from the Clouds and the Earth's Radiant Energy System instrument on the Terra satellite. Part I: Methodology. *J. Atmos. Oceanic Technol*, *22*, 338-351.

Loveland, T. R., Reed, B. C., Brown, J. F., Ohlen, D. O., Zhu, Z., Yang, L. W. M. J., & Merchant, J. W. (2000). Development of a global land cover characteristics database and IGBP DISCover from 1 km AVHRR data. *International Journal of Remote Sensing*, *21*(6-7), 1303-1330.

Mittaz, J.P.D., Harris, A.R. and Sullivan, J.T., (2007), A Physical Method for the Calibration of the AVHRR/3 Thermal IR Channels 1: The Pre-launch Calibration Data, J. Atmos. Oceanic Technol., 26, 996.

Mittaz, J.P.D. and Harris, A.R., (2008), Using AATSR as a Radiance Calibration reference from NOAA Satellites, 2nd MERIS/(A)ATSR Users Workshop, Frascati, Italy, 22-26 Sept. 2008, H. Lacoste & L. Ouwehand (Eds.) (ESA Special Publication Series SP-666), Paper 869.

Rípodas Agudo, P., Calvet, X., Lliso Valverde, L., Lahuerta García, J. A., Martínez Rubio, M. Á., García Pereda, J., ... & Moisselin, J. M. (2019). The nowcasting SAF products and services: recent improvements in the new SW packages PPS v2018 and GEO v2018 and future plans.

Roebeling, R. A., Feijt, A. J., & Stammes, P. (2006). Cloud property retrievals for climate monitoring: Implications of differences between Spinning Enhanced Visible and Infrared Imager (SEVIRI) on METEOSAT-8 and Advanced Very High Resolution Radiometer (AVHRR) on NOAA-17. Journal of Geophysical Research: Atmospheres, 111(D20).

Scarino, B. R., Doelling, D. R., Minnis, P., Gopalan, A., Chee, T., Bhatt, R., ... & Haney, C. (2016). A web-based tool for calculating spectral band difference adjustment factors derived from SCIAMACHY hyperspectral data. *IEEE Transactions on Geoscience and Remote Sensing*, *54*(5), 2529-2542.

Stengel, M., Stapelberg, S., Sus, O., Finkensieper, S., Würzler, B., Philipp, D., ... & McGarragh, G. (2020). Cloud_cci Advanced Very High Resolution Radiometer post meridiem (AVHRR-PM) dataset version 3: 35-year climatology of global cloud and radiation properties. *Earth System Science Data*, *12*(1), 41-60.

Su, W., Corbett, J., Eitzen, Z., & Liang, L. (2015). Next-generation angular distribution models for top-of-atmosphere radiative flux calculation from CERES instruments: Methodology. *Meas. Tech*, *8*(2), 611-632.

Tonboe, R., Lavelle, J., Pfeiffer, R. H., & Howe, E. (2016). Product user manual for OSI SAF global sea ice concentration. *Danish Meteorological Institute, Denmark*.

Townshend, J. R. G. (1992). The 1-km AVHRR global data set: needs of the International Geosphere Biosphere Program. *Int. J. Remote Sensing*, *15*(17), 3319-3332.

Trishchenko, A.P., (2002), Removing unwanted fluctuations in the AVHRR thermal calibration data using robust techniques, J. Atmos. Oceanic Technol., 19, pp1939-1954

Young, D. F., Minnis, P., Doelling, D. R., Gibson, G. G., & Wong, T. (1998). Temporal interpolation methods for the Clouds and the Earth's Radiant Energy System (CERES) experiment. *Journal of Applied Meteorology*, *37*(6), 572-590.

Wang, L and Cao, C, (2008), Calibration Assessment of AVHRR Longwave Channels on Metop-A using IASI, IEEE Transactions on Geoscience and Remote Sensing, 46, 1.

Walton, C.C., Sullivan, J.T., Rao, C.R.N. and Weinreb, M.P., (1998), Corrections for detector nonlinearities and calibration inconsistencies for the infrared channels of the advanced very high resolution radiometer, J. Geophys. Res, 103, pp3323-3357

Wielicki, B. A., Barkstrom, B. R., Harrison, E. F., Lee III, R. B., Smith, G. L., & Cooper, J. E. (1996). Clouds and the Earth's Radiant Energy System (CERES): An earth observing system experiment. *Bulletin of the American Meteorological Society*, *77*(5), 853-868.

9. Annex

9.1. Scene types for ADMs and albedo models: overview

Tables with scene types used to select the shortwave ADM's and albedo models

9.1.1. CERES/TRMM Ed.2B ADMs, scene types and albedo models

More information and graphs can be found on the CERES website: https://ceres.larc.nasa.gov/data/angular-distribution-models/#cerestrmm-ssf-edition2b-adms

For water and land scene types (i.e. all non-snow and non-ice) the CERES TRMM SW ADM's are used: these were derived from the CERES instrument onboard the TRMM satellite (Loeb et al., 2003). For each of the 590 scene types:

- ..a three-dimensional look-up table is available (**ADM**), with dimensions SZA, VZA, and RAA. With the correct angles, the closest corresponding anisotropic factor can be identified in this look-up table, or for more accuracy it can be interpolated using all the closest anisotropic factors.
- ..an **albedo model** is available, with a single dimension (SZA);

In the table, the scene types that are used in the Level-2 processing (calculation of shortwave TOA albedo for every instantaneous AVHRR pixel) are shown in bold green color: this concerns only the 'pure' cloud conditions are (clear, and 100% overcast), as fractional cloud cover is not relevant for a binary cloud mask. For the Level-3 processing, however, also the albedo models for the grayed-out scene types are used, since the aggregation to the 0.25°x0.25° grid generates fractional cloud cover.

Table 14: ADM scene types (non-snow, non-ice)

ADM ID	Scene Type	Wind Speed (m/s)	Cloud Phase	Cloud Fraction (%)	Cloud Opt. Depth
1	**Clear Ocean**	**Ws<=3.5**	**-999**	**-999**	**-999**
2	**Clear Ocean**	**3.5<Ws<=5.5**	**-999**	**-999**	**-999**
3	**Clear Ocean**	**5.5<Ws<=7.5**	**-999**	**-999**	**-999**
4	**Clear Ocean**	**Ws>7.5**	**-999**	**-999**	**-999**
5	**Clear Ocean**	**all ws**	**-999**	**-999**	**-999**
6	Clear Ocean (ADM flx)	ws1	-999	-999	-999
7	Clear Ocean (ADM flx)	ws2	-999	-999	-999
8	Clear Ocean (ADM flx)	ws3	-999	-999	-999
9	Clear Ocean (ADM flx)	ws4	-999	-999	-999
10	Clear Ocean (ADM flx)	all ws	-999	-999	-999
11	**Clear Mod-Hi Tree/Shrub**	**-999**	**-999**	**-999**	**-999**
12	**Clear Low-Mod Tree/Shrub**	**-999**	**-999**	**-999**	**-999**
13	**Clear Dark Desert**	**-999**	**-999**	**-999**	**-999**
14	**Clear Bright Desert**	**-999**	**-999**	**-999**	**-999**
15	**Cloud Ocean**	**-999**	**Liquid**	**0.1 - 10**	**0.01 - 1.0**
16	**Cloud Ocean**	**-999**	**Liquid**	**0.1 - 10**	**1.0 - 2.5**
17	**Cloud Ocean**	**-999**	**Liquid**	**0.1 - 10**	**2.5 - 5.0**
18	**Cloud Ocean**	**-999**	**Liquid**	**0.1 - 10**	**5.0 - 7.5**
19	**Cloud Ocean**	**-999**	**Liquid**	**0.1 - 10**	**7.5 - 10.0**
20	**Cloud Ocean**	**-999**	**Liquid**	**0.1 - 10**	**10.0 - 12.5**
21	**Cloud Ocean**	**-999**	**Liquid**	**0.1 - 10**	**12.5 - 15.0**
22	**Cloud Ocean**	**-999**	**Liquid**	**0.1 - 10**	**15.0 - 17.5**
23	**Cloud Ocean**	**-999**	**Liquid**	**0.1 - 10**	**17.5 - 20.0**
24	**Cloud Ocean**	**-999**	**Liquid**	**0.1 - 10**	**20.0 - 25.0**
25	**Cloud Ocean**	**-999**	**Liquid**	**0.1 - 10**	**25.0 - 30.0**
26	**Cloud Ocean**	**-999**	**Liquid**	**0.1 - 10**	**30.0 - 40.0**
27	**Cloud Ocean**	**-999**	**Liquid**	**0.1 - 10**	**40.0 - 50.0**
28	**Cloud Ocean**	**-999**	**Liquid**	**0.1 - 10**	**> 50.0**
29	Cloud Ocean	-999	Liquid	10 - 20	0.01 - 1.0
30	Cloud Ocean	-999	Liquid	10 - 20	1.0 - 2.5
31	Cloud Ocean	-999	Liquid	10 - 20	2.5 - 5.0

32	Cloud Ocean	-999	Liquid	10 - 20	5.0 - 7.5
33	Cloud Ocean	-999	Liquid	10 - 20	7.5 - 10.0
34	Cloud Ocean	-999	Liquid	10 - 20	10.0 - 12.5
35	Cloud Ocean	-999	Liquid	10 - 20	12.5 - 15.0
36	Cloud Ocean	-999	Liquid	10 - 20	15.0 - 17.5
37	Cloud Ocean	-999	Liquid	10 - 20	17.5 - 20.0
38	Cloud Ocean	-999	Liquid	10 - 20	20.0 - 25.0
39	Cloud Ocean	-999	Liquid	10 - 20	25.0 - 30.0
40	Cloud Ocean	-999	Liquid	10 - 20	30.0 - 40.0
41	Cloud Ocean	-999	Liquid	10 - 20	40.0 - 50.0
42	Cloud Ocean	-999	Liquid	10 - 20	> 50.0
43	Cloud Ocean	-999	Liquid	20 - 30	0.01 - 1.0
44	Cloud Ocean	-999	Liquid	20 - 30	1.0 - 2.5
45	Cloud Ocean	-999	Liquid	20 - 30	2.5 - 5.0
46	Cloud Ocean	-999	Liquid	20 - 30	5.0 - 7.5
47	Cloud Ocean	-999	Liquid	20 - 30	7.5 - 10.0
48	Cloud Ocean	-999	Liquid	20 - 30	10.0 - 12.5
49	Cloud Ocean	-999	Liquid	20 - 30	12.5 - 15.0
50	Cloud Ocean	-999	Liquid	20 - 30	15.0 - 17.5
51	Cloud Ocean	-999	Liquid	20 - 30	17.5 - 20.0
52	Cloud Ocean	-999	Liquid	20 - 30	20.0 - 25.0
53	Cloud Ocean	-999	Liquid	20 - 30	25.0 - 30.0
54	Cloud Ocean	-999	Liquid	20 - 30	30.0 - 40.0
55	Cloud Ocean	-999	Liquid	20 - 30	40.0 - 50.0
56	Cloud Ocean	-999	Liquid	20 - 30	> 50.0
57	Cloud Ocean	-999	Liquid	30 - 40	0.01 - 1.0
58	Cloud Ocean	-999	Liquid	30 - 40	1.0 - 2.5
59	Cloud Ocean	-999	Liquid	30 - 40	2.5 - 5.0
60	Cloud Ocean	-999	Liquid	30 - 40	5.0 - 7.5
61	Cloud Ocean	-999	Liquid	30 - 40	7.5 - 10.0
62	Cloud Ocean	-999	Liquid	30 - 40	10.0 - 12.5
63	Cloud Ocean	-999	Liquid	30 - 40	12.5 - 15.0
64	Cloud Ocean	-999	Liquid	30 - 40	15.0 - 17.5
65	Cloud Ocean	-999	Liquid	30 - 40	17.5 - 20.0
66	Cloud Ocean	-999	Liquid	30 - 40	20.0 - 25.0
67	Cloud Ocean	-999	Liquid	30 - 40	25.0 - 30.0
68	Cloud Ocean	-999	Liquid	30 - 40	30.0 - 40.0
69	Cloud Ocean	-999	Liquid	30 - 40	40.0 - 50.0
70	Cloud Ocean	-999	Liquid	30 - 40	> 50.0
71	Cloud Ocean	-999	Liquid	40 - 50	0.01 - 1.0
72	Cloud Ocean	-999	Liquid	40 - 50	1.0 - 2.5
73	Cloud Ocean	-999	Liquid	40 - 50	2.5 - 5.0
74	Cloud Ocean	-999	Liquid	40 - 50	5.0 - 7.5
75	Cloud Ocean	-999	Liquid	40 - 50	7.5 - 10.0
76	Cloud Ocean	-999	Liquid	40 - 50	10.0 - 12.5
77	Cloud Ocean	-999	Liquid	40 - 50	12.5 - 15.0
78	Cloud Ocean	-999	Liquid	40 - 50	15.0 - 17.5
79	Cloud Ocean	-999	Liquid	40 - 50	17.5 - 20.0
80	Cloud Ocean	-999	Liquid	40 - 50	20.0 - 25.0
81	Cloud Ocean	-999	Liquid	40 - 50	25.0 - 30.0
82	Cloud Ocean	-999	Liquid	40 - 50	30.0 - 40.0
83	Cloud Ocean	-999	Liquid	40 - 50	40.0 - 50.0
84	Cloud Ocean	-999	Liquid	40 - 50	> 50.0
85	Cloud Ocean	-999	Liquid	50 - 60	0.01 - 1.0
86	Cloud Ocean	-999	Liquid	50 - 60	1.0 - 2.5
87	Cloud Ocean	-999	Liquid	50 - 60	2.5 - 5.0
88	Cloud Ocean	-999	Liquid	50 - 60	5.0 - 7.5
89	Cloud Ocean	-999	Liquid	50 - 60	7.5 - 10.0
90	Cloud Ocean	-999	Liquid	50 - 60	10.0 - 12.5
91	Cloud Ocean	-999	Liquid	50 - 60	12.5 - 15.0
92	Cloud Ocean	-999	Liquid	50 - 60	15.0 - 17.5
93	Cloud Ocean	-999	Liquid	50 - 60	17.5 - 20.0
94	Cloud Ocean	-999	Liquid	50 - 60	20.0 - 25.0
95	Cloud Ocean	-999	Liquid	50 - 60	25.0 - 30.0
96	Cloud Ocean	-999	Liquid	50 - 60	30.0 - 40.0
97	Cloud Ocean	-999	Liquid	50 - 60	40.0 - 50.0
98	Cloud Ocean	-999	Liquid	50 - 60	> 50.0

99	Cloud Ocean	-999	Liquid	60 - 70	0.01 - 1.0
100	Cloud Ocean	-999	Liquid	60 - 70	1.0 - 2.5
101	Cloud Ocean	-999	Liquid	60 - 70	2.5 - 5.0
102	Cloud Ocean	-999	Liquid	60 - 70	5.0 - 7.5
103	Cloud Ocean	-999	Liquid	60 - 70	7.5 - 10.0
104	Cloud Ocean	-999	Liquid	60 - 70	10.0 - 12.5
105	Cloud Ocean	-999	Liquid	60 - 70	12.5 - 15.0
106	Cloud Ocean	-999	Liquid	60 - 70	15.0 - 17.5
107	Cloud Ocean	-999	Liquid	60 - 70	17.5 - 20.0
108	Cloud Ocean	-999	Liquid	60 - 70	20.0 - 25.0
109	Cloud Ocean	-999	Liquid	60 - 70	25.0 - 30.0
110	Cloud Ocean	-999	Liquid	60 - 70	30.0 - 40.0
111	Cloud Ocean	-999	Liquid	60 - 70	40.0 - 50.0
112	Cloud Ocean	-999	Liquid	60 - 70	> 50.0
113	Cloud Ocean	-999	Liquid	70 - 80	0.01 - 1.0
114	Cloud Ocean	-999	Liquid	70 - 80	1.0 - 2.5
115	Cloud Ocean	-999	Liquid	70 - 80	2.5 - 5.0
116	Cloud Ocean	-999	Liquid	70 - 80	5.0 - 7.5
117	Cloud Ocean	-999	Liquid	70 - 80	7.5 - 10.0
118	Cloud Ocean	-999	Liquid	70 - 80	10.0 - 12.5
119	Cloud Ocean	-999	Liquid	70 - 80	12.5 - 15.0
120	Cloud Ocean	-999	Liquid	70 - 80	15.0 - 17.5
121	Cloud Ocean	-999	Liquid	70 - 80	17.5 - 20.0
122	Cloud Ocean	-999	Liquid	70 - 80	20.0 - 25.0
123	Cloud Ocean	-999	Liquid	70 - 80	25.0 - 30.0
124	Cloud Ocean	-999	Liquid	70 - 80	30.0 - 40.0
125	Cloud Ocean	-999	Liquid	70 - 80	40.0 - 50.0
126	Cloud Ocean	-999	Liquid	70 - 80	> 50.0
127	Cloud Ocean	-999	Liquid	80 - 90	0.01 - 1.0
128	Cloud Ocean	-999	Liquid	80 - 90	1.0 - 2.5
129	Cloud Ocean	-999	Liquid	80 - 90	2.5 - 5.0
130	Cloud Ocean	-999	Liquid	80 - 90	5.0 - 7.5
131	Cloud Ocean	-999	Liquid	80 - 90	7.5 - 10.0
132	Cloud Ocean	-999	Liquid	80 - 90	10.0 - 12.5
133	Cloud Ocean	-999	Liquid	80 - 90	12.5 - 15.0
134	Cloud Ocean	-999	Liquid	80 - 90	15.0 - 17.5
135	Cloud Ocean	-999	Liquid	80 - 90	17.5 - 20.0
136	Cloud Ocean	-999	Liquid	80 - 90	20.0 - 25.0
137	Cloud Ocean	-999	Liquid	80 - 90	25.0 - 30.0
138	Cloud Ocean	-999	Liquid	80 - 90	30.0 - 40.0
139	Cloud Ocean	-999	Liquid	80 - 90	40.0 - 50.0
140	Cloud Ocean	-999	Liquid	80 - 90	> 50.0
141	Cloud Ocean	-999	Liquid	90 - 95	0.01 - 1.0
142	Cloud Ocean	-999	Liquid	90 - 95	1.0 - 2.5
143	Cloud Ocean	-999	Liquid	90 - 95	2.5 - 5.0
144	Cloud Ocean	-999	Liquid	90 - 95	5.0 - 7.5
145	Cloud Ocean	-999	Liquid	90 - 95	7.5 - 10.0
146	Cloud Ocean	-999	Liquid	90 - 95	10.0 - 12.5
147	Cloud Ocean	-999	Liquid	90 - 95	12.5 - 15.0
148	Cloud Ocean	-999	Liquid	90 - 95	15.0 - 17.5
149	Cloud Ocean	-999	Liquid	90 - 95	17.5 - 20.0
150	Cloud Ocean	-999	Liquid	90 - 95	20.0 - 25.0
151	Cloud Ocean	-999	Liquid	90 - 95	25.0 - 30.0
152	Cloud Ocean	-999	Liquid	90 - 95	30.0 - 40.0
153	Cloud Ocean	-999	Liquid	90 - 95	40.0 - 50.0
154	Cloud Ocean	-999	Liquid	90 - 95	> 50.0
155	Cloud Ocean	-999	Liquid	95 - 99.9	0.01 - 1.0
156	Cloud Ocean	-999	Liquid	95 - 99.9	1.0 - 2.5
157	Cloud Ocean	-999	Liquid	95 - 99.9	2.5 - 5.0
158	Cloud Ocean	-999	Liquid	95 - 99.9	5.0 - 7.5
159	Cloud Ocean	-999	Liquid	95 - 99.9	7.5 - 10.0
160	Cloud Ocean	-999	Liquid	95 - 99.9	10.0 - 12.5
161	Cloud Ocean	-999	Liquid	95 - 99.9	12.5 - 15.0
162	Cloud Ocean	-999	Liquid	95 - 99.9	15.0 - 17.5
163	Cloud Ocean	-999	Liquid	95 - 99.9	17.5 - 20.0
164	Cloud Ocean	-999	Liquid	95 - 99.9	20.0 - 25.0
165	Cloud Ocean	-999	Liquid	95 - 99.9	25.0 - 30.0

166	Cloud Ocean	-999	Liquid	95 - 99.9	30.0 - 40.0
167	Cloud Ocean	-999	Liquid	95 - 99.9	40.0 - 50.0
168	Cloud Ocean	-999	Liquid	95 - 99.9	> 50.0
169	**Cloud Ocean**	**-999**	**Liquid**	**99.9 - 100**	**0.01 - 1.0**
170	**Cloud Ocean**	**-999**	**Liquid**	**99.9 - 100**	**1.0 - 2.5**
171	**Cloud Ocean**	**-999**	**Liquid**	**99.9 - 100**	**2.5 - 5.0**
172	**Cloud Ocean**	**-999**	**Liquid**	**99.9 - 100**	**5.0 - 7.5**
173	**Cloud Ocean**	**-999**	**Liquid**	**99.9 - 100**	**7.5 - 10.0**
174	**Cloud Ocean**	**-999**	**Liquid**	**99.9 - 100**	**10.0 - 12.5**
175	**Cloud Ocean**	**-999**	**Liquid**	**99.9 - 100**	**12.5 - 15.0**
176	**Cloud Ocean**	**-999**	**Liquid**	**99.9 - 100**	**15.0 - 17.5**
177	**Cloud Ocean**	**-999**	**Liquid**	**99.9 - 100**	**17.5 - 20.0**
178	**Cloud Ocean**	**-999**	**Liquid**	**99.9 - 100**	**20.0 - 25.0**
179	**Cloud Ocean**	**-999**	**Liquid**	**99.9 - 100**	**25.0 - 30.0**
180	**Cloud Ocean**	**-999**	**Liquid**	**99.9 - 100**	**30.0 - 40.0**
181	**Cloud Ocean**	**-999**	**Liquid**	**99.9 - 100**	**40.0 - 50.0**
182	**Cloud Ocean**	**-999**	**Liquid**	**99.9 - 100**	**> 50.0**
183	Cloud Ocean	-999	Ice	0.1 - 10	0.01 - 1.0
184	Cloud Ocean	-999	Ice	0.1 - 10	1.0 - 2.5
185	Cloud Ocean	-999	Ice	0.1 - 10	2.5 - 5.0
186	Cloud Ocean	-999	Ice	0.1 - 10	5.0 - 7.5
187	Cloud Ocean	-999	Ice	0.1 - 10	7.5 - 10.0
188	Cloud Ocean	-999	Ice	0.1 - 10	10.0 - 12.5
189	Cloud Ocean	-999	Ice	0.1 - 10	12.5 - 15.0
190	Cloud Ocean	-999	Ice	0.1 - 10	15.0 - 17.5
191	Cloud Ocean	-999	Ice	0.1 - 10	17.5 - 20.0
192	Cloud Ocean	-999	Ice	0.1 - 10	20.0 - 25.0
193	Cloud Ocean	-999	Ice	0.1 - 10	25.0 - 30.0
194	Cloud Ocean	-999	Ice	0.1 - 10	30.0 - 40.0
195	Cloud Ocean	-999	Ice	0.1 - 10	40.0 - 50.0
196	Cloud Ocean	-999	Ice	0.1 - 10	> 50.0
197	Cloud Ocean	-999	Ice	10 - 20	0.01 - 1.0
198	Cloud Ocean	-999	Ice	10 - 20	1.0 - 2.5
199	Cloud Ocean	-999	Ice	10 - 20	2.5 - 5.0
200	Cloud Ocean	-999	Ice	10 - 20	5.0 - 7.5
201	Cloud Ocean	-999	Ice	10 - 20	7.5 - 10.0
202	Cloud Ocean	-999	Ice	10 - 20	10.0 - 12.5
203	Cloud Ocean	-999	Ice	10 - 20	12.5 - 15.0
204	Cloud Ocean	-999	Ice	10 - 20	15.0 - 17.5
205	Cloud Ocean	-999	Ice	10 - 20	17.5 - 20.0
206	Cloud Ocean	-999	Ice	10 - 20	20.0 - 25.0
207	Cloud Ocean	-999	Ice	10 - 20	25.0 - 30.0
208	Cloud Ocean	-999	Ice	10 - 20	30.0 - 40.0
209	Cloud Ocean	-999	Ice	10 - 20	40.0 - 50.0
210	Cloud Ocean	-999	Ice	10 - 20	> 50.0
211	Cloud Ocean	-999	Ice	20 - 30	0.01 - 1.0
212	Cloud Ocean	-999	Ice	20 - 30	1.0 - 2.5
213	Cloud Ocean	-999	Ice	20 - 30	2.5 - 5.0
214	Cloud Ocean	-999	Ice	20 - 30	5.0 - 7.5
215	Cloud Ocean	-999	Ice	20 - 30	7.5 - 10.0
216	Cloud Ocean	-999	Ice	20 - 30	10.0 - 12.5
217	Cloud Ocean	-999	Ice	20 - 30	12.5 - 15.0
218	Cloud Ocean	-999	Ice	20 - 30	15.0 - 17.5
219	Cloud Ocean	-999	Ice	20 - 30	17.5 - 20.0
220	Cloud Ocean	-999	Ice	20 - 30	20.0 - 25.0
221	Cloud Ocean	-999	Ice	20 - 30	25.0 - 30.0
222	Cloud Ocean	-999	Ice	20 - 30	30.0 - 40.0
223	Cloud Ocean	-999	Ice	20 - 30	40.0 - 50.0
224	Cloud Ocean	-999	Ice	20 - 30	> 50.0
225	Cloud Ocean	-999	Ice	30 - 40	0.01 - 1.0
226	Cloud Ocean	-999	Ice	30 - 40	1.0 - 2.5
227	Cloud Ocean	-999	Ice	30 - 40	2.5 - 5.0
228	Cloud Ocean	-999	Ice	30 - 40	5.0 - 7.5
229	Cloud Ocean	-999	Ice	30 - 40	7.5 - 10.0
230	Cloud Ocean	-999	Ice	30 - 40	10.0 - 12.5
231	Cloud Ocean	-999	Ice	30 - 40	12.5 - 15.0
232	Cloud Ocean	-999	Ice	30 - 40	15.0 - 17.5

233	Cloud Ocean	-999	Ice	30 - 40	17.5 - 20.0
234	Cloud Ocean	-999	Ice	30 - 40	20.0 - 25.0
235	Cloud Ocean	-999	Ice	30 - 40	25.0 - 30.0
236	Cloud Ocean	-999	Ice	30 - 40	30.0 - 40.0
237	Cloud Ocean	-999	Ice	30 - 40	40.0 - 50.0
238	Cloud Ocean	-999	Ice	30 - 40	> 50.0
239	Cloud Ocean	-999	Ice	40 - 50	0.01 - 1.0
240	Cloud Ocean	-999	Ice	40 - 50	1.0 - 2.5
241	Cloud Ocean	-999	Ice	40 - 50	2.5 - 5.0
242	Cloud Ocean	-999	Ice	40 - 50	5.0 - 7.5
243	Cloud Ocean	-999	Ice	40 - 50	7.5 - 10.0
244	Cloud Ocean	-999	Ice	40 - 50	10.0 - 12.5
245	Cloud Ocean	-999	Ice	40 - 50	12.5 - 15.0
246	Cloud Ocean	-999	Ice	40 - 50	15.0 - 17.5
247	Cloud Ocean	-999	Ice	40 - 50	17.5 - 20.0
248	Cloud Ocean	-999	Ice	40 - 50	20.0 - 25.0
249	Cloud Ocean	-999	Ice	40 - 50	25.0 - 30.0
250	Cloud Ocean	-999	Ice	40 - 50	30.0 - 40.0
251	Cloud Ocean	-999	Ice	40 - 50	40.0 - 50.0
252	Cloud Ocean	-999	Ice	40 - 50	> 50.0
253	Cloud Ocean	-999	Ice	50 - 60	0.01 - 1.0
254	Cloud Ocean	-999	Ice	50 - 60	1.0 - 2.5
255	Cloud Ocean	-999	Ice	50 - 60	2.5 - 5.0
256	Cloud Ocean	-999	Ice	50 - 60	5.0 - 7.5
257	Cloud Ocean	-999	Ice	50 - 60	7.5 - 10.0
258	Cloud Ocean	-999	Ice	50 - 60	10.0 - 12.5
259	Cloud Ocean	-999	Ice	50 - 60	12.5 - 15.0
260	Cloud Ocean	-999	Ice	50 - 60	15.0 - 17.5
261	Cloud Ocean	-999	Ice	50 - 60	17.5 - 20.0
262	Cloud Ocean	-999	Ice	50 - 60	20.0 - 25.0
263	Cloud Ocean	-999	Ice	50 - 60	25.0 - 30.0
264	Cloud Ocean	-999	Ice	50 - 60	30.0 - 40.0
265	Cloud Ocean	-999	Ice	50 - 60	40.0 - 50.0
266	Cloud Ocean	-999	Ice	50 - 60	> 50.0
267	Cloud Ocean	-999	Ice	60 - 70	0.01 - 1.0
268	Cloud Ocean	-999	Ice	60 - 70	1.0 - 2.5
269	Cloud Ocean	-999	Ice	60 - 70	2.5 - 5.0
270	Cloud Ocean	-999	Ice	60 - 70	5.0 - 7.5
271	Cloud Ocean	-999	Ice	60 - 70	7.5 - 10.0
272	Cloud Ocean	-999	Ice	60 - 70	10.0 - 12.5
273	Cloud Ocean	-999	Ice	60 - 70	12.5 - 15.0
274	Cloud Ocean	-999	Ice	60 - 70	15.0 - 17.5
275	Cloud Ocean	-999	Ice	60 - 70	17.5 - 20.0
276	Cloud Ocean	-999	Ice	60 - 70	20.0 - 25.0
277	Cloud Ocean	-999	Ice	60 - 70	25.0 - 30.0
278	Cloud Ocean	-999	Ice	60 - 70	30.0 - 40.0
279	Cloud Ocean	-999	Ice	60 - 70	40.0 - 50.0
280	Cloud Ocean	-999	Ice	60 - 70	> 50.0
281	Cloud Ocean	-999	Ice	70 - 80	0.01 - 1.0
282	Cloud Ocean	-999	Ice	70 - 80	1.0 - 2.5
283	Cloud Ocean	-999	Ice	70 - 80	2.5 - 5.0
284	Cloud Ocean	-999	Ice	70 - 80	5.0 - 7.5
285	Cloud Ocean	-999	Ice	70 - 80	7.5 - 10.0
286	Cloud Ocean	-999	Ice	70 - 80	10.0 - 12.5
287	Cloud Ocean	-999	Ice	70 - 80	12.5 - 15.0
288	Cloud Ocean	-999	Ice	70 - 80	15.0 - 17.5
289	Cloud Ocean	-999	Ice	70 - 80	17.5 - 20.0
290	Cloud Ocean	-999	Ice	70 - 80	20.0 - 25.0
291	Cloud Ocean	-999	Ice	70 - 80	25.0 - 30.0
292	Cloud Ocean	-999	Ice	70 - 80	30.0 - 40.0
293	Cloud Ocean	-999	Ice	70 - 80	40.0 - 50.0
294	Cloud Ocean	-999	Ice	70 - 80	> 50.0
295	Cloud Ocean	-999	Ice	80 - 90	0.01 - 1.0
296	Cloud Ocean	-999	Ice	80 - 90	1.0 - 2.5
297	Cloud Ocean	-999	Ice	80 - 90	2.5 - 5.0
298	Cloud Ocean	-999	Ice	80 - 90	5.0 - 7.5
299	Cloud Ocean	-999	Ice	80 - 90	7.5 - 10.0

300	Cloud Ocean	-999	Ice	80 - 90	10.0 - 12.5
301	Cloud Ocean	-999	Ice	80 - 90	12.5 - 15.0
302	Cloud Ocean	-999	Ice	80 - 90	15.0 - 17.5
303	Cloud Ocean	-999	Ice	80 - 90	17.5 - 20.0
304	Cloud Ocean	-999	Ice	80 - 90	20.0 - 25.0
305	Cloud Ocean	-999	Ice	80 - 90	25.0 - 30.0
306	Cloud Ocean	-999	Ice	80 - 90	30.0 - 40.0
307	Cloud Ocean	-999	Ice	80 - 90	40.0 - 50.0
308	Cloud Ocean	-999	Ice	80 - 90	> 50.0
309	Cloud Ocean	-999	Ice	90 - 95	0.01 - 1.0
310	Cloud Ocean	-999	Ice	90 - 95	1.0 - 2.5
311	Cloud Ocean	-999	Ice	90 - 95	2.5 - 5.0
312	Cloud Ocean	-999	Ice	90 - 95	5.0 - 7.5
313	Cloud Ocean	-999	Ice	90 - 95	7.5 - 10.0
314	Cloud Ocean	-999	Ice	90 - 95	10.0 - 12.5
315	Cloud Ocean	-999	Ice	90 - 95	12.5 - 15.0
316	Cloud Ocean	-999	Ice	90 - 95	15.0 - 17.5
317	Cloud Ocean	-999	Ice	90 - 95	17.5 - 20.0
318	Cloud Ocean	-999	Ice	90 - 95	20.0 - 25.0
319	Cloud Ocean	-999	Ice	90 - 95	25.0 - 30.0
320	Cloud Ocean	-999	Ice	90 - 95	30.0 - 40.0
321	Cloud Ocean	-999	Ice	90 - 95	40.0 - 50.0
322	Cloud Ocean	-999	Ice	90 - 95	> 50.0
323	Cloud Ocean	-999	Ice	95 - 99.9	0.01 - 1.0
324	Cloud Ocean	-999	Ice	95 - 99.9	1.0 - 2.5
325	Cloud Ocean	-999	Ice	95 - 99.9	2.5 - 5.0
326	Cloud Ocean	-999	Ice	95 - 99.9	5.0 - 7.5
327	Cloud Ocean	-999	Ice	95 - 99.9	7.5 - 10.0
328	Cloud Ocean	-999	Ice	95 - 99.9	10.0 - 12.5
329	Cloud Ocean	-999	Ice	95 - 99.9	12.5 - 15.0
330	Cloud Ocean	-999	Ice	95 - 99.9	15.0 - 17.5
331	Cloud Ocean	-999	Ice	95 - 99.9	17.5 - 20.0
332	Cloud Ocean	-999	Ice	95 - 99.9	20.0 - 25.0
333	Cloud Ocean	-999	Ice	95 - 99.9	25.0 - 30.0
334	Cloud Ocean	-999	Ice	95 - 99.9	30.0 - 40.0
335	Cloud Ocean	-999	Ice	95 - 99.9	40.0 - 50.0
336	Cloud Ocean	-999	Ice	95 - 99.9	> 50.0
337	**Cloud Ocean**	**-999**	**Ice**	**99.9 - 100**	**0.01 - 1.0**
338	**Cloud Ocean**	**-999**	**Ice**	**99.9 - 100**	**1.0 - 2.5**
339	**Cloud Ocean**	**-999**	**Ice**	**99.9 - 100**	**2.5 - 5.0**
340	**Cloud Ocean**	**-999**	**Ice**	**99.9 - 100**	**5.0 - 7.5**
341	**Cloud Ocean**	**-999**	**Ice**	**99.9 - 100**	**7.5 - 10.0**
342	**Cloud Ocean**	**-999**	**Ice**	**99.9 - 100**	**10.0 - 12.5**
343	**Cloud Ocean**	**-999**	**Ice**	**99.9 - 100**	**12.5 - 15.0**
344	**Cloud Ocean**	**-999**	**Ice**	**99.9 - 100**	**15.0 - 17.5**
345	**Cloud Ocean**	**-999**	**Ice**	**99.9 - 100**	**17.5 - 20.0**
346	**Cloud Ocean**	**-999**	**Ice**	**99.9 - 100**	**20.0 - 25.0**
347	**Cloud Ocean**	**-999**	**Ice**	**99.9 - 100**	**25.0 - 30.0**
348	**Cloud Ocean**	**-999**	**Ice**	**99.9 - 100**	**30.0 - 40.0**
349	**Cloud Ocean**	**-999**	**Ice**	**99.9 - 100**	**40.0 - 50.0**
350	**Cloud Ocean**	**-999**	**Ice**	**99.9 - 100**	**> 50.0**
351	Cloud Mod-Hi Tree/Shrub	-999	Liquid	0.1 - 25	0.01 - 2.5
352	Cloud Mod-Hi Tree/Shrub	-999	Liquid	0.1 - 25	2.5 - 6.0
353	Cloud Mod-Hi Tree/Shrub	-999	Liquid	0.1 - 25	6.0 - 10.0
354	Cloud Mod-Hi Tree/Shrub	-999	Liquid	0.1 - 25	10.0 - 18.0
355	Cloud Mod-Hi Tree/Shrub	-999	Liquid	0.1 - 25	18.0 - 40.0
356	Cloud Mod-Hi Tree/Shrub	-999	Liquid	0.1 - 25	> 40
357	Cloud Mod-Hi Tree/Shrub	-999	Liquid	25 - 50	0.01 - 2.5
358	Cloud Mod-Hi Tree/Shrub	-999	Liquid	25 - 50	2.5 - 6.0
359	Cloud Mod-Hi Tree/Shrub	-999	Liquid	25 - 50	6.0 - 10.0
360	Cloud Mod-Hi Tree/Shrub	-999	Liquid	25 - 50	10.0 - 18.0
361	Cloud Mod-Hi Tree/Shrub	-999	Liquid	25 - 50	18.0 - 40.0
362	Cloud Mod-Hi Tree/Shrub	-999	Liquid	25 - 50	> 40
363	Cloud Mod-Hi Tree/Shrub	-999	Liquid	50 - 75	0.01 - 2.5
364	Cloud Mod-Hi Tree/Shrub	-999	Liquid	50 - 75	2.5 - 6.0
365	Cloud Mod-Hi Tree/Shrub	-999	Liquid	50 - 75	6.0 - 10.0
366	Cloud Mod-Hi Tree/Shrub	-999	Liquid	50 - 75	10.0 - 18.0

367	Cloud Mod-Hi Tree/Shrub	-999	Liquid	50 - 75	18.0 - 40.0
368	Cloud Mod-Hi Tree/Shrub	-999	Liquid	50 - 75	> 40
369	Cloud Mod-Hi Tree/Shrub	-999	Liquid	75 - 99.9	0.01 - 2.5
370	Cloud Mod-Hi Tree/Shrub	-999	Liquid	75 - 99.9	2.5 - 6.0
371	Cloud Mod-Hi Tree/Shrub	-999	Liquid	75 - 99.9	6.0 - 10.0
372	Cloud Mod-Hi Tree/Shrub	-999	Liquid	75 - 99.9	10.0 - 18.0
373	Cloud Mod-Hi Tree/Shrub	-999	Liquid	75 - 99.9	18.0 - 40.0
374	Cloud Mod-Hi Tree/Shrub	-999	Liquid	75 - 99.9	> 40
375	**Cloud Mod-Hi Tree/Shrub**	**-999**	**Liquid**	**99.9 - 100**	**0.01 - 2.5**
376	**Cloud Mod-Hi Tree/Shrub**	**-999**	**Liquid**	**99.9 - 100**	**2.5 - 6.0**
377	**Cloud Mod-Hi Tree/Shrub**	**-999**	**Liquid**	**99.9 - 100**	**6.0 - 10.0**
378	**Cloud Mod-Hi Tree/Shrub**	**-999**	**Liquid**	**99.9 - 100**	**10.0 - 18.0**
379	**Cloud Mod-Hi Tree/Shrub**	**-999**	**Liquid**	**99.9 - 100**	**18.0 - 40.0**
380	**Cloud Mod-Hi Tree/Shrub**	**-999**	**Liquid**	**99.9 - 100**	**> 40**
381	Cloud Mod-Hi Tree/Shrub	-999	Ice	0.1 - 25	0.01 - 2.5
382	Cloud Mod-Hi Tree/Shrub	-999	Ice	0.1 - 25	2.5 - 6.0
383	Cloud Mod-Hi Tree/Shrub	-999	Ice	0.1 - 25	6.0 - 10.0
384	Cloud Mod-Hi Tree/Shrub	-999	Ice	0.1 - 25	10.0 - 18.0
385	Cloud Mod-Hi Tree/Shrub	-999	Ice	0.1 - 25	18.0 - 40.0
386	Cloud Mod-Hi Tree/Shrub	-999	Ice	0.1 - 25	> 40
387	Cloud Mod-Hi Tree/Shrub	-999	Ice	25 - 50	0.01 - 2.5
388	Cloud Mod-Hi Tree/Shrub	-999	Ice	25 - 50	2.5 - 6.0
389	Cloud Mod-Hi Tree/Shrub	-999	Ice	25 - 50	6.0 - 10.0
390	Cloud Mod-Hi Tree/Shrub	-999	Ice	25 - 50	10.0 - 18.0
391	Cloud Mod-Hi Tree/Shrub	-999	Ice	25 - 50	18.0 - 40.0
392	Cloud Mod-Hi Tree/Shrub	-999	Ice	25 - 50	> 40
393	Cloud Mod-Hi Tree/Shrub	-999	Ice	50 - 75	0.01 - 2.5
394	Cloud Mod-Hi Tree/Shrub	-999	Ice	50 - 75	2.5 - 6.0
395	Cloud Mod-Hi Tree/Shrub	-999	Ice	50 - 75	6.0 - 10.0
396	Cloud Mod-Hi Tree/Shrub	-999	Ice	50 - 75	10.0 - 18.0
397	Cloud Mod-Hi Tree/Shrub	-999	Ice	50 - 75	18.0 - 40.0
398	Cloud Mod-Hi Tree/Shrub	-999	Ice	50 - 75	> 40
399	Cloud Mod-Hi Tree/Shrub	-999	Ice	75 - 99.9	0.01 - 2.5
400	Cloud Mod-Hi Tree/Shrub	-999	Ice	75 - 99.9	2.5 - 6.0
401	Cloud Mod-Hi Tree/Shrub	-999	Ice	75 - 99.9	6.0 - 10.0
402	Cloud Mod-Hi Tree/Shrub	-999	Ice	75 - 99.9	10.0 - 18.0
403	Cloud Mod-Hi Tree/Shrub	-999	Ice	75 - 99.9	18.0 - 40.0
404	Cloud Mod-Hi Tree/Shrub	-999	Ice	75 - 99.9	> 40
405	**Cloud Mod-Hi Tree/Shrub**	**-999**	**Ice**	**99.9 - 100**	**0.01 - 2.5**
406	**Cloud Mod-Hi Tree/Shrub**	**-999**	**Ice**	**99.9 - 100**	**2.5 - 6.0**
407	**Cloud Mod-Hi Tree/Shrub**	**-999**	**Ice**	**99.9 - 100**	**6.0 - 10.0**
408	**Cloud Mod-Hi Tree/Shrub**	**-999**	**Ice**	**99.9 - 100**	**10.0 - 18.0**
409	**Cloud Mod-Hi Tree/Shrub**	**-999**	**Ice**	**99.9 - 100**	**18.0 - 40.0**
410	**Cloud Mod-Hi Tree/Shrub**	**-999**	**Ice**	**99.9 - 100**	**> 40**
411	Cloud Low-Mod Tree/Shrub	-999	Liquid	0.1 - 25	0.01 - 2.5
412	Cloud Low-Mod Tree/Shrub	-999	Liquid	0.1 - 25	2.5 - 6.0
413	Cloud Low-Mod Tree/Shrub	-999	Liquid	0.1 - 25	6.0 - 10.0
414	Cloud Low-Mod Tree/Shrub	-999	Liquid	0.1 - 25	10.0 - 18.0
415	Cloud Low-Mod Tree/Shrub	-999	Liquid	0.1 - 25	18.0 - 40.0
416	Cloud Low-Mod Tree/Shrub	-999	Liquid	0.1 - 25	> 40
417	Cloud Low-Mod Tree/Shrub	-999	Liquid	25 - 50	0.01 - 2.5
418	Cloud Low-Mod Tree/Shrub	-999	Liquid	25 - 50	2.5 - 6.0
419	Cloud Low-Mod Tree/Shrub	-999	Liquid	25 - 50	6.0 - 10.0
420	Cloud Low-Mod Tree/Shrub	-999	Liquid	25 - 50	10.0 - 18.0
421	Cloud Low-Mod Tree/Shrub	-999	Liquid	25 - 50	18.0 - 40.0
422	Cloud Low-Mod Tree/Shrub	-999	Liquid	25 - 50	> 40
423	Cloud Low-Mod Tree/Shrub	-999	Liquid	50 - 75	0.01 - 2.5
424	Cloud Low-Mod Tree/Shrub	-999	Liquid	50 - 75	2.5 - 6.0
425	Cloud Low-Mod Tree/Shrub	-999	Liquid	50 - 75	6.0 - 10.0
426	Cloud Low-Mod Tree/Shrub	-999	Liquid	50 - 75	10.0 - 18.0
427	Cloud Low-Mod Tree/Shrub	-999	Liquid	50 - 75	18.0 - 40.0
428	Cloud Low-Mod Tree/Shrub	-999	Liquid	50 - 75	> 40
429	Cloud Low-Mod Tree/Shrub	-999	Liquid	75 - 99.9	0.01 - 2.5
430	Cloud Low-Mod Tree/Shrub	-999	Liquid	75 - 99.9	2.5 - 6.0
431	Cloud Low-Mod Tree/Shrub	-999	Liquid	75 - 99.9	6.0 - 10.0
432	Cloud Low-Mod Tree/Shrub	-999	Liquid	75 - 99.9	10.0 - 18.0
433	Cloud Low-Mod Tree/Shrub	-999	Liquid	75 - 99.9	18.0 - 40.0

434	Cloud Low-Mod Tree/Shrub	-999	Liquid	75 - 99.9	> 40
435	**Cloud Low-Mod Tree/Shrub**	**-999**	**Liquid**	**99.9 - 100**	**0.01 - 2.5**
436	**Cloud Low-Mod Tree/Shrub**	**-999**	**Liquid**	**99.9 - 100**	**2.5 - 6.0**
437	**Cloud Low-Mod Tree/Shrub**	**-999**	**Liquid**	**99.9 - 100**	**6.0 - 10.0**
438	**Cloud Low-Mod Tree/Shrub**	**-999**	**Liquid**	**99.9 - 100**	**10.0 - 18.0**
439	**Cloud Low-Mod Tree/Shrub**	**-999**	**Liquid**	**99.9 - 100**	**18.0 - 40.0**
440	**Cloud Low-Mod Tree/Shrub**	**-999**	**Liquid**	**99.9 - 100**	**> 40**
441	Cloud Low-Mod Tree/Shrub	-999	Ice	0.1 - 25	0.01 - 2.5
442	Cloud Low-Mod Tree/Shrub	-999	Ice	0.1 - 25	2.5 - 6.0
443	Cloud Low-Mod Tree/Shrub	-999	Ice	0.1 - 25	6.0 - 10.0
444	Cloud Low-Mod Tree/Shrub	-999	Ice	0.1 - 25	10.0 - 18.0
445	Cloud Low-Mod Tree/Shrub	-999	Ice	0.1 - 25	18.0 - 40.0
446	Cloud Low-Mod Tree/Shrub	-999	Ice	0.1 - 25	> 40
447	Cloud Low-Mod Tree/Shrub	-999	Ice	25 - 50	0.01 - 2.5
448	Cloud Low-Mod Tree/Shrub	-999	Ice	25 - 50	2.5 - 6.0
449	Cloud Low-Mod Tree/Shrub	-999	Ice	25 - 50	6.0 - 10.0
450	Cloud Low-Mod Tree/Shrub	-999	Ice	25 - 50	10.0 - 18.0
451	Cloud Low-Mod Tree/Shrub	-999	Ice	25 - 50	18.0 - 40.0
452	Cloud Low-Mod Tree/Shrub	-999	Ice	25 - 50	> 40
453	Cloud Low-Mod Tree/Shrub	-999	Ice	50 - 75	0.01 - 2.5
454	Cloud Low-Mod Tree/Shrub	-999	Ice	50 - 75	2.5 - 6.0
455	Cloud Low-Mod Tree/Shrub	-999	Ice	50 - 75	6.0 - 10.0
456	Cloud Low-Mod Tree/Shrub	-999	Ice	50 - 75	10.0 - 18.0
457	Cloud Low-Mod Tree/Shrub	-999	Ice	50 - 75	18.0 - 40.0
458	Cloud Low-Mod Tree/Shrub	-999	Ice	50 - 75	> 40
459	Cloud Low-Mod Tree/Shrub	-999	Ice	75 - 99.9	0.01 - 2.5
460	Cloud Low-Mod Tree/Shrub	-999	Ice	75 - 99.9	2.5 - 6.0
461	Cloud Low-Mod Tree/Shrub	-999	Ice	75 - 99.9	6.0 - 10.0
462	Cloud Low-Mod Tree/Shrub	-999	Ice	75 - 99.9	10.0 - 18.0
463	Cloud Low-Mod Tree/Shrub	-999	Ice	75 - 99.9	18.0 - 40.0
464	Cloud Low-Mod Tree/Shrub	-999	Ice	75 - 99.9	> 40
465	**Cloud Low-Mod Tree/Shrub**	**-999**	**Ice**	**99.9 - 100**	**0.01 - 2.5**
466	**Cloud Low-Mod Tree/Shrub**	**-999**	**Ice**	**99.9 - 100**	**2.5 - 6.0**
467	**Cloud Low-Mod Tree/Shrub**	**-999**	**Ice**	**99.9 - 100**	**6.0 - 10.0**
468	**Cloud Low-Mod Tree/Shrub**	**-999**	**Ice**	**99.9 - 100**	**10.0 - 18.0**
469	**Cloud Low-Mod Tree/Shrub**	**-999**	**Ice**	**99.9 - 100**	**18.0 - 40.0**
470	**Cloud Low-Mod Tree/Shrub**	**-999**	**Ice**	**99.9 - 100**	**> 40**
471	Cloud Dark Desert	-999	Liquid	0.1 - 25	0.01 - 2.5
472	Cloud Dark Desert	-999	Liquid	0.1 - 25	2.5 - 6.0
473	Cloud Dark Desert	-999	Liquid	0.1 - 25	6.0 - 10.0
474	Cloud Dark Desert	-999	Liquid	0.1 - 25	10.0 - 18.0
475	Cloud Dark Desert	-999	Liquid	0.1 - 25	18.0 - 40.0
476	Cloud Dark Desert	-999	Liquid	0.1 - 25	> 40
477	Cloud Dark Desert	-999	Liquid	25 - 50	0.01 - 2.5
478	Cloud Dark Desert	-999	Liquid	25 - 50	2.5 - 6.0
479	Cloud Dark Desert	-999	Liquid	25 - 50	6.0 - 10.0
480	Cloud Dark Desert	-999	Liquid	25 - 50	10.0 - 18.0
481	Cloud Dark Desert	-999	Liquid	25 - 50	18.0 - 40.0
482	Cloud Dark Desert	-999	Liquid	25 - 50	> 40
483	Cloud Dark Desert	-999	Liquid	50 - 75	0.01 - 2.5
484	Cloud Dark Desert	-999	Liquid	50 - 75	2.5 - 6.0
485	Cloud Dark Desert	-999	Liquid	50 - 75	6.0 - 10.0
486	Cloud Dark Desert	-999	Liquid	50 - 75	10.0 - 18.0
487	Cloud Dark Desert	-999	Liquid	50 - 75	18.0 - 40.0
488	Cloud Dark Desert	-999	Liquid	50 - 75	> 40
489	Cloud Dark Desert	-999	Liquid	75 - 99.9	0.01 - 2.5
490	Cloud Dark Desert	-999	Liquid	75 - 99.9	2.5 - 6.0
491	Cloud Dark Desert	-999	Liquid	75 - 99.9	6.0 - 10.0
492	Cloud Dark Desert	-999	Liquid	75 - 99.9	10.0 - 18.0
493	Cloud Dark Desert	-999	Liquid	75 - 99.9	18.0 - 40.0
494	Cloud Dark Desert	-999	Liquid	75 - 99.9	> 40
495	**Cloud Dark Desert**	**-999**	**Liquid**	**99.9 - 100**	**0.01 - 2.5**
496	**Cloud Dark Desert**	**-999**	**Liquid**	**99.9 - 100**	**2.5 - 6.0**
497	**Cloud Dark Desert**	**-999**	**Liquid**	**99.9 - 100**	**6.0 - 10.0**
498	**Cloud Dark Desert**	**-999**	**Liquid**	**99.9 - 100**	**10.0 - 18.0**
499	**Cloud Dark Desert**	**-999**	**Liquid**	**99.9 - 100**	**18.0 - 40.0**
500	**Cloud Dark Desert**	**-999**	**Liquid**	**99.9 - 100**	**> 40**

501	Cloud Dark Desert	-999	Ice	0.1 - 25	0.01 - 2.5
502	Cloud Dark Desert	-999	Ice	0.1 - 25	2.5 - 6.0
503	Cloud Dark Desert	-999	Ice	0.1 - 25	6.0 - 10.0
504	Cloud Dark Desert	-999	Ice	0.1 - 25	10.0 - 18.0
505	Cloud Dark Desert	-999	Ice	0.1 - 25	18.0 - 40.0
506	Cloud Dark Desert	-999	Ice	0.1 - 25	> 40
507	Cloud Dark Desert	-999	Ice	25 - 50	0.01 - 2.5
508	Cloud Dark Desert	-999	Ice	25 - 50	2.5 - 6.0
509	Cloud Dark Desert	-999	Ice	25 - 50	6.0 - 10.0
510	Cloud Dark Desert	-999	Ice	25 - 50	10.0 - 18.0
511	Cloud Dark Desert	-999	Ice	25 - 50	18.0 - 40.0
512	Cloud Dark Desert	-999	Ice	25 - 50	> 40
513	Cloud Dark Desert	-999	Ice	50 - 75	0.01 - 2.5
514	Cloud Dark Desert	-999	Ice	50 - 75	2.5 - 6.0
515	Cloud Dark Desert	-999	Ice	50 - 75	6.0 - 10.0
516	Cloud Dark Desert	-999	Ice	50 - 75	10.0 - 18.0
517	Cloud Dark Desert	-999	Ice	50 - 75	18.0 - 40.0
518	Cloud Dark Desert	-999	Ice	50 - 75	> 40
519	Cloud Dark Desert	-999	Ice	75 - 99.9	0.01 - 2.5
520	Cloud Dark Desert	-999	Ice	75 - 99.9	2.5 - 6.0
521	Cloud Dark Desert	-999	Ice	75 - 99.9	6.0 - 10.0
522	Cloud Dark Desert	-999	Ice	75 - 99.9	10.0 - 18.0
523	Cloud Dark Desert	-999	Ice	75 - 99.9	18.0 - 40.0
524	Cloud Dark Desert	-999	Ice	75 - 99.9	> 40
525	**Cloud Dark Desert**	**-999**	**Ice**	**99.9 - 100**	**0.01 - 2.5**
526	**Cloud Dark Desert**	**-999**	**Ice**	**99.9 - 100**	**2.5 - 6.0**
527	**Cloud Dark Desert**	**-999**	**Ice**	**99.9 - 100**	**6.0 - 10.0**
528	**Cloud Dark Desert**	**-999**	**Ice**	**99.9 - 100**	**10.0 - 18.0**
529	**Cloud Dark Desert**	**-999**	**Ice**	**99.9 - 100**	**18.0 - 40.0**
530	**Cloud Dark Desert**	**-999**	**Ice**	**99.9 - 100**	**> 40**
531	Cloud Bright Desert	-999	Liquid	0.1 - 25	0.01 - 2.5
532	Cloud Bright Desert	-999	Liquid	0.1 - 25	2.5 - 6.0
533	Cloud Bright Desert	-999	Liquid	0.1 - 25	6.0 - 10.0
534	Cloud Bright Desert	-999	Liquid	0.1 - 25	10.0 - 18.0
535	Cloud Bright Desert	-999	Liquid	0.1 - 25	18.0 - 40.0
536	Cloud Bright Desert	-999	Liquid	0.1 - 25	> 40
537	Cloud Bright Desert	-999	Liquid	25 - 50	0.01 - 2.5
538	Cloud Bright Desert	-999	Liquid	25 - 50	2.5 - 6.0
539	Cloud Bright Desert	-999	Liquid	25 - 50	6.0 - 10.0
540	Cloud Bright Desert	-999	Liquid	25 - 50	10.0 - 18.0
541	Cloud Bright Desert	-999	Liquid	25 - 50	18.0 - 40.0
542	Cloud Bright Desert	-999	Liquid	25 - 50	> 40
543	Cloud Bright Desert	-999	Liquid	50 - 75	0.01 - 2.5
544	Cloud Bright Desert	-999	Liquid	50 - 75	2.5 - 6.0
545	Cloud Bright Desert	-999	Liquid	50 - 75	6.0 - 10.0
546	Cloud Bright Desert	-999	Liquid	50 - 75	10.0 - 18.0
547	Cloud Bright Desert	-999	Liquid	50 - 75	18.0 - 40.0
548	Cloud Bright Desert	-999	Liquid	50 - 75	> 40
549	Cloud Bright Desert	-999	Liquid	75 - 99.9	0.01 - 2.5
550	Cloud Bright Desert	-999	Liquid	75 - 99.9	2.5 - 6.0
551	Cloud Bright Desert	-999	Liquid	75 - 99.9	6.0 - 10.0
552	Cloud Bright Desert	-999	Liquid	75 - 99.9	10.0 - 18.0
553	Cloud Bright Desert	-999	Liquid	75 - 99.9	18.0 - 40.0
554	Cloud Bright Desert	-999	Liquid	75 - 99.9	> 40
555	**Cloud Bright Desert**	**-999**	**Liquid**	**99.9 - 100**	**0.01 - 2.5**
556	**Cloud Bright Desert**	**-999**	**Liquid**	**99.9 - 100**	**2.5 - 6.0**
557	**Cloud Bright Desert**	**-999**	**Liquid**	**99.9 - 100**	**6.0 - 10.0**
558	**Cloud Bright Desert**	**-999**	**Liquid**	**99.9 - 100**	**10.0 - 18.0**
559	**Cloud Bright Desert**	**-999**	**Liquid**	**99.9 - 100**	**18.0 - 40.0**
560	**Cloud Bright Desert**	**-999**	**Liquid**	**99.9 - 100**	**> 40**
561	Cloud Bright Desert	-999	Ice	0.1 - 25	0.01 - 2.5
562	Cloud Bright Desert	-999	Ice	0.1 - 25	2.5 - 6.0
563	Cloud Bright Desert	-999	Ice	0.1 - 25	6.0 - 10.0
564	Cloud Bright Desert	-999	Ice	0.1 - 25	10.0 - 18.0
565	Cloud Bright Desert	-999	Ice	0.1 - 25	18.0 - 40.0
566	Cloud Bright Desert	-999	Ice	0.1 - 25	> 40
567	Cloud Bright Desert	-999	Ice	25 - 50	0.01 - 2.5

568	Cloud Bright Desert	-999	Ice	25 - 50	2.5 - 6.0
569	Cloud Bright Desert	-999	Ice	25 - 50	6.0 - 10.0
570	Cloud Bright Desert	-999	Ice	25 - 50	10.0 - 18.0
571	Cloud Bright Desert	-999	Ice	25 - 50	18.0 - 40.0
572	Cloud Bright Desert	-999	Ice	25 - 50	> 40
573	Cloud Bright Desert	-999	Ice	50 - 75	0.01 - 2.5
574	Cloud Bright Desert	-999	Ice	50 - 75	2.5 - 6.0
575	Cloud Bright Desert	-999	Ice	50 - 75	6.0 - 10.0
576	Cloud Bright Desert	-999	Ice	50 - 75	10.0 - 18.0
577	Cloud Bright Desert	-999	Ice	50 - 75	18.0 - 40.0
578	Cloud Bright Desert	-999	Ice	50 - 75	> 40
579	Cloud Bright Desert	-999	Ice	75 - 99.9	0.01 - 2.5
580	Cloud Bright Desert	-999	Ice	75 - 99.9	2.5 - 6.0
581	Cloud Bright Desert	-999	Ice	75 - 99.9	6.0 - 10.0
582	Cloud Bright Desert	-999	Ice	75 - 99.9	10.0 - 18.0
583	Cloud Bright Desert	-999	Ice	75 - 99.9	18.0 - 40.0
584	Cloud Bright Desert	-999	Ice	75 - 99.9	> 40
585	**Cloud Bright Desert**	**-999**	**Ice**	**99.9 - 100**	**0.01 - 2.5**
586	**Cloud Bright Desert**	**-999**	**Ice**	**99.9 - 100**	**2.5 - 6.0**
587	**Cloud Bright Desert**	**-999**	**Ice**	**99.9 - 100**	**6.0 - 10.0**
588	**Cloud Bright Desert**	**-999**	**Ice**	**99.9 - 100**	**10.0 - 18.0**
589	**Cloud Bright Desert**	**-999**	**Ice**	**99.9 - 100**	**18.0 - 40.0**
590	**Cloud Bright Desert**	**-999**	**Ice**	**99.9 - 100**	**> 40**

Albedo models are shown below for a selection of scene types. General features are the increase of albedo with SZA. For clear-sky scene types (ADMs 1-14), the SZA-dependent variation is highest. However, higher cloud fraction and higher cloud optical thickness result in higher TOA albedo with less SZA-dependency (curve is more flat).

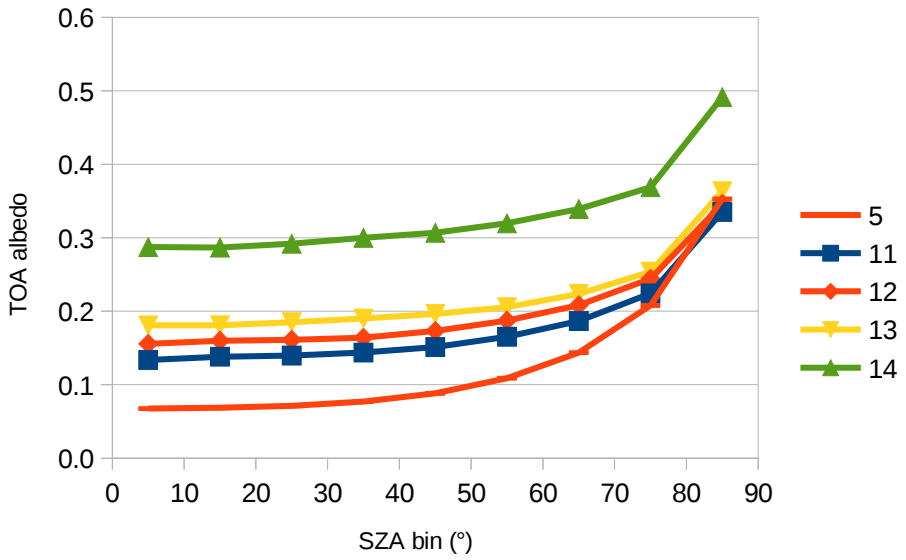

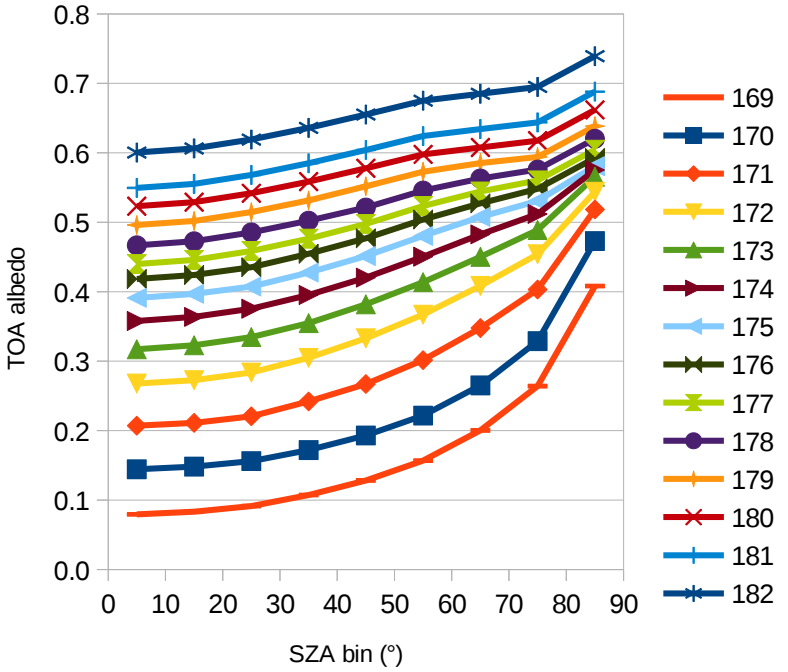
TOA albedo
SZA bin (°)
0.0
0.1
0.2
0.3
0.4
0.5
0.6
0.7
0.8
0 10 20 30 40 50 60 70 80 90
169
170
171
172
173
174
175
176
177
178
179
180
181
182

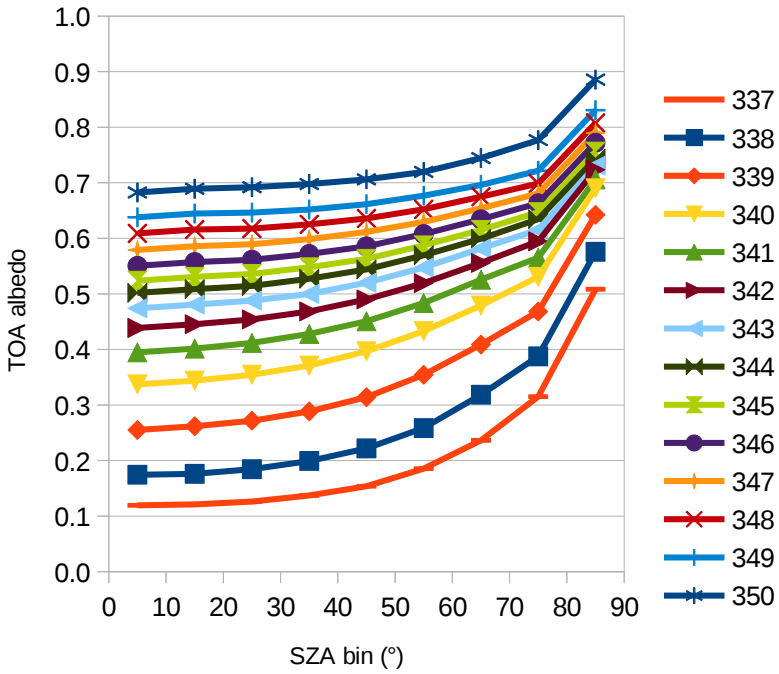
TOA albedo
SZA bin (°)
0.0
0.1
0.2
0.3
0.4
0.5
0.6
0.7
0.8
0.9
1.0
0 10 20 30 40 50 60 70 80 90
337
338
339
340
341
342
343
344
345
346
347
348
349
350

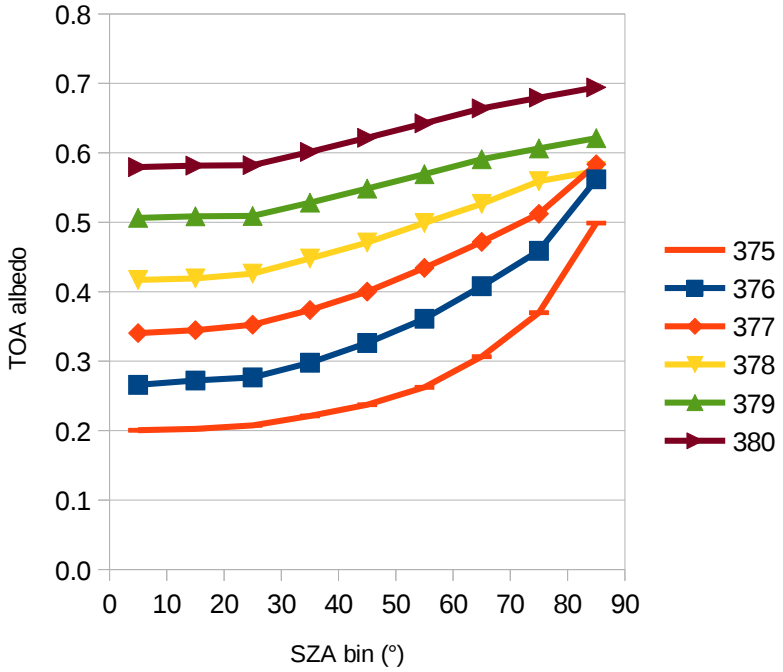

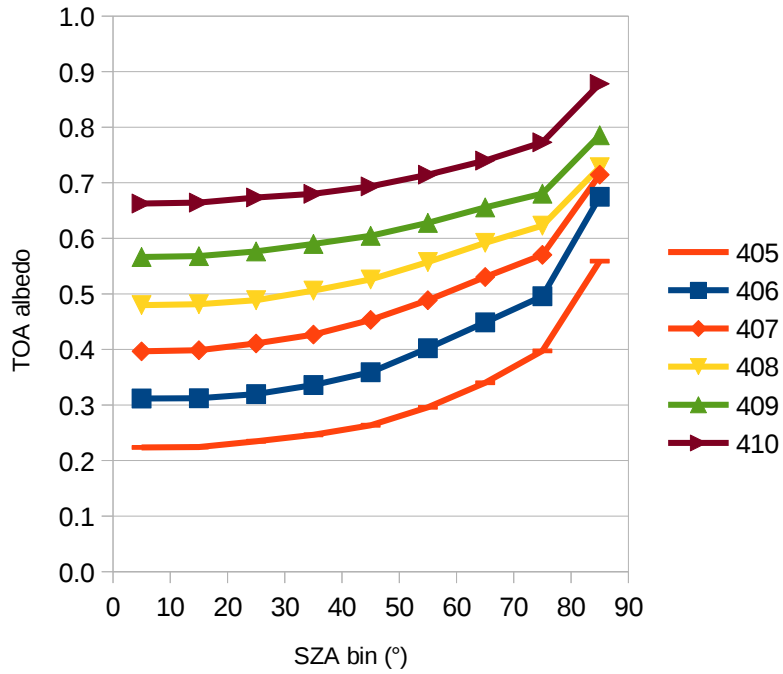

INTERPOLATION OF MISSING VALUES

Some of these models are interpolated where the *original* models contain missing values: The following graph depicts albedo (y-axis) as a function of SZA bin (x-axis), for 14 *original* albedo models (line colors). It is clear that many *original* models do not have a correct curve, due to the wrong treatment of missing values (albedo value is simply copied from corresponding SZA bin in a different albedo model).

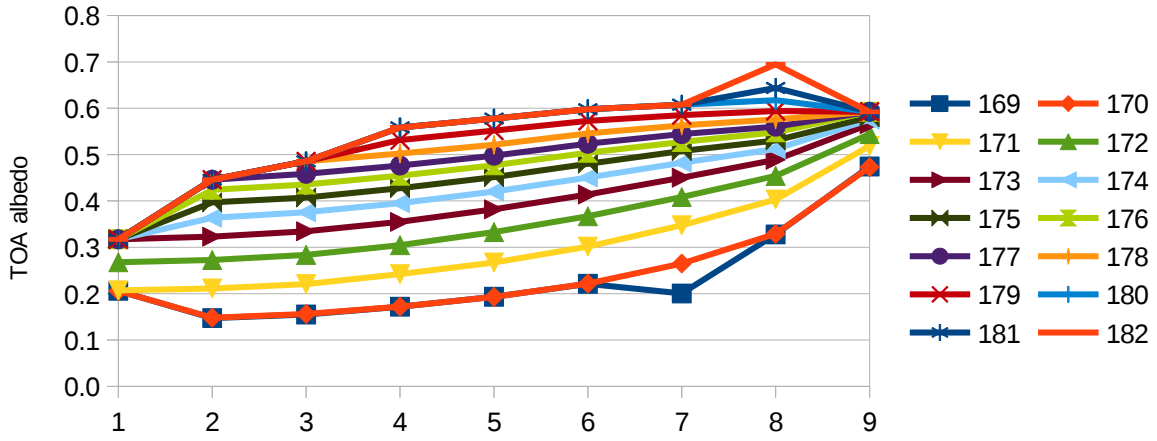

SOLUTION

Instead of simply copying the albedo value from the corresponding SZA bin in a different albedo model, we now **interpolate** to obtain the missing values. The result is shown in figure below, showing exactly the same data but now corrected:

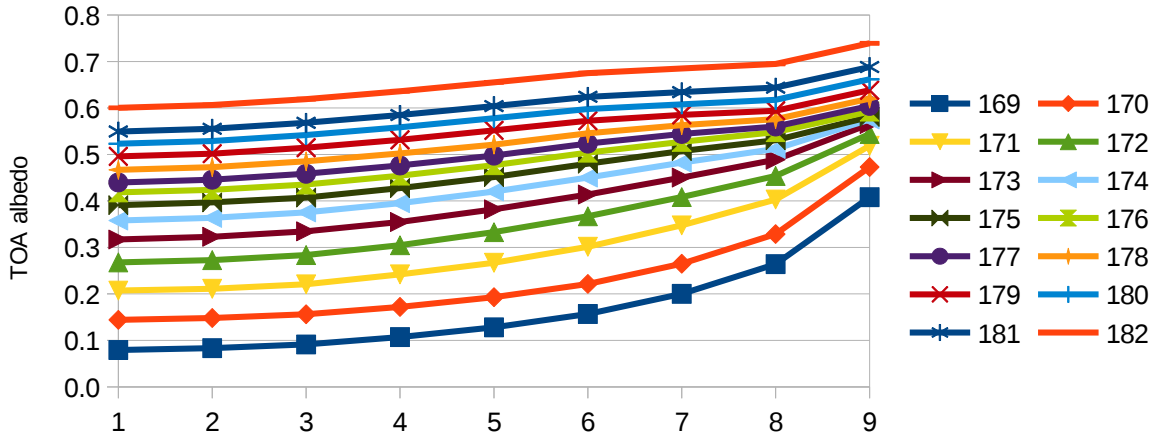

The method of interpolating is simple. We demonstrate it here with an extract of real data. The rows represent three albedo models, the columns represent three SZA bins. The three cells in the left-below corner were missing in the original CERES ADM, but wrongly converted to the RMIB ADM format by taking the value from the closest albedo model with valid albedo value for that SZA bin (for the first SZA bin, i.e. first column, this is the first albedo model, i.e. first row; for the second SZA bin, for the second SZA bin, this is the second albedo model, etc.).
Original:

0.445740	0.458550	0.476350
0.445740	0.485400	0.502230
0.445740	0.485400	0.531450

The correction is done by using only differences (no fractional or multiplicative operations): we look to the albedo difference between current and nearest SZA bin from the previous albedo model. This difference is then applied to the current albedo model, by subtracting it from the nearest valid SZA bin albedo.
Resulting table after correction (red = corrected):

0.445740	0.458550	0.476350
0.472590	0.485400	0.502230
0.501810	0.514620	0.531450

The missing value of (row 2, column 1) is taken by the following operation:

```
0.472590 = 0.485400 + ( 0.445740 - 0.458550 )
```

9.1.2. CERES/Terra SSF Ed.2B ADMs, scene types and albedo models

More information and graphs can be found on the CERES website: https://ceres.larc.nasa.gov/data/angular-distribution-models/#ceresterra-ssf-edition2b-adms

For snow and ice, the ADM's are derived from the CERES instrument onboard the Terra satellite (Loeb et al., 2005):

Table 15: ADM scene types (permanent snow/ice, fresh snow, sea-ice)

ADM ID	Scene Type	Snow/Sea-Ice Fraction (%)	Cloud Fraction (%)	Cloud Opt. Depth
591	Permanent Snow AVG B and D	100	0.0 - 0.1	
592	Permanent Snow	100	0.1 - 25.0	
593	Permanent Snow	100	25.0 - 50.0	
594	Permanent Snow	100	50.0 - 75.0	
595	Permanent Snow	100	75.0 - 99.9	
596	Permanent Snow AVG B and D	100	99.9 - 100.0	0.01 - 10.0
597	Permanent Snow AVG B and D	100	99.9 - 100.0	> 10
598	Theoretical Snow	100	0	
599	Theoretical Snow	100	100	
600	Sea Ice AVG B and D	99.0 - 100.	0.0 - 0.1	
601	Sea Ice	75.0 - 99.0	0.0 - 0.1	
602	Sea Ice	50.0 - 75.0	0.0 - 0.1	
603	Sea Ice	25.0 - 50.0	0.0 - 0.1	
604	sea Ice	01.0 - 25.0	0.0 - 0.1	
605	Sea Ice	75.0 - 99.0	0.1 - 25.0	
606	Sea Ice	75.0 - 99.0	25.0 - 50.0	
607	Sea Ice	75.0 - 99.0	50.0 - 75.0	
608	Sea Ice	75.0 - 99.0	75.0 - 99.0	
609	Sea Ice	50.0 - 75.0	0.1 - 25.0	
610	Sea Ice	50.0 - 75.0	25.0 - 50.0	
611	Sea Ice	50.0 - 75.0	50.0 - 75.0	
612	Sea Ice	50.0 - 75.0	75.0 - 99.0	
613	Sea Ice	25.0 - 50.0	0.1 - 25.0	
614	Sea Ice	25.0 - 50.0	25.0 - 50.0	
615	Sea Ice	25.0 - 50.0	50.0 - 75.0	
616	Sea Ice	25.0 - 50.0	75.0 - 99.0	
617	Sea Ice	01.0 - 25.0	0.1 - 25.0	
618	Sea Ice	01.0 - 25.0	25.0 - 50.0	
619	Sea Ice	01.0 - 25.0	50.0 - 75.0	
620	Sea Ice	01.0 - 25.0	75.0 - 99.0	
621	Fresh Snow AVG B and D	99.0 - 100.	0.0 - 0.1	
622	Fresh Snow	75.0 - 99.0	0.0 - 0.1	
623	Fresh Snow	50.0 - 75.0	0.0 - 0.1	
624	Fresh Snow	25.0 - 50.0	0.0 - 0.1	
625	Fresh Snow	01.0 - 25.0	0.0 - 0.1	
626	Fresh Snow	75.0 - 99.0	0.1 - 25.0	
627	Fresh Snow	75.0 - 99.0	25.0 - 50.0	
628	Fresh Snow	75.0 - 99.0	50.0 - 75.0	
629	Fresh Snow	75.0 - 99.0	75.0 - 99.0	
630	Fresh Snow	50.0 - 75.0	0.1 - 25.0	
631	Fresh Snow	50.0 - 75.0	25.0 - 50.0	
632	Fresh Snow	50.0 - 75.0	50.0 - 75.0	
633	Fresh Snow	50.0 - 75.0	75.0 - 99.0	
634	Fresh Snow	25.0 - 50.0	0.1 - 25.0	
635	Fresh Snow	25.0 - 50.0	25.0 - 50.0	
636	Fresh Snow	25.0 - 50.0	50.0 - 75.0	
637	Fresh Snow	25.0 - 50.0	75.0 - 99.0	
638	Fresh Snow	01.0 - 25.0	0.1 - 25.0	
639	Fresh Snow	01.0 - 25.0	25.0 - 50.0	
640	Fresh Snow	01.0 - 25.0	50.0 - 75.0	
641	Fresh Snow	01.0 - 25.0	75.0 - 99.0	
642	Averaged Theoretical Snow ADMs : 598 - 599			
643	Averaged Permanent Snow ADMs: 591B – 597D			
644	Averaged Fresh Snow ADMs: 26 models			

645	Averaged Sea Ice ADMs: 26 models			
646	AVG B and D Fresh Snow	SF: 0.0 - 0.1	CF: 99.9 - 100	TAU: < 10
647	AVG B and D Fresh Snow	SF: 0.0 - 0.1	CF: 99.9 - 100	TAU: > 10
648	AVG B and D Sea Ice	IF: 0.0 - 0.1	CF: 99.9 - 100	TAU: < 10
649	AVG B and D Sea Ice	IF: 0.0 - 0.1	CF: 99.9 - 100	TAU: > 10

9.1.3. CERES Terra/Aqua Edition4 ADMs

More information and graphs can be found on the CERES website: https://ceres.larc.nasa.gov/data/angular-distribution-models/#ceres-terraaqua-edition4-adms

9.2. CERES TRMM SW ADM interpolation bias correction

The correction term is based on Loeb et al., 2003. Note that the corrections are here considered in terms of albedo, whereas the original formulas by Loeb et al., 2003 (*p.248, eq.16 in that reference*) are given in terms of flux, and shown here as equation 24:

$$F = \frac{\pi \cdot I}{R} + \delta F_{bin} \tag{24}$$

Where δF_{bin} stands for the bin-average flux correction term (available for each scene type and SZA,VZA, RAA angular bin). However, the bin-average correction terms in the RMIB database are available in terms of albedo, instead of flux (i.e. $\delta\alpha_{SW,bin}$ instead of δF_{bin}). To be able to apply our albedo correction, it would **not** be correct to simply re-write equation 24 like this (eq.25):

$$\alpha_{SW} = \frac{\rho_{SW}}{R} + \delta\alpha_{SW,bin} \quad (NOT\ \ correct\ \ !) \tag{25}$$

Indeed, the solar zenith angle (θ_0), required for an albedo→flux conversion, is different for the bin-averaged correction term δF_{bin} (eq.26 with bin-averaged solar zenith angle $\theta_{0,bin}$) than for the instantaneous quantities α_{SW} and ρ_{SW} (eqs.27 with instantaneous solar zenith angle θ_0):

$$\delta\alpha_{SW,bin} = \delta F_{bin} \cdot \frac{d^2}{TSI \cdot \cos(\theta_{0,bin})} \tag{26}$$

$$\alpha_{SW} = F \cdot \frac{d^2}{TSI \cdot \cos(\theta_0)} \quad \text{(and)} \quad \rho_{SW} = \pi \cdot I \cdot \frac{d^2}{TSI \cdot \cos(\theta_0)} \tag{27}$$

Hence the correct conversion term is derived as follows: the entire equation 24 is multiplied by $[d^2/(TSI \cdot \cos(\theta_0))]$, as shown in equation 28:

$$F \cdot \left[\frac{d^2}{TSI \cdot \cos(\theta_0)}\right] = \frac{\pi \cdot I}{R} \cdot \left[\frac{d^2}{TSI \cdot \cos(\theta_0)}\right] + \delta F_{bin} \cdot \left[\frac{d^2}{TSI \cdot \cos(\theta_0)}\right] \tag{28}$$

After substituting the left hand and first right hand terms in equation 28, we get equation 29:

$$\alpha_{SW} = \frac{\rho_{SW}}{R} + \left(\alpha_{SW,bin} \cdot \frac{TSI \cdot \cos(\theta_{0,bin})}{d^2}\right) \cdot \left[\frac{d^2}{TSI \cdot \cos(\theta_0)}\right] \tag{29}$$

And after resolving the second right hand term in equation 29, the *interpolation bias correction* in terms of albedo is given by equation 30:

$$\delta\alpha_{SW} = \delta\alpha_{SW,bin} \cdot \frac{\cos(\theta_{0,bin})}{\cos(\theta_0)} \tag{30}$$

This explains why the bin-average albedo correction terms ($\delta\alpha_{SW,bin}$), as available in the RMIB database, are multiplied by $[\cos(\theta_{0,bin})/\cos(\theta_0)]$ to obtain the directly applicable correction terms in terms of instantaneous albedo ($\delta\alpha_{SW}$) which may then be applied in equation 9.

9.3. Updated Narrowband-to-Broadband regressions

This sections provides updates on the tables and figures from Akkermans and Clerbaux, 2020. The values' modifications were caused by:

- small bug fixes in the code, most notably a (cosine) solar zenith angle correction for the channel 2 reflectance.
- broadening of cloud cover range for cloud classes "clear-sky" (0% to 0-10%) and "overcast" (100% to 90-100%).

The corresponding table and figure numbers from the original article are supplied in the captions of the following tables and figures.

Surface Type	IGBP Category	Nr. (Clear 0-10%)	Nr. (Overcast 90-100%)	Nr.(All)
Ocean	17	132298	576279	874832
Forests	1,2,3,4,5	7379	19036	44401
Savannas	8,9	12611	7491	28290
Grass/crop	6,10,11,12,13,14	24163	31423	76893
Dark deserts	7,18	36789	11045	61334
Bright deserts	16	140012	18667	191642
Perm. snow/ice	15	100818	71656	196848
Fresh snow	19	131996	180127	481537
Sea ice 100%		55449	49005	130281
Sea ice 95-99%		80198	132466	272334
Sea ice 90-95%		19461	75752	118277
Sea ice 80-90%		23501	137368	198221
Sea ice 60-80%		12969	95339	136376
Sea ice 10-60%		10183	108997	144779
Sea ice 0-10%		18350	303079	381240
(total)		806177	1817730	3337285

Table 16: NTB: Number of matched NTB pairs with strict matching criteria (update of Table 2 in Akkermans and Clerbaux, 2020)

	Clear-Sky (0-10%)				Overcast (90-100%)				All-Sky			
Surface Type	R^2_{adj}	RMSr	rRMSr	SEr	R^2_{adj}	RMSr	rRMSr	SEr	R^2_{adj}	RMSr	rRMSr	SEr
Ocean	0.880	0.31	5.57%	0.001	0.981	1.75	4.54%	0.002	0.990	1.70	5.86%	0.002
Forests	0.940	0.44	3.55%	0.005	0.973	1.97	4.47%	0.014	0.987	1.75	5.83%	0.008
Savannas	0.975	0.39	2.77%	0.003	0.977	1.97	5.61%	0.023	0.985	1.30	6.13%	0.008
Grass/crop	0.960	0.54	3.35%	0.003	0.977	1.75	3.88%	0.010	0.990	1.50	5.01%	0.005
Dark deserts	0.980	0.58	3.16%	0.003	0.971	1.85	4.30%	0.018	0.986	1.24	5.20%	0.005
Bright deserts	0.980	0.69	2.34%	0.002	0.969	1.60	3.75%	0.012	0.973	1.01	3.31%	0.002
Perm. snow/ice	0.975	0.63	1.04%	0.002	0.954	1.33	2.20%	0.005	0.880	1.78	2.94%	0.004
Fresh snow	0.992	1.03	2.69%	0.003	0.976	1.41	2.93%	0.003	0.976	1.74	4.12%	0.003
Sea ice 100%	0.959	0.62	1.18%	0.003	0.958	0.91	1.71%	0.004	0.871	1.39	2.63%	0.004
Sea ice 95-99%	0.973	0.63	1.21%	0.002	0.966	1.06	1.95%	0.003	0.900	1.69	3.19%	0.003
Sea ice 90-95%	0.990	0.72	1.50%	0.005	0.965	1.14	2.12%	0.004	0.934	1.75	3.37%	0.005
Sea ice 80-90%	0.973	0.72	1.91%	0.005	0.968	1.19	2.33%	0.003	0.964	1.52	3.17%	0.003
Sea ice 60-80%	0.955	0.90	2.92%	0.008	0.969	1.30	2.72%	0.004	0.972	1.52	3.44%	0.004
Sea ice 10-60%	0.944	1.39	8.22%	0.014	0.975	1.45	3.44%	0.004	0.982	1.59	4.22%	0.004
Sea ice 0-10%	0.960	0.33	5.24%	0.002	0.973	1.57	3.89%	0.003	0.984	1.64	4.60%	0.003
(generic*)	0.998	0.80	2.39%	0.001	0.982	1.58	3.54%	0.001	0.985	1.93	4.92%	0.001

R^2_{adj}: adjusted coefficient of determination; RMSr: root-mean-square residual; rRMSr : relative RMSr;
SEr: standard error of residuals
(*) surface-type-independent regression, that combines all matched NTB pairs (regardless the surface type)

*Table 17: NTB validation: Regression metrics based on calibration subset, here using **100%** of the NTB pairs with strict matching criteria (update of Table 4 in Akkermans and Clerbaux, 2020)*

	Clear-Sky (0-10%)				Overcast (90-100%)				All-Sky			
Aggregation Type	MB_{flux}	MB	rMB	$rRMSr$	MB_{flux}	MB	rMB	$rRMSr$	MB_{flux}	MB	rMB	$crRMSr$
Ocean	-0.85*	-0.084*	-1.46%*	6.84%	-1.29*	-0.179*	-0.46%*	5.51%	-1.15*	-0.148*	-0.49%*	6.81%
Forests	-0.31	-0.011	-0.09%	4.01%	+0.09	-0.018	-0.04%	4.91%	+0.24	+0.013	+0.04%	6.31%
Savannas	+0.36	+0.034	+0.23%	3.13%	-0.21	-0.013	-0.04%	5.91%	+0.10	+0.011	+0.05%	6.57%
Grass/crop	-0.32*	-0.037*	-0.23%*	3.62%	-0.05	-0.028	-0.06%	4.44%	+0.06	-0.005	-0.02%	5.62%
Dark deserts	-0.72*	-0.066*	-0.35%*	3.35%	+0.24	+0.015	+0.04%	4.83%	-0.46	-0.042	-0.17%	5.57%
Bright deserts	-0.16	-0.022	-0.08%	2.47%	+0.38	+0.035	+0.08%	4.37%	+0.13	+0.010	+0.03%	3.52%
Perm. snow/ice	-0.72*	-0.146*	-0.24%*	1.28%	-0.67*	-0.215*	-0.35%*	2.71%	-0.57*	-0.152*	-0.25%*	3.31%
Fresh snow	+0.31	+0.014	+0.04%	2.93%	-0.24*	-0.117*	-0.24%*	3.33%	-0.63*	-0.150*	-0.34%*	4.43%
Sea ice 100%	+0.01	-0.009	-0.02%	1.26%	-0.25	-0.039	-0.07%	1.96%	-0.11	-0.010	-0.02%	2.88%
Sea ice 95-99%	-0.14*	-0.042*	-0.08%*	1.34%	-0.30*	-0.059*	-0.11%*	2.17%	-0.37*	-0.066*	-0.12%*	3.34%
Sea ice 90-95%	-0.11	-0.029	-0.06%	1.64%	-0.33*	-0.055*	-0.10%*	2.34%	-0.26*	-0.044*	-0.09%*	3.57%
Sea ice 80-90%	+0.09	+0.009	+0.02%	2.05%	-0.04	+0.002	+0.00%	2.50%	+0.27*	+0.058*	+0.12%*	3.31%
Sea ice 60-80%	+0.21	+0.036	+0.12%	2.96%	-0.58*	-0.070*	-0.15%*	2.96%	-0.31	-0.034	-0.08%	3.63%
Sea ice 10-60%	+0.82*	+0.097*	+0.58%*	8.07%	-0.74*	-0.100*	-0.24%*	3.90%	-0.38	-0.054	-0.14%	4.66%
Sea ice 0-10%	+0.11	+0.003	+0.05%	6.00%	-0.85*	-0.174*	-0.43%*	4.44%	-0.96*	-0.195*	-0.54%*	5.16%
Global mean[1]	-0.70	-0.077	-0.79%	n.a.[2]	-0.31	-0.067	+0.24%	n.a.[2]	-0.65	-0.092	+0.64%	n.a.[2]

MB_{flux}: mean bias expressed as isotropic flux (Wm^{-2}); rMB: relative mean bias; rRMSr: relative rms residual
$*$ statistically significant on the 99% confidence level
[1] *After spatial aggregation of all NTB pairs on a 5°×5° grid with area-weighting.*
[2] *Since rRMSr is calculated with respect to all NTB pairs within that scene type, this metric cannot be globally aggregated*

Table 18: NTB validation: regression performance on expanded database with relaxed matching criteria (update of Table 6 in Akkermans and Clerbaux, 2020)

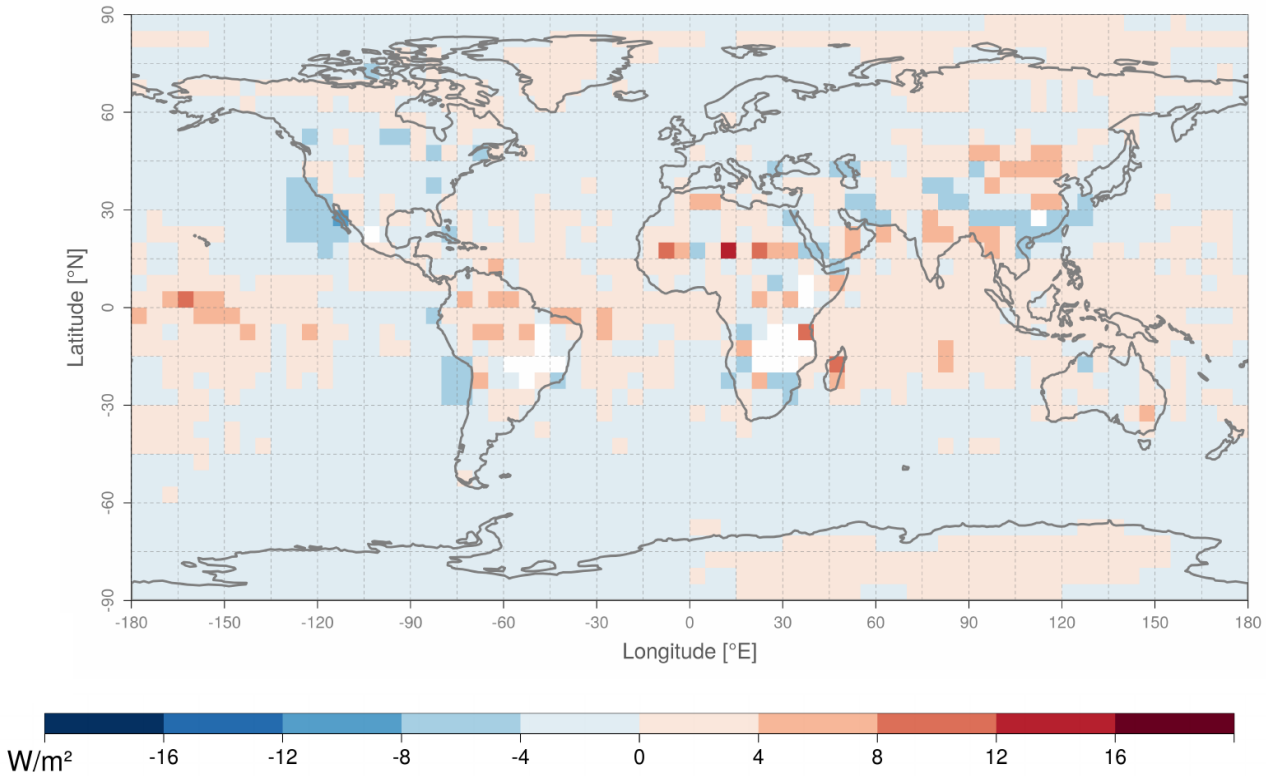

*Figure 78: Flux-equivalent Mean Bias (MB_{flux}) between observed and estimated broadband reflectance, for **overcast conditions** (update of Figure 4c in Akkermans and Clerbaux, 2020).*

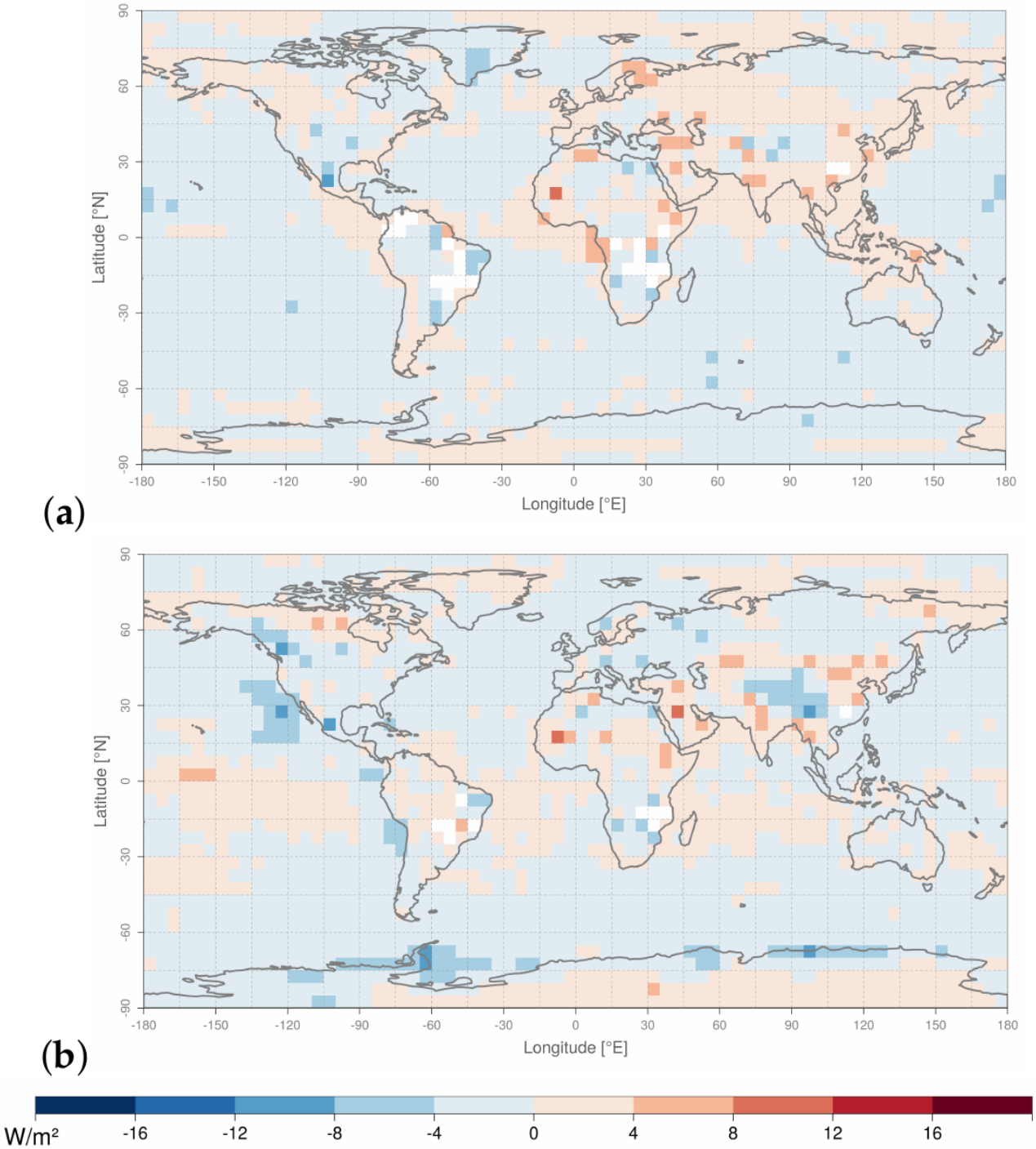

Figure 79: Flux-equivalent Mean Bias (MB_{flux}) between observed and estimated broadband reflectance, for (a) clear-sky and (b) all-sky conditions (update of Figure 5 in Akkermans and Clerbaux, 2020).

		Clear-Sky (0-10%)		Overcast (90-100%)		All-Sky	
Statistic	**Validation Subset**	MB_{flux}	MB	MB_{flux}	MB	MB_{flux}	MB
global mean (on 5° × 5° grid)	NOAA17+Terra	-0.69	-0.105	+0.33	-0.008	+0.32	+0.015
	NOAA19+Aqua	-0.52	-0.023	-0.56	-0.075	-0.86	-0.086
	NOAA18+Aqua	-0.67	-0.120	-1.13	-0.192	-1.42	-0.240

MB_{flux}: mean bias expressed as isotropic flux (Wm^{-2}); MB: mean reflectance bias (Wm^{-2})

Table 19: NTB: Global stability statistics from bias map, based on expanded database, with relaxed matching criteria (update of Table 7 in Akkermans and Clerbaux, 2020)

		Clear-Sky		Overcast		All-Sky	
Statistic	**Regression Predictors**	MB_{flux}	MB	MB_{flux}	MB	MB_{flux}	MB
global RMSB	Ch1,Ch2,SZA,VZA	1.76	0.213	2.08	0.288	2.08	0.316
	Ch1,Ch2,SZA	1.88	0.258	2.42	0.453	2.31	0.417
	Ch1,Ch2	2.01	0.283	2.75	0.465	2.30	0.418
global MAB	Ch1,Ch2,SZA,VZA	1.35	0.166	1.62	0.226	1.58	0.225
	Ch1,Ch2,SZA	1.49	0.201	1.86	0.296	1.77	0.281
	Ch1,Ch2	1.55	0.208	2.08	0.327	1.72	0.287

Global statistics: RMSB: root mean square of biases (Wm^{-2}); MAB Mean of absolute biases (Wm^{-2})
On pixel-level: MB_{flux}: mean bias expressed as isotropic flux (Wm^{-2}); MB: mean reflectance bias (Wm^{-2})

Table 20: NTB: Global accuracy statistics from bias map, based on surface-type-dependent regressions from expanded database, with relaxed matching criteria (update of Table 8 in Akkermans and Clerbaux, 2020)

9.4. Application of NTB regressions on GAC/AVHRR pixel scale (new)

For the validation of the obtained NTB regressions, Akkermans and Clerbaux (2020) applied each of these regressions to aggregated narrowband AVHRR reflectances (i.e. aggregated to CERES footprint), compared the resulting broadband reflectance with the corresponding CERES broadband reflectance, and from that calculated a bias (Figure 80). In other words, the regressions are applied **AFTER** pixel aggregation. The "all-sky" NTB regression is applied on **all** aggregated pixels, including those with fractional cloud cover (*e.g. mixed fields of "broken clouds", patchwork of alternating clearsky and overcast AVHRR pixels*), cfr. Figure 80c.

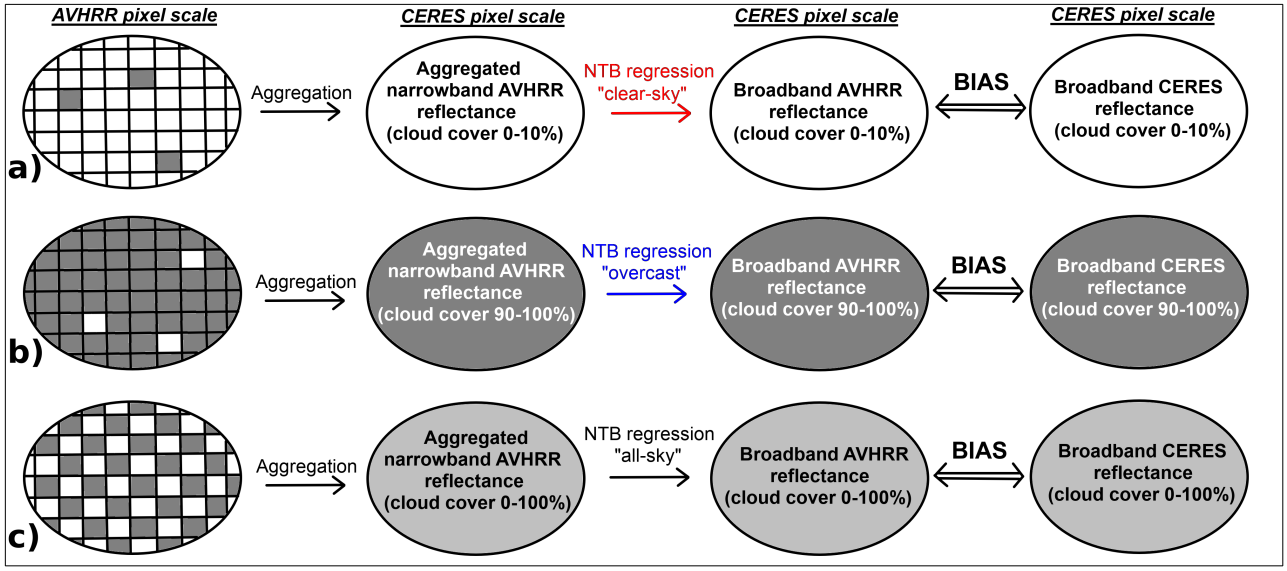

Figure 80: NTB regression validation in Akkermans and Clerbaux (2020)

However, in the CLARA-A3 TOA RSF processing, described in this document, the AVHRR (GAC) pixels are **not** a priori aggregated to homogeneous entities that match the relatively large CERES footprints, but processed separately as smaller independent entities (AVHRR pixels). Given the binary nature of the cloud mask (each AVHRR pixel is assigned either a clear-sky or an overcast cloud cover), only one of the first two 'pure' NTB regressions will be applied on each individual AVHRR pixel (either for 'clearsky' or 'overcast' scenes). Hence, situations with *mixed fields of "broken clouds" (patchwork of alternating clearsky and overcast AVHRR pixels)* require a different validation approach, in which the regressions are applied on each individual AVHRR pixel **BEFORE** their aggregation, after which the resulting broadband reflectances from all AVHRR pixels are aggregated to the CERES footprint and compared with the observed CERES broadband reflectance to calculate the bias (Figure 81). Similar to the all-sky validation approach from Akkermans and Clerbaux (2020) depicted in Figure 80c, the all-sky validation approach in Figure 81c aims to be representative for all situations, however the latter is specifically tailored to CLARA-A3 since it mimics what happens in the CLARA-A3 processing, i.e. only making use of the 'pure' binary regressions for clearsky and overcast situations, which are applied on AVHRR pixels with the same 2 (binary) cloud classes.

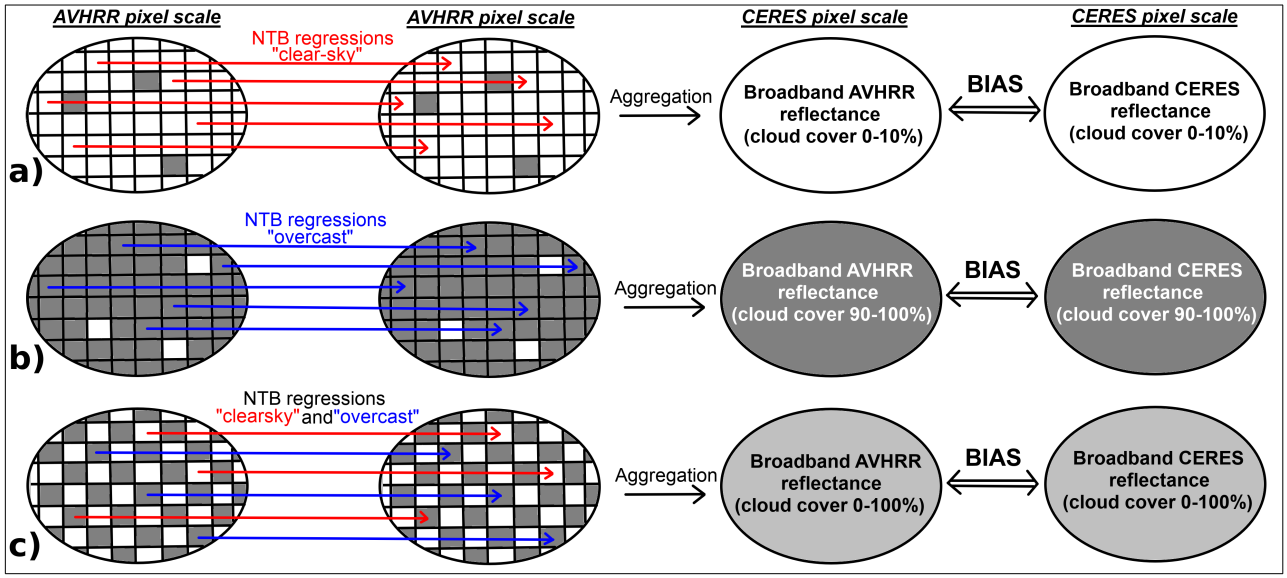

Figure 81: NTB regression validation for individual GAC/AVHRR pixels

The results of the all-sky validation approach depicted in Figure 81c is shown below for the actual reflectance expressed as percentage with range 0-100% (Figure 82), and for the flux-equivalent reflectance expressed as W/m² (Figure 83).

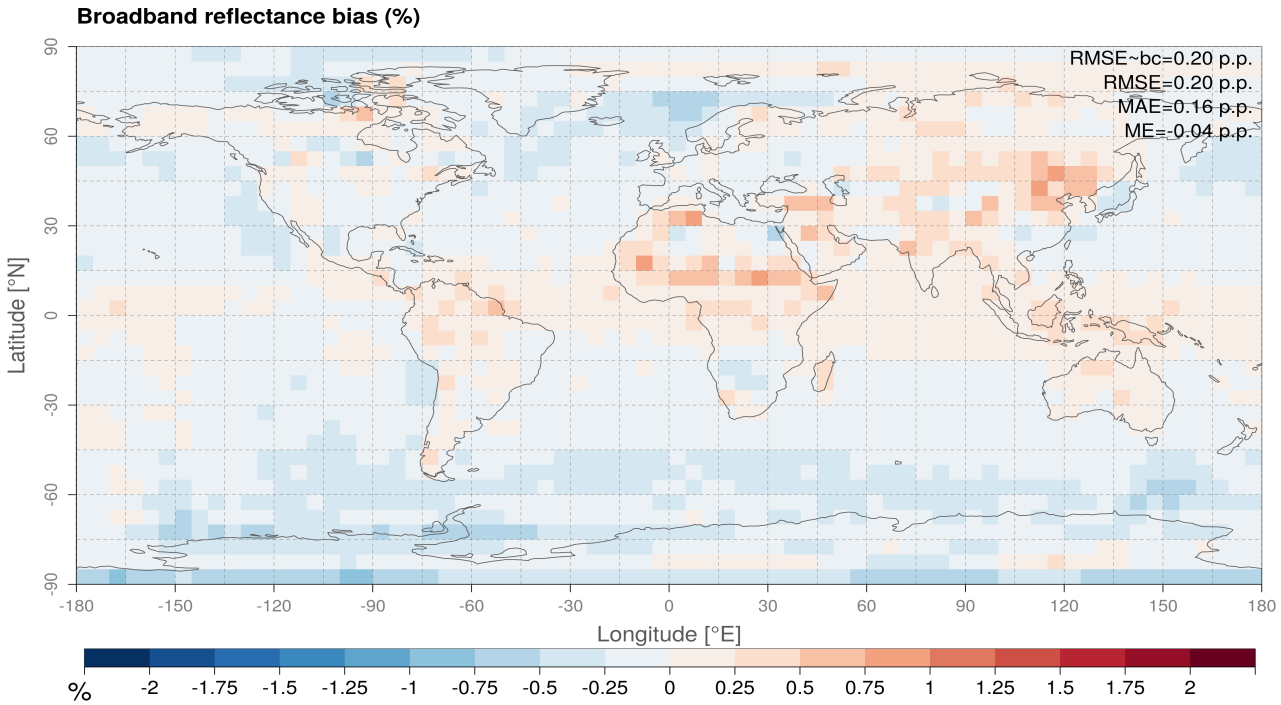

Figure 82: Mean bias of reflectance (in percentage points p.p.) between observed and estimated broadband reflectance, for all-sky conditions

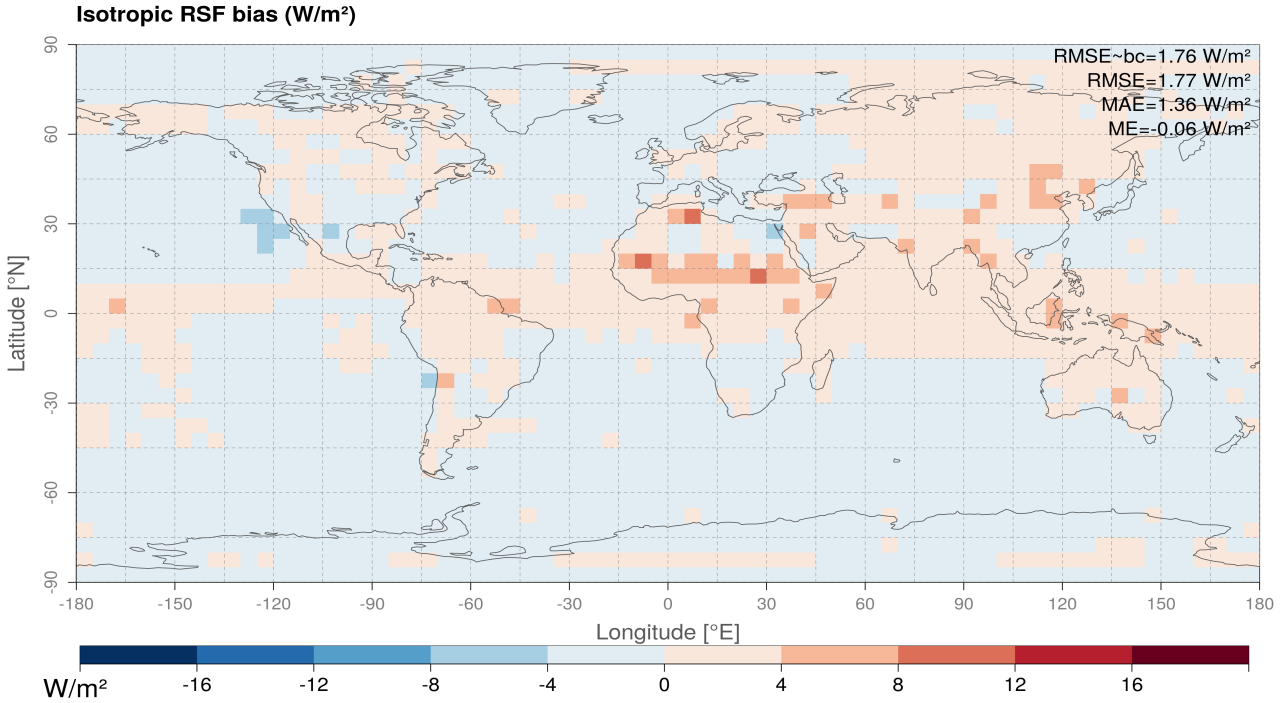

Figure 83: Mean bias of flux-equivalent reflectance (in W/m^2) between observed and estimated broadband reflectance, for all-sky conditions

Conclusion: good performance, so we can trust the 'pure' NTB regressions to perform well, also in mixed cloud patchwork situations.

9.5. Land cover classes for NTB analyses

Akkermans and Clerbaux (2020) aggregated the same groups of IGBP land cover classes as Loeb et al. (2005), where it was used to generate longwave ADM's. In the current document, these aggregated IGBP subidivions are referred to as "NTB surface types", and differ from the "CERES surface types" in terms of class definition and also in class detail: for instance, it has an additional class "Savanna". Figure 84 shows that this IGBP class grouping is also suitable for shortwave analyses: the 'savanna' class is clearly a transitional class between dark and bright vegetation. Note that the units here are scaled radiance (cfr Section 3.1.2.b), i.e. not normalized for anisotropy: inter-class differences may be partially biased due to preferential anisotropy in the sampling.

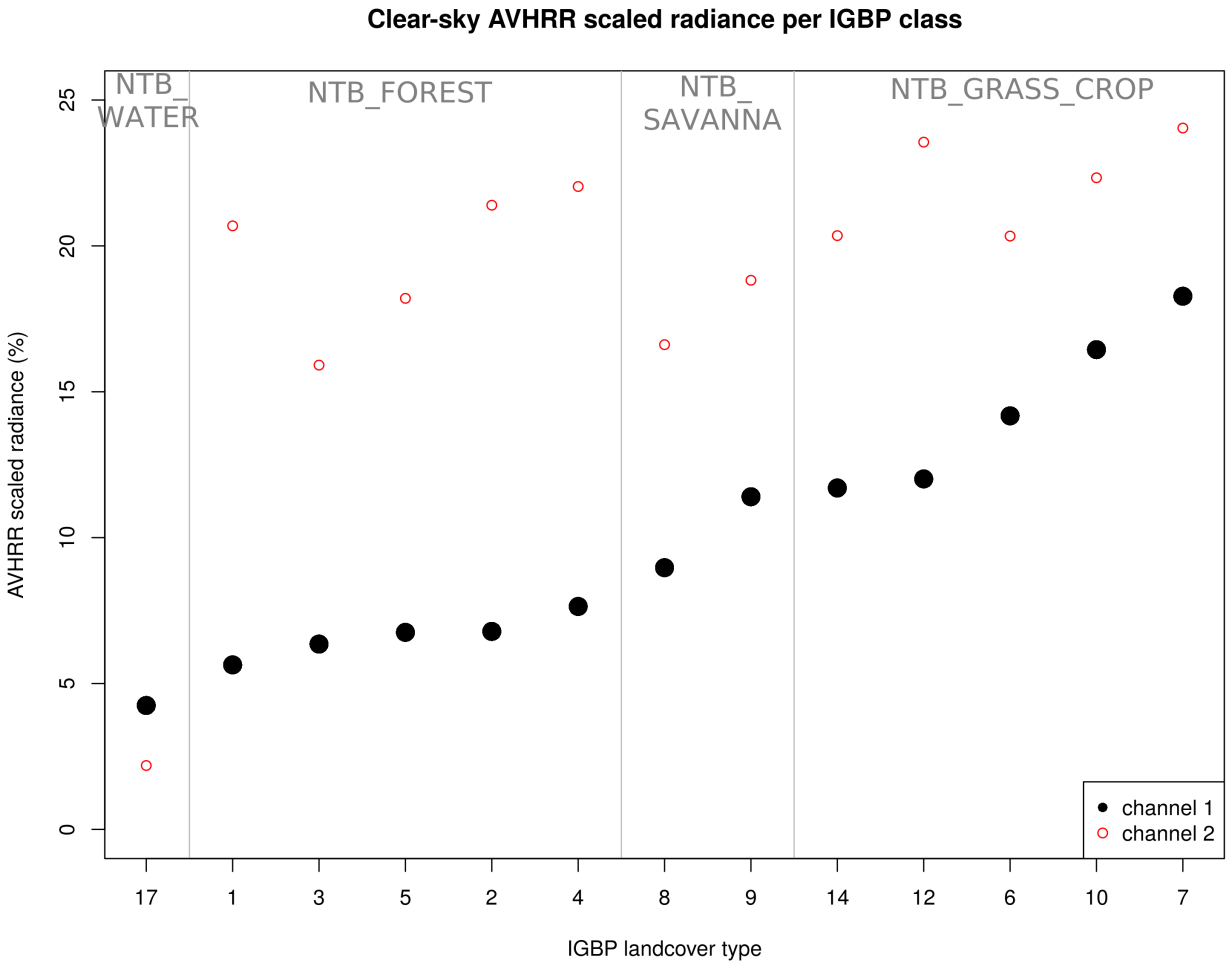

Figure 84: Clear-sky scaled radiance for AVHRR channels 1 and 2, stratified per IGBP class

9.6. Bit Flags, and Bit Flag variable IDs

9.6.1. Bit flag variable ID's

Note that the ID is only given for the LAST variable that was affected by an issue (indicated by one of the bit flags) before the routine terminated for a given pixel. For instance, it is possible that there is an issue with multiple variables, but that only the last variable causes a fatal termination (and hence invalid albedo for current pixel): in such a case, only for the last variable the ID is stored.

Table 21 contains the short variable identifiers that are used by the configuration file and by the program code. The corresponding full (human-readable) variable names can also be found in the configuration file.

Table 21: Bit flag Variable ID's

Input Program Part 1		**Output Program Part 1**		**Output Program Part 2**		**Output Program Part 3**	
ID	Variable in configfile	ID	Variable in configfile	ID	Variable in configfile	ID	Variable in configfile
1	REFL_CH1	30	TIME	60	TWILIGHT_A	101	SW_FLUX
2	REFL_CH2	31	LW_FLUX	61	TWILIGHT_B	102	SW_FLUX_TWL
3	TB_CH4	32	LW_RAD	62	SURF1_FRAC	103	NR_INST_SW
4	TB_CH5	33	SW_ALB	63	SURF2_FRAC	104	NR_INST_LW
5	LON	34	SW_ALB_ISO	64	SURF3_FRAC	105	RELSHARE_SUNGLINT
6	LAT	35	CLOUDCOV	65	SURF4_FRAC	106	RELSHARE_TWILIGHT
7	SZA	36	COT_WRITE	66	SURF5_FRAC	107	RELSHARE_DAYLIGHT
8	VZA	38	WINDSP	67	SURF6_FRAC	108	BITFLAGS_SW
9	RAA	39	BITFL	68	SURF7_FRAC	109	BITFLAGS_LW
10	CMA	40	SURFTYPE	69	SURF8_FRAC	118	BITFLAGS_SW_SAT
11	CMAPROB	41	SEAICE_WRITE	70	SURF_TOTAL	119	BITFLAGS_LW_SAT
12	COT_READ	42	SNOWCOV	71	CPHASE_WRITE	110	LW_FLUX_HIRS1
13	CPHASE_READ	43	BITFLAGS	72	NR_AVHRR_SUNGLINT	111	LW_FLUX_HIRS2
14	CPPQUAL	44	GLINTANGLE	73	NR_AVHRR_SW	112	LW_FLUX_HIRS3
15	SEAICE_READ	45	CLOUDCOVNBH	74	NR_AVHRR_LW	113	LW_FLUX_HIRSN
16	SNOWDEPTH			75	SZA_CALC	114	LW_FLUX_HIRS1CORR
17	IWV	*49*	*SZA_WRITE**			115	LW_FLUX_HIRS2CORR
18	TSUR					116	LW_FLUX_HIRS3CORR
19	U10M					117	NR_DLB
20	V10M						
21	LANDUSGS					130	NR_DM_SW
22	FRLAND					131	NR_DM_LW
23	TIMESTAMP						
24	CPPCOND						
(*) development/debug purposes only							

9.6.2. Bit flags for Program Part 1

The variable “bitflags” is an unsigned short integer, meaning that it can contain up to 16 bitflags (max combined value amounts 65535). These are numbered from right to left, so the rightmost bit is “bit number 1”, the second from the right is “bit number 2”, etc. Critical flags indicate non-processed pixels, i.e. situations in which the pixel could not be processed due to a number of reasons, and has no valid output (NA, NaN, fill value,..), and are shown in red in Table 22; *these pixels will be ignored in the aggregation program (Program Part 2) and not be included in the aggregated pixel.* ***Note that this can be different for shortwave and longwave part (!)***

Table 22: Bit flags for Program Part 1

Bit nr.	**Binary representation**	**Value**	**Bitflag name**	**Interpretation**
1	0000000000000001	1	BITFLAG_FILL	pixel is **not** processed (SW and/or LW) due to *inputdata* which is missing, for the variable indicated by Bitflag_variable_ID)
2	0000000000000010	2	BITFLAG_RANGE	pixel is **not** processed (SW and/or LW) due to *inputdata* which is out of range (invalid), for the variable indicated by Bitflag_variable_ID)

3	0000000000000100	4	BITFLAG_ERROR	pixel is **not** processed (SW and/or LW) due to *intermediate/output data* processing errors, for the variable indicated by Bitflag_variable_ID
4	0000000000001000	8	BITFLAG_NB_OLR	pixel is **not** processed (LW) due to *invalid LW NB-to-OLR conversion*, e.g. due to unrealistic input brightness temperatures Tb_ch4 or Tb_ch5. This flag is for non-fatal errors, which lead to non-valid longwave processing (only for current pixel). Some cases lead to fatal errors that terminate the entire program (affecting entire orbit), such as too high VZA as input.
5	0000000000010000	16	BITFLAG_ADM4	Specific conditions (overcast sea-ice) for which newer ADMs are used (CERES ADM Ed.4 from Su et al. 2015, ADM nrs. 1049-1058)
6	0000000000100000	32	BITFLAG_ADM4ERR	Error in Ed.4 ADM: unrealistic anisotropic factor (R) value, e.g. negative or too high, so classic ADMs are used instead
7	0000000001000000	64	BITFLAG_CORR	Due to issues with calculation or outputdata, the result is corrected (e.g. SW albedo exceeds 100% and is therefore corrected to 100%); variable is indicated by Bitflag_variable_ID
8	0000000010000000	128	*(spare bit)*	*(spare bit)*
9	0000000100000000	256	BITFLAG_BADCOT	Cloud optical thickness inputdata is labeled as bad quality, and is substituted by long-term average from CERES
10	0000001000000000	512	BITFLAG_SZA	Solar Zenith Angle is higher than the threshold (default is 84°, but adjustable in config file), preventing SW albedo calculation
11	0000010000000000	1024	BITFLAG_COAST	Coastal water pixels may suffer from albedo underestimation because they may actually consist of land or mixed water/land, thereby misleading the NTB routine which erroneously uses the regression for water surfaces. In that case, resulting albedo's between 0%-6% are not set to "invalid" but to a fixed value of 6%, and this flag is activated.
12	0000100000000000	2048	BITFLAG_CMASNOW	Following situations are covered by this bit flag: **1.** Ocean pixel (not included in OSI SAF sea ice) for which cloudmask says "clearsky surface snow/ice" (valid CMA=3) but this is very unlikely, therefore the pixel has been set to "cloudy ocean" with liquid cloud and COT taken from CERES **[Bitflag variable ID: cloudmask]** **2.** Cases in which the cloudmask 'CMAextended' fails to detect sea ice [e.g. 1996/03/10, 13:00-15:00UTC, Gulf of Bothnia (north part of Baltic Sea)], i.e. false CMA=0 case; (only done for sea-ice and not for fresh snow, since the latter has quite low spatial accuracy, so the cloudmask should be the only source (CMA=3) **[Bitflag variable ID: seaice_write]** **3.** Cases in which the cloudmask 'CMAextended' CANNOT be used to detect clearsky snow/ice because there is a mismatch between cloudmasks (CMA=1 or CMA=2, whereas CMAPROB<50%, which renders CMAext useless for clearsky snow/ice detection): flag_CMAext_notvalid=1 **[Bitflag variable ID: cloudcover]**
13	0001000000000000	4096	BITFLAG_GLINT	Sunglint conditions, i.e. the "exposed water fraction" is higher than the threshold [*GLINT_MIN_WATER_FRACTION in configfile*], and the sunglint angle is lower than the threshold [*GLINT_ANGLE_THRESHOLD_MILD in configfile*].
14	0010000000000000	8192	*(spare bit)*	*(spare bit)*
15	0100000000000000	16384	BITFLAG_GLINT_ERR	Sunglint: pixel is **not** processed due to an adjustable flag in the configuration file [FLAG_SUNGLINT=1] which excludes all pixels in sunglint conditions (see BITFLAG_GLINT). *To be clear: this is not the default setting!*
16	1000000000000000	32768	BITFLAG_VZA	Pixel is **not** processed (SW+LW) due to inputdata namely Viewing Zenith Angle which is higher than the threshold (max. 70° but adjustable in config file)

The flags are added and the resulting value is a combination of the different bitflags; a combined value of e.g. 9 consists of bitflags nr.1 (value 1) and nr.4 (value 8). The flags can be read manually using a **binary** "AND" operation *[e.g. checking existence of SZA bitflag in C can be done with:* `if((BITFLAG_SZA & bitflag)==BITFLAG_SZA)` *]*, or with specialized routines.

9.6.3. Bit flags for Program Part 3

The variable "bitflags" is an unsigned short integer, meaning that it can contain up to 16 bitflags (max combined value amounts 65535). These are numbered from right to left, so the rightmost bit is "bit number 1", the second from the right is "bit number 2", etc. Critical flags indicate non-processed pixels, i.e. situations in which the pixel could not be processed due to a number of reasons, and has no valid output (NA, NaN, fill value,..), and are shown in red in Table 22; *these pixels will be ignored in the aggregation program (Program Part 2) and not be included in the aggregated pixel.* ***Note that this can be different for shortwave and longwave part (!)***

Table 23: Bit flags for Program Part 3

Bit nr.	Binary representation	Value	Bitflag name	Interpretation
1	0000000000000001	1	BITFLAG_NO_DLB	No so-called 'daylight-blocks' (DLB's) detected for current day, i.e. all timebins permanently have SZA>84° (or mu0<SZA084MU)

2	0000000000000010	2	BITFLAG_INVALID_L2	At least 1 DLB contains at least 1 invalid Level-2 observation (e.g. when Level-1 input data were invalid, or when e.g. effective SZA cutoff is lower than 84°), i.e. an observation that belongs to the timerange of the DLB but are not used due to (counts_level2==0)
3	0000000000000100	4	BITFLAG_ALB_ADM4ERR	***(SW only)*** error in Ed.4 ADM: unrealistic (clim.average) albedo value, e.g. negative or too high, so albedo from classic ADMs is used instead
4	0000000000001000	8	BITFLAG_ALB_MISMATCH	***(SW only)*** too large mismatch between theoretical albedo curve (from CERES TRMM ADM) and observed albedo, leading to a shift of the theoretical curve outside the physical range [0.0-1.0]; as a "fix", the cloud cover is artificially and iteratively increased (leading to another scene type) until the theoretical albedo curve doesnt shift outside the physical range anymore; if cloudcover increase does not help, the Cloud Optical Thickness is iteratively increased by steps of 5, until the curve fits within physical limits
5	0000000000010000	16	BITFLAG_ERA5	***(LW only)*** ERA5 has been used to model the diurnal cycle
6	0000000000100000	32	BITFLAG_TWL_EXT	***(SW only)*** At least 1 *entire* DLB has SZA >= 80° and has no valid observations, and is therefore filled using extrapolated twilight model (in 80°-84° SZA range) [this overrules BITFLAG_EMPTY_DLB and BITFLAG_INVALID_DLB for the current daylightblock, i.e. at least for this DLB (!) those flags are not activated]
7	0000000001000000	64	BITFLAG_EMPTY_DLB	pixel is **not** processed (SW and/or LW): At least 1 DLB has no (zero) Level-2 observations, e.g. due to missing inputfiles, or low probability of observations in short-timerange-DLB, when SZA is almost always >84°
8	0000000010000000	128	BITFLAG_INVALID_DLB	pixel is **not** processed (SW and/or LW): At least 1 DLB has all INVALID Level-2 observations (e.g. when input data were invalid, or when e.g. effective SZA cutoff is lower than 84°), i.e. observations that belong to the timerange of the DLB but are not used due to (counts_sw_inst==0), i.e. no Level-2 observation; there are no valid Level-2 pixels (all suffer from counts_sw_inst==0)
9	0000000100000000	256	BITFLAG_INVALID_ALL	pixel is **not** processed (SW and/or LW): There are more than 0 DLB's, and *all of them* have each either no level-2, or all invalid level-2 observations

9.7. Post-processing from ERA5 OLR and cloud cover

MARS: https://confluence.ecmwf.int/display/UDOC/MARS+user+documentation

The data request goes from ${date_prev}:07:00 to ${date_nextnext}:06:00, i.e. 72 hours of data. The timestamp indicates the accumulated past hour, so "06:00" means the integral between "05:00 – 06:00"; From that, we extract the range between ${date_prev}:12:00 (timestep 6) until ${date_next}:13:00 (timestep 55). Since these are hourly cumulated times, the effective extracted time range is between 11h UTC (instant.) previous day until 13h UTC (instant.) next day, i.e. 50 full hours.

General MARS request parameters

```
# General MARS request parameters
MARS_type="fc"  #Type of field (an, fc, pf, cf)
MARS_time="06:00:00/18:00:00"
MARS_step="1/2/3/4/5/6/7/8/9/10/11/12"  #Forecast time step  (HH)
MARS_area="89.875/0.125/-89.875/359.875"  #Spatial area
MARS_date=${date_prev}/to/${date_next}
Area="global"
MARS_stream="oper"  #Forecasting system (oper, wave, moda, mnth)
MARS_levtype="sfc"  #Type of level (sfc, ml, pl, pv, pt, dp)
MARS_grid="0.25/0.25"  #Output grid mesh
MARS_format="netcdf"  #Output format
MARS_param="40.235/164.128"   # for OLR use "40.235" [indicatorOfParameter=40;
table2Version=235], do NOT use its short name ("mtnlwrf") this will yield wrong
variable! For cloud cover use “164.128”
```

Once the requested file is downloaded, the following steps are performed:

- convert from GRIB to Netcdf
- select time steps 6 to 55